Cyprus University of Technology
Faculty of Engineering and Technology

Doctoral Dissertation

Evaluation of a flat, rectangular MR compatible ultrasonic transducer for cardiac applications

Michalis Sotiriou

Limassol, May 2023

CYPRUS UNIVERSITY OF TECHNOLOGY

FACULTY OF ENGINEERING AND TECHNOLOGY

DEPARTMENT OF ELECTRICAL ENGINEERING, COMPUTER

ENGINEERING AND INFORMATICS

Doctoral Dissertation

Evaluation of a flat, rectangular MR compatible ultrasonic transducer for cardiac applications

Michalis Sotiriou

Limassol, May 2023

Approval Form

Doctoral Dissertation

Evaluation of a flat, rectangular MR compatible ultrasonic transducer for cardiac applications

Presented by

Michalis Sotiriou

Supervisor: Faculty of Engineering, Christakis Damianou, Professor

Signature

Member of the committee: Faculty of Engineering, Takis Kasparis, Professor

Signature

Member of the committee: Faculty of Pure and Applied Sciences, Costas Pattichis, Professor

Signature

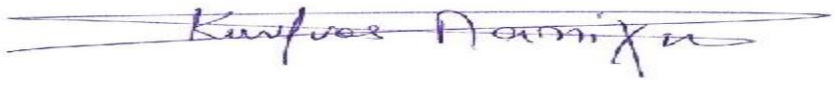

Cyprus University of Technology

Limassol, May 2023

Approval Form of Advisory Committee

Doctoral Dissertation

Evaluation of a flat, rectangular MR compatible ultrasonic transducer for cardiac applications

Presented by

Michalis Sotiriou

Supervisor: Faculty of Engineering, Christakis Damianou, Professor

Signature

Member of the committee: Faculty of Engineering, Takis Kasparis, Professor

Signature

Member of the committee: Faculty of Pure and Applied Sciences, Costas Pattichis, Professor

Signature

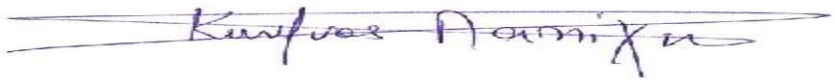

Cyprus University of Technology

Limassol, May 2023

Copyrights

Acknowledgements

First, I would like to express my sincere appreciation and thankfulness to my supervisor, Prof. Christakis Damianou for his supervision, support and useful critique during my PhD study.

Moreover, I would like to express gratitude to my lab colleagues and research team (Marinos Giannakou, Antria Filippou, Nikolas Evripidou and Anastasia Antoniou) for their support during my dissertation.

Finally, I would like to thank especially my wife Isavella and my family for all their support all these years to complete my dissertation.

Abstract

High Intensity Focused Ultrasound (HIFU) is a non-invasive therapeutic technique that can cause localized hyperthermia at predictable depths without injuring intervening tissues. Atherosclerosis is a condition that develops when a substance called plaque builds up in the walls of the arteries and is related with numerous problems on heart and blood vessels. HIFU can be used to ablate atherosclerotic plaque from these arteries and avoid fatal problems such as heart failure and stroke.

In this study the main objective is the design of an in vitro model to assess the thermal ablation of atherosclerotic plaque using different parameters of intravascular transducers. The experiments were initially conducted in different phantoms and in freshly excised turkey tissue phantom. A flat rectangular transducer was assessed in an arterial atherosclerotic plaque phantom which was created in the laboratory with a very low cost. The proposed phantom mimics the human atherosclerotic plaque. Atherosclerotic plaque is mainly consists of fibrous tissue, lipid core, calcium and necrotic core. Different percentages of those components would categorize different types of plaques. Agar was used for mimicking fibrous tissue, gypsum for calcium and butter for lipid core. The only limitation is that macrophages were not used for mimicking the necrotic core. The artery phantom follows the elastic properties of an artery. The amount of plaque removal was evaluated visually and using an X-Ray system. The main complications of thermal ablation were the increased artery temperature above a safe level (1 °C) and the rupture of atherosclerotic plaque during the ablation. Furthermore, different parameters of intravascular transducers were assessed with different composition percentages of atherosclerotic plaque. The frequency was 4.0 MHz and acoustical power and sonication time were between 6–15 W and 15–30 s respectively for achieving the optimum combination. Moreover, the specific flat, rectangular transducer is MR compatible and thermometry images were obtained during this evaluation. The intended application is to use it for atherosclerotic plaque ablation using a single element transducer. Finally, an evaluation of acoustic and thermal properties of plaque phantoms to test their suitability mainly for ultrasound imaging and therapy was performed. This is very important for the effective implementation of ultrasound not only in diagnosis, but especially for therapy. The evaluation included measurements of the acoustic propagation speed using the pulse-echo technique, the ultrasonic attenuation coefficient using through transmission immersion technique, and the absorption coefficient. Moreover, thermal

properties (thermal conductivity, volumetric specific heat capacity and thermal diffusivity) were measured with the transient method using a needle probe. The mean value of acoustic and thermal properties and their standard deviation of plaque phantoms were 1523±23 m/s for acoustic speed, 0.50±0.02 W/mK for thermal conductivity, 0.30±0.21 dB/cm-MHz for ultrasonic absorption coefficient and 1.63±0.46 dB/cm-MHz for ultrasonic attenuation coefficient.

Future studies should be focused on the optimum recipe of the atherosclerotic plaque phantoms that mimics the human atherosclerotic plaque (agar 4% w/v, gypsum 10% w/v and butter 10% w/v) and can be used for HIFU therapy. In future clinical trials the transducer (1-3mm wide) will be incorporated in a catheter which will be inserted intravascular, and then transferred to the heart arteries where ultrasonic ablation will take place for a minimum amount of time. This technology can be used in the future for clinical trials to treat plaques in the coronary arteries.

Keywords: HIFU, Ultrasound, Atherosclerosis, Cardiac treatment, Therapeutic Ultrasound, Atherosclerotic plaque, MRI, Attenuation; Absorption; Conductivity; Phantoms.

Table of Contents

List of Tables

List of Figures

List of Abbreviations

HIFU: High Intensity Focused Ultrasound

MRI: Magnetic Resonance Imaging

MRgFUS: MR-guided Focused Ultrasound

VT: Ventricular Tachycardia

RFA: Radiofrequency Ablation

AF: Atrial Fibrillation

PVI: Pulmonary Vein Isolation

RFC:RadiofrequencyCatheter

AV: AtrioVentricular

LA: Left Atrial

HIFU-BC: HIFU Balloon Catheter

EPS: Electrophysiological Study

HA: Hydroxyapatite

LAD: Left Anterior Descending

PRF: Pulse Repetition Frequency

DF:DutyFactor

PAD: Peripheral Artery Disease

SWT: Shock Wave Therapy

TUS: Therapeutic Ultrasound

HA-PLA: Hydroxyapatite-Polyactide

DDFP: Dodecafluoropentane

PESDA: Perfluorocarbon-Exposed Sonicated Dextrose Albumin

rt-PA: Recombinant Tissue Plasminogen Activator

UCA: Ultrasound Contrast Agents

MBs: Microbubbles

AHA: American Heart Association

PIT: Pathological Intimal Thickening

TCFA: Thin Cap Fibroatheroma

VH-IVUS: Virtual Histology Intravascular Ultrasound

ThCFA: Thick-Capped Fibroatheroma

FC: Fibrocalcific

FA: Fibroatheroma

ICAD: Intracranial Atherosclerotic Disease

PAT: Photo Acoustic Tomography

OCT: Optical Coherence Tomography

CT: Computed Tomography

TPU: Thermoplastic Polyurethane

CPE+: Co-Polyester Extended

ABS: Acrylonitrile Butadiene Styrene

CR: Computed Radiography

FSE: Fast Spin Echo

TE: Echo Time

TR: Repetition Time

ETL: Echo Train Length

FOV: Field Of View

TMM: Tissue Mimicking Material

FUS: Focused Ultrasound

EPI: Echo-Planar Imaging

GRE: Gradient Echo

TTM: Transient Thermoelectric Method

1. Introduction

Ultrasound is a pressure wave at a frequency above the threshold of human hearing (20.000 Hz). It is produced by passing an electrical current through quartz or ceramic materials (such as barium titanate, lead zirconatetitanate) causing thermo resonate; this resonance is referred to as the piezoelectric effect [1].Ultrasound waves can be targeted to produce an elliptical focus. The potential for medical use exists because this focusing allows precise delivery of energy and its harmless passage through intervening structures. Most of the medically-relevant effects of ultrasound are associated with its thermal effects. Ultrasonic heat generation depends on the intensity (W/cm^2), duration of exposure, extent of focusing, and attenuation (dB/cm/MHz) of the treated tissue [1].

Diagnostic ultrasound examination is a widely practiced technique in the evaluation of patients with cardiovascular diseases. Conventional diagnostic ultrasound systems operate at high ultrasound frequency (5–12 MHz) delivering low-intensity ultrasound power. The bioeffects of ultrasound, however, can be exploited for therapeutic applications by appropriate changes in instrumentation and delivery approaches. Therapeutic ultrasound is being used today in a number of medical scenarios such as cataract, glaucoma [2], dental plaque removal [3], lithotripsy of renal stones [4], vasectomy [5], essential tremor [6], treatment of prostatic hyperplasia [7], prostate cancer [8-9] and testicular tumors [10]. A considerable body of experimental and clinical investigations point to the therapeutic potential of ultrasound in a variety of cardiovascular applications as well, such as thrombolysis [11], atherosclerotic plaque dissolution [12], local drug and targeted gene delivery [13] and angiogenesis [14].

High-intensity focused ultrasound (HIFU) is a therapeutic technique which uses a focused piezoelectric transducer to converge ultrasonic energy into a tissue target and produced localized destruction. The focal zone is the only position where the ultrasound energy is high enough to produce change in the tissue, and create a lesion. A typical ultrasound concave transducer beam, has surface intensity of 10 $W/cm^2$and 2000 W/cm^2 at the focal point [15]. HIFU beams can be precisely focused within a small focal volume, resulting in a rapid rise of the local tissue temperature. This temperature elevation causes localized tissue damage through coagulative necrosis [16-17]. With proper choice of operating frequency and transducer design, this can be achieved without significant biological damage to the intervening tissue [18-19]. The

advent of image guidance modalities such as magnetic resonance imaging (MRI) and ultrasound has allowed for completely non-invasive thermal therapy procedures [20-23].

Moreover, HIFU energy can pass through different types of tissue en route to the target. The main energy loss is due to attenuation, absorption and scattering within the tissue layers. Some other techniques such as radiofrequency ablation (RFA) and microwave energy have poor tissue penetration so these are invasive methods [24]. Ultrasound can be converted to thermal energy and when temperatures in excess of 50-60 ^{0}C are produced for minimum 1-10 s [25], this causes coagulative necrosis due to protein denaturation [26], cellular destruction and tissue stiffening [27]. HIFU is a non invasive extracorporeal technique capable of thermally ablating subsurface structures without injuring intervening tissues [28].A sharp boundary between the damaged tissue and the surrounding unaffected tissue has been demonstrated using light and electron microscopy [29]. Ultrasonic energy can be applied in a target volume to induce molecular agitation, absorptive heating and ultimately thermal coagulative tissue necrosis.

Ultrasound technology started in 1880 by Curie et al. [30], who found the piezoelectric effect. In 1917, P. Langevin discovered the effect of high intensity on biological tissues [31] and in 1932, H. Freundlich et al. [32], suggested the therapeutic use for ultrasound, the application of unfocused ultrasound to therapeutically heat tissue. After ten years, HIFU was designed as approach for destruction of human tissue by Lynn et al. [33] and in 1954 Fry et al. [34] introduced HIFU to disrupt tissue in the central nervous system. Since then, lesions have been created in murine and canine kidney and liver [35], rabbit brain and kidney [36-37], canine prostate, human prostate and testicles [9-10]. Moreover, this technology has been used to treat benign and malignant tumours of the bone, breast, and uterus and prostate for more than 10 years [38-42].Further studies have demonstrated the feasibility of HIFU application for ablating cardiac tissue in animal models [43-45].

HIFU can be used to cause localized hyperthermia at predictable depths without injuring intervening tissues [46].Damianou et al. [47] investigated in vitro and in vivo brain ablation created by HIFU and monitored by MRI. A single-element spherically focused transducer of 5 cm diameter, focusing at 10 cm and operating at 1 MHz was used. The transducer was tested in freshly excised lamb brain and in rabbit brain in vivo. The length of the lesions in vivo brain was much higher than the length in vitro, indicating that the penetration in the in vitro brain is

limited; possibly by reflection due to trapped bubbles in the blood vessels.The results have shown that HIFU has the potential to treat brain tumours in humans.

Couppis et al. [48] explored the feasibility of creating lesions in heart at a depth of at least 15 mm using HIFU with MRI guidance. The average lesion depth for the 14 in vivo experiments was almost 12 mm. The system was tested in an excised lamb heart. HIFU can create rapid tissue modification in small volumes (as small as 20 mm^3) without coming in touch with myocardium. The transducer was capable to create thermal lesions despite the motion of the heart. Lee et al. [49] investigated the ability of HIFU to create lesions in mammalian cardiac tissues ex vivo. Porcine valve leaflet, canine pericardium, human newborn atrial septum and right atrial appendage were studied. Specimens were mounted and immersed in a water bath at room temperature. Using a 1-MHz phased array transducer, ultrasound energy was applied with an acoustic intensity of 1630 W/cm^2 and 2547 W/cm^2 until a visible defect was created with a duration of 3 to 25 sec. Macroscopic and microscopic examination demonstrated precise defects ranging from 3 to 4 mm in diameter and no damage was identified to the surrounding tissues. It was concluded that HIFU can create precise defects in different cardiac tissue without damage to the surrounding tissue [49]. Moreover, other studies have documented the use of HIFU to enhance thrombolysis [50-57].

On the other hand, HIFU has some limitations, such as atrial-esophageal fistula, pulmonary embolism and phrenic nerve damage [58]. Okumura et al. [59] studied direct HIFU effects as the mechanism of phrenic nerve injury occurring within4-7 mm from balloon surface. Borchert et al. [60] investigated the thermal injury of oesophagus with development of atrioesophageal fistula after pulmonary vein isolation using HIFU. Furthermore, one limitation during HIFU cardiac ablation challenge is the beating heart. This affects the ablation size and accuracy to various extents. A β-blocker can be used to reduce the heartbeat and blood flow. This reduction provided efficient ultrasonic energy deposition within the target [61].

The combination of HIFU with MRI guidance known as MR-guided focused ultrasound (MRgFUS) appears to be promising to ablate tissues located deep in the brain. HIFU heats and non-invasively destroys the targeted tissue and MRI is used for visualization of anatomical structures and treatment control. The main advantage of the method is that does not require anaesthesia and offers an incision less treatment through the intact skull. Moreover, it provides immediately therapeutic effect and a quick return to normal activities [62].Many clinical trials

have shown the effectiveness of MRgFUS on neurological disorders such as essential tremor, Parkinson's disease and neuropathic pain [63-65].

2. Heart diseases and HIFU

2.1 Cardiovascular diseases

Cardiovascular diseases are diseases that are related with numerous problems on heart and blood vessels, many of which are related to a process called atherosclerosis. Atherosclerosis is a condition that develops when a substance called plaque builds up in the walls of the arteries. This buildup narrows the arteries, making it harder for blood to flow through. If a blood clot forms, it can stop the blood flow and this can cause a heart attack or stroke.HIFU has been demonstrated to produce a spectrum of vascular changes: vascular occlusion of non-bleeding arteries and veins [66-75], haemostasis of lacerated arteries and veins [76-79], thrombus generation [80], vascular spasm and reduction in blood flow and arterial rupture [81].

2.2 Coronary Heart Disease

Coronary heart disease is a disease in which a waxy substance called plaque builds up inside the coronary arteries. These arteries supply oxygen-rich blood to the heart muscle and this plaque can harden or rupture over time. Also, hardened plaque narrows the coronary arteries and reduces the flow of oxygen-rich blood to the heart. If the flow of oxygen-rich blood to the heart muscle is reduced or blocked, angina (chest pain or discomfort) or a heart attack can occur and without a quick treatment, this can lead to serious heart problems or death. Coronary heart disease continues to be a leading cause of morbidity and mortality among adults in Europe and North America [82]. Since today, a variety of interventions have been proposed to treat coronary artery disease. The most effective treatment is usually coronary artery bypass grafting where problematic lesions in the coronary arteries are bypassed using external grafts. Moreover, focused disease can often be treated intravascularly using a variety of catheter based approaches, such as balloon angioplasty, atherectomy [83], radiation treatment, stenting, and often combinations of these approaches [84].

2.3 Arrhythmias

Arrhythmia is an abnormal rhythm of the heart. There are various types of arrhythmias, such as bradycardia, tachycardia and atrial fibrillation. Bradycardia is when the heart rate is less

than 60 beats per minute, tachycardia is when the heart rate is more than 100 beats per minute and fibrillation is when the heart beats irregularly. An arrhythmia can affect how well the heart works and the heart may not be able to pump enough blood to meet the needs of the body. Most arrhythmias are not serious, but some of them can lead to stroke or cardiac arrest.

An important strategy for cardiac arrhythmia treatment [85] is the catheter ablation which is used to cut some electrical abnormalities in the myocardium. On the other hand, this procedure is related with certain complications and limitations [86-87]. HIFU has been considered an ideal tool to explore non-invasive, efficient, strategy for myocardial ablation.

Animal studies for arrhythmias

Wu et al. [88] achieved a complete atrioventricular block without thoracotomy, X-ray guidance and catheter intervention in a large animal model using HIFU in 21 canines. The right side of the central fibrous body was targeted by HIFU guided echocardiography and ablation was received by 10 canines, 8 canines received ablation and cardiac pacing for 2 h, and 3 canines received ablation and cardiac pacing for 3 months. No complications were observed during this study. Lu et al. [89] evaluated the feasibility of targeted ablation of cardiac tissues using HIFU for noninvasive ablation of ventricular tachycardia (VT) in anesthetized closed-chest dogs. The results have shown that HIFU is potentially useful for noninvasive ablation of targeted localized myocardial tissues, and it may be potentially applicable for VT ablation, particularly for those with intramyocardial and epicardial origins. On the other hand, during radiofrequency ablation (RFA) for treatment in patients with ventricular and atrial tachyarrhythmias, some important complications had raised, such as coronary artery injury which can be clinically devastating [90]. In general, important complications should be limited and lesion formation and safe arrhythmia treatments should be optimized when tissue is ablated in the vicinity of coronary arteries.

2.4 Atrial Fibrillation

As mentioned before there are different types of arrhythmias. The most common is atrial fibrillation (AF) which is connected with cardiovascular morbidity and mortality [91]. This is irregular beating of the atrial chambers - nearly always too fast (350 – 600 beats per minute) and instead of producing a single, strong contraction, the chamber fibrillates. AF mainly affects older patients rather than younger.

More than 7 million people all over the world are died every year from cardiac arrhythmia [92] and all types of AF have a high risk of stroke or heart failure [93]. AF surgical treatment started in 1987 using the Maze procedure but due to technical complexity and because of the required additional cardiopulmonary bypass time was not widely accepted[94].The catheter ablation is one of the most widely method that used for cardiac arrhythmia treatment but has some limitations and complications [95-96].The aim of the procedure is to delete some abnormalities of electrical conduction in the myocardium and different energy sources like microwave, radiofrequency, laser and cryotherapy were devised to simplify the procedure of creating pulmonary vein isolation (PVI)[97]. The main limitation that should be solved isthe creation of large thermal gradients due to energy propagation through the epicardial fat and the damage of adjacent structures such as oesophagus [98].

New non-pharmacological techniques and energy sources are being developed for AF treatment. PVI has become the cornerstone of catheter ablation for atrial fibrillation and is currently the first choice of therapy if patients fail ant arrhythmic drugs [99-103]. Moreover, radiofrequency catheter RFC-based PVI may be associated with serious complications such as PV stenosis, stroke, atrialesophagealfistula [104-105] and in order to improve outcome and reduce complications, techniques for creating more extensive linear lesions were used [106-107].In comparison with radiofrequency catheter (RFC) based pulmonary isolation procedures, HIFU balloon catheters show long term success [108].

Animal studies for atrial fibrillation

Zimmer et al. [109] performed HIFU guided ablations in beating canine hearts using catheter mounted HIFU transducers. Seven in vivo experiments in open-chest dogs were performed and the US transducers were mounted on the tip of angiographic catheters. Lesions on the epicardium and left ventricle were produced and it was concluded that may be useful for ablation of cardiac arrhythmias. Strickberger et al. [110] investigated if HIFU can be used to ablate the atrioventricular (AV) junction within the beating heart. Ten dogs were anesthetized and underwent a throracotomy. The maximum US intensity for ablation (2.8 kW/cm^2) was delivered to the AV junction only during electrical diastole and complete AV block was achieved in each of the 10 dogs within 30 s. It was concluded that HIFU can be used for ablation of cardiac arrhythmias. Nestor et al. [111] tried to achieve transmural tissue ablation using HIFU

energy system which may be necessary for successful treatment for atrial fibrillation. Nine heparinized bovines underwent a beating heart left atrial (LA) ablation with a single application of the HIFU device. The thickness of calf LA lesion (2.5–20.1 mm) was greater than human LA thickness (1.2–6 mm), and in this range HIFU ablation achieved 100%.

Clinical studies for atrial fibrillation

Nakagawa et al. [112] investigated the safety and efficacy of the HIFU balloon catheter (HIFU-BC) for PV isolation in patients with AF. Twenty- seven patients with paroxysmal (19 patients) or persistent (8 patients) AF were studied. It was showed that after a single HIFU ablation, 67% (after 6 months) and 56% (after 12 months) of patients were free of AF episodes or atrial tachycardia. The complications included transient bleeding from a distal branch of the left superior PV resulting from guide wire manipulation in one patient and right phrenic nerve injury in another patient but no PV stenosis (>50% narrowing) and no LA-esophageal fistula occurred.

Schmidt et al. [113] assessed the short-term and long-term success rates of PV isolation in patients with paroxysmal AF using HIFU balloon catheter. A total of 15 patients with a long history of drug-refractory, symptomatic paroxysmal AF were enrolled. The results have shown that patients with paroxysmal AF, acute PV isolation can be achieved in 89% using a steerable HIFU balloon; 58% of all patients were free of AF and 75% reached the primary end point defined as a reduction of AF episodes to less than 50%. However, further studies are needed to improve identification of patients at risk for phrenic nerve injury and any other complications. Pizon et al. [114] showed that HIFU ablation caused a significant improvement of atrial mechanical function for patients that suffered from AF. The study included 78 patients who underwent elective cardiac surgery. Forty - two patients underwent HIFU ablation (11.9% paroxysmal, 23.8% persistent, 64.3% longstanding persistent), 16 underwent cardiac surgery without ablation and 20 had preoperatively normal sinus rhythm control. Moreover, six months follow up have shown that HIFU ablation caused improvement of atrial filling fraction and A-wave velocity.

Another clinical study for treatment of atrial fibrillation with HIFU was performed by Garcia et al [115]. The aim was to assess endocardial atrial lesions 6 months after epicardial HIFU ablation and to evaluate the benefit of a combined ablation approach. Thirty patients undergone HIFU atrial fibrillation ablation during cardiac surgery and electrophysiological study

(EPS) was performed after 6 months. The results have shown that 60% of the patients were free of atrial arrhythmia symptoms improving to 81% at 12 months after a percutaneous endocardial approach was performed.

2.5 Diseases of Arteries

Atherosclerosis, is also called as hardening of the arteries, is a common condition in which fatty material collects along the walls of arteries [116]. The disease arises when plaque (cholesterol, fat, and calcium) accumulates inside the arteries, restricting blood flow. Eventually the arteries can become blocked and cause serious problems like a heart attack or stroke. The composition of the plaque includes a fibrous cap comprised of smooth muscle cells and fibrotic tissue, and lipid core containing fat-laden macrophages and extracellular lipids. The size of the plaque is increased in the advanced stage by large amounts of calcium salt or hydroxyapatite (HA) [117]. Calcium is a critical component of atherosclerotic plaque. The sequence of events in plaque development following injury is inflammation, followed by calcification of the damaged tissue, ending ultimately in the formation of a necrotic core [118-119].

Atherosclerosis treatment requires special surgical procedures such as balloon angioplasty [120-122], balloon angioplasty and stenting [123-124], cutting balloon [125-127], atherectomy [128-129] and surgical bypass [130-131], to open an artery and improve blood flow. The degree of luminal stenosis and patient's symptomatology, among other factors, determine the best treatment option for each patient [132]. The treatment of atherosclerotic plaques by HIFU was investigated by feasibility studies.

Animal studies for treating atherosclerotic plaques

Shehata et al. [133] investigated the feasibility and acute safety of targeting atherosclerotic plaques by HIFU in vivo through a noninvasive extracorporeal approach. Four swine were included in this prospective study, three of which were familial hypercholesterolemic swine. After US identification of atherosclerotic plaques within the femoral arteries, plaques were targeted by HIFU with an integrated dual-mode US array system. All swine tolerated the procedure well, with no arterial dissection, perforation, or rupture. The results demonstrated the feasibility and acute safety of targeting atherosclerotic plaques by HIFU in vivo. One important

limitation of targeting atherosclerotic plaques by HIFU is that the artery temperature should not exceed a safe level during the ultrasound ablation for destroying atherosclerotic plaque. Moreover, the safety of HIFU applications delivered directly over the left anterior descending (LAD) artery in an open-chest swine model was evaluated by Koruth et al. [134]. Ten swine underwent median sternotomy and 43 therapies along the LAD were analyzed. It was found that HIFU has the potential to create deep ventricular lesion with relative sparing of the LAD. The incremental arterial damage noted over time warrants further evaluation.

Carotid artery disease affects the two large arteries in the neck that supply blood to the brain. This condition increases the risk for stroke, and it causes more than half of stroke cases. Carotid artery disease is often linked to atherosclerosis. The main treatment for carotid artery is endarterectomy [135-137]. On the other hand, ablation treatments can be used for removing atherosclerotic plaque. Damianou et al. [12] used pulsed ultrasound to remove atherosclerotic plaque in an in vivo model. The plaque in 17 New Zealand rabbits was created using high cholesterol diet for 4 months and the amount of plaque removed was studied in terms of intensity, with a fixed pulse repetition frequency (PRF), and duty factor (DF). The results have shown that the amount of plaque removed is directly related to the acoustic intensity. It was found also that the presence of bubbles accelerates the removal of plaque. No temperature elevation above 1 ^{0}C was produced and the atherosclerotic plaque removes up to a depth of 2 mm in 25 min in the carotid of rabbits. The results were very promising with the limitation that the dissolved material in humans should be collected, preventing blockage of other arteries thus creating stroke.

Peripheral arterial disease (PAD) is often associated with atherosclerosis and becomes much more likely as the person get older. In peripheral arterial disease, the arteries further from the heart, usually in the pelvis and legs, become narrowed because of plaque buildup. Decreased blood flow to the muscles may cause pain and fatigue in the legs. Shock wave therapy (SWT) and therapeutic ultrasound (TUS) were compared in a rat hind limb ischemia model by Nazer et al. [138] for their ability to promote angiogenesis and reperfusion. Direct comparison between them demonstrates that TUS is more effective than SWT at promoting reperfusion, whereas both therapies promote angiogenesis in ischemic gastrocnemius muscle. The results suggested that TUS should be more effective than SWT for the treatment of ischemic heart disease and peripheral arterial disease.

The efficacy of intravascular sonotherapy treatment on in-stent restenosis in a swine model was assessed by Fitzgerald et al. [139]. After balloon injury, billiary stents were implanted in the femoral arteries of 14 swine. An 8-French catheter intravascular sonotherapy system (URX, PharmaSonics Inc.) was used for sonotherapy or sham treatment. At 28 days, percent stenosis was significantly less in the sonotherapy group than in the sham group (36% versus 44%) and was concluded that intravascular sonotherapy may be an effective form of nonionizing energy to reduce in-stent restenosis.

In vitro studies

A simulation study of the thermal and mechanical effects of flat rectangular (3x10 mm^2), MRI compatible transducer operating at 5.0 MHz, for destroying atherosclerotic plaque was done by Damianou et al. [140]. This study focused on measuring the plaque destruction as a function of power, time, frequency, DF and pulse duration. The main goal was to keep the temperature in the artery at a safe level. The results have shown that with the thermal mode the temperature in the artery cannot be kept at a safe level while in mechanical mode ultrasound created no severe temperature elevation in the arteries. Finally, it was concluded that the size of plaque removal depended on power, time, frequency, and duty factor and pulse duration.

Damianou et al. [141] investigated the effectiveness of a therapeutic protocol in removing calcified material using pulsed ultrasound with a planar unfocused transducer operating at 5.3 MHz. The effect of various parameters such as intensity, PRF, DF, and the presence of bubbles were explored. Moreover, cylindrical chalks and hydroxyapatite-polyactide (HA-PLA) composites were used during in vitro experiments. The results have shown that the removed calcified material as expected increases with the intensity, PRF, DF and the presence of bubbles. With this transducer and protocol HA-PLA material up to a depth of 3 mm in just 30 min was removed. This technology looks promising provided that the dissolves material from the plaque is collected, so that it does not flow from the blood stream to other arteries, thus causing the blockage of arteries. Suction mechanism can be used to collect the removed particles [142-143].

Siegel et al. [144] assessed catheter-delivered ultrasound for arterial recanalization as well as for assessment of the size of particulate debris from 11 postmortem atherosclerotically occluded coronary arteries. All 11 postmortem coronary occlusions were recanalized, and 99% of the particulates generated were smaller than 10 microns in diameter. It was found that after

ultrasound, mean coronary arterial stenosis fell from 80% to 60% and no ultrasound-related complications were identified.

In vivo studies

Almekkaway et al. [145] simulated the effect of HIFU in non-homogenous medium for targeting atherosclerotic plaques in vivo. A finite-difference time-domain heterogeneous model for acoustic and thermal tissue response in the treatment region was derived from ultrasound images of the treatment region. A 3.5 MHz dual mode ultrasound array suitable for targeting peripheral vessels was used and two cases were simulated where seven adjacent HIFU shots (~5000 W/cm^2, 2s exposure time) were targeted on the plaque tissue within the femoral artery. The transient bioheat equation with a convective term to account for blood flow was used to predict the thermal dose. The results have suggested that a realistic, image-based acoustic and thermal model of the treatment region is capable of predicting the extent of thermal damage to target plaque tissue. The model considered the effect of the wall thickness of large arteries and the heat-sink effect of flowing blood. The model is used for predicting the size and pattern of HIFU damage in vivo.

Clinical studies

Ultrasound ablation was used to treat peripheral arterial obstructive disease by Monteverde-Grether et al [146]. Angiosonoplasty, with a prototype ultrasonic system was undergone in 32 patients (mean age 67). The procedure was successful in 26 patients and angiography before and after angiosonoplasty confirmed that the lesions were successfully opened. Reocclusion occurred in 4 patients immediately after the procedure and vascular spasm in 2 patients. The ultrasound ablation of atherosclerotic plaque appeared safe and has shown no restenosis and a low incidence of complication over a six month period.

The treatment of carotid atherosclerotic plaques with external ultrasound was evaluated from Zhang et al [147]. In this study, 357 patients with 363 carotid atherosclerotic plaques were divided into an ultrasound treatment group and a control group. After treatment, the maximum thickness and area of 79.94 % of the plaques in the ultrasound group were reduced, while in the control group, the thickness and area of 18.52 % were reduced. Siegel et al [148] described the use of percutaneous therapeutic ultrasound for coronary angioplasty. The treatment of

obstructive coronary atherosclerosis with a prototype 4.6F coronary catheter ultrasound ablation device with a 1.7 mm diameter ball tip was performed in 19 patients. The ultrasound coronary catheter delivered energy at 19.5 kHz, with a power output of 16 to 20 W, in a pulsed mode with a 50% duty cycle of 30 ms. Patients were treated for a mean of 493 s with intracoronary ultrasound ablation and all lesions were treated with adjunctive balloon angioplasty.

In another clinical study, the safety and feasibility of intracoronary sonotherapy (IST) and its effect on the coronary vessel at 6 months was studied by Regar et al [149]. After successful angioplasty on 37 patients, IST was performed using a 5F catheter with three serial ultrasound transducers operating at 1 MHz. The results have shown that IST performed successfully in 90% of the lesions.

2.6 Stroke and thrombosis

Stroke is one of the most frequent causes of mortality, morbidity and disability of population in developed countries [150-151]. A stroke occur when the blood supply to part of the brain is interrupted or reduced, preventing brain cells and tissue of oxygen and nutrients. After minutes, brain cells died. A stroke may be caused by a blocked artery (ischemic stroke) or the leaking or bursting of a blood vessel (hemorrhagic stroke). About 87% of strokes are ischemic strokes and the remaining roughly 13% hemorrhagic [152]. Ischemic stroke occurs when the arteries to the brain become narrowed or blocked, causing severely reduced blood flow. A blood clot (thrombus) forms in one of the arteries that supply blood to your brain. A clot may be caused by plaque that builds up in arteries and cause reduced blood flow or other artery conditions. Either thrombolytic therapy [153] or sonothrombolysis [154] can be used for the treatment of stroke.

In 1968, micro bubbles were introduced as an ultrasound contrast agent [155] and nowadays are widely accepted as a clinical agent in diagnostic ultrasound. However, during in vitro and in vivo studies, has revealed that the presence of ultrasound with microbubbles except of diagnostic has also therapeutic possibilities and increased clot lysis [156].

Animal studies for stroke

Siegel et al. [157] evaluated the efficacy of peripheral and coronary thrombolysis in vivo in animals by using noninvasive transcutaneous ultrasound combined with thrombolytic drugs and/or micro bubbles agents such as dodecafluoropentane (DDFP) and perfluorocarbon-exposed sonicated dextrose albumin (PESDA). Thrombotic occlusions were induced in 74 rabbit iliofemoral arteries and 24 canine left anterior descending (LAD) coronary arteries in this in vivo study. The results have shown that noninvasive transcutaneous ultrasound can greatly enhance the effect of clot dissolution with thrombolytic drugs and/or micro bubbles.

Damianou et al. [158] evaluated the potential of MRgFUS combined with recombinant tissue plasminogen activator (rt-PA) to dissolve clots in the carotid of a New Zealand rabbit in vivo. It was found that the time needed for opening the carotid artery using MRgFUS and rt-PA was decreased compared with just using rt-PA. The time needed to completely open the artery was 70 minutes.

In vitro and in vivo studies

Tachibana et al. [159] proved that the addition of micro bubbles during ultrasound (US) application could enhance clot lysis even further. Artificial thrombus was produced by Chandler's loop method with blood extracted from a healthy object and fibrinolysis was determined by the percentage of weight loss of thrombus. The results have shown that fibrinolysis with urokinase (UK) alone was 26.6%, with UK and US treatment was 33.3% and fibrinolysis with the presence of UK, US and albumin micro bubbles used for echo-contrast material (Albunex) was 51.3%. Porter et al. [160] hypothesized that PESDA micro bubble, which are more stable than air filled microbubbles, may also enhance US-induced thrombolysis. The percentage clot lysis of equally sized thrombi, made from freshly drawn blood incubated for 2 hours and then exposed to 20 kHz, was measured. The thrombi were bathed in 4ml of saline solution, urokinase (UK) alone, PESDA alone and a combination of them. The results have shown that PESDA microbubbles alone may be capable of inducing thrombolysis when insonified with a low frequency transducer. Nishioka et al. [161] examined the effectiveness of dodecafluoropentane (DDFP) emulsion, to enhance low frequency ultrasound clot disruption in vitro and in vivo. For in vitro studies, the disruption rate of fresh human clots by ultrasound (24 kHz, 2.9 W/cm^2) was examined in saline and DDFP emulsion, and for in vivo studies, a rabbit

iliofemoral thrombotic occlusion model was used. The results have shown that DDFP emulsion significantly enhances the clot-disrupting effect of low frequency ultrasound.

Thrombolytic therapy can also be achieved by using rt-PA. Many studies have shown that HIFU can be used to enhance rt-PA thrombolysis. Kondo et al. [162] evaluated the effect of a galactose based ultrasound contrast agents (UCA) on the efficacy of ultrasonic enhancement of rt-PA thrombolysis and observed the serial changes in the acoustic property and histopathology. The rt-PA thrombolysis was studied in 30 artificial white thrombi and the results have shown that UCA enhanced the effect of ultrasound on rt-PA thrombolysis. Holland et al. [163] explored various US settings to determine the thrombolytic efficacy of US therapy with and without rt-PA administration. They assessed in vitro, a porcine clot model and demonstrated that treatment with US and rt-PA can significantly increase clot dissolution by as much as 104% compared to rt-PA alone and the clot mass loss enhancement increased with square root of the treatment duration.

Spengos et al. [164] examined the effects of US on rt-PA mediated thrombolysis in a flow model in vitro. Fibrin clots were placed in a continuous pressure flow model and treated with rt-PA during 1 MHz US exposure. The results have shown that recanalization rate during 30 min was 90-100% in the US-exposed clots in comparison with 30% in the clots treated only with rt-PA. The shortening of recanalization rate could help to optimizing the effects of acute thrombolytic stroke therapy.

On the other hand, some studies focused on the macrovascular system and applied different ultrasound frequencies and acoustic pressures [162-168]. Papadopoulos et al. [169] evaluated the performance of a flat rectangular (2x10 mm^2) transducer operating at 4.0 MHz for intravascular treatment of thrombosis and atherosclerosis. This in vitro study was tested in two different gel phantoms and MR thermometry was used to demonstrate the thermal capabilities of this type of transducer. The results have shown that the destruction of thrombi using pulsed ultrasound requires long exposure time and high microbubble dosage. Damianou et al. [170] evaluated the potential of an MRgFUS system combined with thrombolytic drugs to dissolve clots using in vitro and in vivo models. It was found that the volume of dissolved clot increases with acoustic intensity and beam size and decreases with frequency. Moreover, the thrombus in the in vivo model (ear artery) was destroyed with the therapeutic protocols investigated in the in vitro models. Schaefer et al. [171] investigated physical factors that influenced ultrasound thrombolysis. The results have shown that ultrasound in the 2.0-4.5 MHz frequency range ablates

fresh thrombus at a distance without the use of adjuvant thrombolytic or contrast agents. The thrombolytic efficacy depended directly on mode of operation, duration and inversely on the frequency of insolation.

Clinical studies

A clinical study was performed by Doomernik et al. [109] where a systematic literature search was performed using MEDLINE, EMBASE and Cochrane databases. A total of 77 reports related with focusing on catheter – delivered ultrasound – accelerated thrombolysis were identified. Experimental studies have shown that HIFU may induce thrombolysis, with and without the addition of plasminogen activators. In 340 clinical cases of thromboembolic condition, sonothrombolysis was compared to standard thrombolysis. The results have shown that sonothrombolysis in comparison with standard thrombolysis was related to rapid revascularization and a reduction in treatment time, drug dosage, hospitalization time and bleeding complications.

Another clinical study was evaluated by Molina et al. [172]. It was founded that administration of microbubbles (MBs) induces further acceleration of ultrasound-enhanced thrombolysis in acute stroke, leading to a more complete recanalization outcome. An evaluation of 111 patients with acute stroke attributable to middle cerebral artery occlusion treated with rt-PA was done. Thirty – eight patients were treated with rt-PA and MBs and were compared with 73 patients who were allocated to receive only rt-PA. Finally, Alexandrov et al. [173] assigned 126 stroke patients to receive continuous ultrasound or placebo following treatment with rt-PA within three hours after the onset of symptoms. Their results have shown a significant increase of complete recanalisation in the ultrasound group compared with placebo.

2.7 Valvular Heart Disease

Valvular heart disease is characterized by damage to or a defect in one of the four heart valves: the mitral, aortic, tricuspid or pulmonary. The mitral and tricuspid valves control the flow of blood between the atria and the ventricles (the upper and lower chambers of the heart). The pulmonary valve controls the flow of blood from the heart to the lungs, and the aortic valve governs blood flow between the heart and the aorta, and thereby the blood vessels to the

rest of the body. The mitral and aortic valves are the ones most frequently affected by valvular heart disease. Normally functioning valves ensure that blood flows with proper force in the proper direction at the proper time. In valvular heart disease, the valves become too narrow and hardened (atherosclerosis) to open fully, or are unable to close completely. The severity of valvular heart disease varies. In mild cases there may be no symptoms, while in advanced cases, valvular heart disease may lead to congestive heart failure and other complications. HIFU has the potential to reduce the severity of the cardiac valve stenosis by disrupting adhesions.

HIFU can create superficial thermal lesions and perforation in mitral valve and aortic valve tissues. Otsuka et al. [174] examined 15 calf mitral and 15 aortic valves and found that HIFU ablation could be performed on all valves. The creation of perforated lesions in the cardiac valves was very consistent and reproducible. Focused US energy was applied with an operating frequency of 4.67 MHz at a nominal acoustic power of 58 W for 0.2s, 0.3s and 0.4 s at 4-s intervals and the mean diameter of the perforated area was 1.09 ± 0.11 mm. In contrast with RF ablation [175], HIFU energy is focused and precise lesions can be created. Picardo et al. [176] investigated the feasibility of using HIFU for inducing partial shrinkage of the saphenous vein wall. The position and size of valvular deformations are well suited to being heated and consequently reduced with HIFU and the resulting shrinkage of deformations should restore normal function of the valve. An experimental protocol was used in which in vitro segments of human saphenous vein were exposed with a monochromatic signal produced by a real-time HIFU probe. Results showed that HIFU is suitable for partial shrinkage of the saphenous vein and suggest that correction of dysfunctional of valvular tissue is feasible.

The ex vivo effectiveness of a portable HIFU for transcutaneous venous ablation was determined by Henderson et al [177]. An ex vivo testing platform consisting of two different models comprised of sequentially layered skin-muscle-vein or skin-fat-vein was developed, and specimen were treated with HIFU. It was found that this portable device has the potential to allow clinicians to easily perform venous ablation in a manner that is entirely noninvasive and without the expense or inconvenience of large, complicated devices. HIFU was hypothesized by Abe et al. [178] that might be useful as a noninvasive extracorporeal technique for cutting mitral chordate. They examined the in vitro feasibility of using HIFU to cut calf mitral chordate with diameters from 0.2-1.6 mm. The results showed that mitral chordate cutting by HIFU depended on the diameter of chordate but was controllable by HIFU settings.

3. Different types of atherosclerotic plaque

3.1 Introduction

Coronary heart disease is a leading cause of death in the Western world [179]. The majority of this disease is related with atherosclerosis where the development of thrombosis can cause acute myocardial infarction and sudden death [180]. The process of atherosclerotic plaque progression is considered to be dynamic and complicated. An understanding of the histromorphological characteristics of coronary plaques is of particular importance for both basic and clinical researchers who investigate the pathogenesis of atherosclerotic coronary disease [181].

Atherosclerotic plaque lesions can be classified into 7 categories [182]. These categories include intimal xanthoma, intimal thickening, pathological intimal thickening, fibrous cap atheroma, thin fibrous cap atheroma, calcified nodule and fibrocalcific plaque. The definition of these categories is based on the accretion of lipid in relationship to formation of the fibrous cap, changes over time in the lipid to form a necrotic core, thickening or thinning of the fibrous cap and thrombosis.

3.2 Different types of atherosclerotic plaque

3.2.1 Intimal Xanthoma

“Xanthoma’’ is a general pathological term that describes focal accumulations of fat-laden macrophages. The presence of an intimal xanthoma is not a fact for categorizing lesions in current animal models as atherosclerotic. This is based on the fact that the composition of lesions

in animal models is very different from that in the adult human population and the potential for these lesions to regress. They usually do not develop into progressive atherosclerotic lesions and contain macrophage, T lymphocytes and varying degrees of smooth muscle cells [182].

3.2.2 Intimal Thickening

Most adult human lesions originate as preexisting intimal masses according to American heart association (AHA) classification scheme [183-185]. Intimal thickening consists mainly of smooth muscle cells in a proteoglycan – rich matrix.

3.2.3 Fibrous Cap Atheromata

A fibrous cap is a distinct layer of connective tissue completely covering the lipid core. The fibrous cap consists of smooth muscle cells in a collagenous-proteoglycan matrix, with varying degrees of infiltration by macrophages and lymphocytes. Moreover, fibrous cap atheroma can have thin or thick cap overlying a lipid-rich core [182]. Lesions with thin, fibrous caps are those that are most likely to rupture. A thin fibrous cap is smaller than 65 μm thick [186]. The thin fibrous cap is separated from the earlier fibrous cap lesions by the loss of smooth muscle cells, extracellular matrix and inflammatory infiltrate. Moreover, the necrotic core underlying the thin, fibrous cap is large and calcification is usually present [187-188].

3.2.4 Thrombosis and Atherosclerotic Plaque Lesions

Three processes are responsible for lesions with thrombi: rupture, erosion and calcified nodule [184]. The two types related with those thrombi are fibrous cap atheroma and pathological intimal thickening. Sometimes, a lesion can contain both rupture and erosion evidence. Ruptured lesions typically have a large necrotic core, a disrupted fibrous cap infiltrated by macrophages and lymphocytes. Plaque ruptures are found in 60% of individuals dying suddenly with luminal thrombi and are the most frequent cause of death in young men (<50 years) and older women (>50 years) [185]. In women > 50 years old, ruptured plaques consist of the main part of atherosclerotic lesions related with acute thrombi, and similar to men, there is an association with increased total cholesterol levels [188].

For plaque erosion, the endothelium is absent at the erosion part of the plaque. The erosion region consists mainly of smooth muscle and proteoglycans and the corroded site contains minimal inflammation [189-190]. Erosion is about 40% of cases of thrombotic sudden coronary death. A lesion with an infrequent cause of thrombotic occlusion without rupture is referred to a calcified nodule. This type of lesion is mainly related with fibrous cap disruption and thrombi associated with dense calcified nodules. Thin fibrous cap with calcified nodules are not related with fibrocalcific lesions that are not associated with thrombi. Plaques with thick fibrous caps, small lipid-laden necrotic core and overlying extensive accumulations of calcium in the intima close to the media are referred as fibrocalcific lesions [191].

Major types of progressive atherosclerotic lesions can be separated into 5 different types. Pathologic intimal thickening (PIT) composites of smooth muscle cell in a proteoglycan-rich matrix with areas of extracellular lipid accumulation without necrosis. Thrombus is most often mural and infrequently occlusive. Fibrous cap atheroma is composed of well-formed necrotic core with overlying fibrous cap. Thrombus is most often mural and infrequently occlusive. Thin

cap fibroatheroma (TCFA) is a thin fibrous cap infiltrated with macrophages and lymphocytes, rare smooth muscle cells and an underlying necrotic core. TCFA with rupture creates thrombus that usually is occlusive [192]. Fibrocalcific plaque contains collagen-rich plaque usually with significant stenosis; contains large areas of calcification with few inflammatory cells and necrotic core may be present.

At the beginning, both high-risk and low-risk groups develop fatty streaks, but after the start of development, fibrous plaques become dominant and progressively expand to cover about 20% to 46% of the coronary arterial surface. For males, a comparison between the high and low risk groups, fatty streaks were noted at about the same ages (11 to 12 years) and similar growth rates about 0.3% of surface per year were reported. On the other hand, in the high-risk group compared with the low-risk group, fibrous plaques tended to start at a younger age (17 to 23 years) and to grow more rapidly (0.8% and 0.5% of surface per year) respectively [193].

Four major classes of plaques are associated with the acute coronary syndromes and sudden cardiac death. Three classes of plaque are known to cause terminal events due to thrombosis. The first is due to rupture of TCFA, 50% - 60%; thrombosis due to erosion of the endothelium (PIT), 20 %; and thrombosis due to protrusion of a calcified nodule into the arterial lumen, 2 %. The last class, fibrocalcific plaques, there is an advanced stenosis in the absence of thrombosis, with a prevalence of 20% to 30%. This stenosis can lead to myocardial ischemia and fatal arrhythmia [194]. Multiple cycles of subclinical plaque rupture or erosion, followed by thrombosis and healing, occur in 60% of sudden cardiac deaths before the fatal event.

When an atherosclerotic plaque is treated the usual goal of treatment is to make it disappear or regress [195]. The risks of clinical manifestations of atherosclerosis can be reduced by 20% to 40% with statin treatment. Clinical trials of statins have shown reduction in atherosclerotic cardiovascular morbility and mortality, including angina pectoris, nonfatal and

fatal myocardial infarction, uses of coronary bypass surgery and coronary artery angioplasty and stenting, transient ischemic attacks, stroke and total mortality [196 – 199].

3.3 Virtual histology intravascular ultrasound (VH – IVUS)

Although fibroatheromata can be identified at postmortem, identifying high-risk plaque subtypes before a fatal event such as myocardial infarction remains a major challenge [200]. VH–IVUS is based upon spectral analysis of ultrasound backscatter, with different plaque components exhibiting a defined spectrum [201]. The radiofrequency signal is mathematically transformed into a color-coded representation, separating different components of atherosclerotic plaque such as lipid, fibrous tissue, calcification, and necrotic core [202]. VH-IVUS spectral analysis correlates well with histopathology in a predictive accuracy 87.1%, 87.1%, 88.3% and 96.5% for fibrous, fibro fatty, necrotic core and dense calcium respectively [203-204]. VH-IVUS can also identify TCFA and other plaque subtypes [205], follow plaque composition after treatment [206].

The following plaque classifications are used, consistent with subsequently published VH-IVUS classifications [182]:

1) Plaque: Plaque burden of > 40% vessel cross-sectional area for 3 consecutive frames.
2) Fibroatheroma (FA): Plaque burden > 40 %, confluent necrotic core > 10% plaque cross-sectional area.
3) Thin-capped fibroatheroma (TCFA): fibroatheroma in contact with vessel lumen for 3 consecutive frames. TCFA were subdivided into calcified TCFA (dense calcium > 10% plaque cross-sectional area in 3 consecutive frames) and noncalcified TCFA.
4) Thick-capped fibroatheroma (ThCFA): fibroatheroma not fulfilling ThCFA conditions. ThCFA were subdivided into calcified ThCFA (dense calcium > 10% plaque cross-sectional area in 3 consecutive frames) and noncalcified ThCFA.
5) Fibrocalcific plaque (FC): plaque with dense calcium > 10% plaque cross-sectional area in 3 consecutive frames, not meeting fibroatheroma definition.
6) Pathological intimal thickening (PIT): plaque not meeting plaque definitions and predominantly fibrous tissue.

4. US thermal ablation of atherosclerotic plaque phantoms

4.1 Introduction

In this chapter, the effect of therapeutic ultrasound for destruction of atherosclerotic plaque phantoms was investigated. Using an in vitro model, different atherosclerotic plaque phantoms were treated using different acoustic parameters such as acoustic power and treatment time. The goal of this study was to create the optimum treatment process that maximizes the destruction of atherosclerotic plaque in minimum time duration. In order to succeed this, the influence of acoustic parameters such as acoustic power and treatment time was investigated.

Many studies for atherosclerotic plaque phantoms have been made during the last seven years. These studies are summarized in table 4.1. A suitable lesion composition phantom was developed for evaluating the application of computed tomography for differentiation of *in vitro* lipid-rich vs fibrotic plaque samples by Kasraie et al [215]. An atherosclerotic plaque phantom also was prepared using a biological tissue model, bovine fat, and saline or heparinised porcine blood for observation by Near – Infrared Hyper spectral Imaging by Ishii et al [216].

Different plaque phantoms composed of a stenotic vessel wall and plaque components, including fibrous cap and a lipid core, were successfully constructed for a multi-center High Resolution magnetic resonance imaging (MRI) standardization in two different studies by Chueh et al [217, 219]. Another plaque phantom by Chueh et al. composed of a stenotic vessel wall, a fibrous cap and a lipid core was successfully constructed for diagnosis of intracranial atherosclerotic disease (ICAD) [218].

A 3D-printed coronary plaque model was successfully designed for quantifying coronary computed tomography angiography image quality and stenosis measurement accuracy by Richards et al [213].A lipid plaque phantom was created by Wu et al. [208] for a rapid identification of thin-cap lipid-rich atherosclerotic plaque in coronary arteries with two-wavelength intravascular photo acoustics. A model with lipid-rich plaque phantoms was used to accurately predict the presence of chemicals and molecules, including lipid, collagen and calcium using spectroscopy optical coherence tomography [24].

Shang et al. [220] proposed a method for detecting vascular plaques in the vessel. They created different plaque phantoms (lipid-rich cap, thick fibrous cap, thin fibrous cap and rabbit vascular plaques) for detecting arterial atherosclerosis using a dual-mode photo acoustic

tomography (PAT) and optical coherence tomography (OCT). Nam et al. [214] used lipid phantom models and *in vivo* atherosclerotic rabbit models for characterization of lipid-rich plaque in intravascular OCT images based on spectroscopic absorption properties of lipids.

A calcified plaque phantom was created by Gholampour et al. [207] for investigating the thermal damage to vascular nerves while drilling calcified plaque. The results have shown that drilling time is one of the most important factors in increasing temperature. Four plaque phantoms were prepared by Cormode et al. [226] for analyzing atherosclerotic plaque composition using multicolor computed tomography (CT) and targeted gold nanoparticles.

Six vascular phantoms with six types of calcified plaque were made by Jin et al. [214] for evaluating the accuracy of lumen area measurement in calcified plaque by subtraction of dual energy CT. Phantom models were made by Callum et al. [210] for three-dimensional (3-D) imaging of biological tissue across millimetre-scale regions for system characterization and clinical training. Cao et al. [221] created a lipid-mimicked phantom and a collinear catheter for high-sensitivity intravascular photo acoustic imaging of lipid laden plaque.

A carotid artery plaque phantom fabricated from sheep and pig intestines was created by Kumagai et al. [211] for identifying the lipid areas on the artery by ultrasound velocity change imaging method. Jansen et al. [212] investigated atherosclerotic lipids in a vessel phantom for assessing the lipid detection and distinction capabilities of spectroscopic intravascular photo acoustic imaging in two absorption bands.

A tissue mimicking phantom made of porcine fat and gelatine was created by Choi et al. [222] for establishing the feasibility of the intravascular photo thermal strain imaging system and overcoming the limitations of conventional intravascular imaging methods that struggle to image the plaque lipid. Guo et al. [223] assessed the impact of artificial plaque composition on drug transport by using gelatine hydrogels with varying gelatine and lipid concentrations. Kingstone et al. [224] created phantoms that simulated various types of atherosclerotic plaque pathology using 2D and 3D ultrasound for measuring the differences for specific plaque imaging analyses. Atherosclerotic plaque phantoms [37] were used for evaluating the lipid volume fraction in plaques using near-infrared multispectral imaging at wavelengths 1200nm.

As seen in table 4.1, many studies have been performed for assessing atherosclerotic plaque phantoms for medical imaging but only one [207] was for assessing plaque phantoms for medical treatment. Some of the studies specified only mimicking lipid plaques[208-212],

calcified plaques[207, 213–214], lipid and fibrous cap/tissue plaques[215–225]; lipid and calcified plaque[226] and only one study[227]mimicked the main three components (fibrous tissue, lipid core and calcium). This study also mimicked all three main components. To our knowledge, no previous study was performed for evaluating atherosclerotic plaque phantoms *in vitro* for ultrasound therapy.

Table 4.1: Studies for atherosclerotic plaque phantoms and the ingredients for mimicking the main components of atherosclerotic plaque

Author	Fibrous cap – Fibrous/soft tissue	Lipidcore	Calcium
Gholampouretal. 2019 [207]	-	-	Cubebone of bovine
Wu etal. 2015 [208]	-	a) Human peri-adventitial fat b) Pure cholesterol, cholesterol oleate and cholesterol linoleate samples	-
Nametal. 2016 [209]	-	Mayonnaise (Soybeanoil 80 %)	-
Littleetal. 2019 [210]	-	Coconutoil	-
Kumagaietal. 2018 [211]	-	Fat	-
Jansenetal. 2013 [212]	-	Cholesterol, cholesterol oleate, cholesterol linoleate	-
Richardsetal. 2018 [213]	-	-	Dentalresinmixture
Jinetal. 2017 [214]	Agar	-	Calciumhydroxypatitepowder
Kasraieetal. 2014 [215]	Elastin, Type I Collagen	25 % Free cholesterol, 19 % Cholesteryl oleate, 20 % Triglycerid	-
Ishiietal. 2014 [216]	Hemoglobin, Gelatin, intralipid, saline or blood	Bovinefat	-
Chuehetal. 2016 [217]	Agarose, carrageenan, sodium azide, water	Vegetable fat, sodium azide and carrageenan mixture	-
Chuehetal. 2015 [218]	Gadolinium chloride, agarose, carrageenan, sodium azide, water, sodium chloride	Milk, sodium azide, carrageenan mixture	-
Chuehetal. 2018 [219]	Gadolinium chloride, agarose, carrageenan, sodium azide, water, sodium chloride	Milk, sodium azide, carrageenan mixture	-
Shangetal. 2017 [220]	Collagen, agar and gelatin	Fat, cholesterol, phospholipid and triglyceride	-
Caoetal. 2016 [221]	Agar gel (Agar powder and D_2O)	Butter fat, a portion of porcine intramuscular fat	-
Choietal. 2018 [222]	Gelatin	a) Cornstarch, b) Porcine fat	-
Guoetal. 2014 [223]	Gelatin, glutaraldehyde	Lipidmixtures	-
Kingstoneetal. 2014 [224]	Modelingcompound, compoundputty	Wholecornkernels, olives	Mustardseeds
Nagaoetal. 2015 [225]	Hemoglobin, gelatin, intralipid	Bovinefat	-
Commodeetal. 2010 [226]	-	Lipids, Meat (raw ground beef)	Calciumphosphate
Flemingetal. 2013 [227]	Collagen	Cholesterol, glycerol trioleate, mayonnaise, melted butter and vegetable oil	Calcium

4.2 Arterial Mimic Tube

The arterial atherosclerotic plaque phantom created in the laboratory was of low cost. Different types of atherosclerotic plaques were mimicked with different percentages. The arterial mimic tube base was made by thermoplastic polyurethane (TPU) and the other components from co-polyester extended (CPE+) material for mimicking the elastic properties of the artery. Agar was used for mimicking fibrous tissue, gypsum for calcium and butter for lipid core.

The arterial mimic tube base was made by TPU and the other components from CPE+ material for mimicking the elastic properties of the artery. Both parts printed using a 3D printer (ULTIMAKER3 extended, Ultimaker B.V, Zaltbommel, Netherlands). Fig. 4.1A shows the cross – sectional area of the arterial mimic tube with atherosclerotic plaque. The diameter of the tube is 13.50 mm. The mean available lumen range of the artery is between 5.52 mm and 6.49 mm and the mean atherosclerotic plaque thickness is between 3.01 mm and 3.98 mm. Fig. 4.1B shows the arterial mimic tube (black) with the cap (white) and a smaller tube (yellow) for creating the lumen of the artery. The length of the arterial mimic tube is 106.50 mm. The thickness of the cap is 3.00 mm and the length of the smaller tube 27 mm.

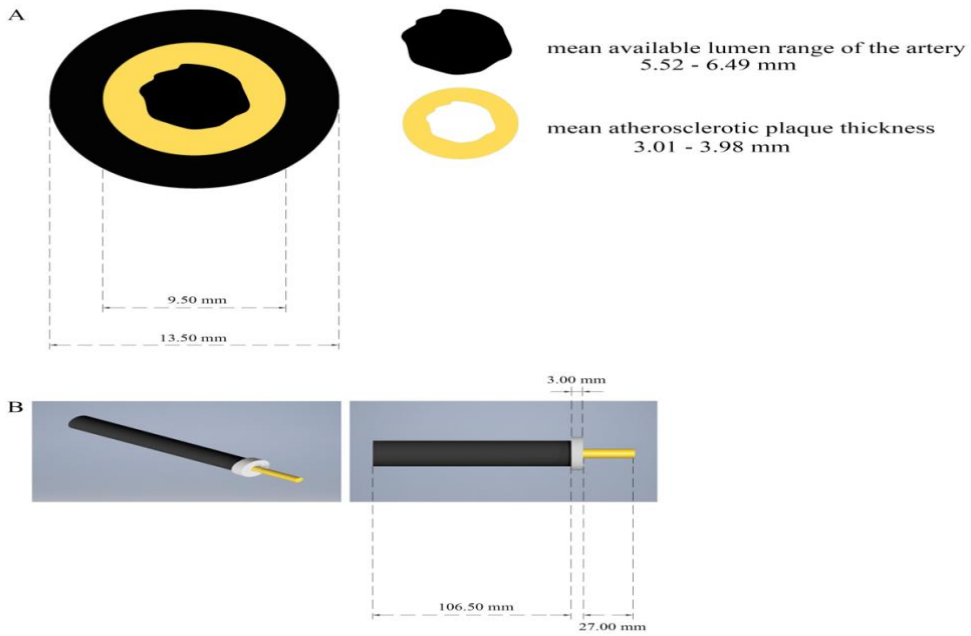

Figure 4.1: A) The cross – sectional area of the arterial mimic tube with atherosclerotic plaque, B) The arterial mimic tube (black) with the cap (white) and smaller tube (yellow) for creating the lumen of the artery.

The atherosclerotic plaque phantom consisted of Agar (Agar-agar granulated, purified and free from inhibitors for microbiology, Merck KGaa, Darmstadt, Germany), gypsum (Peletico Building Gypsum, Peletico Ltd, Strovolos, Cyprus), butter (FLORA original, UNILEVER TC LTD, Nicosia, Cyprus) and water. The ingredients were similar to that of Chueh et al. [217-219], Shang et al [220], Jin et al. [214] and Cao et al. [221] for agar. Regarding butter, Fleming et al. [227] and Cao et al. [221] used similar materials. Gypsum mimicked calcium and it was inspired by Fleming et al. [227] and Cormodeet al. [226]. The percentage of each component for classifying different plaques was based on previous studies [228-229]. Atherosclerotic plaques with less than 10 % of calcium were assessed. These types of atherosclerotic plaques are mainly PIT and fibrotic plaques [228-229]. Agar was used for mimicking fibrous tissue, gypsum for calcium and butter for lipid core. The produced sample was isotropic and homogeneous. The overall volume of the phantom was 230 ml. For the arterial atherosclerotic plaque phantom 10 ml was used and 220 ml for creating another plaque phantom for further investigation. The recipe of the atherosclerotic plaque phantom was agar 4% w/v, gypsum 1% w/v, butter 2% w/v and 93% water. The volume of the phantom was 10 ml. The phantom was poured in the 3D arterial mimic tube and was left to solidify overnight. The steps for the preparation were similar to the preparation of the agar/silica evaporated milk phantom as described in Menicou et al. [230]. The water was boiled to 50 ℃ with a magnetic stirrer and agar was added. Agar and water were boiled together until 90 ℃ and gypsum was added. The magnetic stirrer was turn off and when temperature reached again at 50 ℃ butter was added for creating the phantoms. Figure 4.2 shows the preparation of the atherosclerotic plaque phantoms using the magnetic stirrer.

Figure 4.2: The preparation of the atherosclerotic plaque phantoms using the magnetic stirrer.

Fig 4.3 shows the similarity between our model and the plaque in humans [228]. Fig. 4.3A shows the morphology of a human plaque with VH-IVUS. Fig. 4.3B shows the morphology of a human plaque with intravascular ultrasound (IVUS). Fig.4.3C shows the atherosclerotic plaque model created for this study. The tube that mimics the artery is shown in black and the atherosclerotic plaque is shown in gray.

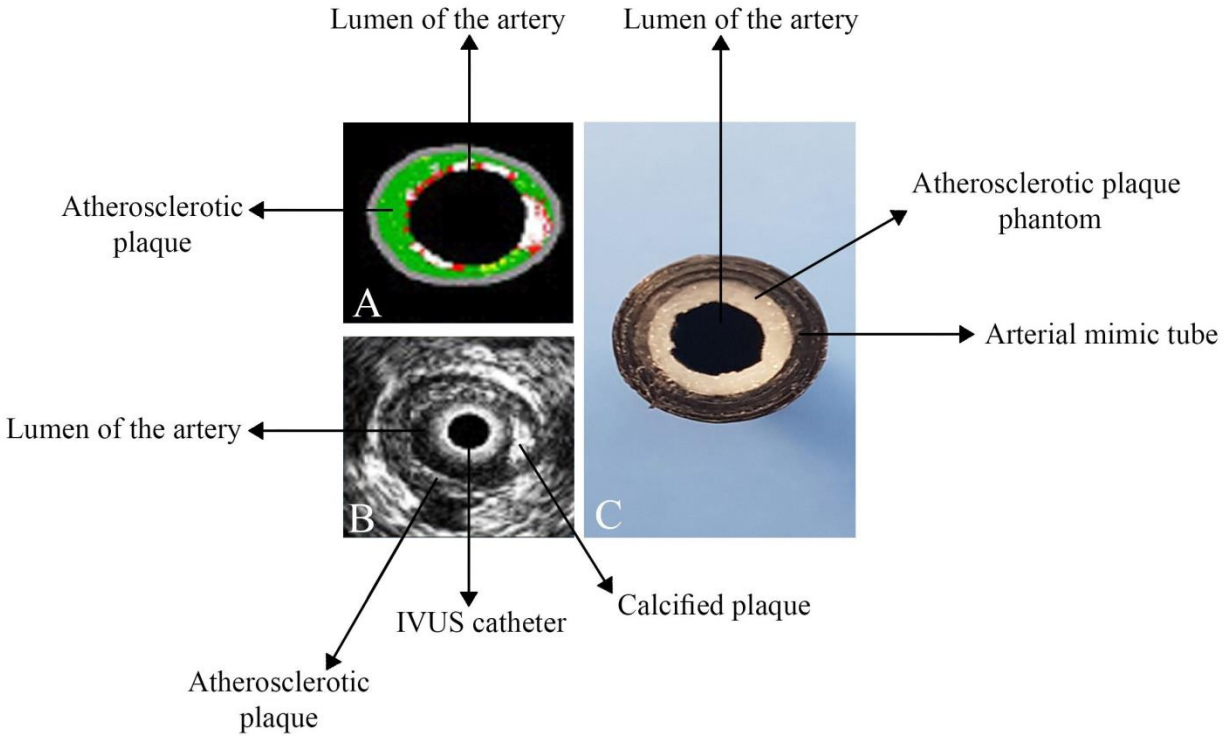

Figure 4.3: A) The morphology of a human plaque with VH-IVUS, B) The morphology of a human plaque with intravascular ultrasound (IVUS), C) The atherosclerotic plaque model created for this study.

4.3 HIFU System

The HIFU system was composed of a signal generator (33220A, Agilent Technologies, Englewood, CO, USA), an RF amplifier (AG 1012 LF Generator &Amplifier, T & C Power Conversion, Rochester, USA), and a planar rectangular transducer (Fig.4.4). The active size of the transducer was 2x10 mm^2. The transducer material was made out of P762-type piezoceramic (Ferroperm, Kvistgaard, Denmark), operating at 4 MHz ($\pm$5%). The thickness of the transducer was 0.5 mm.The transducer holder was made using Acrylonitrile Butadiene Styrene (ABS). The ABS parts of the transducer holder were produced by a 3D Printer (Ultimaker3 extended,

Ultimaker B.V, Zaltbommel, Netherlands). The internal structure includes a cavity to accommodate the 1 mm thick coaxial cable. In order to heat the atherosclerotic plaque for the purpose of treating atherosclerosis, the transducer should be placed in a catheter. The arteries are only 3-4 mm wide, so the transducer element should be as compact as possible.

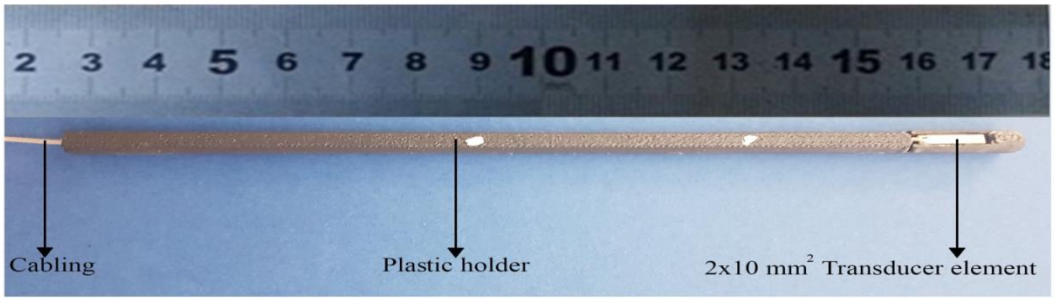

Figure 4.4: Main components of a planar transducer.

4.4 Experimental Setup

Figure 4.5 shows the schematic diagram of the experimental setup. The transducer was placed inside the arterial atherosclerotic plaque tube which was balanced with a holder. The transducer and the arterial atherosclerotic plaque tube were placed in the water container which was filled with de-ionised, degassed water, providing a good acoustical coupling between the transducer and atherosclerotic plaque phantom. The signal generator and amplifier were controlled (frequency, power, sonication time etc), by a user-friendly program written in C # (Visual Studio 2010 Express, Microsoft Corporation, USA).

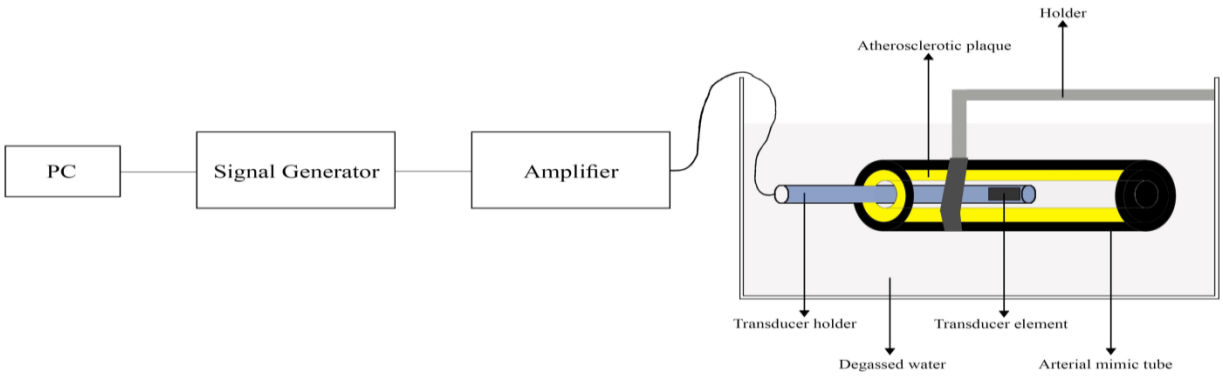

Figure 4.5: The schematic diagram of the experimental setup.

4.5 X-Ray Imaging

An X-Ray (Portable X-Ray System IMS001, Shenzhen Browiner Tech Co. Ltd, Shenzhen, P.R. China) system was used for evaluating the atherosclerotic plaque phantoms for ultrasound therapy. A computed radiography (CR) reader was used (Carestream Vita Flex CR Systems, Carestream Health Inc., New York, United States) to store the X-ray images. The X-Ray parameters used for acquiring the images was 50 kV voltages, 45 mA current, 45 ms time of exposure and 2 mAs.

4.6 MR imaging

The device was tested in a 1.5 T MR system (Signa, General Electric, Fairfield, CT, USA) using a GPFLEX coil (USA instruments, Cleveland, OH, USA). MR thermometry data was produced a coronal T2-weighted Fast Spin Echo (FSE) image was initially obtained for localization and setup checking. Main parameters used to obtain the T2-FSE image were the following: echo time (TE) = 55 ms, repetition time (TR) = 3000 ms, number of averages= 0.55, echo train length (ETL) = 1, field of view (FOV) = 20 cm, slice thickness= 2 mm, matrix= 512x512, and flip angle= 90^{o}.

4.7 MR thermometry

The temperature during the sonication was evaluated using the proton resonance frequency shift equation. The equation relates the measured phase with the temperature elevation (ΔT). This relationship is given by:

$$\Delta T = \frac{\varphi(T) - \varphi(T_0)}{\gamma \alpha B_0 TE} \quad (1)$$

Where φ(T) and φ(To) are the phases at a starting and final temperature T and T_o respectively, γis the gyromagnetic ratio, αis the proton resonant frequency shift coefficient, Bo is the magnetic field strength and TE is the echo time. The SPGR pulse sequence was used to extract the MRI thermometry maps with a 2 s temporal resolution. The amplifier used was AR-313601, Model 75A250M4, Amplifier Research, Souderton, USA.

4.8 Fibrotic and Pathological Intimal Thickening (PIT) plaque phantoms for ultrasound therapy

4.8.1 Evaluation of Fibrotic and PIT plaque phantom

Materials and methods

The first step was to assess fibrotic and PIT plaque phantom for ultrasound therapy. Different parameters of ultrasound such as acoustical power and time duration were used for achieving the optimum result (maximum destruction of atherosclerotic plaque phantom for a minimum treatment time). The recipe of the fibrotic atherosclerotic plaque phantom was agar 4% w/v, gypsum 1% w/v, butter 2% w/v and 93% water and for the PIT atherosclerotic plaque phantom was agar 4% w/v, gypsum 1% w/v, butter 20% w/v and 75% water respectively. Figure 4.6 shows the eight arterial atherosclerotic plaque phantoms from the top. Fibrotic plaque phantoms (left) and PIT plaque phantoms (right).

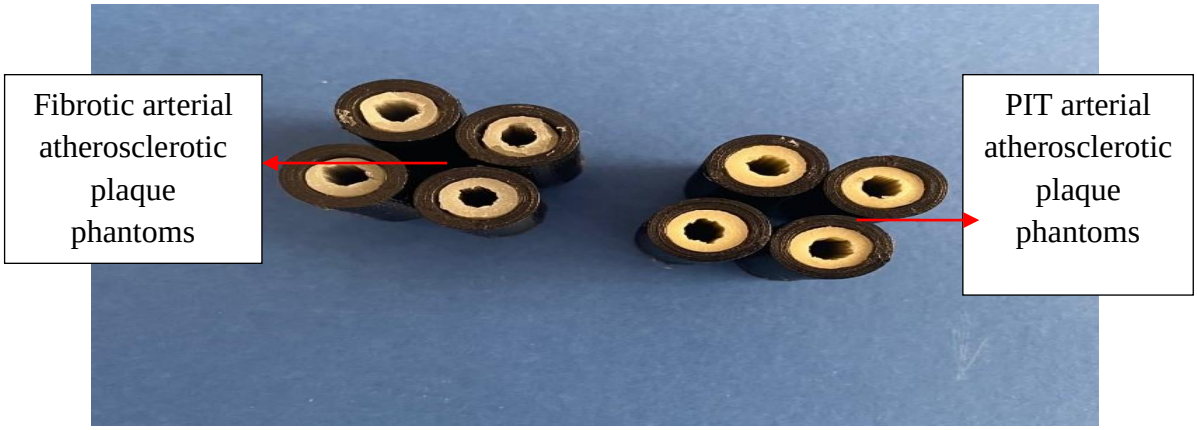

Figure 4.6: Fibrotic (left) and PIT (right) arterial atherosclerotic plaque phantoms.

Figure 4.7 shows the arterial plaque phantom and the ultrasound transducer with the plastic holder.

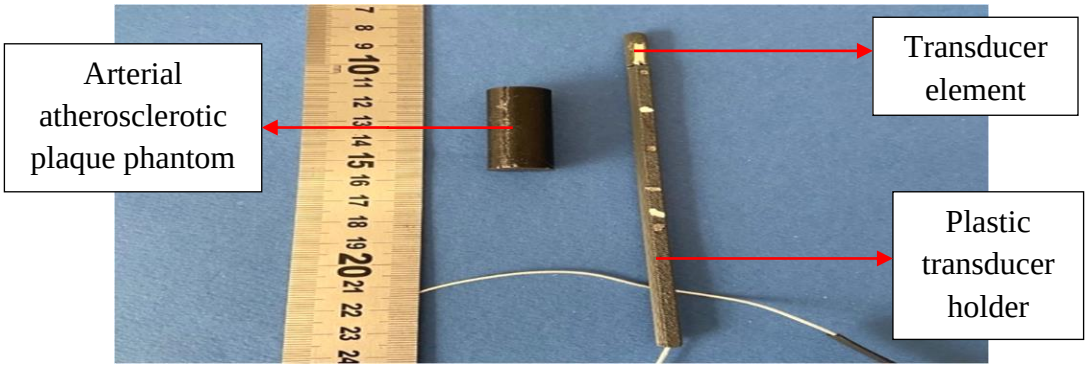

Figure 4.7: Arterial atherosclerotic plaque phantom and the ultrasound transducer with the plastic holder.

Figure 4.8 shows the experimental setup for investigating the ability of therapeutic ultrasound to ablate atherosclerotic plaque. The acoustical power was 6 W and 8 W respectively for 30 s time of duration. The amount of plaque removal was evaluated visually and using an X-Ray system

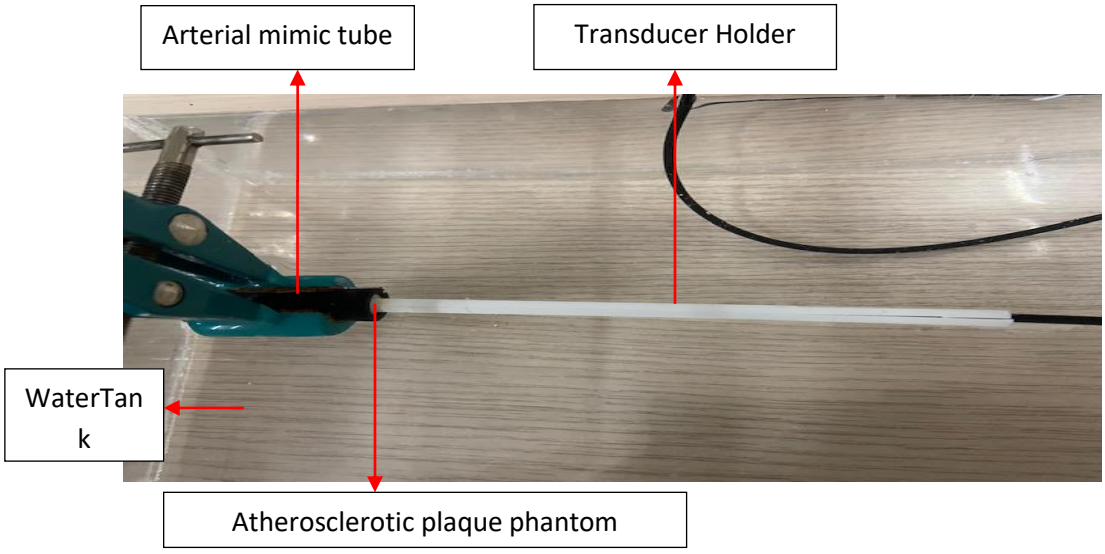

Figure 4.8: The experimental setup for investigating the ability of therapeutic ultrasound to ablate atherosclerotic plaque phantoms.

Figure 4.9 shows the X-Ray images for a fibrotic atherosclerotic plaque phantom. Fig. 4.9A shows the cross-sectional image. The thickness of the tube was 2.1 mm and 2.12 mm at two different points respectively. The thickness of the plaque was 2.6 mm and 2.61 mm at two different points respectively. Fig. 4.9B shows the horizontal image of the fibrotic atherosclerotic

plaque phantom. The thickness of the lumen of the artery, plaque and tube was 3.95 mm, 2.71 mm and 2.10 mm respectively.

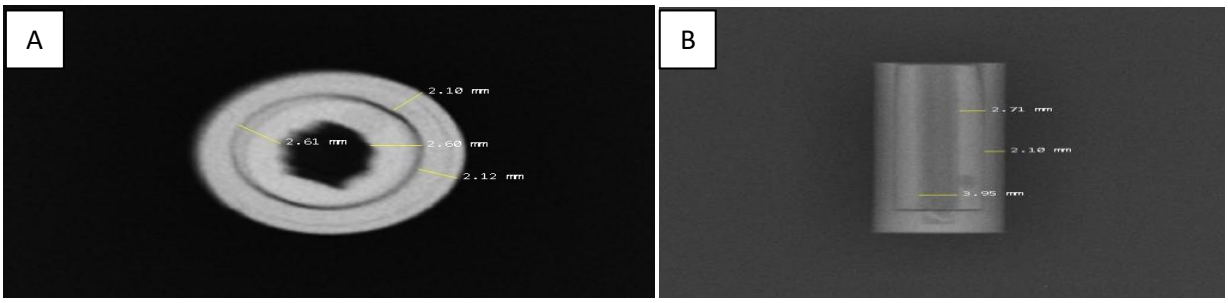

Figure 4.9: A) The cross-sectional image with tube and plaque thickness at two points respectively, B) The horizontal image of the fibrotic atherosclerotic plaque phantom with the thickness of the lumen of the artery, plaque and tube respectively.

Results

Figure 4.10 shows the X-ray images of the fibrotic atherosclerotic plaque phantom after thermal ablation. Fig. 4.10A shows the X-Ray image of the cross-sectional of the phantom after ablation. The size of the lesion was almost 2.34 mm. Fig. 4.10B shows the X-Ray image of the horizontal position of the phantom after ablation. The depth of the lesion was 2.22 mm and 1.77 mm at two different points respectively. Figure4.10C shows the image of the cross-sectional area of the phantom and fig.4.10D the corresponding X-Ray image after the ultrasonic ablation. The acoustical power was 8 W for 30 s.

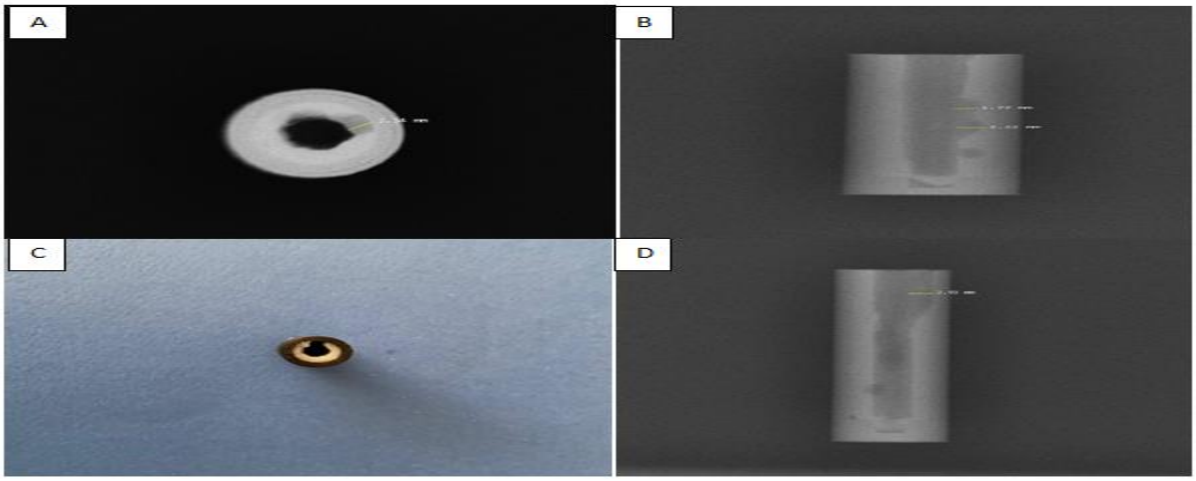

Figure 4.10: A) The X-Ray image of the cross-sectional of the phantom after ablation and B) The corresponding X-Ray image C) The image of the cross-sectional area of the phantom after the ultrasonic ablation and D) The corresponding X-ray image.

Figure 4.11 shows the X-ray images of the second atherosclerotic plaque phantom before and after thermal ablation. Fig. 4.11A shows the horizontal X-Ray image of the phantom before ablation. Fig. 4.11B shows the horizontal X-Ray image of the phantom after ablation. The depth of the lesion was almost 1.62 mm. The acoustical power was 6 W for 30 s.

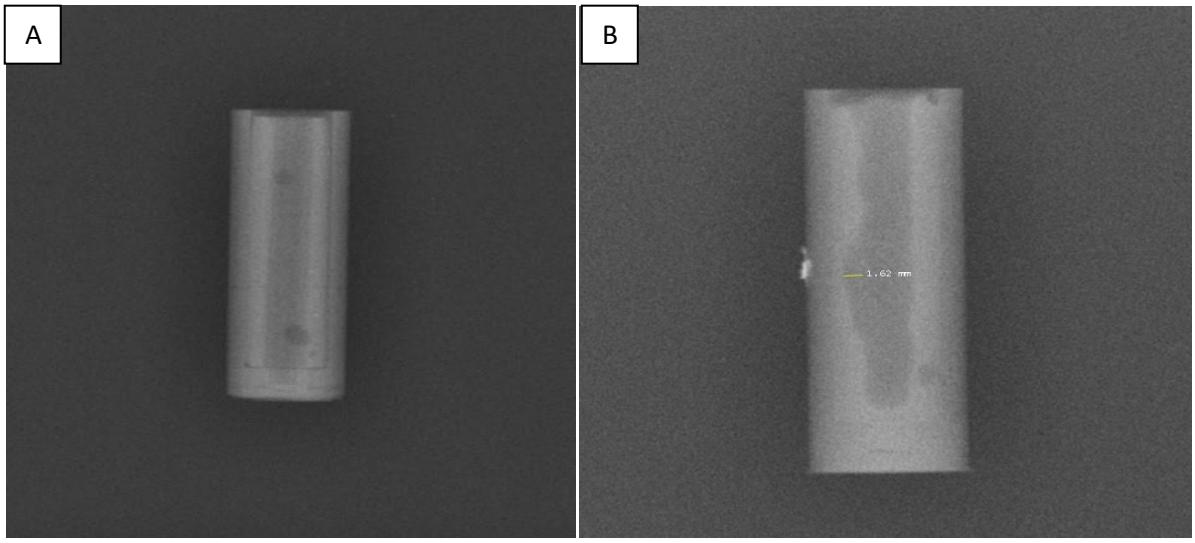

Figure 4.11: A) The horizontal X-Ray image of the fibrotic phantom before ablation, B) The horizontal X-Ray image of the phantom after ablation.

Figure 4.12 shows the X-ray images of the PIT atherosclerotic plaque phantom before and after thermal ablation. Fig. 4.12A shows the horizontal X-Ray image of the phantom before the ultrasonic ablation. Fig. 4.12B shows the horizontal X-Ray image of the phantom after ultrasonic ablation. The depth of the lesion was almost 0.86 mm. The acoustical power was 8 W for 30 s.

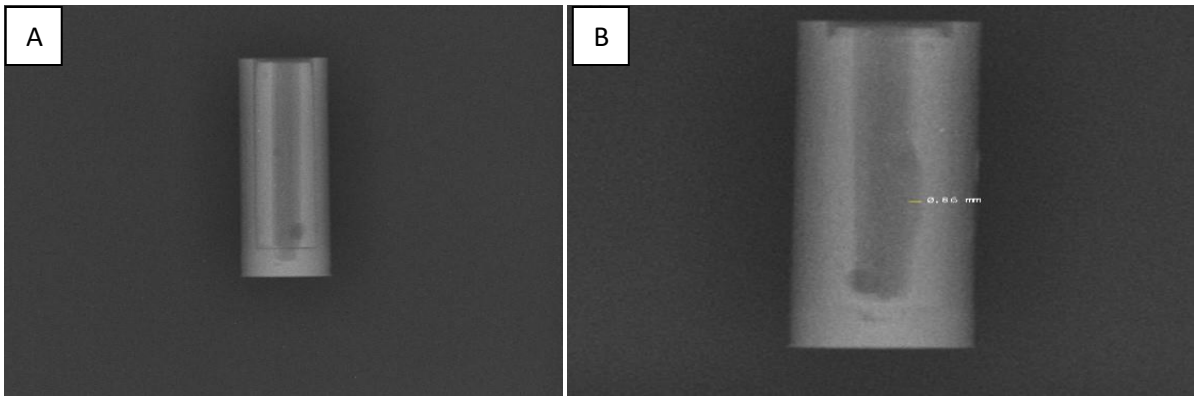

Figure 4.12: A) The horizontal X-Ray image of the PIT phantom before the ultrasonic ablation, B) The horizontal X-Ray image of the phantom after ultrasonic ablation.

4.8.2 Fibrotic and PIT plaque phantoms with 8 W acoustical power and different treatment time

Materials and methods

The next step of our investigation was to evaluate the relationship between acoustical power and different treatment times for fibrotic and PIT plaque phantoms. The acoustical power was 8 W and the plaque phantoms were assessed for a time interval between 15–30 s. The amount of plaque removal was evaluated visually and using an X-Ray system. The recipe of the fibrotic atherosclerotic plaque phantom was agar 4% w/v, gypsum 1% w/v, butter 2% w/v and 93% water and for the PIT atherosclerotic plaque phantom was agar 4% w/v, gypsum 1% w/v, butter 20% w/v and 75% waterrespectively.Table4.2 shows the list of atherosclerotic plaque phantoms with their ingredients.

Table 4.2: List of atherosclerotic plaque phantoms with their ingredients

Phantom	Plaquetype	Volume (ml)	Agar (%w/v)	Gypsum (%w/v)	Butter (%w/v)	Water (%)
1-3	Fibrotic	10	4	1	2	93
4-6	PIT	10	4	1	20	93

Results

Table 4.3 shows the different types of atherosclerotic plaque, ultrasonic parameters and average lesion depths.

Table 4.3: Atherosclerotic plaques, ultrasonic parameters and average lesion depth.

Phantom	Atherosclerotic plaquetype	Acoustical power (W)	Sonication time (s)	Average depth of the lesion (mm)
1	Fibrotic	8	25	1.45
2	Fibrotic	8	20	0.76

3	**Fibrotic**	**8**	**15**	**0.60**
5	**PIT**	**8**	**30**	**1.69**
6	**PIT**	**8**	**25**	**0.87**
7	**PIT**	**8**	**20**	**0.75**

Figure 4.13 shows the lesion depth against time for the fibrotic plaque phantom for 8 W acoustical powers.

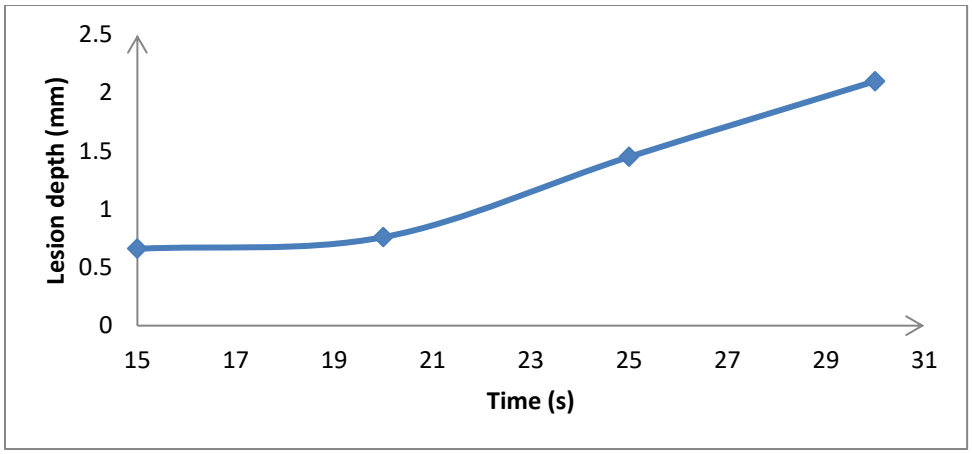

Figure 4.13: Lesion depth against time for the fibrotic phantom for 8 W acoustical powers.

Figure 4.14 shows the lesion depth against time for the PIT plaque phantom for 8 W acoustical powers.

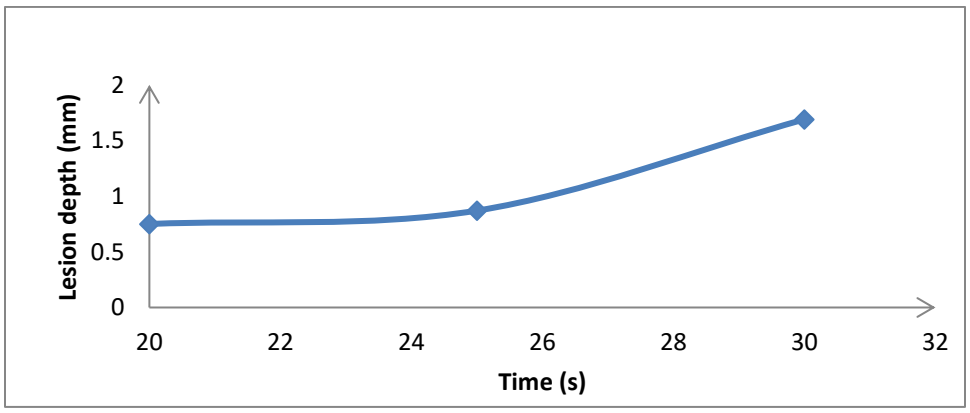

Figure 4.14: Lesion depth against time for the PIT phantom for 8 W acoustical powers.

Figure 4.15 shows the lesion depth against time for both PIT and fibrotic plaque phantoms. The acoustical power was 8 W. The blue and the red line correspond to the fibrotic and PIT plaque phantoms respectively.

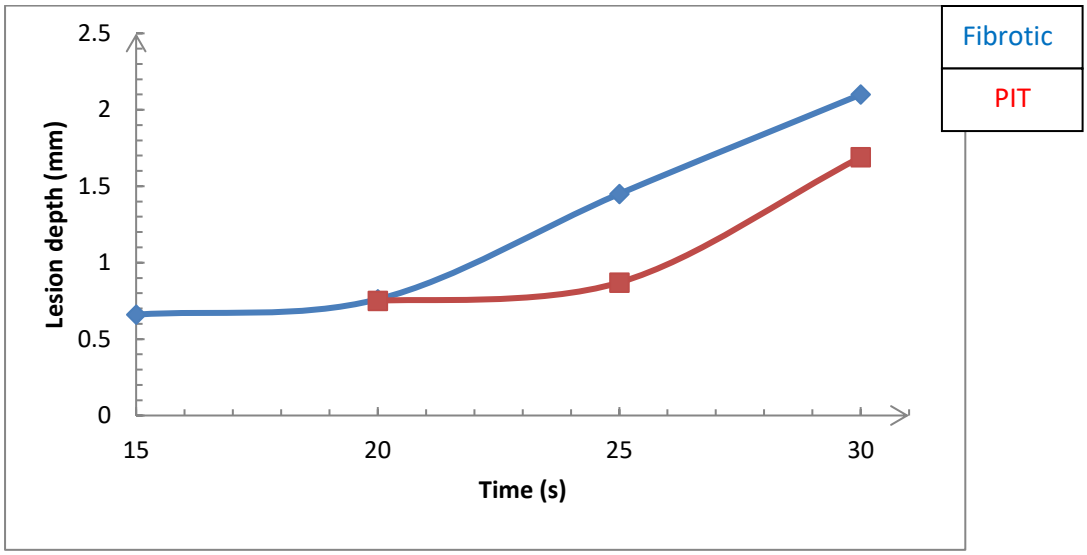

Figure 4.15: The lesion depth against time for both PIT and fibrotic plaque phantoms for 8 W acoustical powers. The blue and the red line correspond to the fibrotic and PIT plaque phantoms respectively

4.8.3 Effect of different percentage of lipid core for fibrotic and PIT plaque phantoms

Materials and Methods

The next step of our investigation was to evaluate the relationship between acoustical power and different treatment times for fibrotic and PIT plaque phantoms with different percentages of the lipid core. The acoustical power was 8 W and the plaque phantoms were assessed for a time interval between 15 – 30 s. The amount of plaque removal was evaluated visually and using an X-Ray system. The recipe of the fibrotic atherosclerotic plaque phantom was agar 4% w/v, gypsum 1% w/v, butter 10% w/v and 85% water. The recipe of the PIT atherosclerotic plaque phantom was agar 4% w/v, gypsum 1% w/v, butter 25% w/v and 70% water. Table 4.4 shows the list of atherosclerotic plaque phantoms with their ingredients.

Table 4.4: List of fibrotic and PIT atherosclerotic plaque phantoms with their ingredients

Phantom	Plaque type	Volume (ml)	Agar (%w/v)	Gypsum (%w/v)	Butter (%w/v)	Water (%)
1-4	Fibrotic	10	4	1	10	85
5-8	PIT	10	4	1	25	70

Results

Table 4.5 shows the different types of atherosclerotic plaque, ultrasonic parameters and average lesion depths.

Table 4.5: Fibrotic and PIT plaque phantoms, ultrasonic parameters and average lesion depth

Phantom	Atherosclerotic plaquetype	Power (W)	Time (s)	Average depth of the lesion (mm)
1	Fibrotic	8	30	1.73
2	Fibrotic	8	25	1.15
3	Fibrotic	8	20	0.56
4	Fibrotic	8	15	0.43
5	PIT	8	30	0.73
6	PIT	8	25	0.58
7	PIT	8	20	0.43
8	PIT	8	15	0.00

Figure 4.16 shows the lesion depth against time for the fibrotic plaque phantom. The lipid core was mimicked by butter with 10%. The acoustical power was 8 W.

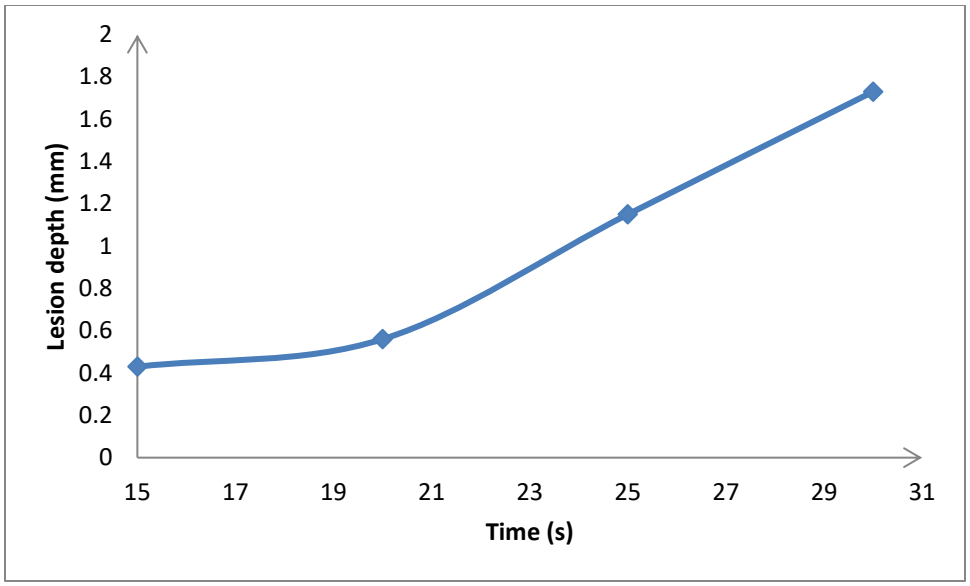

Figure 4.16: The lesion depth against time for the fibrotic plaque phantom with 10 % butter for 8 W acoustical powers.

Figure 4.17 shows the lesion depth against time for the PIT plaque phantom with 25 % butter for 8 W acoustical powers.

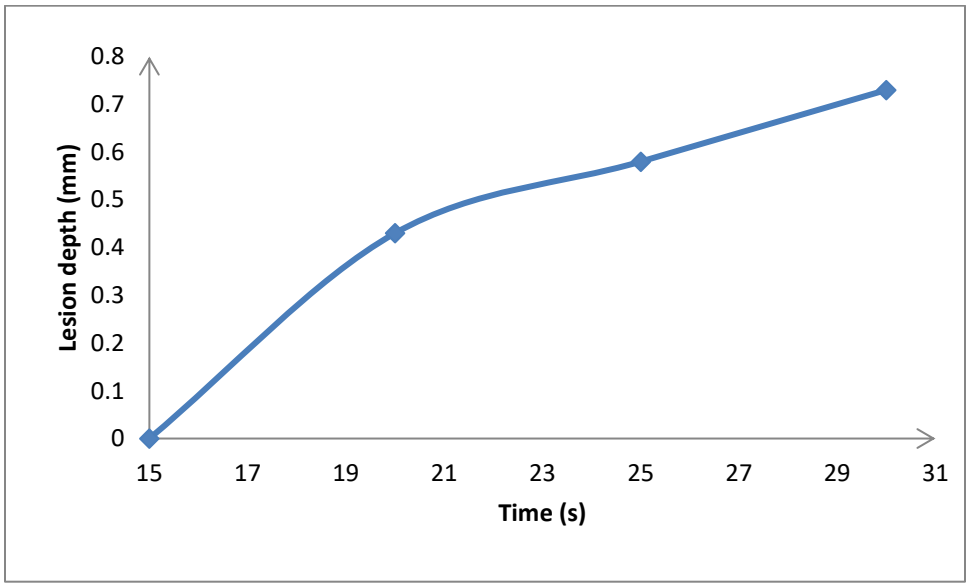

Figure 4.17: The lesion depth against time for the PIT plaque phantom with 25 % butter for 8 W acoustical powers.

Figure 4.18 shows the lesion depth against time for both PIT and fibrotic plaque phantoms. The acoustical power was 8 W. The blue and the red line correspond to the fibrotic and PIT plaque phantoms respectively.

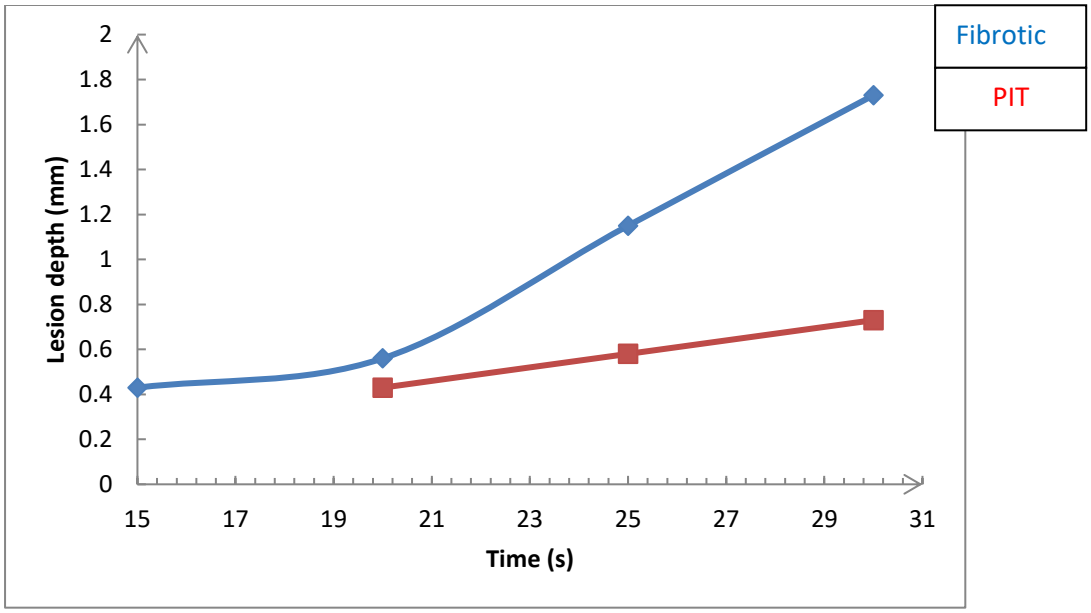

Figure 4.18: The lesion depth against time for both PIT and fibrotic plaque phantoms for 8 W acoustical powers. The blue and the red line correspond to the fibrotic and PIT plaque phantoms respectively.

4.8.4 Fibrotic and PIT plaque phantoms with 10 W acoustical power and different time

Materials and methods

The next step of our investigation was to evaluate the relationship between acoustical power and different treatment times for fibrotic and PIT plaque phantoms with different percentages of lipid core. The acoustical power was 10 W and the plaque phantoms were assessed for 15–30 s sonication time interval. The amount of plaque removal was evaluated visually and using an X-Ray system. The recipe of the fibrotic atherosclerotic plaque phantom was agar 4% w/v, gypsum 1% w/v, butter 10% w/v and 85% water. The recipe of the PIT atherosclerotic plaque phantom was agar 4% w/v, gypsum 1% w/v, butter 25% w/v and 70% water.

Results

Table 4.6 shows the different types of atherosclerotic plaque, ultrasonic parameters, average lesion depth and the percentage of plaque destruction. The percentage of plaque destruction was calculated by dividing the average depth of the lesion with the average length of atherosclerotic plaque at the point of destruction.

Table 4.6: Fibrotic and PIT plaque phantoms with 10 W acoustical power, 15-30s treatment time and average lesion depth

Phantom	Atherosclerotic plaque type	Power (W)	Time (s)	Average depth of the lesion (mm)	Percentage plaque destruction (%)
1	Fibrotic	10	30	2.59	100
2	Fibrotic	10	25	1.94	78
3	Fibrotic	10	20	1.09	44
4	Fibrotic	10	15	0.62	25
5	PIT	10	30	2.13	85
6	PIT	10	25	1.81	72
7	PIT	10	20	1.15	46
8	PIT	10	15	0.91	36

Figure 4.19 shows the lesion depth against time for the fibrotic plaque phantom with 10% butter. The acoustical power was 10 W.

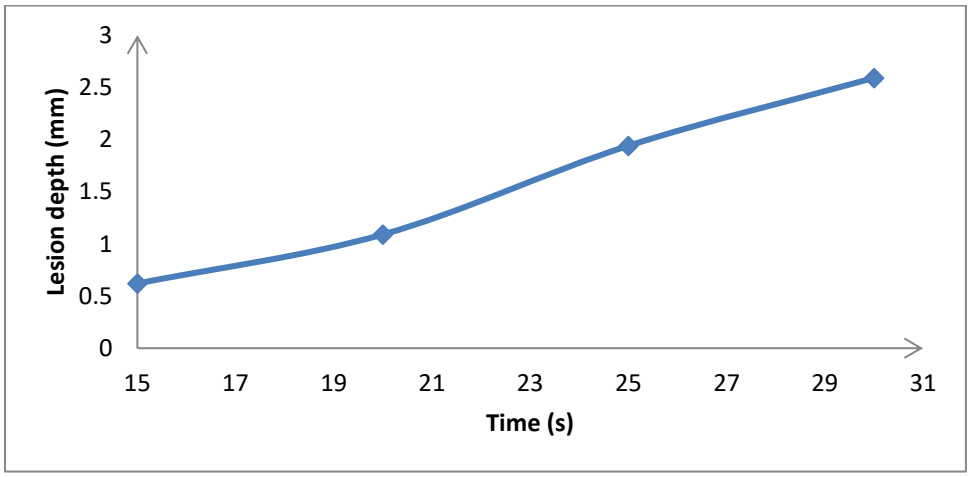

Figure 4.19: The lesion depth against time for the fibrotic plaque phantom with 10% butter for 10 W acoustical powers.

Figure 4.20 shows the lesion depth against time for the PIT plaque phantom with 25% butter for acoustical power was 10 W.

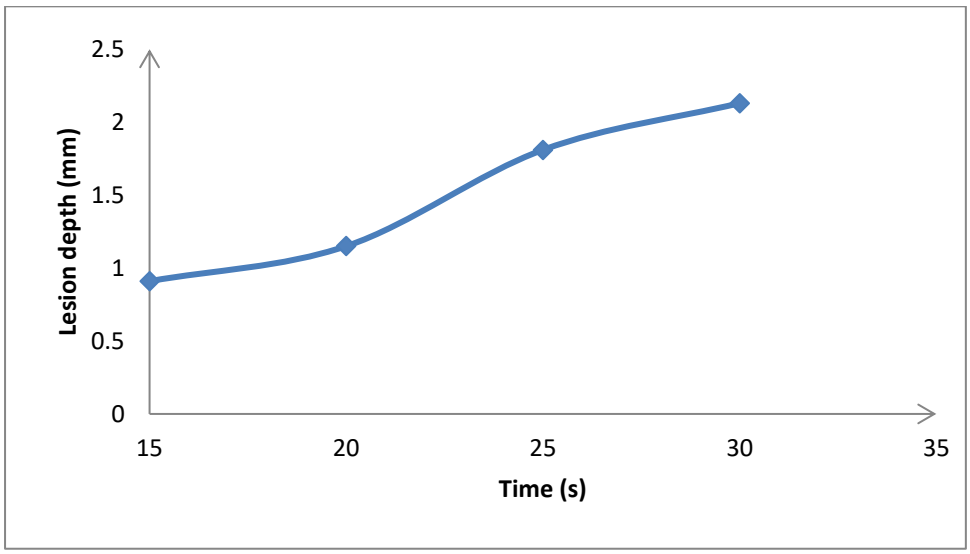

Figure 4.20: The lesion depth against time for the PIT plaque phantom for 10 W acoustical powers.

Figure 4.21 shows the lesion depth against time for both PIT and fibrotic plaque phantoms. The acoustical power was 10 W. The blue and the red line correspond to the fibrotic and PIT plaque phantoms respectively.

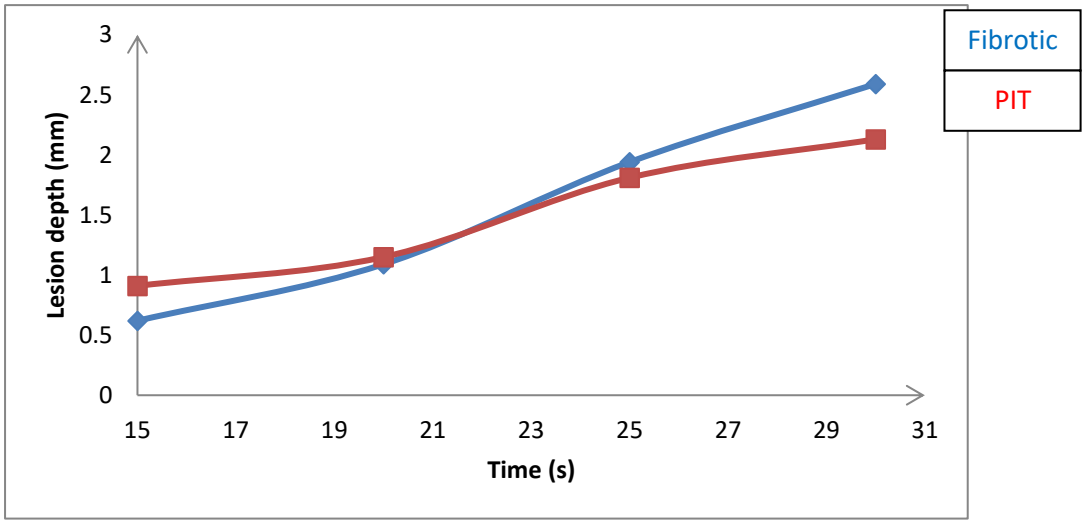

Figure 4.21: The lesion depth against time for both PIT and fibrotic plaque phantoms for 10 W acoustical powers. The blue and the red line correspond to the fibrotic and PIT plaque phantoms respectively.

.

Figure 4.22 shows the percentage plaque destruction against sonication time for both PIT and fibrotic plaque phantoms. The acoustical power was 10 W. The blue and the red line correspond to the fibrotic and PIT plaque phantoms respectively.

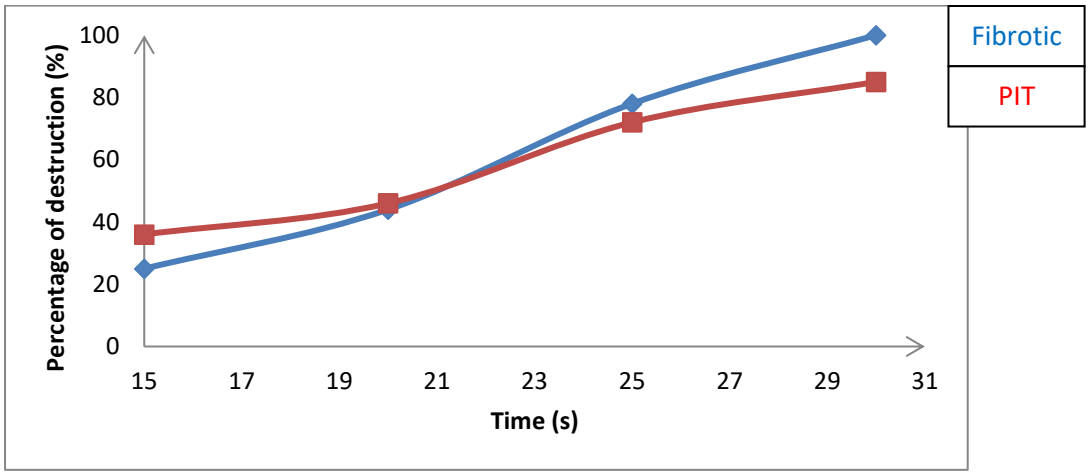

Figure 4.22: The plaque destruction in percentage against time for both PIT and fibrotic plaque phantoms. The acoustical power was 10 W. The blue and the red line correspond to the fibrotic and PIT plaque phantoms respectively.

Figure 4.23 shows the lesion depth against time for both PIT and fibrotic plaque phantoms. The acoustical power was 10 W and 8 W respectively. The green and the purple line correspond to the fibrotic and PIT plaque phantoms for 10 W acoustical powers respectively. The blue and the red line correspond to the fibrotic and PIT plaque phantoms for 8 W acoustical powers respectively.

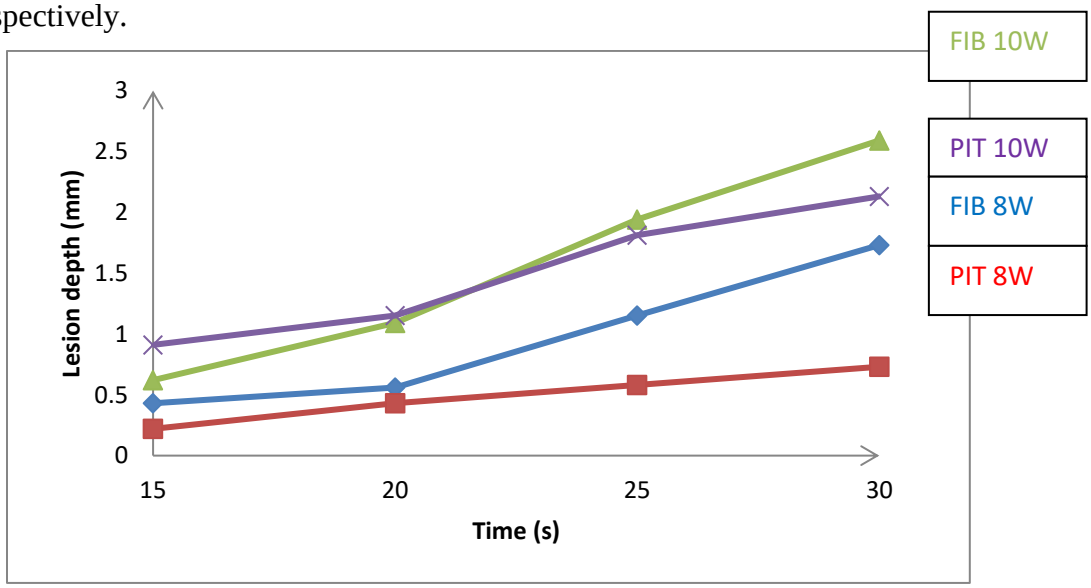

Figure 4.23: The lesion depth against sonication time for both PIT and fibrotic plaque phantoms.

4.9 PIT, TCFA, ThCFA and fibrocalcific plaque phantoms with 10 W acoustical power and different treatment time

Materials and methods

An evaluation of the relationship between acoustical power and different treatment times for PIT, TCFA, ThCFA and fibrocalcific plaque phantoms has been evaluated. The acoustical power used was 10 W and the plaque phantoms were assessed for 20 – 25 s time interval. The amount of plaque removal was evaluated visually and using an X-Ray system. The recipe of the PIT atherosclerotic plaque phantom was agar 4% w/v, gypsum 1% w/v, butter 20% w/v and 75% water. For TCFA were agar 4 % w/v, gypsum 10 % w/v, butter 18 % w/v and 68% water. For ThCFA were agar 4% w/v, gypsum 7% w/v, butter 2.5% w/v and 86.5% water and for fibrocalcific were agar 4% w/v, gypsum 50% w/v, butter 1 % w/v and 36% water.Table4.7 shows the atherosclerotic plaque phantoms with their ingredients.

Table 4.7: PIT, TCFA, ThCFA and FC plaque phantoms with their ingredients

Phantom	Atherosclerotic plaquetype	Volume (ml)	Agar (%w/v)	Gypsum (%w/v)	Butter (%w/v)	Water (%)
1-2	PIT	10	4	1	10	85
3-4	TCFA	10	4	10	18	68
5-6	ThCFA	10	4	7	2.5	86.5
7-8	FC	10	4	50	10	36

Results

Table 4.8 shows the different types of atherosclerotic plaque, ultrasonic parameters, average lesion depth and the percentage of plaque destruction.

Table 4.8: PIT, TCFA, ThCFA and FC plaque phantoms, ultrasonic parameters, average lesion depth and percentage plaque destruction

Phantom	Atherosclerotic plaque type	Power (W)	Time (s)	Average depth of the lesion (mm)	Percentage plaque destruction (%)
1	PIT	10	20	1.37	58
2	PIT	10	25	2.09	85
3	TCFA	10	20	1.66	65
4	TCFA	10	25	2.09	91
5	ThCFA	10	20	0.80	31
6	ThCFA	10	25	1.29	49
7	FC	10	20	0.00	0
8	FC	10	25	0.00	0

Figure 4.24A shows the lesion depth against time for the PIT, TCFA and ThCFA plaque phantoms and figure 4.24B the corresponding percentage of plaque destruction. The acoustical power was 10 W. The red, blue and green line corresponds to ThCFA, TCFA and PIT respectively.

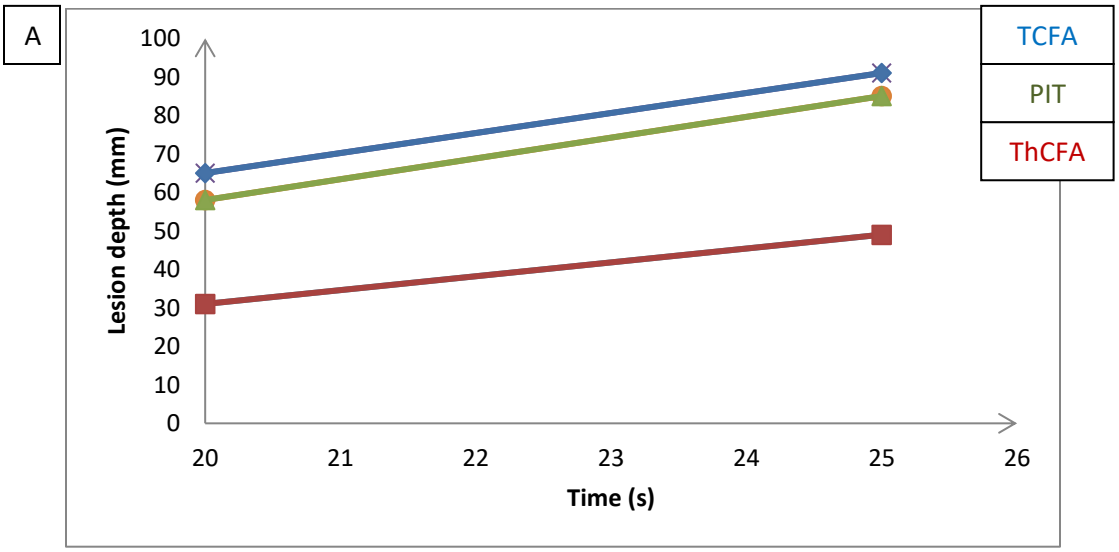

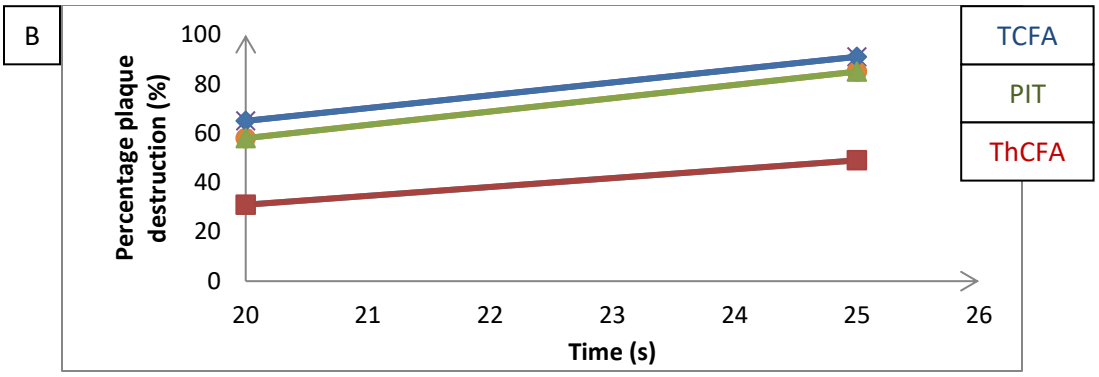

Figure 4.24: A) The lesion depth against time for the PIT, TCFA and ThCFA plaque phantoms. The acoustical power was 10 W, B) The percentage plaque destruction against time for the PIT, TCFA and ThCFA plaque phantoms.

4.10 PIT and TCFA plaque phantoms with 15 W acoustical power and different treatment time

Materials and methods

The next step of our evaluation was focused on PIT and TCFA atherosclerotic plaque phantoms. The acoustical power was 15 W and the plaque phantoms were assessed for 15 – 30 s time interval. The amount of plaque removal was evaluated visually and using an X-Ray system. The recipe of the PIT atherosclerotic plaque phantom was agar 4% w/v, gypsum 1% w/v, butter 20% w/v and 75% water. For TCFA were agar 4% w/v, gypsum 10% w/v, butter 18% w/v and 68% water. Figure 4.25 shows the slightly new experimental setup for investigating the ability of therapeutic ultrasound to ablate atherosclerotic plaque. The only difference with previous experiments was the plastic arterial mimic tube holder. This holder was designed for MR-thermometry experiments.Table4.9 shows the PIT and TCFA atherosclerotic plaque phantoms with their ingredients.

Table 4.9: List of PIT and TCFA atherosclerotic plaque phantoms with their ingredients

Phantom	Atherosclerotic plaquetype	Volume (ml)	Agar (%w/v)	Gypsum (%w/v)	Butter (%w/v)	Water (%)
1-4	PIT	10	4	1	10	85
5-8	TCFA	10	4	10	18	68

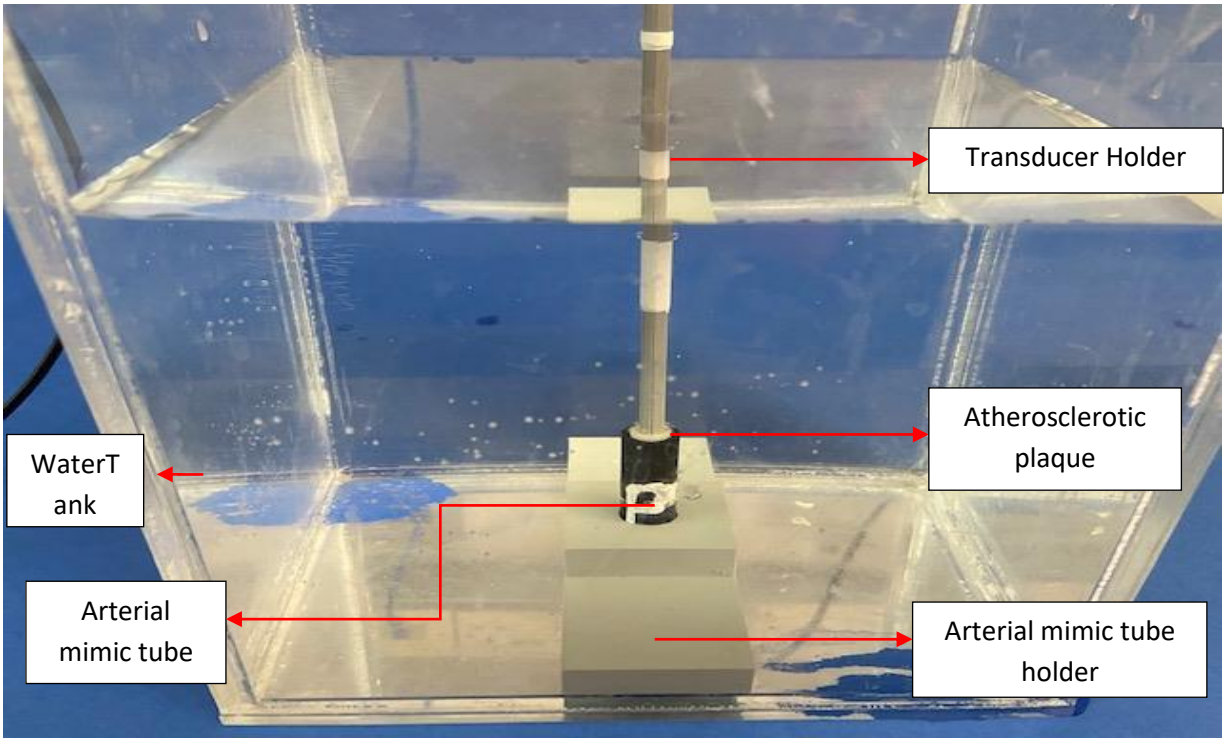

Figure 4.25: Experimental setup for investigating the ability of therapeutic ultrasound to ablate atherosclerotic plaque using a new arterial mimic tube holder.

Results

Table 4.10 shows the different types of PIT and TCFA atherosclerotic plaques, ultrasonic parameters, average lesion depth and the percentage of plaque destruction.

Table 4.10: PIT and TCFA atherosclerotic plaque phantoms with 15 W acoustical powers, 15-30 s treatment time, average lesion depth and percentage plaque destruction

Phantom	Atherosclerotic plaque type	Power (W)	Time (s)	Average depth of the lesion (mm)	Percentage plaque destruction (%)
1	PIT	15	15	0.72	29
2	PIT	15	20	2.15	87
3	PIT	15	25	2.24	96
4	PIT	15	30	2.61	98

5	TCFA	15	15	2.33	94
6	TCFA	15	20	2.33	100
7	TCFA	15	25	2.13	95
8	TCFA	15	30	2.38	100

Figure 4.26A shows the lesion depth against time for the PIT and TCFA plaque phantoms. The acoustical power was 15 W. The red and blue line corresponds to PIT and TCFA respectively.Figure4.26B shows the percentage plaque destruction against time for the PIT and TCFA plaque phantoms. The acoustical power was 15 W. The green and purple line corresponds to TCFA and PIT respectively.

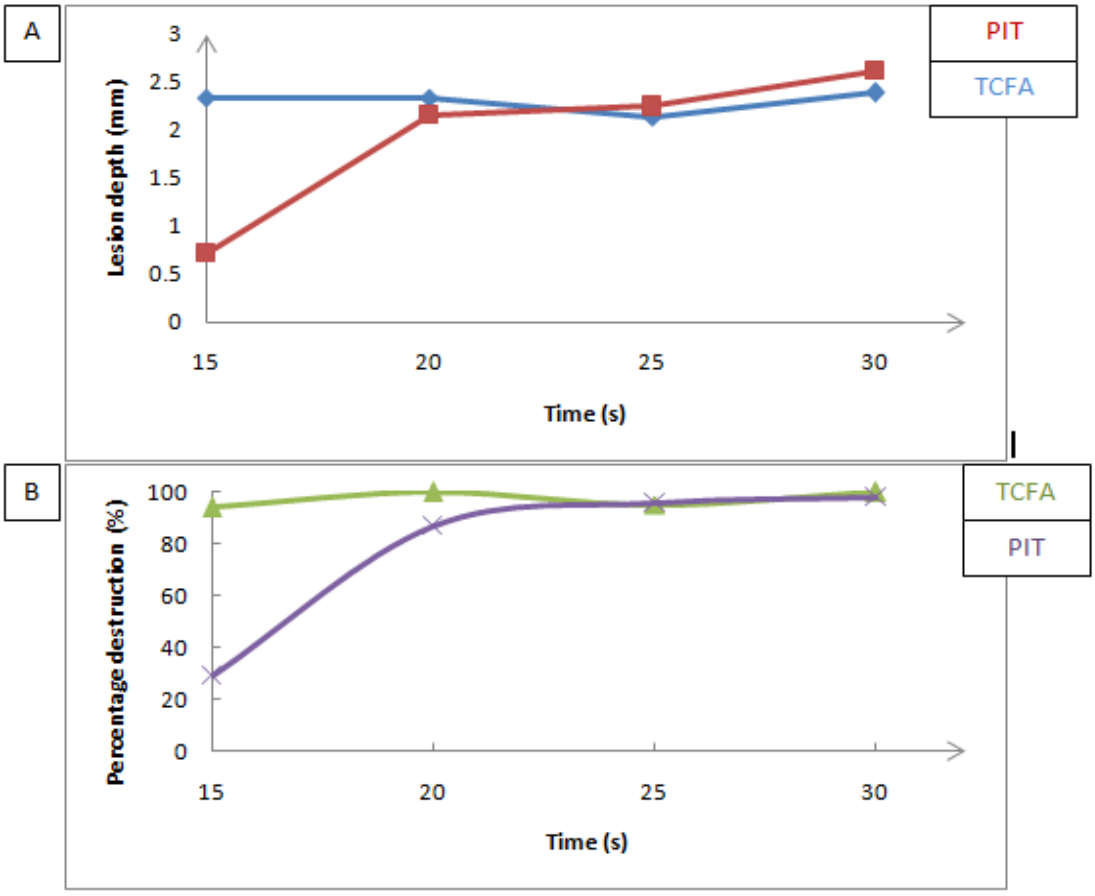

Figure 4.26: A) The lesion depth against time for the PIT and TCFA plaque phantoms. The acoustical power was 15 W, B) The percentage plaque destruction against time for the PIT and TCFA plaque phantoms.

4.11 TCFA plaque phantoms with 12 W and 15 W acoustical powers and different treatment times

Materials and methods

Plaque rupture can lead to cardiac ischemia and stroke. TCFA plaques are often ruptured in comparison with other types of plaques and so an evaluation of TCFA atherosclerotic plaque phantom has been made. The acoustical powers were 12 W and 15 W for 6 – 12 s treatment times. The amount of plaque removal was evaluated visually and using an X-Ray system. The recipe of the TCFA atherosclerotic plaque phantom were agar 4 % w/v, gypsum 10 % w/v, butter 18 % w/v and 68 % water.

Results

Table 4.11 shows TCFA atherosclerotic plaques, ultrasonic parameters, average lesion depth and the percentage of plaque destruction.

Table 4.11: TCFA atherosclerotic plaque phantoms, ultrasonic parameters, average lesion depth and percentage plaque destruction

Phantom	Atherosclerotic plaque type	Power (W)	Time (s)	Average depth of the lesion (mm)	Percentage plaque destruction (%)
1	TCFA	12	6	0.90	45
2	TCFA	12	8	1.47	60
3	TCFA	12	10	1.58	70
4	TCFA	12	12	2.38	92
5	TCFA	15	6	1.69	62
6	TCFA	15	8	1.92	90
7	TCFA	15	10	1.92	70
8	TCFA	15	12	2.26	95

Figure 4.27Ashows the lesion depth against time for the TCFA plaque phantoms. The red and blue line corresponds to 15 W and 12 W acoustical powers respectively.Figure4.27B shows

the percentage plaque destruction against time for TCFA plaque phantoms. The green and purple line corresponds to 12 W and 15 W acoustical powers respectively.

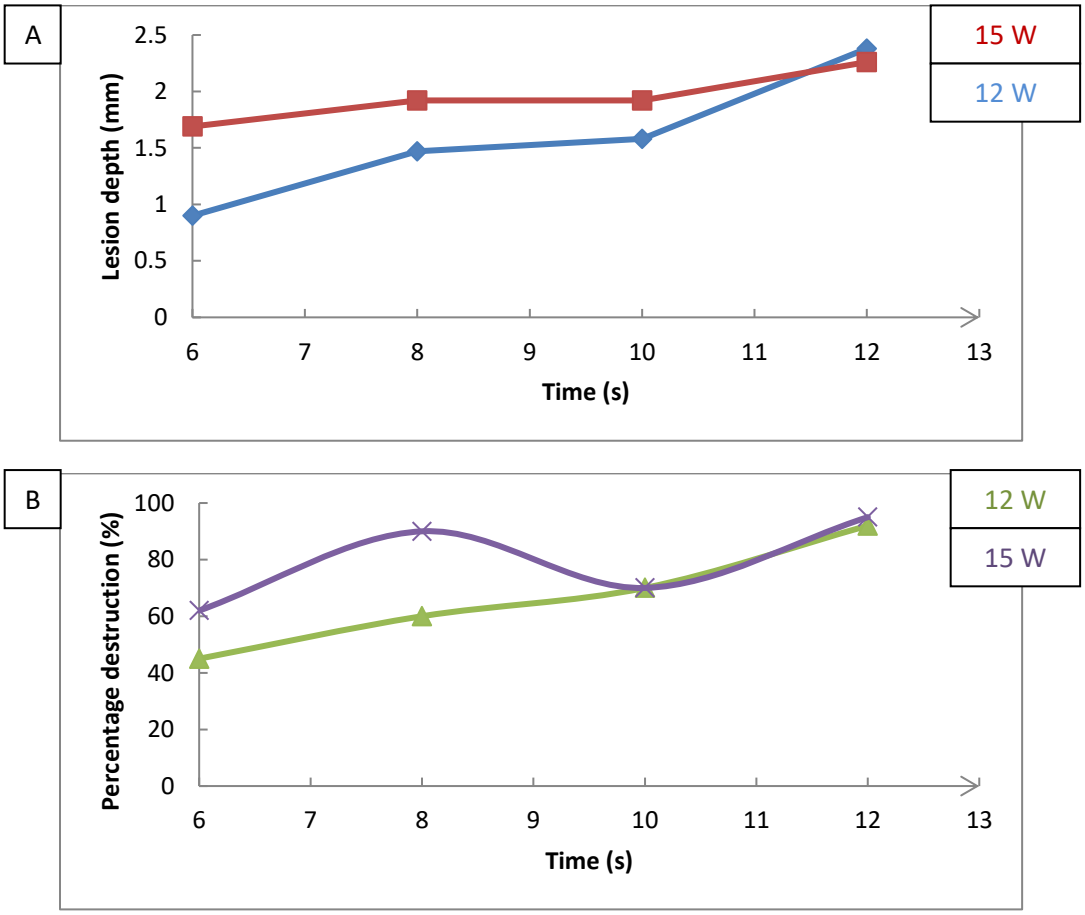

Figure 4.26: A): The lesion depth against time for the TCFA plaque phantoms, B) The percentage plaque destruction against time for TCFA plaque phantoms.

4.12 Conclusion

In this chapter, the effect of therapeutic ultrasound for destruction of atherosclerotic plaque phantoms was described. A low cost arterial plaque model was evaluated with different atherosclerotic plaque phantoms using different acoustic parameters such as acoustic power and treatment time. Atherosclerotic plaques were mimicked with their three main components: fibrous tissue with agar, lipid core with butter and calcium with gypsum. The optimum treatment process that maximized the destruction of atherosclerotic plaque in minimum time duration was achieved. In order to succeed this, the influence of acoustic parameters such as acoustic power and treatment time was investigated. A summary for the evaluation is given below. Same plaque phantoms are evaluated separately and then an overall conclusion have been analyzed for all the

phantoms. The max and minimum percentage plaque destruction is evaluated for same plaque phantoms and the relationship between the percentage plaque destruction and their ingredients is analyzed.

The first step of this evaluation was to assess fibrotic and PIT plaque phantoms for ultrasound therapy. The results were shown that the fibrotic (2% butter) atherosclerotic plaque phantoms were properly ablated by thermal ultrasound. The 1st fibrotic atherosclerotic plaque phantom was destructed completely for acoustical power 8 W for 30 s. The 4th plaque phantom was destructed by more than 70% with acoustical power 6 W for 30 s. PIT atherosclerotic plaque phantom with 20% butter remained unaffected by the ultrasonic ablation with acoustical power of 6 W for 30 s. The last PIT atherosclerotic plaque phantom was ablated by almost 30% with acoustical power of 8 W for 30 s. The size of the lesion for the atherosclerotic plaque phantom is similar to the size of the transducer and depends on acoustical power and sonication time. The X-Ray images of the arterial plaque phantoms have shown that the arterial plaque phantoms were properly mimicked. The experiment has shown that the ultrasonic ablation affected by the lipid concentration as the lipid concentration of PIT phantom was higher than the fibrotic phantom.

The next step of this investigation was to evaluate the relationship between acoustical power and different treatment times for fibrotic and PIT plaque phantoms. It was shown that for acoustical power of 8 W until 15 s the destruction of the fibrotic plaque was almost 25%. After 20 s sonication time and for every 5 s the amount of plaque destruction was doubled. Moreover, the results showed that the PIT atherosclerotic plaque phantom with 20% butter was properly ablated by thermal ultrasound. For 8 W acoustical power and 15 s sonication time an anomalous result was produced and should be assessed again. It seems that the amount of lipid concentration plays a significant role to the amount of plaque destruction. The size of the lesion for the atherosclerotic plaque phantom is similar to the size of the transducer and depends on acoustical power and sonication time.

As the amount of lipid core played a significant role to the amount plaque destruction, the next evaluation was focused to the relationship between acoustical power and different treatment times for fibrotic and PIT plaque phantoms with different percentages of the lipid core. It was shown that for acoustical power of 8 W until 15 s the destruction of the fibrotic plaque was almost 25 %. There is a linear relationship after 20 s sonication time between the lesion depth and sonication time. Moreover, the results were shown that the PIT atherosclerotic plaque

phantoms with 25 % butter were properly ablated by thermal ultrasound. For the last PIT phantom with 15 s sonication time, no effect was produced probably because of the imaging angle between the phantom and the X-ray plane. The PIT plaque phantom lesion depth is less than the fibrotic phantom depth mainly due to the higher concentration of the lipid core. There is a difference of 15 % between the two lipid concentrations and these affect the amount of plaque removal. As the amount of lipid increases, the amount of plaque depth decreases.

The last part of the evaluation of fibrotic and PIT plaque phantoms have been done with 10 W acoustical power and different treatment times. The results showed that the fibrotic atherosclerotic plaque phantoms with 10% butter were properly ablated by thermal ultrasound. It was shown that for acoustical power of 10 W until 15 s the destruction of the fibrotic plaque was almost 25% and 36% for the PIT plaque respectively. For 10 W acoustical powers, the lesion depth for PIT phantoms was higher than 8 W while for fibrotic plaque phantoms was similar. The fibrotic plaque was completed destructed with 10 W acoustical power and 30 s sonication time. However, for each 5 s after 20 s it seems to follow a linear relationship. For 10 W acoustical powers up to 20 s sonication times, the higher the lipid percentage the higher the lesion depth.

Moreover, the relationship between 10 W acoustical power and different treatment times for PIT, TCFA, ThCFA and FC plaque phantoms has been evaluated. The results showed that PIT, TCFA and ThCFA atherosclerotic plaque phantoms were properly ablated by thermal ultrasound. FC atherosclerotic plaque phantom was not ablated, mainly due to the very high 50% percentage of gypsum. It was shown that for 10 W acoustical powers for 25 s sonication times the percentage destruction of TCFA and PIT plaque phantom had a 6% difference. Furthermore, the percentage destruction of the plaque phantom at the point of sonication was 65% to 91% for TCFA, 31% to 49% for ThCFA and 50% to 85% for the PIT plaque phantoms respectively. The 91 % higher percentage plaque destruction at the point of sonication was created in TCFA phantom with 10 W acoustical power and 25 s sonication time. The size of the lesion for the atherosclerotic plaque phantom was similar to the size of the transducer. The size of the lesion depends on acoustical power and sonication time. The X-Ray images of the arterial plaque phantoms have shown that the arterial plaque phantoms were properly mimicked. The components of arterial atherosclerotic plaque model can be clearly defined by X-Ray images of the TCFA and ThCFA rather than fibrotic and PIT because of the higher amount of gypsum.

Furthermore, the next step of this evaluation was focused on PIT and TCFA atherosclerotic plaque phantoms with 15 W acoustical power and 15 – 30 s treatment time interval. TCFA atherosclerotic plaque phantoms had a minimum 95 % plaque lesion at the point of sonication with 15 W acoustical power and different sonication times. PIT atherosclerotic plaque phantoms had a minimum 96 % plaque lesion at the point of sonication with 15 W acoustical powers for sonication times higher than 25 s. The minimum percentage plaque lesion at the point of sonication was 30% for 15 s sonication time. A specific note should be placed for TCFA atherosclerotic plaque, which is the most vulnerable plaque leading to stroke and cardiac ischemia. The X-Ray images of the arterial plaque phantoms have shown that the arterial plaque phantoms were properly mimicked. The components of arterial atherosclerotic plaque model can be clearly defined by X-Ray images of the TCFA rather than PIT plaque phantom because of the higher amount of gypsum.

Plaque rupture can lead to cardiac ischemia and stroke. TCFA plaques are often ruptured in comparison with other types of plaques and so finally an evaluation of TCFA atherosclerotic plaque phantom has been made. The results were shown that TCFA atherosclerotic plaque phantoms were properly ablated by thermal ultrasound. It was shown that for 12 W acoustical powers the minimum plaque percentage destruction was almost 45% and for 15 W acoustical powers was 62%. The maximum percentage plaque destructions were similar and close to 95% for both acoustical powers. For a very small 6 s duration of sonication time, it was shown that the TCFA plaque phantom was destructed at the point of sonication by 45% and 62% for 12 W and 15 W acoustical powers respectively. An anomalous result produced for 15 W acoustical power and 10 s sonication time and should be assessed again. The size of the lesion for the atherosclerotic plaque phantom is similar to the 2 x10 mm^2 size of the transducer. The size of the lesion depends on acoustical power and sonication time. The X-Ray images of the arterial plaque phantoms have shown that the arterial plaque phantoms were properly mimicked.

Table 4.12 shows the fibrotic plaque phantoms with their ingredients, ultrasonic parameters, and average lesion depth with the percentage destruction. Figure 4.28 shows the percentage plaque destruction against time for fibrotic plaque phantoms. Only the last three phantoms are shown in the graph because for the first two only one sonication was taken place. For the third fibrotic plaque phantom the value of the first was included to compare and the maximum treatment time with the last two fibrotic phantoms.

Table 4.12: Fibrotic atherosclerotic plaque phantoms with their ingredients, ultrasonic parameters, average lesion depth and percentage plaque destruction

Plaquephantom	Fib 1	Fib 2	Fib 3	Fib 4	Fib 5
Agar (%w/v)	4	4	4	4	4
Gypsum (%w/v)	1	1	1	1	1
Butter (%w/v)	2	2	2	10	10
Water (%)	93	93	93	85	85
AcousticalPower (W)	8	6	8	8	10
Sonicationtime (s)	30	30	15-25	15-30	15-30
Averagelesiondepth (mm)	2.2	1.62	0.60-1.45	0.43-1.73	1.19-1.51
Percentagedestruction (%)	100	70	21 - 56	17-67	36-57

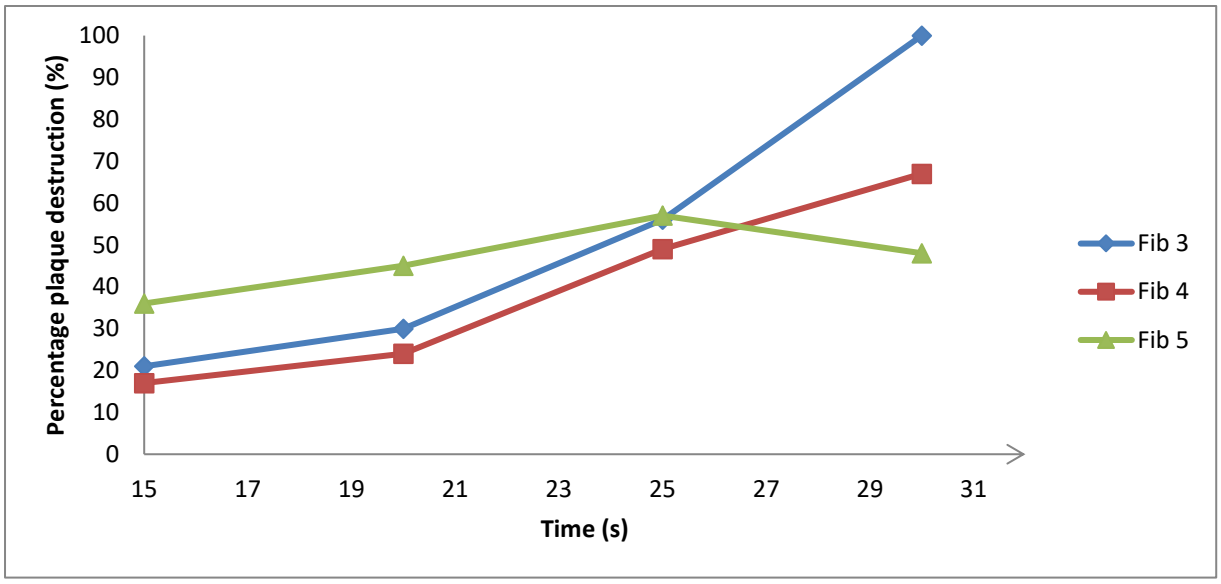

Figure 4.27: The percentage plaque destruction against time for fibrotic plaque phantoms.

Important conclusions can be derived from table 4.12 and fig. 4.28 related to fibrotic plaque phantoms and ultrasonic parameters. Regarding 8 W acoustical powers with 2% w/v butter, it can be deduced that the fibrotic plaque phantom was destructed 100% for a sonication time of 30 s, and minimum 21% plaque destruction occurred for 15 s sonication times. An increase of the butter percentage which mimics the lipid core of atherosclerotic plaques showed that the percentage destruction is smaller. Specifically, an increase of 8% w/v of butter (fib4) led to a decrease of about 23% of the maximum destruction of the plaque phantom and 4% of the minimum respectively. Finally, a raise of 2 W acoustical powers (fib5) led to an increase of

about 20 % to the minimum destruction of the plaque phantom and 8% to the maximum. The last point of the last fibrotic phantom is anomalous.

Table 4.13 shows the PIT plaque phantoms with their ingredients, ultrasonic parameters, and average lesion depth with the percentage destruction. Figure 4.29 shows the percentage plaque destruction against time for PIT plaque phantoms. Only the last five phantoms are shown in the graph because for the first two only one sonication was taken place.

Table 4.13: PIT atherosclerotic plaque phantoms with their ingredients, ultrasonic parameters, average lesion depth and percentage plaque destruction

Plaquephantom	PIT 1	PIT 2	PIT 3	PIT 4	PIT 5	PIT 6	PIT 7
Agar (%w/v)	4	4	4	4	4	4	4
Gypsum (%w/v)	1	1	1	1	1	1	1
Butter (%w/v)	20	20	20	25	25	20	20
Water (%)	75	75	75	70	70	75	75
Acoustical Power(W)	8	6	8	8	10	10	15
Sonication time (s)	30	30	20-30	15-30	15-30	20-25	15-30
Average lesion depth (mm)	0.86	0	0.75-1.69	0-0.73	0.53-1.01	1.37-2.09	0.72-2.61
Percentage destruction (%)	30	0	25-74	0-30	20-38	58-85	29-98

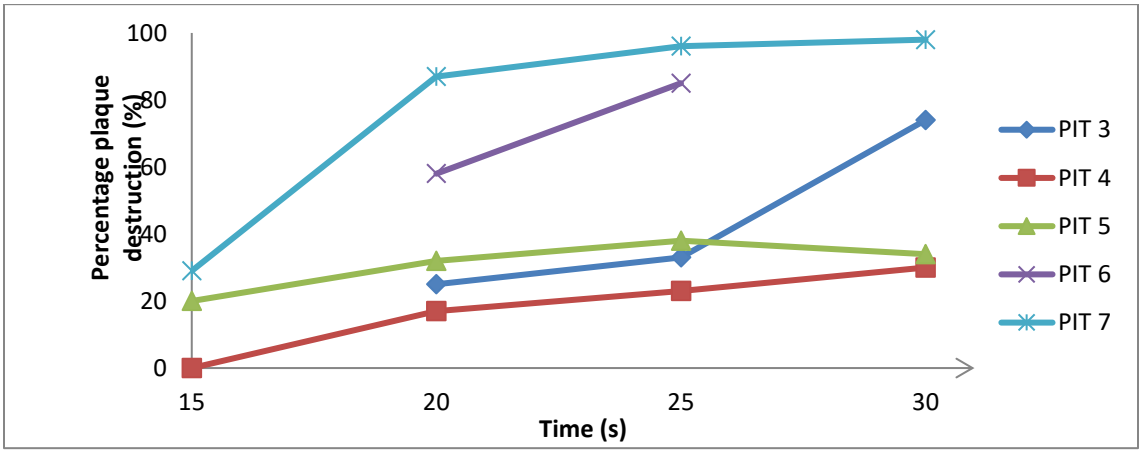

Figure 4.28: The percentage plaque destruction against time for PIT plaque phantoms.

Looking carefully to table 4.13 and fig. 4.29, an interesting conclusion for PIT plaque phantoms and ultrasonic parameters can be derived. No plaque destruction created with 6 W acoustical power and 30 s sonication time. The minimum plaque destruction was 20% for 10 W

acoustical powers, 15 s sonication times and 25% butter and the maximum was 98% for 15 W acoustical powers, 30 s sonication times and 20% butter. Moreover, the percentage plaque destruction was affected by the percentage of butter which mimics the lipid core of atherosclerotic plaque. An increase of 5% w/v butter with 8 W acoustical powers showed that the amount of plaque destruction decreased by 8% for 20 s sonication times, 10% for 25 s sonication times and 44% for 30 s sonication times. An increase of 5% w/v butter with 10 W acoustical powers decreases the amount of destruction by 26% for 20 s sonication times and 47% for 25 s sonication times. The results are given on figure 4.30 below.

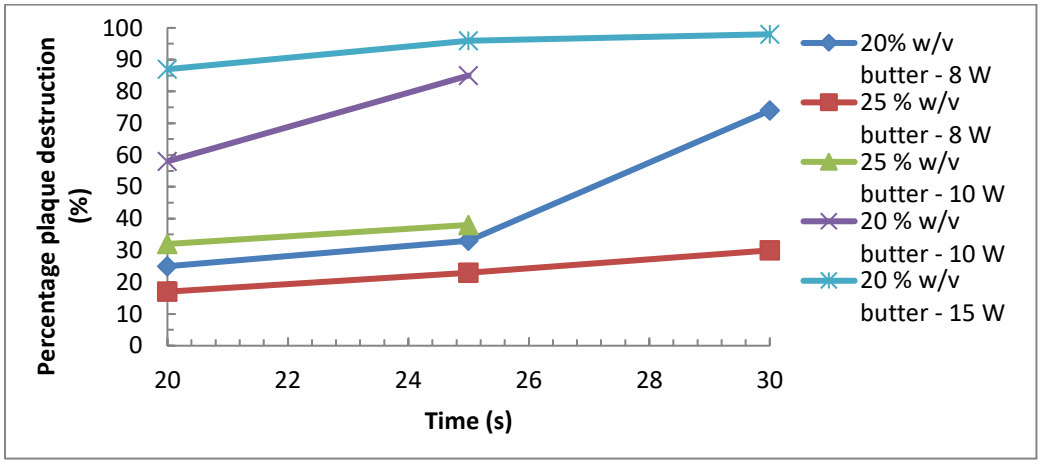

Figure 4.29: Percentage plaque destruction against time, for different percentage lipid cores and acoustical powers.

Table 4.14 shows the TCFA plaque phantoms with their ingredients, ultrasonic parameters, and average lesion depths with the percentage destructions. Figure 4.31 shows the percentage plaque destruction against time for TCFA plaque phantoms and 6-12 s sonication times. Figure 4.32 shows the percentage plaque destruction against time for TCFA plaque phantoms and 15-30 s sonication times.

Table 4.14: TCFA atherosclerotic plaque phantoms with their ingredients, ultrasonic parameters, average lesion depths and percentage plaque destructions

Plaquephantom	TCFA 1	TCFA 2	TCFA 3	TCFA 4
Agar (%w/v)	4	4	4	4
Gypsum (%w/v)	10	10	10	10
Butter (%w/v)	18	18	18	18
Water (%)	68	68	68	68

AcousticalPower (W)	10	15	12	15
Sonicationtime (s)	20-25	15-30	6-12	6-12
Average lesion depth (mm)	1.66-2.09	2.33-2.38	0.72-2.61	2.33 -2.38
Percentage destruction (%)	65-91	94-100	45-92	62-95

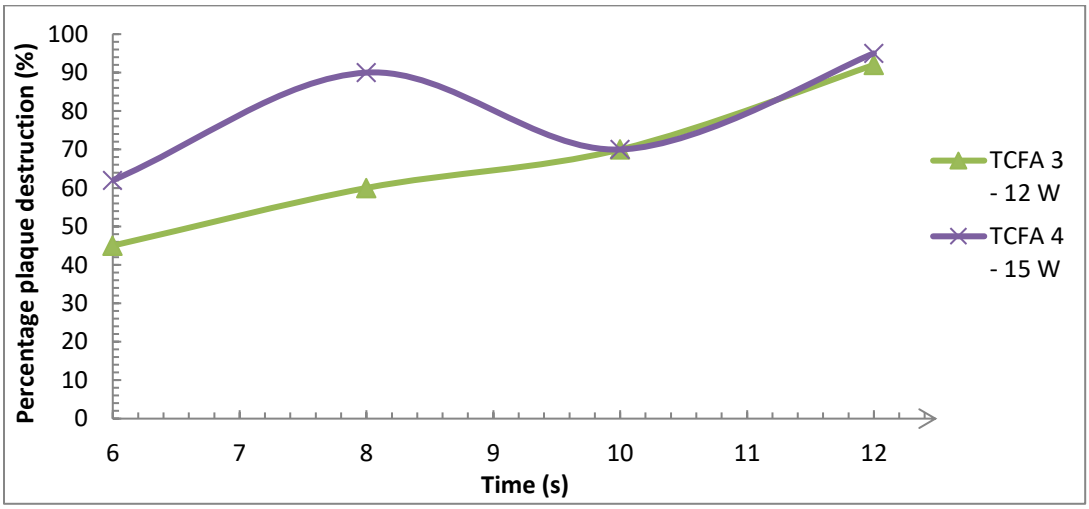

Figure 4.30: The percentage plaque destruction against time for TCFA plaque phantoms and 6-12 s sonication times.

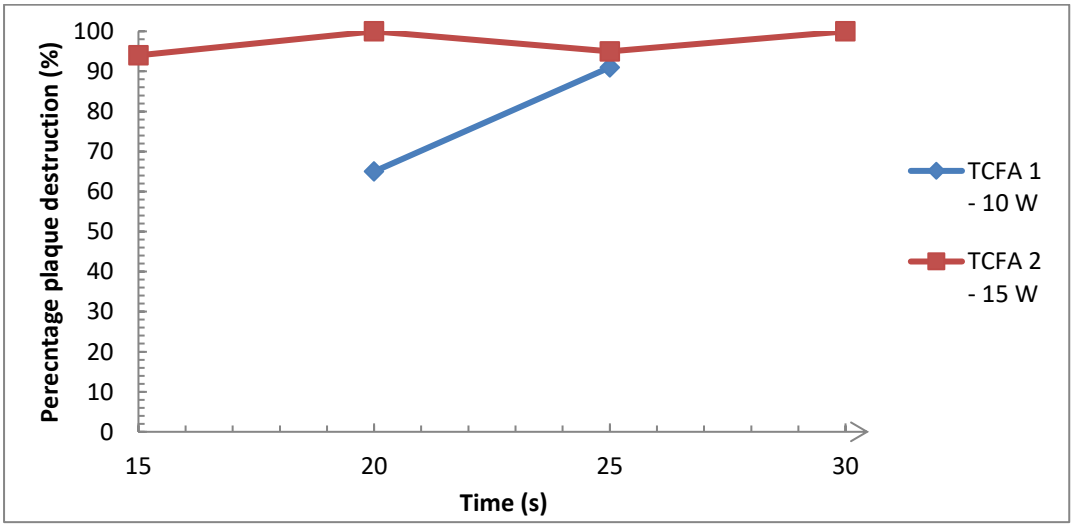

Figure 4.31: The percentage plaque destruction against time for TCFA plaque phantoms and 15-30 s sonication times.

TCFA plaques are often ruptured in comparison with other types of plaques and so the investigation for atherosclerotic plaque phantoms should be focused on this type of plaque,

especially for future work. For our study two different combinations of sonication time and acoustical power have been evaluated. The first investigation assessed the 12 W and 15 W acoustical powers with the same 6 s to 12 s sonication time interval. The minimum percentage destructions were 45 % and 62 % for 12 W and 15 W acoustical powers and 6 s sonication time respectively. The maximum percentage destructions were 92% and 95% for 12 W and 15 W acoustical powers and 12 s sonication time respectively. These results are very promising as the evaluation showed that the optimum treatment maximized the percentage of plaque destruction to 95 % and minimized the sonication time to 12 s. In future clinical trials the transducer will be incorporated in a catheter which will be inserted intravascular (1-3 mm) wide and can be used to treat atherosclerotic plaques in the coronary arteries, creating close to 50 % plaque destruction for 6 s and close to 100 % for 12 s respectively.

All atherosclerotic plaque phantoms with their ingredients, acoustical powers, sonication times, average lesion depths and percentage plaque destructions are summarized on table 4.15. The percentage plaque destruction against time for all the phantoms is given in figure 4.33.

Table 4.15: Fibrotic, PIT, TCFA, ThCFA and FC phantoms with their ingredients, acoustical powers, sonication times, average lesion depths and percentage plaque destructions.

Plaque phantom	**Fib 1**	**PIT 1**	**Fib 2**	**PIT 2**	**Fib 3**	**PIT 3**
Agar (%w/v)	4	4	4	4	4	4
Gypsum (%w/v)	1	1	1	1	1	1
Butter (%w/v)	2	20	2	20	2	20
Water (%)	93	75	93	75	93	75
AcousticalPower (W)	8	8	6	6	8	8
Sonicationtime (s)	30	30	30	30	15-25	20-30
Average lesion depth (mm)	2.2	0.86	1.62	0	0.60-1.45	0.75-1.69
Percentage destruction (%)	100	30	70	0	21-56	33-56
Plaque phantom	**Fib 4**	**PIT 4**	**Fib 5**	**PIT 5**	**PIT 6**	**TCFA 1**
Agar (%w/v)	4	4	4	4	4	4
Gypsum (%w/v)	1	1	1	1	1	10
Butter (%w/v)	10	25	10	25	20	18
Water (%)	85	70	85	70	75	68
Acoustical Power (W)	8	8	10	10	10	10
Sonication time (s)	15-30	15-30	15-30	15-30	20-25	20-25
Average lesion depth (mm)	0.43-1.73	0-0.73	1.19-1.51	0.53-1.01	1.37-2.09	1.66-2.09
Percentage destruction (%)	17-67	0-30	36-57	20-38	58-85	65-91

Plaque phantom	ThCFA 1	FC	PIT 7	TCFA 2	TCFA 3	TCFA 4
Agar (%w/v)	4	4	4	4	4	4
Gypsum (%w/v)	7	50	1	10	10	10
Butter (%w/v)	2.5	10	20	18	18	18
Water (%)	86.5	36	75	68	68	68
Acoustical Power (W)	10	10	15	15	12	15
Sonication time (s)	20-25	20-25	15-30	15-30	6-12 s	6-12 s
Average lesion depth (mm)	0.80-1.29	0	0.72-2.61	2.33-2.38	0.72-2.61	2.33 - 2.38
Percentage destruction (%)	31 - 49	0	29-98	94-100	45-92	62-95

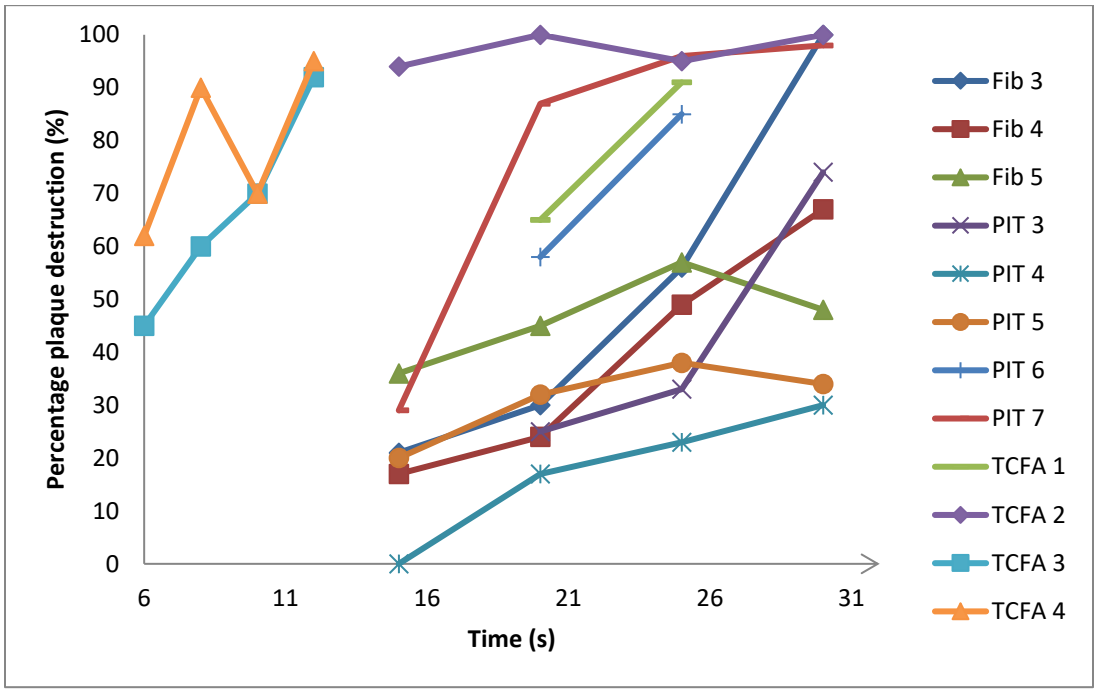

Figure 4.32: The percentage plaque destruction against time for all the phantoms.

All atherosclerotic plaque phantoms with their ingredients, ultrasonic parameters, average lesion depths and percentage plaque destructions are summarized on table 4.15 and figure 4.33. ThCFA and FC plaque phantoms were not included on previous discussions. The percentage plaque destruction for FC plaque phantoms was zero, mainly because of the very high percentage of gypsum (50%) that mimics calcium. In future trials a much lower percentage of gypsum should be used, for identifying the relationship between percentage plaque destruction and gypsum and how different percentages of gypsum would affect the average lesion depth. ThCFA

plaque phantoms are different from TCFA plaque phantoms mainly due to the size of the fibrous cap (<65µm for TCFA) and different percentage of plaque components. For our investigation, ThCFA 1 had a decrease of 3% w/v gypsum and 15.5% w/v butter in comparison with TCFA 1. The results showed that the percentage plaque destruction for ThCFA 1 related to TCFA 1 phantom was 34 % smaller for 10 W acoustical power and 20 s sonication time and 42% smaller for 10 W acoustical power and 25 s sonication time. Only two phantoms were totally destructed. Fib 1 phantom was destructed 100% with 8 W acoustical power and 30 s sonication time while TCFA 2 phantoms was destructed 100 % with 15 W acoustical power and 20 s sonication time.

Two plaque phantoms (11.1%) were not affected by the ultrasound waves, 16 plaque phantoms (89 %) were destructed by at least 30 %, 12 plaque phantoms (66.7 %) were destructed by at least 50 %, 8 plaque phantoms (44.4%) were destructed by at least 70 %, 6 plaque phantoms (30%) at least 90% and 2 (11.1%) destructed 100 %.The percentage plaque destruction against number of phantoms is given in fig. 4.34. The red colour represents the minimum percentage plaque destruction. Fig. 4.35 shows the percentage of phantoms and the corresponding range of average lesion depths. The maximum average lesion depth from all the phantoms was 2.61mm for PIT 7 and TCFA 3 respectively. The minimum average lesion depth was 0.43 mm for fib 4 plaque phantom. Figure 4.35 shows the average lesion depth range with the percentage of phantoms.

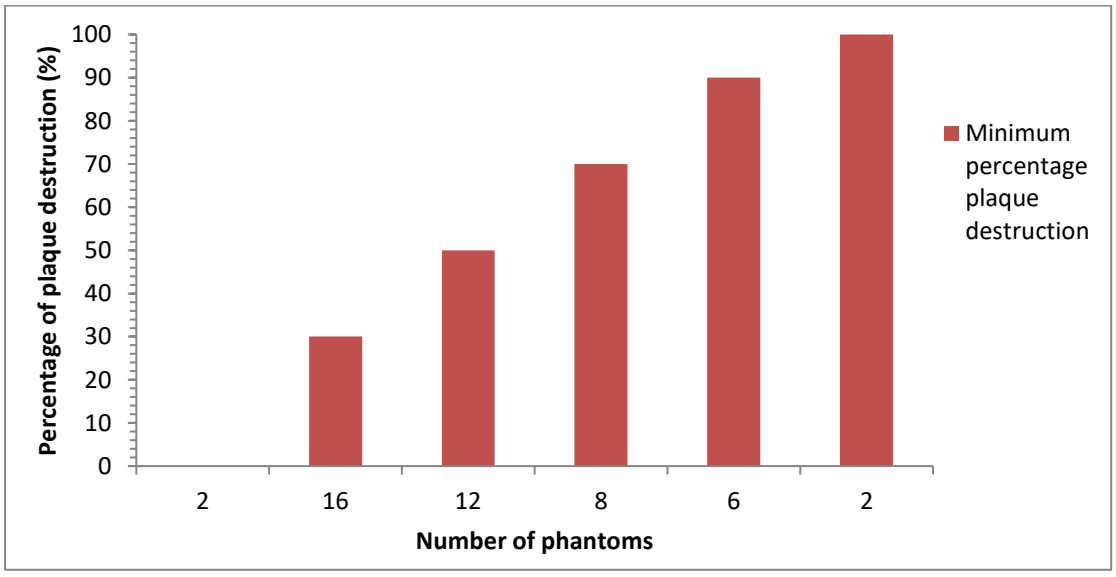

Figure 4.33: The percentage plaque destruction against number of phantoms.

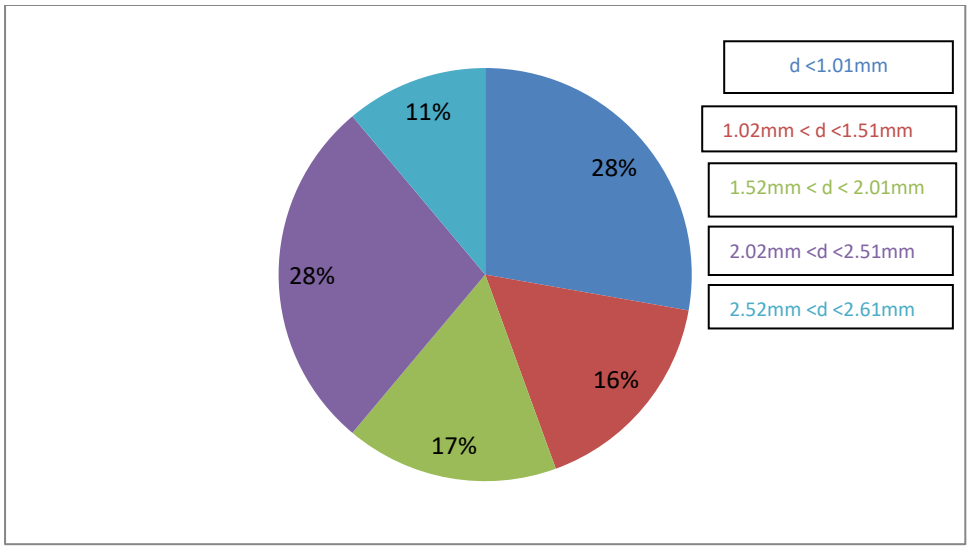

Figure 4.34: The percentage of phantoms and the corresponding range of average lesion depths.

5. Porcine atherosclerotic plaque phantoms for US therapy

5.1 Introduction

The following chapter describes the creation and evaluation of porcine atherosclerotic plaque phantoms for ultrasound therapy. Abdominal porcine arteries were selected rather than coronary arteries because the lumen of the artery was much larger and the transducer holder could fit inside them. The lumen of porcine coronary arteries was close to 3 mm while the lumen of porcine abdominal arteries was between 12 mm to 14 mm. The elastic properties of porcine arteries mimic the elasticity of human arteries. The experimental setup and methods are presented in the following sections.

5.2 Porcine PIT and TCFA plaque phantoms with 10 W acoustical powers and different treatment times

Materials and methods

The next step of our evaluation was focused on porcine PIT and TCFA atherosclerotic plaque phantoms. The acoustical power was 10 W and the plaque phantoms were assessed for 15 – 30 s time interval. The amount of plaque removal was evaluated visually and using an X-Ray system. The recipe of the PIT atherosclerotic plaque phantom was 4% w/v agar, 1% w/v gypsum, 20% w/v butter and 75% water. For TCFA were 4% w/v agar, 10% w/v gypsum, 18% w/v butter and 68% water. Four freshly abdominal excited porcine arteries were used for this experiment. The arteries were cut in 60 mm length for investigating atherosclerotic plaque phantoms for ultrasound therapy. Fig. 5.1A shows the horizontal length of the arteries, fig. 5.1Bshows the vertical length of the arteries and fig. 5.1C shows the lumen of the arteries.

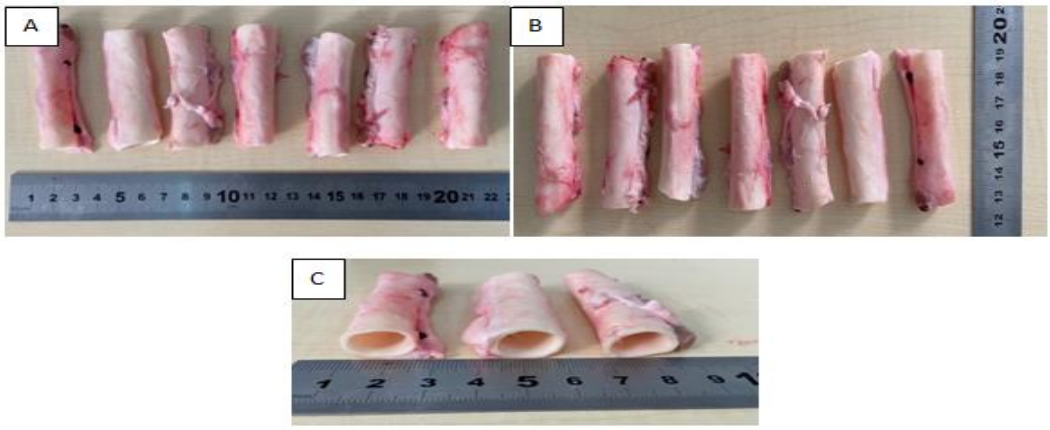

Figure 5. 1: A) The horizontal length, B) The vertical length and C) The lumen of the porcine arteries.

The atherosclerotic plaque phantoms poured into the arteries and the two ends were tightening up with plastic strips. A white plastic tube was used for creating the lumen of the artery. Fig.5.2 shows the porcine arterialatherosclerotic plaque phantoms.

Figure 5. 2: Porcine atherosclerotic plaque phantoms.

Figure 5.3 shows the experimental setup for investigating the ability of therapeutic ultrasound to ablate atherosclerotic plaque.

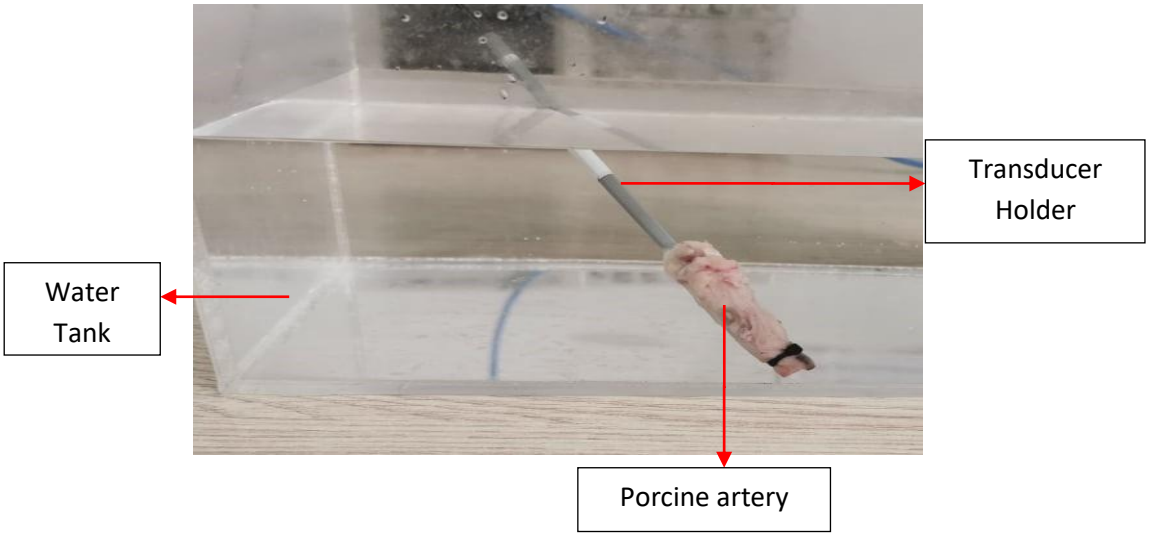

Figure 5. 3: The experimental setup for ablating porcine atherosclerotic plaque phantoms with ultrasound.

The next step of the experiment was to access the ablation of the porcine arterial plaque phantom using X-Ray imaging. Figure 5.4 shows the vertical position of the arterial atherosclerotic plaque phantoms at the CR reader for acquiring the X-Ray image.

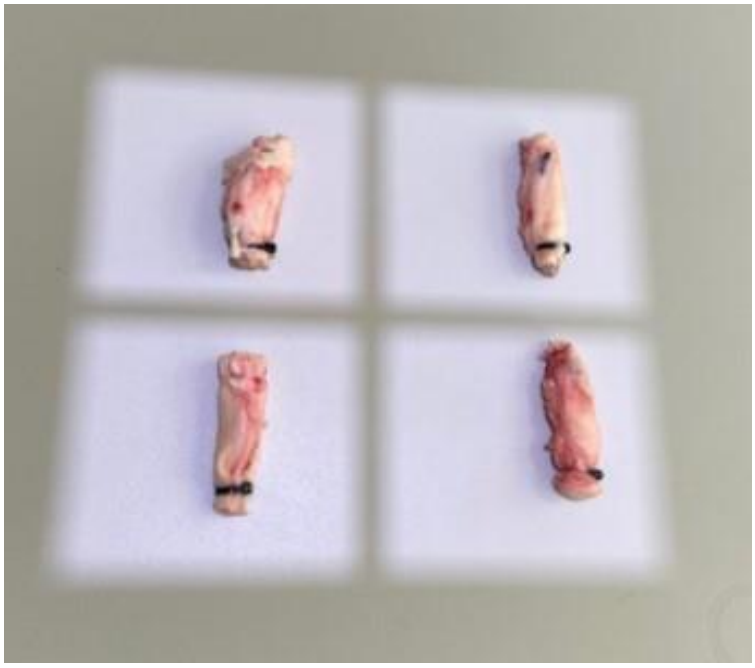

Figure 5. 4: Acquiring X-Ray images for porcine arterial atherosclerotic plaque phantoms.

Thermal mode was used for ablating atherosclerotic plaque using different ultrasonic parameters. Table 5.1 shows the ultrasonic parameters used for each PIT and TCFA phantom.

Table 5. 1: Ultrasonic parameters used for each PIT and TCFA phantom.

Phantom	Atherosclerotic plaque type	Power (W)	Time (s)
1	PIT	10	30
2	PIT	10	25
3	PIT	10	20
4	PIT	10	15
5	TCFA	10	30
6	TCFA	10	25
7	TCFA	10	20
8	TCFA	10	15

Results

Figure 5.5 shows the X-Ray images for the porcine PIT atherosclerotic plaque phantoms before (5.5A-D) and after (5.5E-H) thermal ablation with ultrasound. The acoustical power was 10 W. Fig. 5.5E shows the depth of the lesion that was close to 2.49 mm for 30 s. Fig. 5.5F shows that the depth of the lesion was almost 1.90 mm for 25 s. Fig.

5.5G shows the depth of the lesion was close to 1.12 mm for 20 s. Fig. 5.5H shows the depth of the lesion was almost 0.90 mm for 15 s.

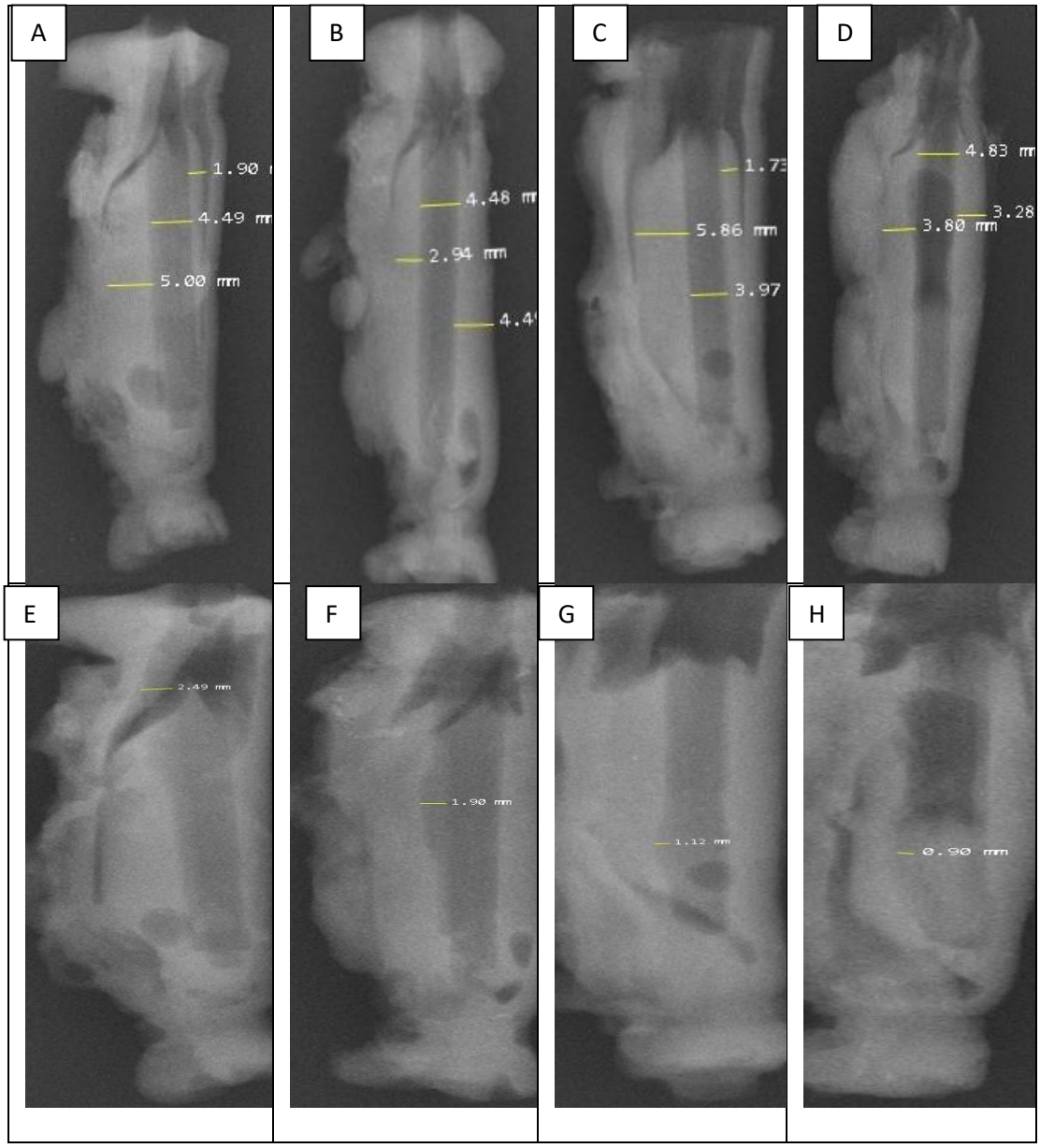

Figure 5.5: The X-Ray images for the porcine PIT atherosclerotic plaque phantoms before (A-D) and after (E-H) thermal ablation with ultrasound. The acoustical power was 10 W.

Figure 5.6 shows the X-Ray images for the porcine TCFA atherosclerotic plaque phantoms before (5.6A-D) and after (5.6E-F) thermal ablation with ultrasound. The acoustical power was 10 W. Fig. 5.6E shows the horizontal X-Ray image of the first TCFA phantom after the ultrasonic ablation. The depth of the lesion was close to 1.05 mm for 30 s. Fig. 5.6F shows the horizontal X-Ray image of the second TCFA phantom after ultrasonic

ablation. The depth of the lesion was almost 1.25 mm for 25 s. No destruction was created for the last two TCFA phantoms.

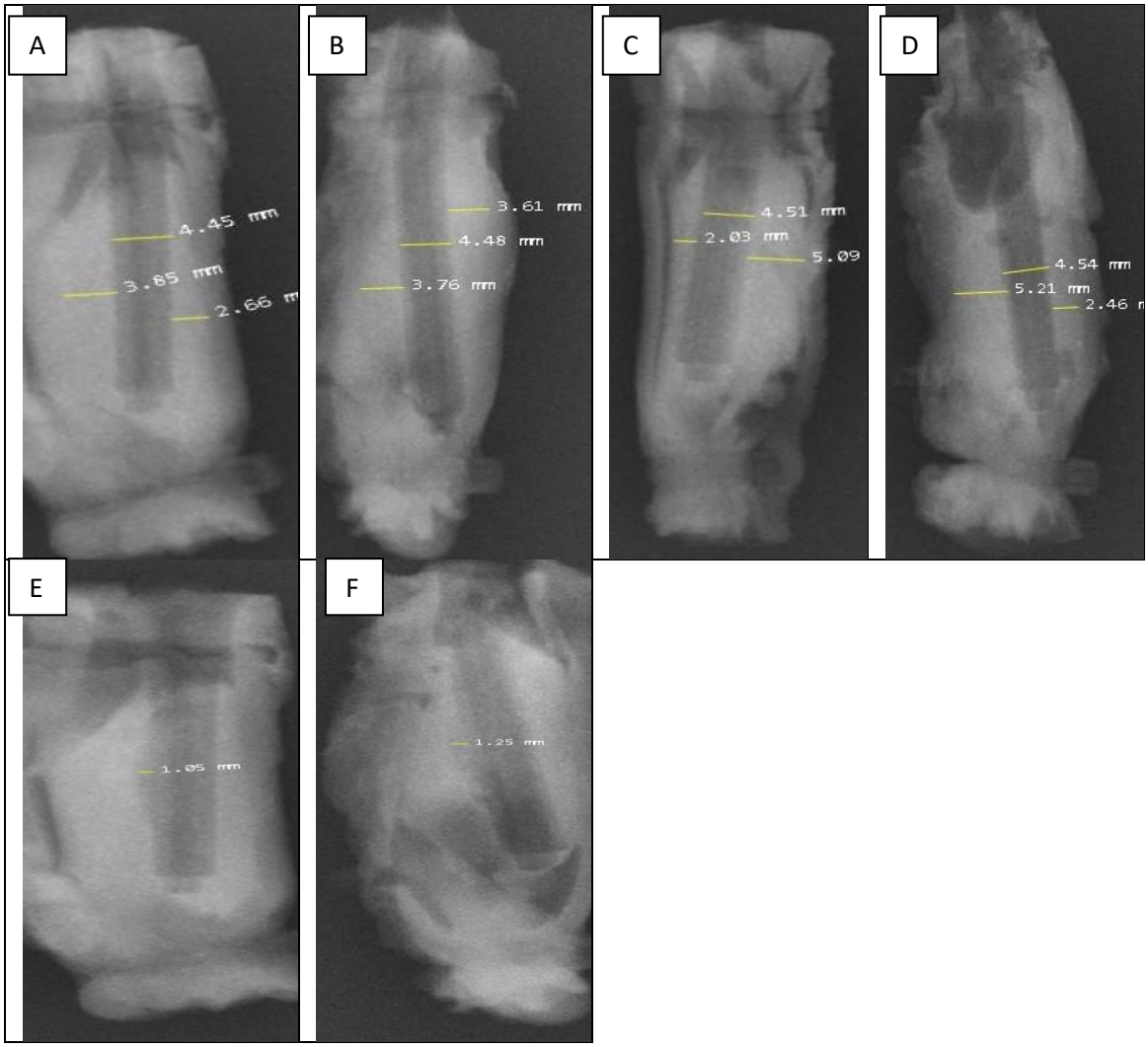

Figure 5.6: The X-Ray images for the porcine TCFA atherosclerotic plaque phantoms before (A-D) and after (E-F) thermal ablation with ultrasound. The acoustical power was 10 W.

Figure 5.7 shows the lesion depth against time for the PIT and TCFA plaque phantoms. The acoustical power was 10 W. The red and blue line corresponds to PIT and TCFA respectively.

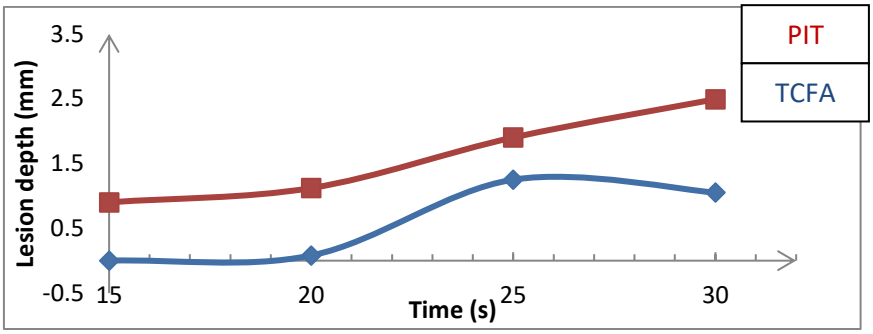

Figure 5.7: The lesion depth against time for the PIT and TCFA plaque phantoms. The acoustical power was 10 W.

Conclusions

An investigation of porcine arterial atherosclerotic plaque phantoms for medical imaging and therapy was made during this experiment. The results showed that PIT and TCFA porcine arterial atherosclerotic plaque phantoms were properly ablated by thermal ultrasound. No destruction was shown in TCFA phantoms for 15 s and 20 s sonication times and 10 W acoustical powers. The higher destruction was shown in PIT phantom with acoustical power of 10 and 30 s sonication times. The size of the lesion for the atherosclerotic plaque phantom is similar to 2x10 mm^2size of the transducer. The size of the lesion depends on sonication time. As the sonication time increases, the depth of the lesion increases. TCFA phantom seems to follow a different way as up to 20 s no destruction was detected and after 30 s the depth of lesion decreased. The X-Ray images of the porcine arterial plaque phantoms have shown that the porcine arterial plaque phantoms were properly mimicked.

5.3 Porcine PIT and TCFA plaque phantoms with 15 W acoustical power and different treatment times

Materials and methods

The next step of our evaluation was focused on porcine PIT and TCFA atherosclerotic plaque phantoms with 15 W acoustical powers and 15 – 30 s sonication times. The amount of plaque removal was evaluated visually and using an X-Ray system. The recipe of the PIT atherosclerotic plaque phantom was agar 4% w/v, gypsum 1% w/v, butter 10% w/v and 85% water. For TCFA were agar 4% w/v, gypsum 10% w/v, butter 18% w/v and 68% water.

Results

Thermal mode was used for ablating atherosclerotic plaque using different ultrasonic parameters. Table 5.2 shows the ultrasonic parameters used for each PIT and TCFA phantom with 15 W acoustical powers.

Table 5.2: The ultrasonic parameters used for each PIT and TCFA phantom with 15 W acoustical powers and the average lesion depth.

Phantom	Atherosclerotic plaquetype	Power (W)	Time (s)	Average depth of the lesion (mm)
1	PIT	15	15	2.00
2	PIT	15	20	1.52
3	PIT	15	25	2.94
4	PIT	15	30	0.93
5	TCFA	15	15	0.97
6	TCFA	15	20	1.33
7	TCFA	15	25	1.75
8	TCFA	15	30	2.90

Figure 5.8 shows the lesion depth against time for the PIT and TCFA plaque phantoms. The acoustical power was 15 W. Figure 5.9 shows the lesion depth against time for the PIT and TCFA plaque phantoms. The acoustical power was 10 W and 15 W respectively.

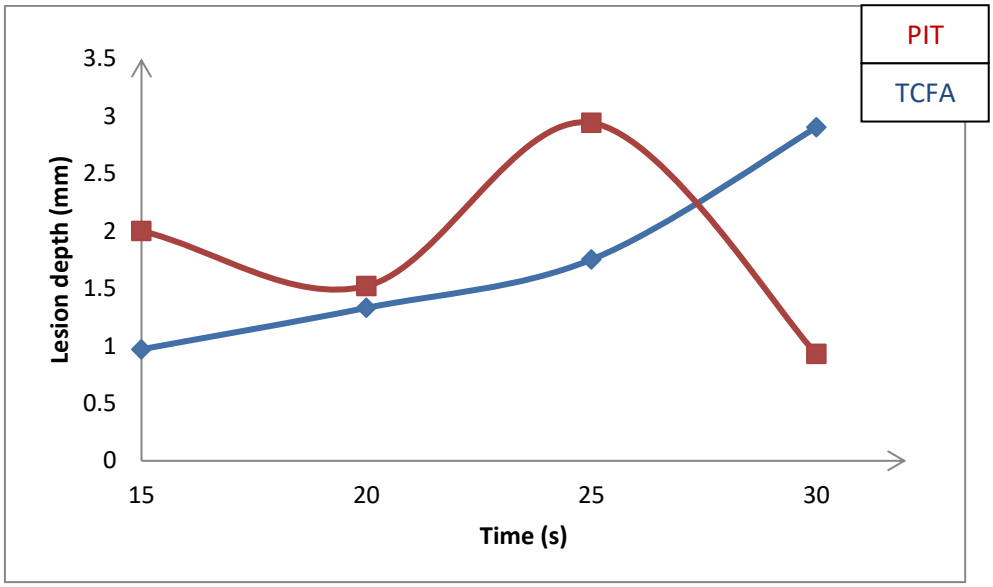

Figure 5.8: The lesion depth against time for the PIT and TCFA plaque phantoms. The acoustical power was 15 W.

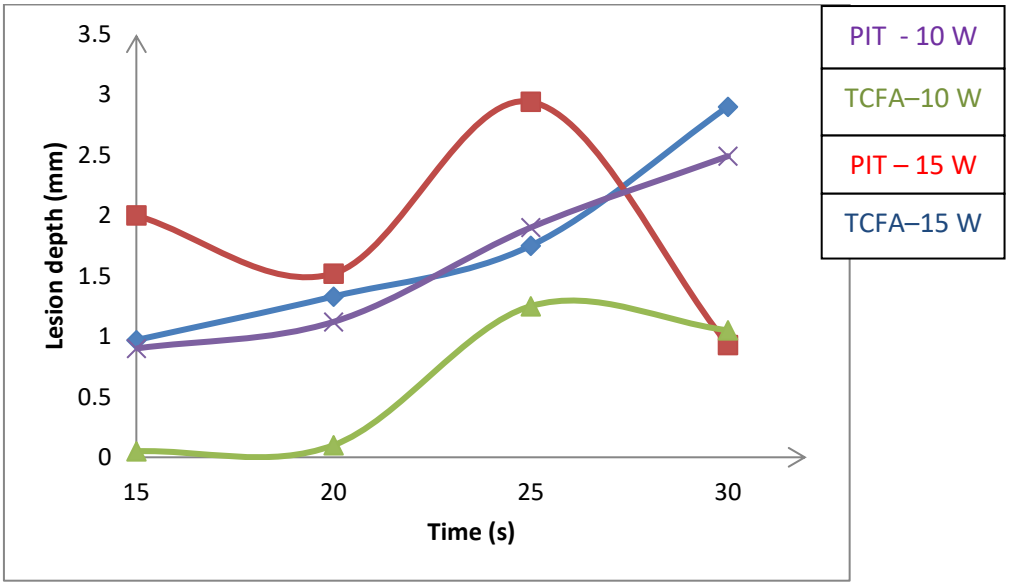

Figure 5.9: The lesion depth against time for the PIT and TCFA plaque phantoms. The acoustical power was 10 W and 15 W respectively.

Conclusions

An investigation of porcine arterial atherosclerotic plaque phantoms for medical imaging and therapy was made during this experiment. The results showed that PIT and TCFA porcine arterial atherosclerotic plaque phantoms were properly ablated by thermal

ultrasound. Similar results have been detected on PIT phantoms for 20 s and 30 s sonication times and 15 W acoustical powers. The size of the lesion for the atherosclerotic plaque phantom is similar to 2x10 mm^2 size of the transducer. The size of the lesion depends on sonication time. As the sonication time increases, the depth of the lesion increases mainly for the TCFA phantom. For the PIT phantom and 30 s sonication time a decrease of close to 2 mm average lesion depth detected. The higher lesion 2.95 mm depth was shown in PIT atherosclerotic plaque phantom with acoustical power of 15 W for 25 s sonication time. The second higher lesion 2.90 mm depth was shown in TCFA atherosclerotic plaque phantom with 15 W acoustical power and 30 s sonication time. The X-Ray images of the porcine arterial plaque phantoms have shown that the porcine arterial plaque phantoms were properly mimicked.

5.4 Discussion

In this chapter the creation and evaluation of porcine atherosclerotic plaque phantoms for ultrasound therapy was described. Abdominal porcine arteries were selected rather than coronary arteries because the lumen of the artery was much larger and the transducer holder could fit inside them. The first evaluation was focused on porcine PIT and TCFA atherosclerotic plaque phantoms which cover the main types of human atherosclerotic plaques. The results showed that PIT and TCFA porcine arterial atherosclerotic plaque phantoms were properly ablated by thermal ultrasound. No destruction was shown in TCFA phantoms for 15 s and 20 s sonication times and 10 W acoustical powers. The higher destruction was shown in PIT phantom with acoustical power of 10 W and 30 s sonication times. TCFA phantom seems to follow a different way as up to 20 s no destruction was detected and after 30 s the depth of lesion decreased. The X-Ray images of the porcine arterial plaque phantoms have shown that the porcine arterial plaque phantoms were properly mimicked.

The next step was focused on the same phantoms with 15 W acoustical power and 15-30 s sonication time.The maximum depth lesion for the PIT porcine plaque phantom was 2.94 mm for 15 W acoustical power and 25 s sonication time and for the TCFA porcine plaque phantom was 2.90 mm for 15 W acoustical power and 30 s sonication time. Moreover, the minimum depth lesion for the PIT porcine plaque phantom was 0.9 mm for 10 W acoustical power and 15 s sonication time and for the TCFA porcine plaque phantom was 0.97 mm for 15 W acoustical powers and 15 s sonication times.

5.5 Conclusion

The creation and evaluation of porcine atherosclerotic plaque phantoms for ultrasound therapy was described in this chapter. Abdominal porcine arteries were selected rather than coronary arteries because the lumen of the abdominal artery was much larger than the coronary and the transducer holder could fit inside them. The porcine arterial plaque phantoms have been properly mimicked and destructed from ultrasound as it was confirmed by X-Ray images.

6. MR Thermometry for TCFA plaque and TMM phantoms

6.1 Introduction

The following chapter describes the evaluation of atherosclerotic plaque and a tissue mimicking material (TMM) phantom for ultrasound therapy using MR thermometry which is a noninvasive temperature real time MR monitoring during minimally invasive thermal therapy as local treatment of benign and malignant diseases. The main benefits of this method is due to the attractive properties of MRI, such as its non-invasiveness, lack of ionizing radiation, and the ability to image in any scan orientation with good spatial and temporal resolution. However, it is the ability of MRI to construct maps of in vivo body temperature that make it particularly well suited for guiding and monitoring minimally invasive thermal therapy. Thermal therapy can be divided into two sections. The first is low-temperature hyperthermia, where temperatures in the range of 43–45 °C are applied for a time of several tens of minutes to kill cancer cells directly or to sensitize them to cytotoxic agents and/or radiation [231]. The second is high-temperature thermal ablation, where temperatures in the range of 50–80°C or higher are applied for a shorter amount of time to rapidly coagulate the tissue and induce necrosis through processes such as protein denaturation [232]. The goal of MR image-guided thermal therapy is to use real-time temperature mapping to provide more control over the treatment outcome. Therefore, it is not only necessary to accurately measure the temperature during treatment, but also to be able to relate treatment temperature to actual thermal tissue damage. Focused ultrasound (FUS), also referred to as high intensity focused ultrasound (HIFU), is a completely non-invasive method that uses an external transducer to focus the ultrasound beam from outside the patient without an incision [233]. Moving the focus of the beam through the tissue allows ablation of irregular shaped regions. Interstitial, transurethral [234] and transrectal ultrasound use MRI compatible, multi-element ultrasound transducers and provide spatial control over the heating area.

6.2 Evaluating ultrasound therapy for plaque phantoms using MR thermometry

Materials and methods

The purpose of this experiment was to destroy an area of a plaque-mimicking phantom using a planar transducer, obtain MR thermometry images during the sonication and observe the destroyed area of the phantom using high-resolution imaging. X-ray image was obtained and the destroyed area was confirmed. The tube and the phantom were placed in an ABS 3D-printed holder to remain at a fixed position inside the acrylic tank. The acrylic tank was filled with degassed water. The transducer was carefully placed in the tube with the

piezoelectric element facing the MRI bore. The recipe of TCFA phantom was agar 4% w/v, gypsum 10% w/v, butter 18% w/v and 68% water. Figure 6.1 shows the experimental setup as placed in the MRI scanner and figure 6.2the coronal T2-weighted Fast Spin Echo (FSE) image which was initially obtained for localization and setup checking. Main parameters used to obtain the T2-FSE image were the following: echo time (TE) =55 ms, repetition time (TR) = 3000 ms, number of averages= 0.55, echo train length (ETL) = 1, field of view (FOV) = 20 cm, slice thickness= 2 mm, matrix= 512x512, and flip angle= 90^{o}.

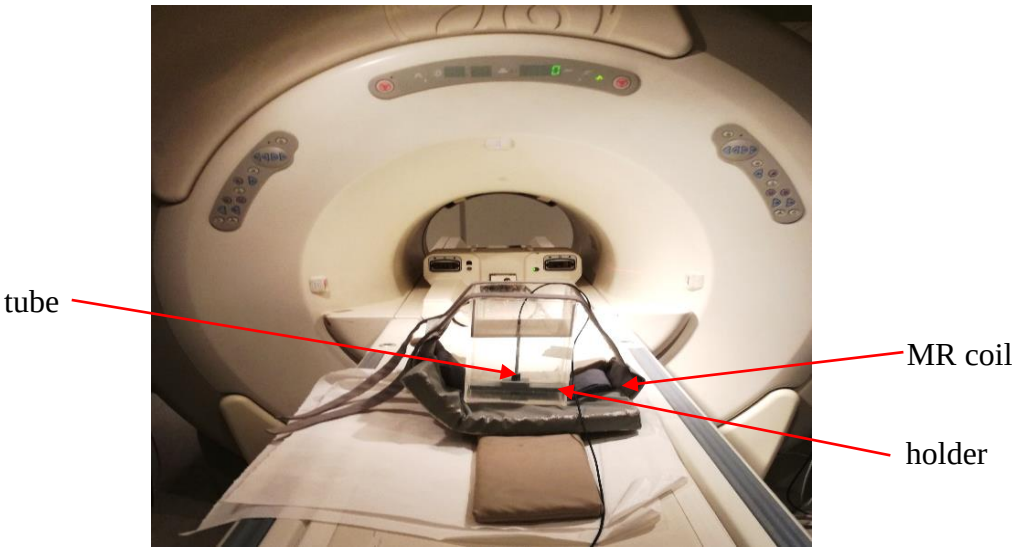

Figure 6.1: Experimental setup in the MRI room.

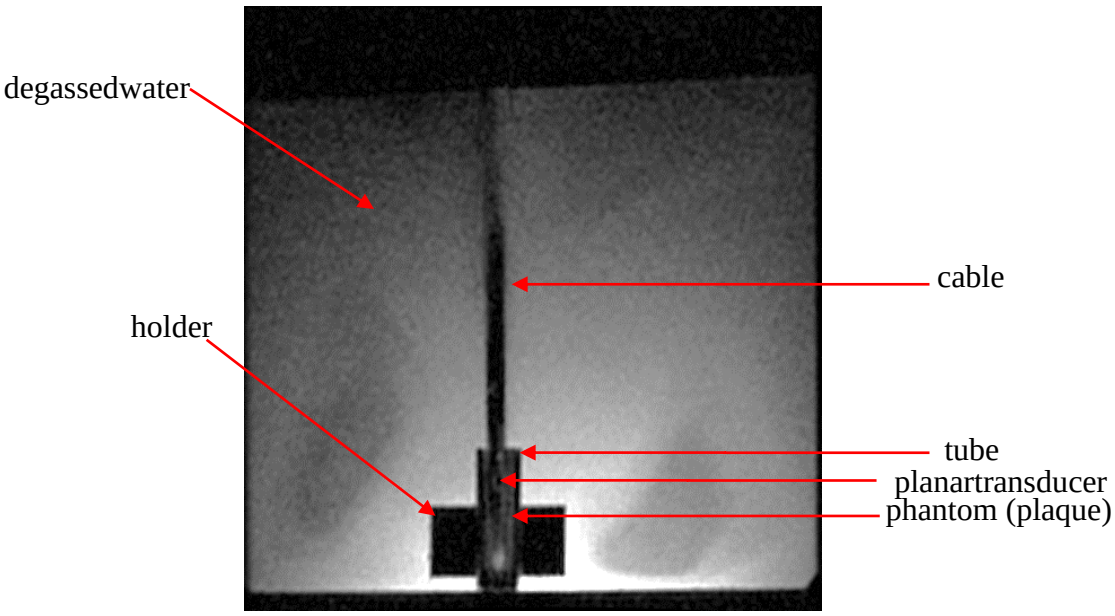

Figure 6.2: T2-FSE image of experimental setup.

Results

MR thermometry images were obtained in sagittal plane in order to monitor the temperature change in the phantom. Acoustic powers of 5 W (voltage 80 mV) and 10 W (voltage 160 mV) were applied to the phantom for 30 s sonication time. Figure 6.3 shows the temperature maps produced after data processing which was obtained on sagittal plane for 5 W acoustic power using single-shot echo-planar imaging (EPI) gradient echo (GRE) multiphase sequence and figure 6.4 shows the corresponding temperature change versus time as calculated from the MR thermometry images. Main parameters used to obtain these images were: TE = 63.1 ms, TR= 272 ms, number of averages = 8, ETL= 1, FOV= 20 cm, slice thickness = 2 mm, matrix= 128x128, and flip angle = 30^{o}.

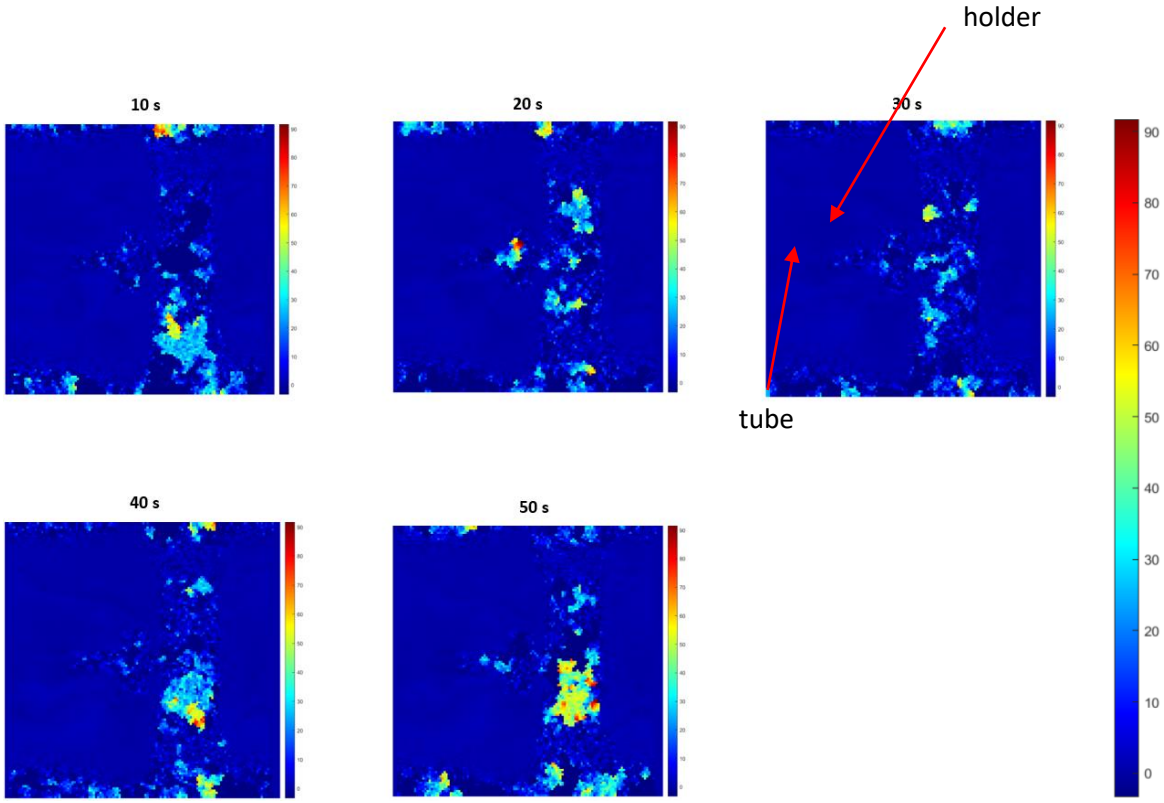

Figure 6.3: Temperature maps (sagittal plane) recorded using single-shot EPI sequence and the transducer (f=4.01 MHz, Pa= 5 W, voltage= 80 mV) for sonication of 10 s, 20 s, 30 s and cooling-off time of 10 s, and 20 s.

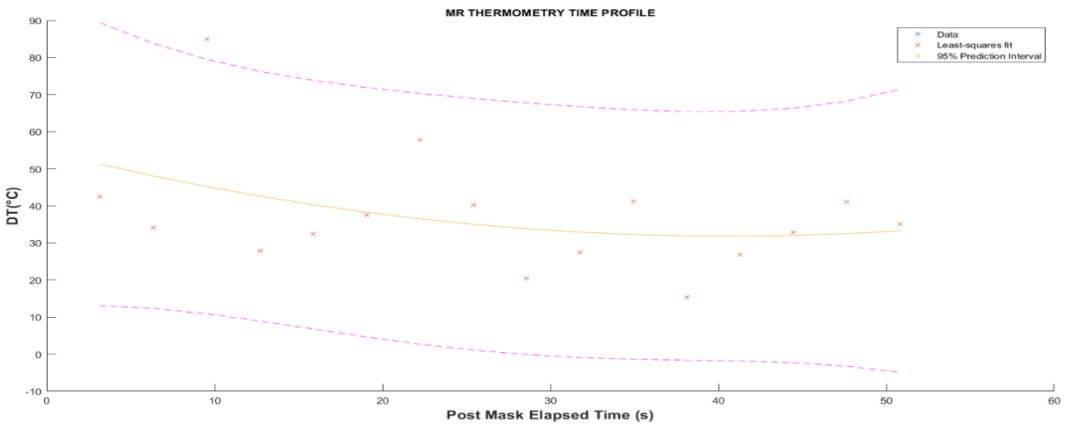

Figure 6.4: Temperature change versus sonication time as calculated from the above sagittal plane MR images with acoustical power of 5 W (voltage= 80 mV).

Figure 6.5 shows the temperature maps produced after data processing and which were obtained on sagittal plane for acoustic power of 10 W (voltage160 mV) using the EPI single-shot sequence and figure 6.6shows the corresponding temperature change versus time as calculated from the MR thermometry images.

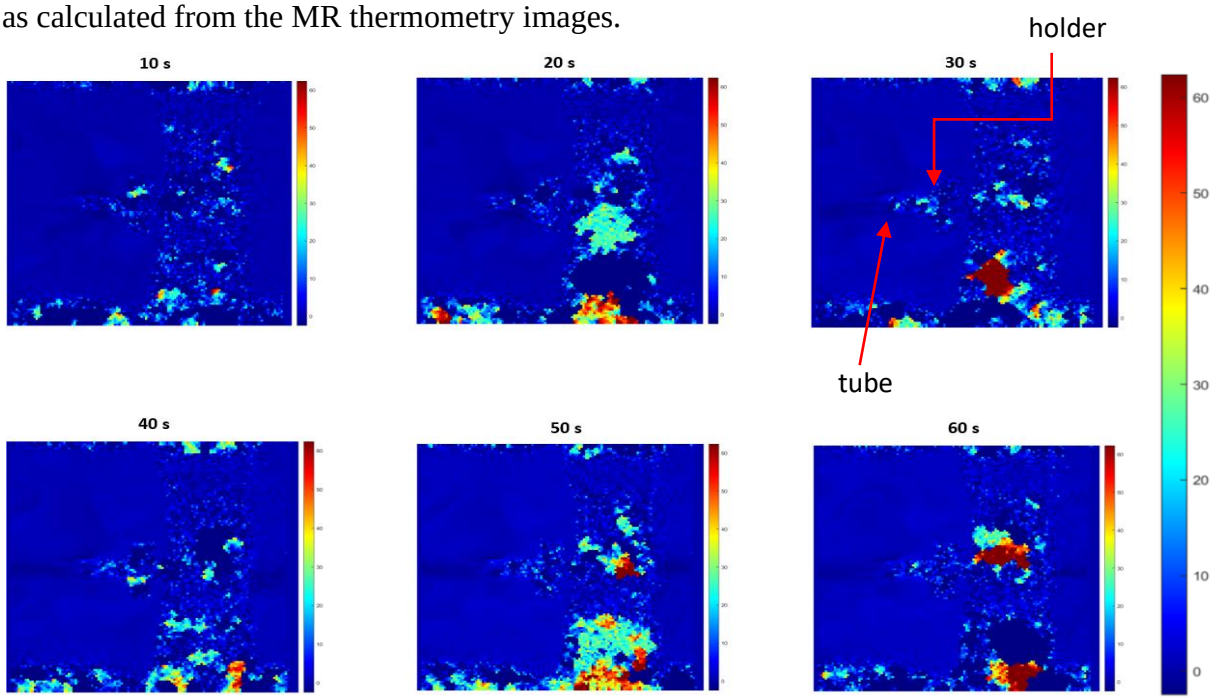

Figure 6.5:Temperature maps (sagittal plane) recorded using single-shot EPI sequence and the transducer (f=4.01 MHz, Pa= 10 W, voltage= 160mV) for sonication of 10 s, 20 s, 30 s and cooling-off time of 10 s, 20 s, and 30 s.

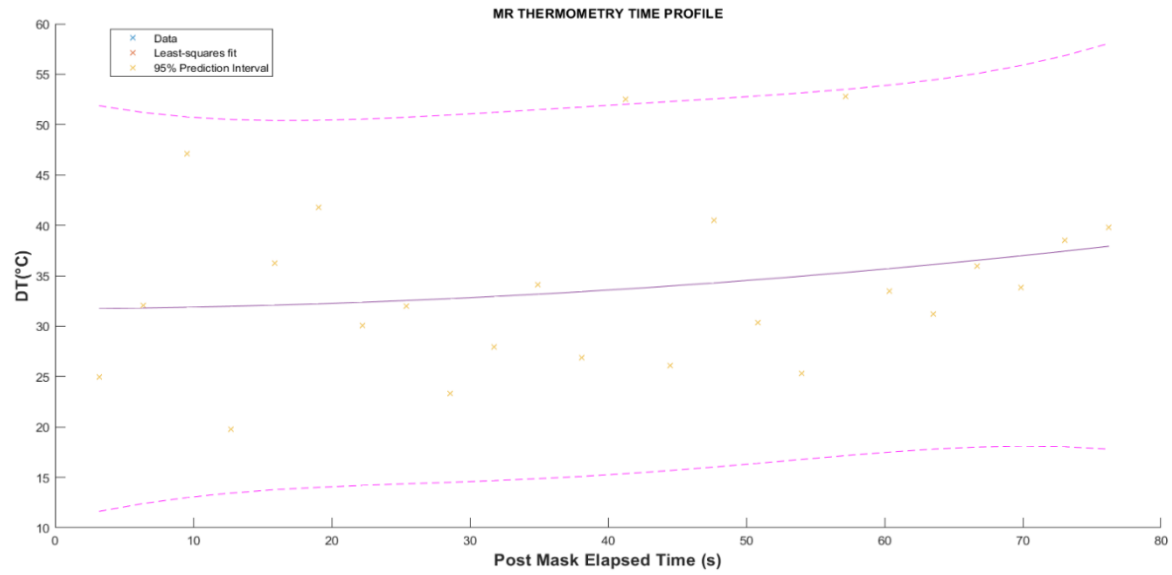

Figure 6.6: Temperature change versus sonication time as calculated from the above sagittal plane MR images with acoustical power of 10 W (voltage= 160mV).

After the sonication, a T2-FSE image was acquired on coronal plane in order to detect and measure possible destruction of the mimicking plaque phantom. The destroyed area of the phantom was observed as shown in figure 6.7.

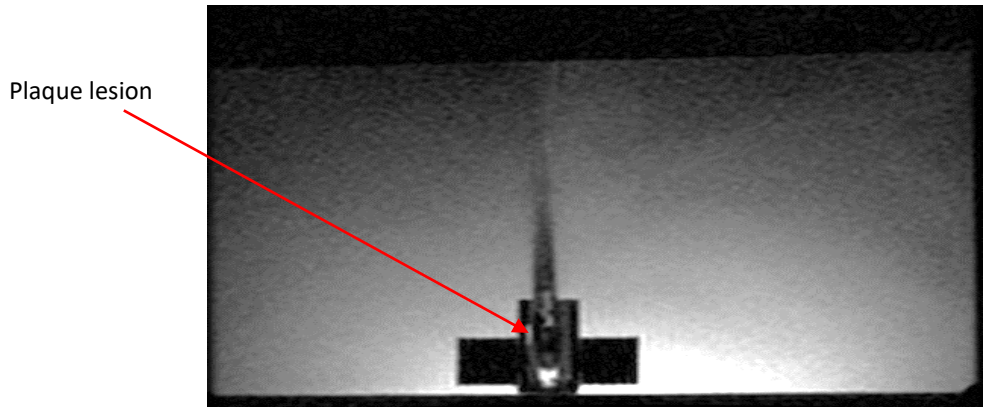

Figure 6.7: T2-FSE image (sagittal plane) that was obtained after the completion of the sonication.

Figure 6.8 shows the length of the destroyed area of the plaque-mimicking phantom after the sonication as measured using a DICOM software tool (RadiAntDicom Viewer). The size of the lesion for the atherosclerotic plaque phantom was 9.08 mm and it was similar to 2x10 mm^2 size of the transducer.

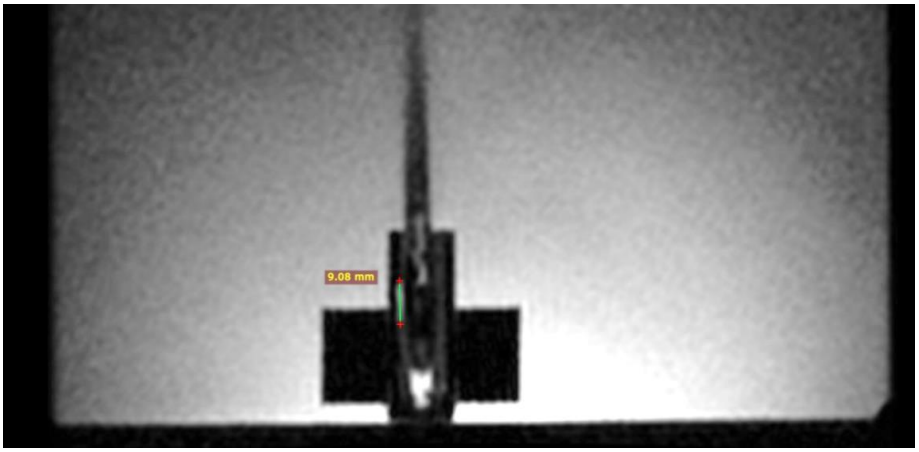

Figure 6.8: Measurement of the destroyed area after the sonication.

Another phantom was sonicated for 30 s and acoustic power of 10 W (voltage 160 mV). Figure 6.9 shows the phantom before the sonication and figure 6.10 shows the phantom after the sonication. The plaque lesion appeared bright since the whole setup was immersed in degassed water and the destroyed area was possibly covered with water. This can be an advantage to observe the destroyed area after a sonication.

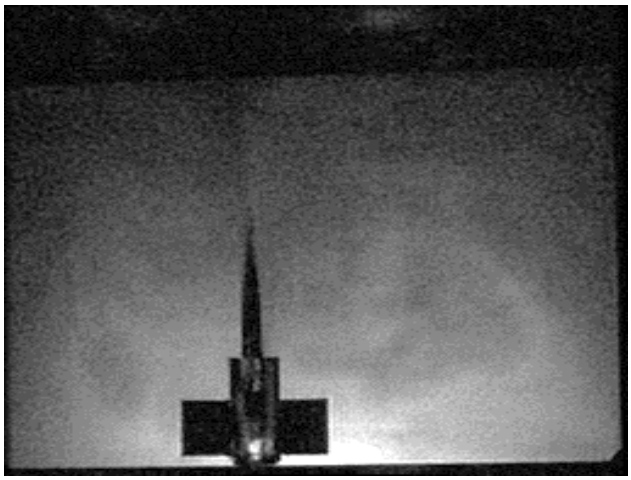

Figure 6.9: T2-FSE image (sagittal plane) before the sonication.

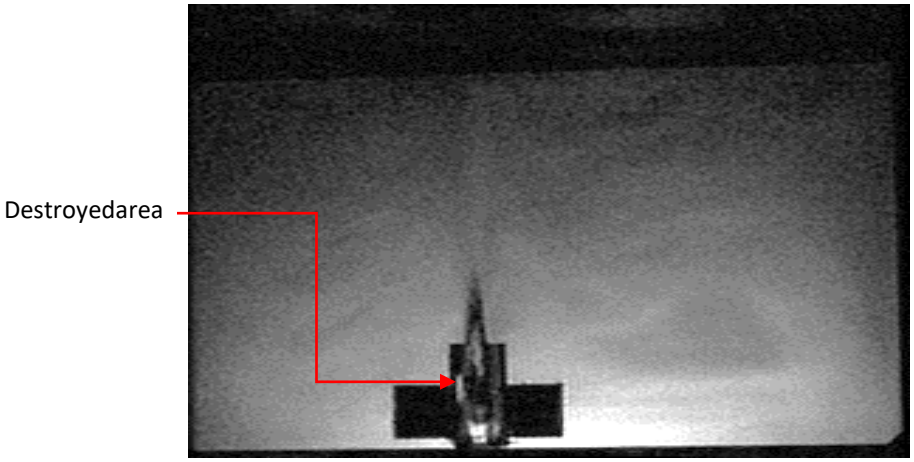

Figure 6.10:T2-FSE image (sagittal plane) after the completion of the sonication.

Figure 6.11 shows the length of the destroyed plaque-mimicking phantom after the sonication as measured using a DICOM software tool (RadiAntDicom Viewer). The size of the lesion for the atherosclerotic plaque phantom was 1.01cm and it was similar to 2x10 mm^2 size of the transducer.

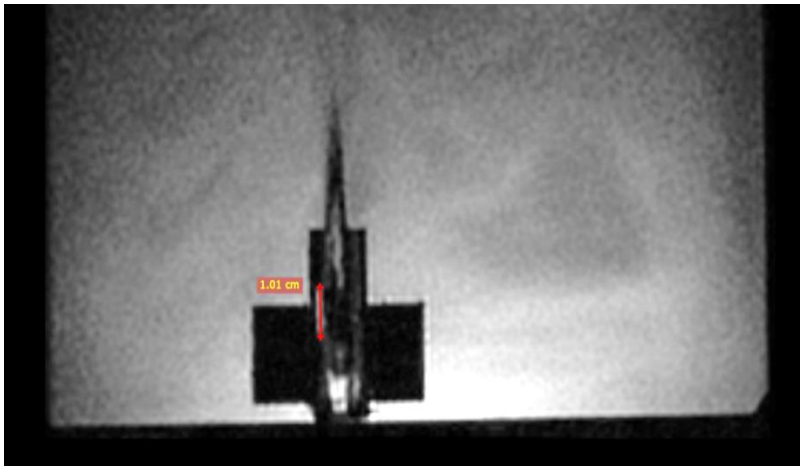

Figure 6.11: Plaque lesion length for 10 W acoustical power and 30 s sonication time.

An X-ray image of the phantom after the sonication was also acquired as shown in figure 6.12.The X-Ray parameters used for acquiring the image was 50 kV voltages, 45 mA current, 45 ms time of exposure and 2 mAs. The X-Ray image confirmed the destruction of the atherosclerotic plaque phantom. The difference that was created between the lumen of the artery and the thickness of the tube was the lesion of the atherosclerotic plaque phantom. The average lesion depth was 1.77 mm.

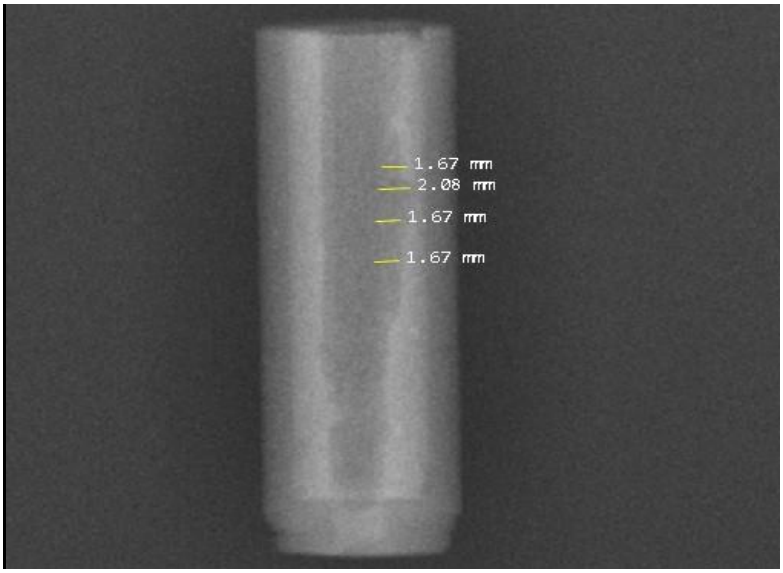

Figure 6.12: X-ray image of the phantom after the sonication.

Conclusions

Sonications using a planar transducer were performed on a plaque-mimicking phantom. The size of the tube that mimics the artery and the phantom that mimics the plaque

was a challenge for MR thermometry results. The minimum slice which the MRI could obtain was2 mm thickness, thus the temperature change using MR thermometry was difficult to be achieved. However, from the T2-FSE images was possible to observe and measure the length of plaque lesion in the tube. The destruction area was also confirmed through an X-ray image. The average lesion depth was 1.77 mm for 30 s sonication time and acoustic power of 10 W (voltage 160 mV).The size of the lesion for the atherosclerotic plaque phantom was similar to 2x10 mm^2 size of the transducer. The size of the lesion was evaluated with the same accuracy with X-Ray image and T2W-FSE image (sagittal plane). The depth of the lesion was evaluated more precisely with the X-Ray image.

6.3Heating of a tissue mimicking material TMM phantom using a planar transducer and monitoring it with MR thermometry

Materials and methods

An evaluation of heating a tissue mimicking material (TMM) phantom using a planar transducer as a model for cardiac applications has been done. The heating effect was monitored using MR thermometry. The recipe of the TMM phantom was 2% w/v agar and 25% v/v evaporated milk. The transducer was operating at 4.0 MHz ($\pm$5%). The experimental setup is shown in fig. 6.13.

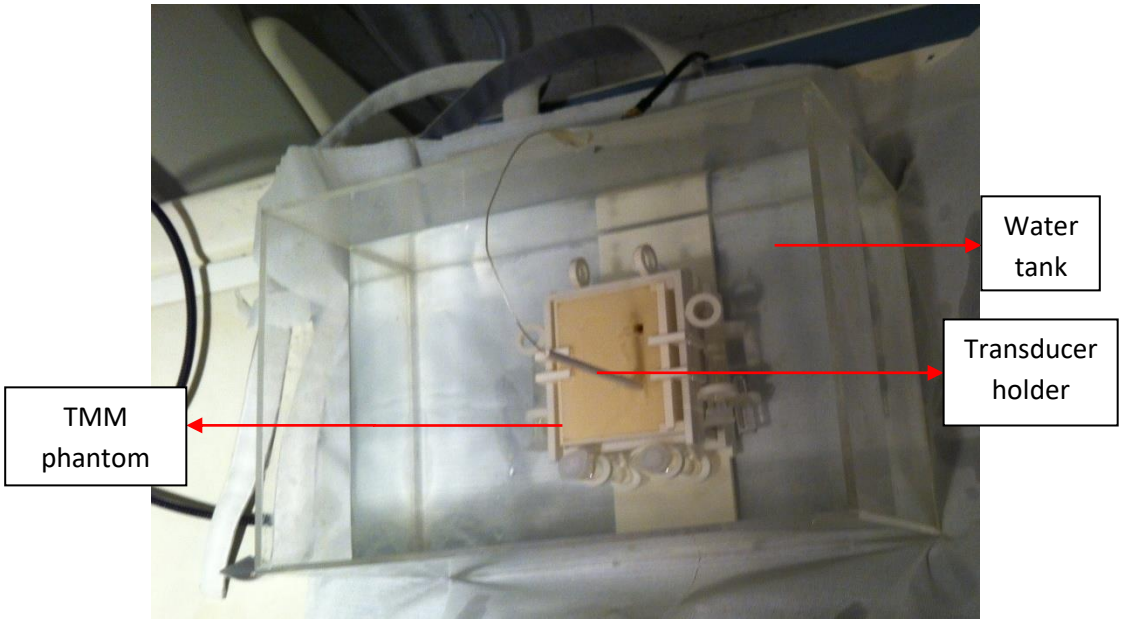

Figure 6.13: Experimental setup for investigating heating of a TMM phantom using a planar transducer.

TMM phantom was sonicated with 5 W and 15 W acoustical power levels respectively. MR thermometry was repeated for different orientations and slice thickness.

The sonication time was 60 s. Fig. 6.14 shows the T2 FGRE image of our transducer embedded inside TMM phantom.

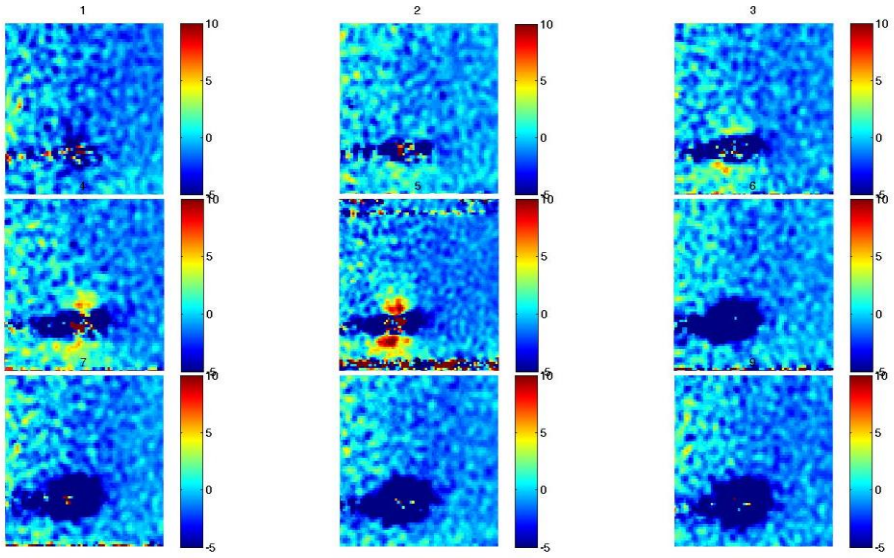

Figure 6.14: T2 FGRE image of our transducer embedded inside TMM phantom**.**

Results

Fig.6.15 shows the sagittal MR thermometry images for 5 mm slice thickness and different acoustical power levels. The acoustical power levels were 5 W and 15 W for fig.6.15A and fig.6.15B respectively.

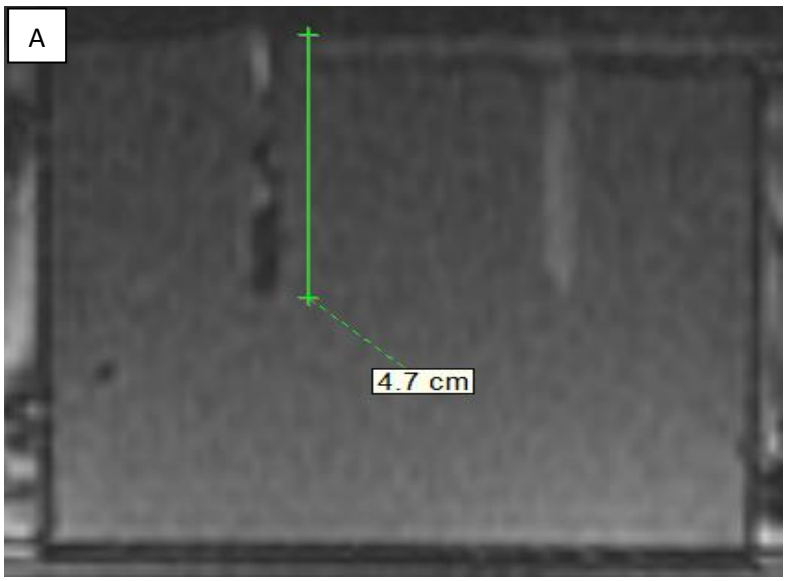

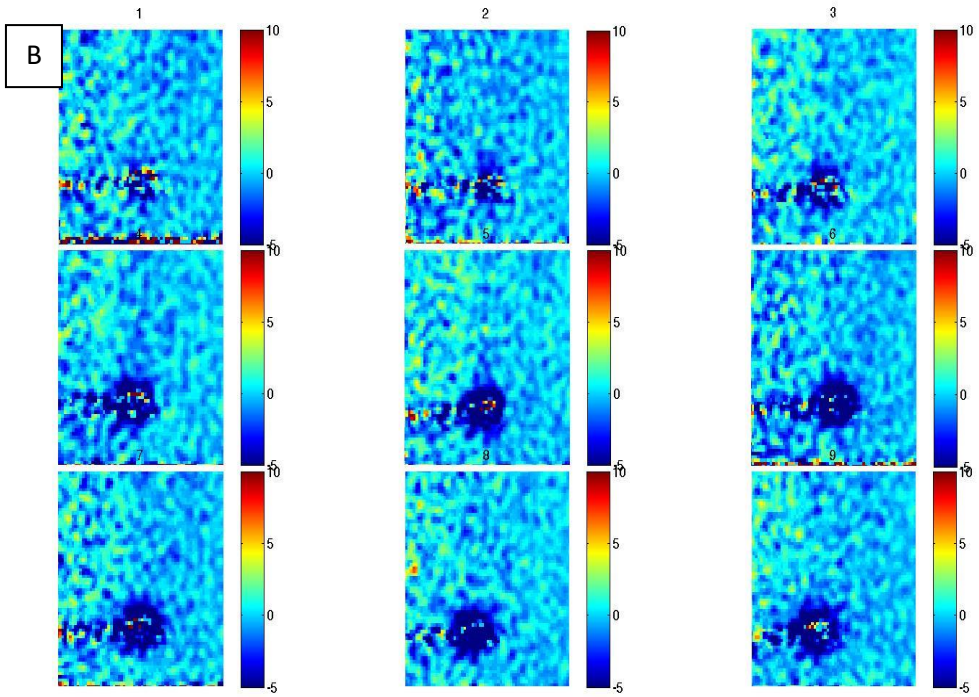

F

Figure 6.15: A) The sagittal MR thermometry images for 5 mm slice thickness for 5 W acoustical powers, B) 15 W acoustical power.

Fig.6.16 shows the coronal MR thermometry images for 5 mm slice thickness and different acoustical power levels. The acoustical power levels were 5 W and 15 W for fig.6.16A and fig.6.16B respectively.

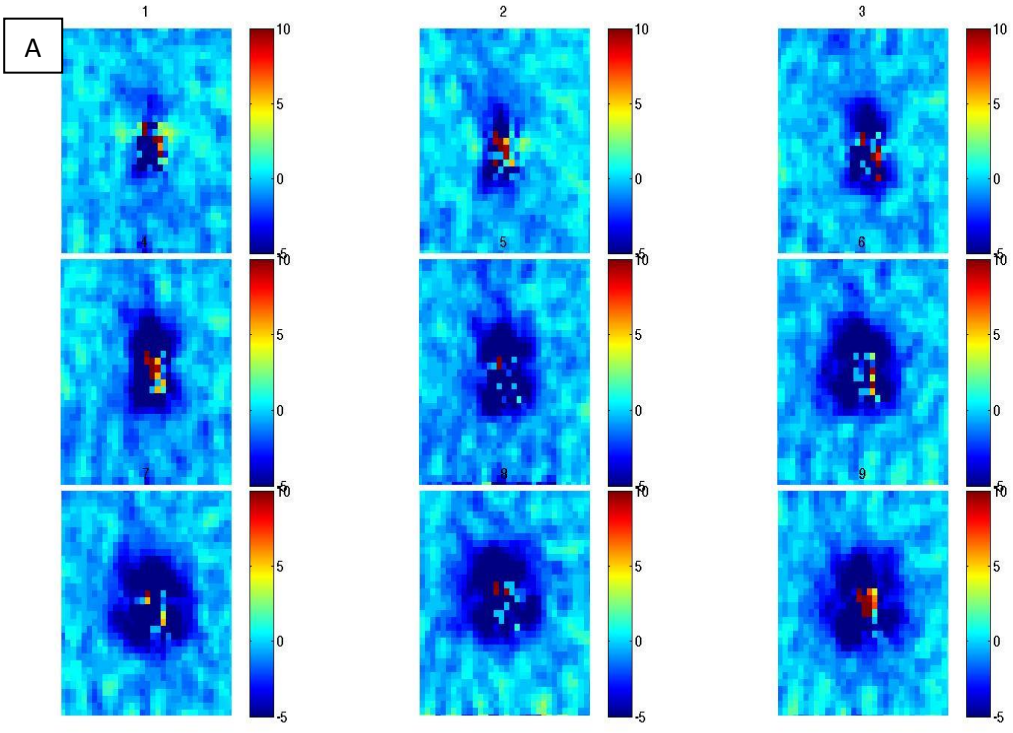

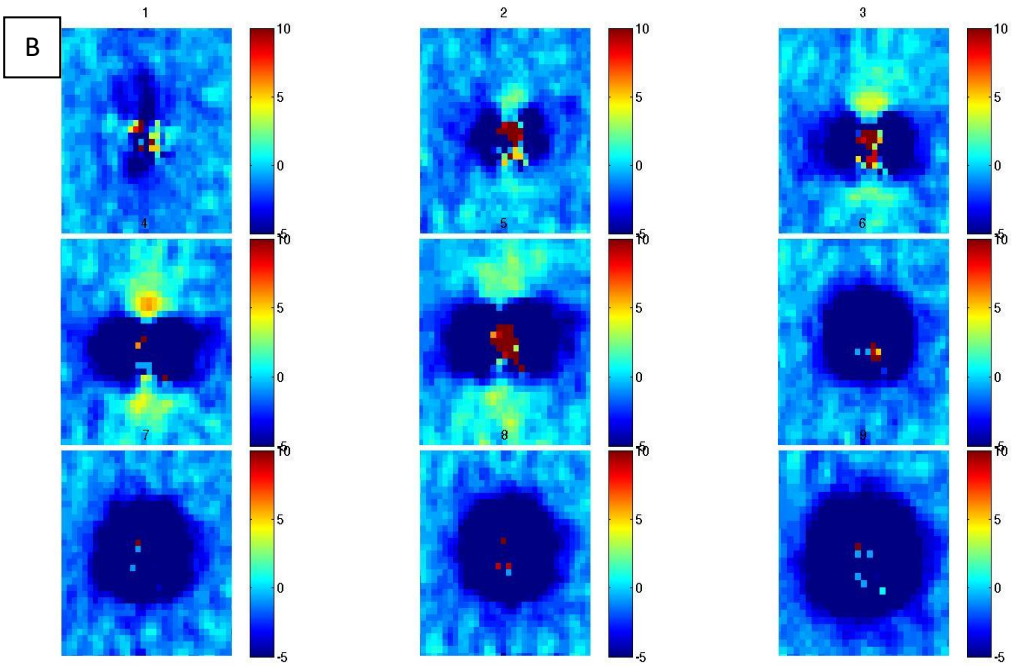

Figure 6.16: A) The coronal MR thermometry images for 5 mm slice thickness for 5 W acoustical power level, B) 15 W acoustical power.

Fig.6.17 shows the coronal MR thermometry images for 10 mm slice thickness and different acoustical power levels. The acoustical power levels were 5 W and 15 W for fig.6.17A and fig.6.17B respectively.

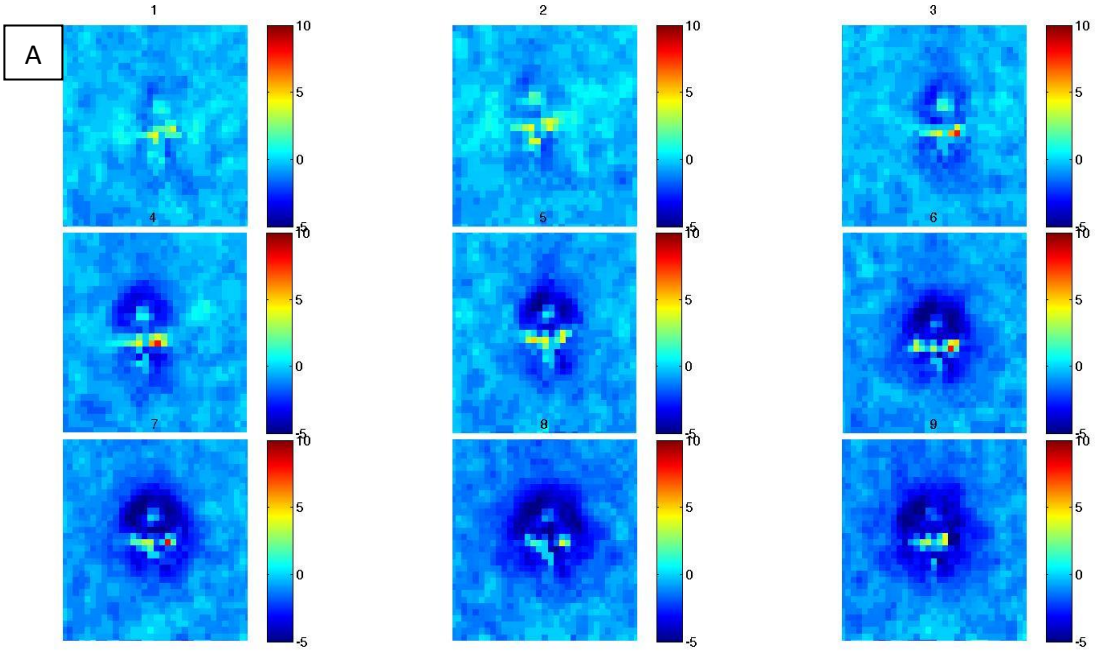

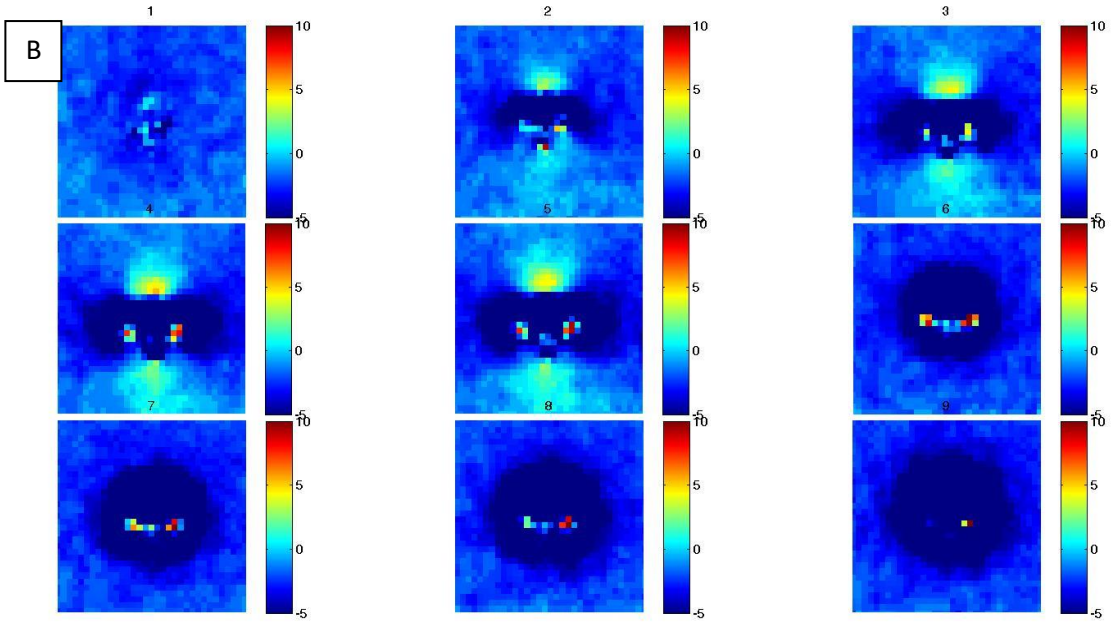

Figure 6.17: A) The coronal MR thermometry images for 10 mm slice thickness for 5 W acoustical power level, B) 15 W acoustical power.

Conclusions

Temperature readings near planar transducer are completely masked by electricity artifacts. At low power (5W) no significant temperature elevation can be detected since it was not adequate to compensate the artifact. At higher powers (15 W) some temperature elevation is detected since temperatures developed were adequate to compensate artifact. Maximum detected temperatures in sagittal plane were of the order of 10 ℃ whilst for the same power settings in the coronal plane the temperature was about 5 ℃.

6.4 Heating of a different tissue mimicking material TMM phantom using a planar transducer and monitoring it with MR thermometry

Materials and methods

An evaluation of heating a different tissue mimicking material (TMM) phantom using a planar transducer as a model for cardiac applications have been done. The heating effect was monitored using MR thermometry. The recipe of the TMM phantom was 2% w/v agar, 1.2% w/v silica and 25% v/v evaporated milk. The transducer was operating at 4.0 MHz (±5%). TMM phantom was sonicated with 20 W and 26 W acoustical power levels. MR thermometry was repeated for different orientations and slice thickness. The sonication time was 60 s.

Results

Fig.6.18 shows the sagittal MR thermometry images for 5 mm slice thickness and different acoustical power levels. The acoustical power levels were 20 W and 26 W for fig.6.18A and fig.6.18B respectively.

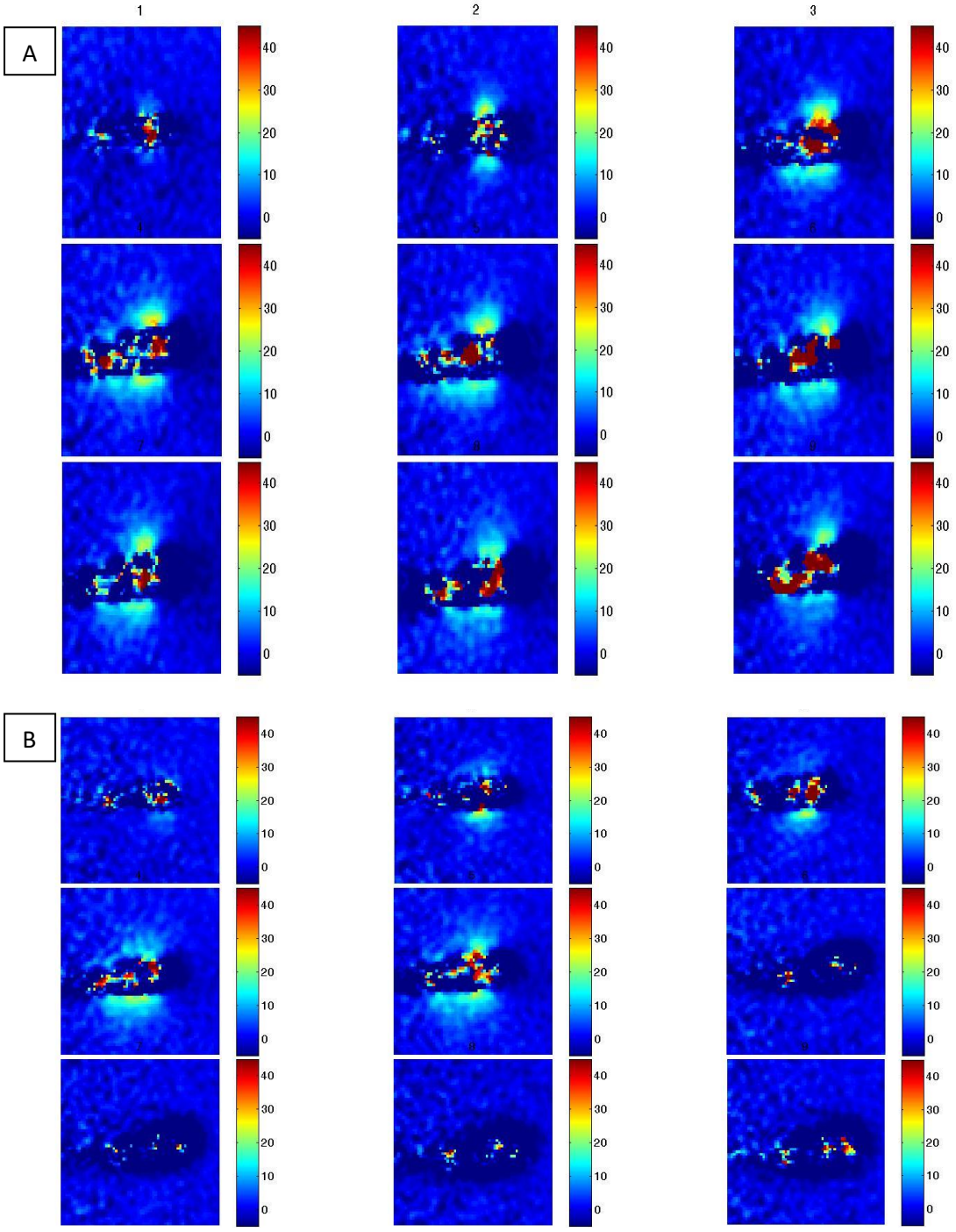

Figure 6. 18: A) The sagittal MR thermometry images for 5 mm slice thickness and 20 W acoustical power level, B) 26 W acoustical power.

Fig.6.19 shows the coronal MR thermometry images for 5 mm slice thickness and different acoustical power levels. The acoustical power levels were 20 W and 26 W for fig.6.19A and fig.6.19B respectively.

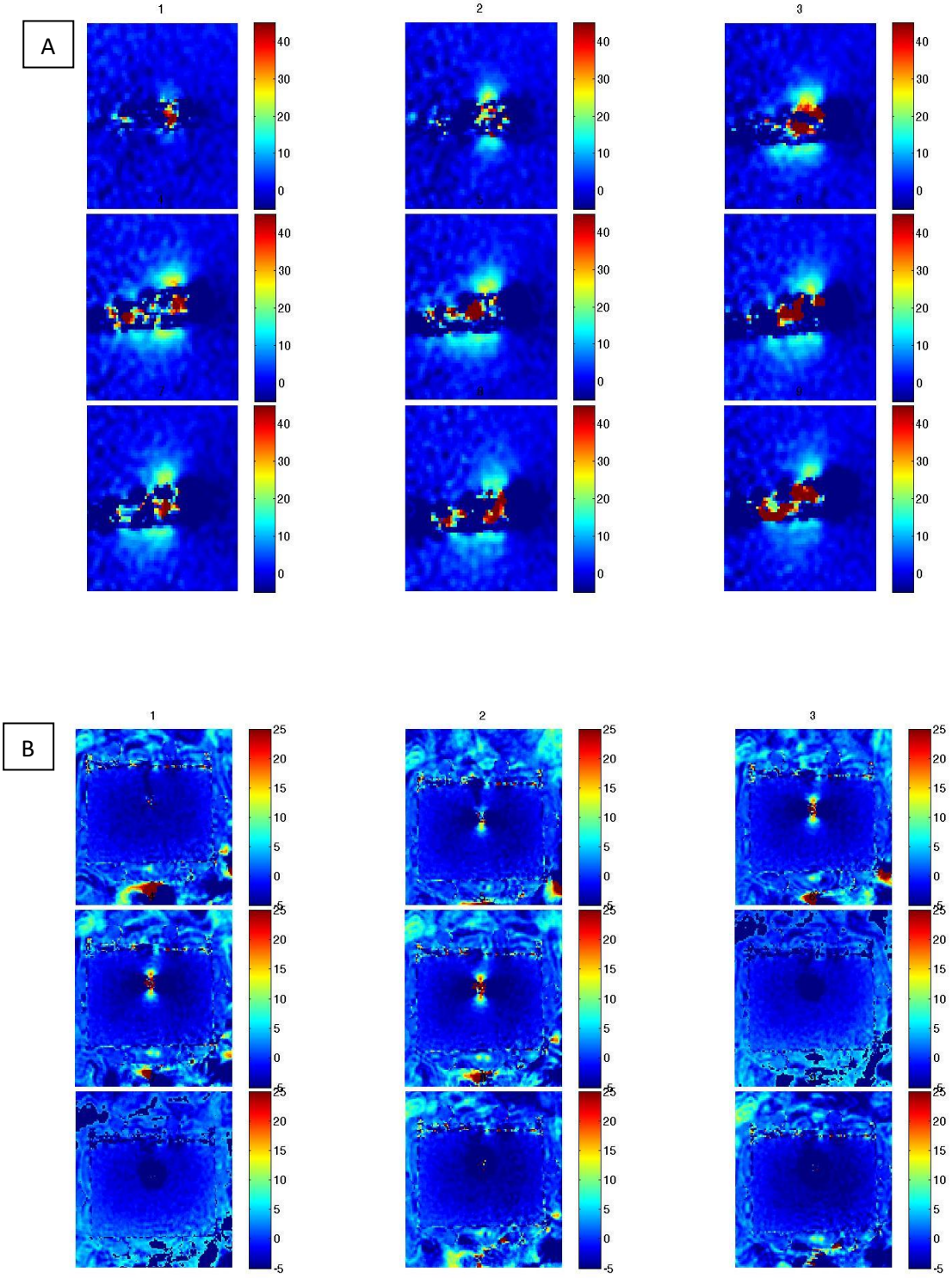

Figure 6.19: A) The coronal MR thermometry images for 5 mm slice thickness and 20 W acoustical power level, B) 26 W acoustical power.

Conclusions

Heating from the planar transducer was detected using MR thermometry. Temperatures along the direction of transmission were higher than temperatures developed on the back side of the planar transducer. The 20 W sonication produced temperatures that exceeded 20 ℃ and 26 W were more than 40℃. Sagittal plane thermometry produced temperatures exceeding 50 ℃ and 70 ℃ respectively. Temperature between coronal and sagittal plane for the same power-duration settings differ due to partial volume and considering the extremely small hot spot created it was very difficult to estimate the maximum temperature accurately. The planar transducer induces artifacts that perturb phase images and affect thermometry results. There is no clear margin of the planar transducer in the sagittal plane due to increased artifacts compared with the coronal plane. The 120 s sonication did not create higher temperatures probably because the gel melted from sonication. Temperature elevation depends on acoustical power and sonication time. For the same acoustical powers there is a temperature difference of 30 ℃ between sagittal and coronal MRI images.

6.5 Discussion

This chapter describes the evaluation of atherosclerotic plaque and a tissue mimicking material (TMM) phantom for ultrasound therapy using MR thermometry. The purpose of the first part of this evaluation was to destroy an area of a plaque-mimicking phantom using a planar transducer, obtain MR thermometry images during the sonication and observe the destroyed area of the phantom using high-resolution imaging. The minimum slice which the MRI could obtain was 2 mm thickness. The average lesion depth was 1.77 mm for 30 s sonication time and acoustic power of 10 W (voltage 160 mV). The size of the lesion for the atherosclerotic plaque phantom was similar to the 2x10 mm^2 size of the transducer. The size of the lesion was evaluated with similar accuracy using X-Ray image and MRI (T2W-FSE). The depth of the lesion was evaluated more precisely with X-Rays.

Moreover, an evaluation of heating a tissue mimicking material (TMM) phantom using a planar transducer as a model for cardiac applications has been done using MR thermometry. Temperature readings near the transducer are completely masked by electricity artifacts. Maximum detected temperatures in sagittal plane were of the order of 10 ℃ whilst for the same power settings in the coronal plane the temperature was about 5 ℃. The next part of the evaluation was to assess the heating of different tissue mimicking material (TMM)

phantom with 1.2% w/v silica and higher acoustical power. The higher acoustical power produced higher temperature elevation. Sagittal plane thermometry produced temperatures exceeding 50 ℃ and 70 ℃ respectively. The planar transducer induces artifacts that perturb phase images and affect thermometry results. Increasing sonication time did not produce higher temperatures probably because the phantom material was melted due to the sonication.

6.6 Conclusion

An evaluation of atherosclerotic plaque and TMM phantom for ultrasound therapy using MR thermometry was described in this chapter. For the plaque-mimicking phantom the temperature change using MRI was difficult to achieve due to artifacts. The size of the plaque phantom lesion was similar to the size of the transducer. For the TMM phantom, for low acoustical power no significant temperature elevation was detected. Moreover, the 70 ℃ maximum temperature elevation was detected for sagittal MRI imageand 26 W acoustical powers.

7. Ultrasonic thermal ablation of phantoms and tissue

7.1 Introduction

Ultrasonic ablation in different tissue phantoms is presented in this chapter. Different sonication parameters were used such as acoustical power and sonication time. Tissue phantoms consisted of agar/silica evaporated milk gel phantom, a commercial polyacrylamide gel and freshly excited turkey tissue. The temperature elevation was assessed because is an important part during destruction of atherosclerotic plaque in human arteries. The temperature elevation should be kept up to 1 ℃. MR thermometry experiments performed with different tissue phantoms.

7.2 HIFU system

The HIFU system used for the next experiment was composed of a signal generator (33220A, Agilent Technologies, Englewood, CO, USA), an RF amplifier (AG 1012 LF Generator &Amplifier, T & C Power Conversion, Rochester, USA), and a planar rectangular transducer. The ABS parts of the transducer holder were produced by a 3D Printer (Ultimaker3 extended, Ultimaker B.V, Zaltbommel, Netherlands). The internal structure includes a cavity to accommodate the 1 mm thick coaxial cable. A VXM positioning system (VXM, VELMEX INC, Bloomfield, NY, USA) was used for guiding the transducer's face.

7.3Agar/Silica evaporated milk phantom

For investigating the ability to increase the temperature using intravascular transducers, an agar/silica evaporated milk phantom was used. The phantom consists of Agar (Agar-agar granulated, purified and free from inhibitors for microbiology, Merck KGaa, Darmstadt, Germany), crystalline silica dioxide powder (Merck Millipore, Darmstadt, Germany), evaporated milk (NOUNOU condensed milk, Friesland Campina, Marousi, Greece) and water. Silica dioxide is insoluble in water and has a high melting point close to 1700 ℃. Evaporated milk was added in the gel following a recipe described by Madsen et al. [222]. Being a low scatter and rich in proteins and fats, evaporated milk served to control attenuation of the gel primarily through the process of acoustic absorption. The produced sample was isotropic and homogeneous. The recipe of the tissue mimicking agar gel was 2% w/v agar, 1.2% w/v silica dioxide and 25% v/v evaporated milk. The details of the recipe and

the steps for the preparation of the agar/silica evaporated milk phantom are described in Menicou et al. [221].

7.4 Temperature measurement

A temperature reader (Omega Thermometer, HH806AU, Omega engineering, USA) was used. The temperature reader sends the data in viewing software via a universal serial bus (USB) interface. A 100 μm in diameter thermocouple was placed between the transducer face and the agar/silica evaporated milk phantom to measure the temperature elevation at the transducer element in order to avoid overheating. In the agar/silica evaporated milk phantom, the thermocouple was placed in front of the face of the transducer.

7.5 Polyacrylamide phantom for assessing lesions

A commercial polyacrylamide gel (ONDA Corporation, Sunnyvale, CA, USA) was used in order to evaluate thermal lesions created by this transducer. The material of this gel becomes white when the temperature exceeds 70 ℃. The attenuation coefficient of this gel is 0.5 dB/cm–MHz.

7.6 Thermal ablation in a freshly excited turkey tissue phantom

Materials and methods

The first step of our investigation was to assess thermal lesions in freshly excited turkey tissue. The experimental setup is shown in fig. 7.1.

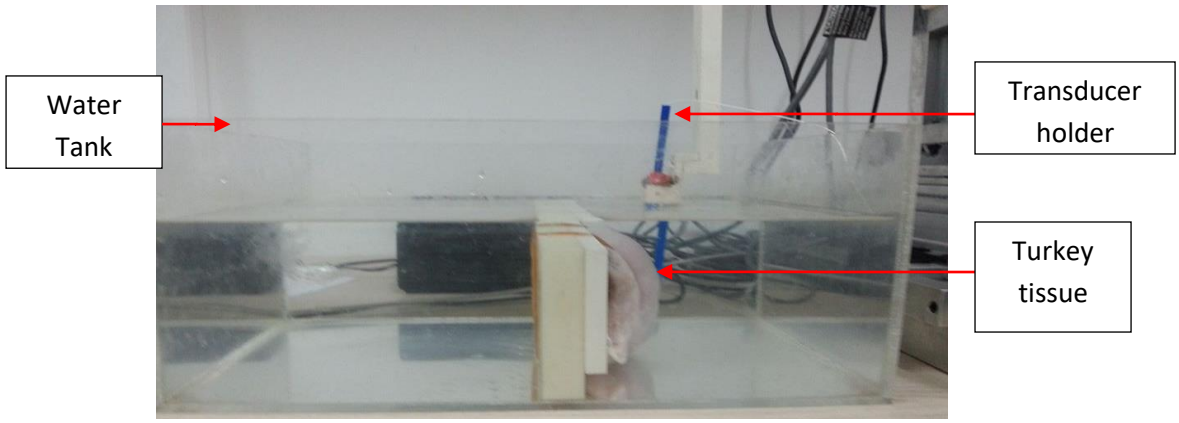

Figure 7.1: Experimental setup for investigating thermal lesion in a freshly turkey tissue.

Results

Figure 7. 2: Thermal lesions in a freshly turkey tissue phantom with acoustical power 20 W for 10 s.

Thermal lesions in the freshly excited turkey tissue phantom using the 2x10 mm^2 transducer operating at 4.0 MHz with acoustical power 20 W for 10 s is shown in fig. 7.2. The size and the shape of the lesions are similar to the geometry of the transducer. The mean area of thermal lesions (n=6) was 38.5 ± 4.0 mm^2 and the mean depth (n=6) was 1.2± 0.2 mm.

The same experiment with 13 W acoustical power and 10 s sonication time was performed (fig.7.3). The size and the shape of the lesions are similar to the geometry of the transducer. The mean area of thermal lesions (n=6) was 27.0 ± 1.6 mm^2 and the mean depth (n=6) was 1.0 ± 0.2 mm.

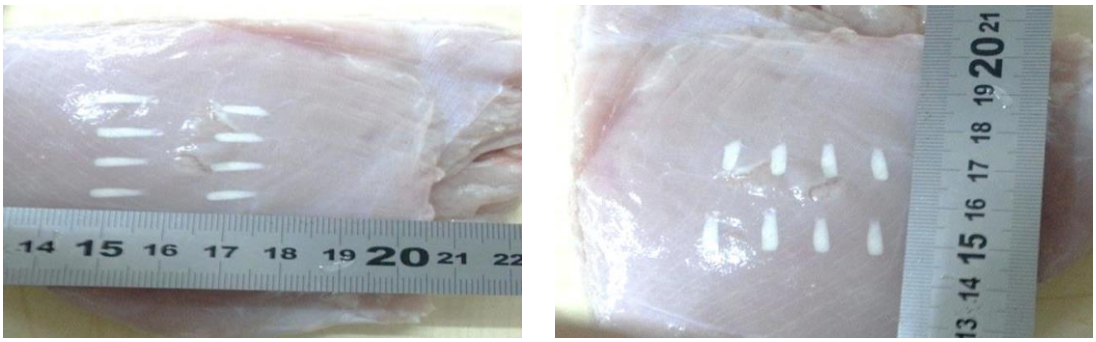

Figure 7. 2: Thermal lesions in freshly turkey tissue phantom with acoustical power 13 W for 10 s.

7.7 Thermal ablation in commercial polyacrylamide gel phantom

Materials and methods

The next step of our investigation was to assess the creation of thermal lesions in a commercial polyacrylamide gel phantom. The experimental setup is shown in fig. 7.4.

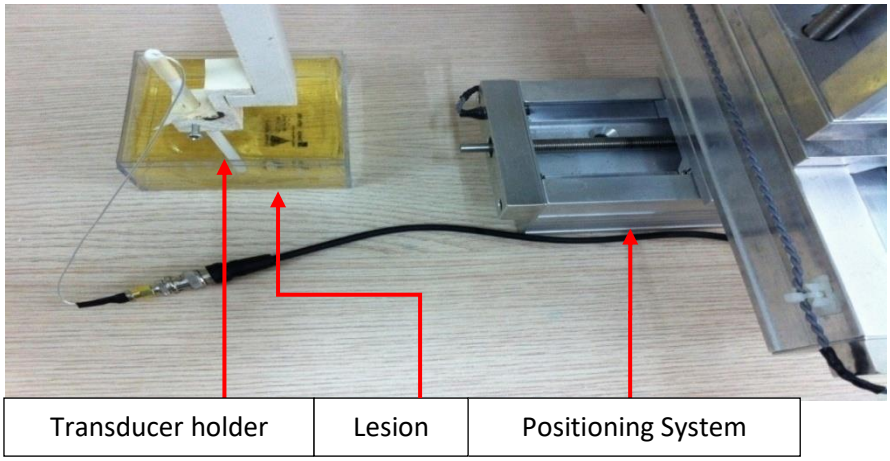

Figure 7.3: Experimental setup for investigating thermal lesion in a commercial polyacrylamide gel phantom.

Results

Thermal lesions in the commercial polyacrylamide gel using the 2 x 10 mm^2transducer operating at 4.0 MHz with acoustical power 10 W for 5 s is shown in fig. 7.5 and fig.7.6. The size and the shape of the lesions are similar to the geometry of the transducer. The mean area of thermal lesions (n=7) was 24.4 ± 11.1 mm^2 and the mean depth (n=7) was 2.1 ± 0.6 mm.

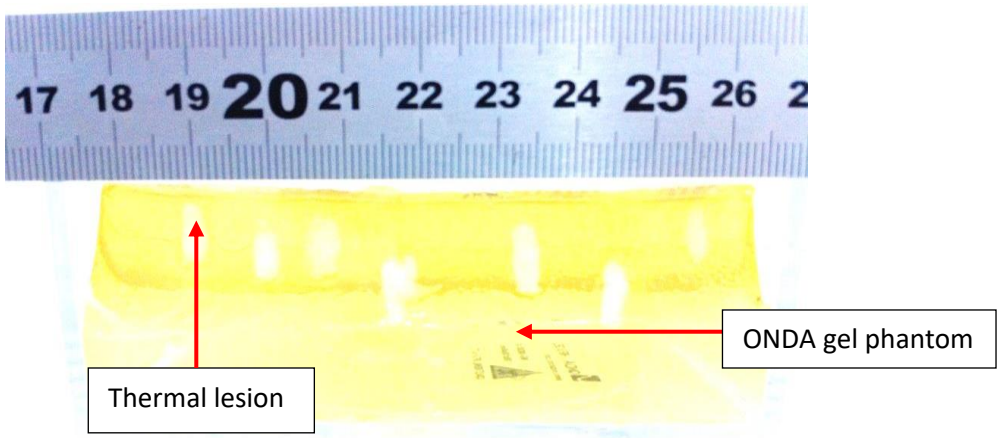

Figure 7.4: Thermal lesions in a commercial polyacrylamide gel with acoustical power 10 W for 5 s.

Figure 7.5: Thermal lesions in a commercial polyacrylamide gel with acoustical power 10 W for 5 s from the top.

7.8 Investigating the ability of increasing temperature on the agar/silica evaporated milk gel phantom using intravascular transducers

Materials and methods

The next step of the evaluation was to assess the temperature elevation on the agar/silica evaporated milk gel phantom. The experimental setup is shown in fig.7.7.

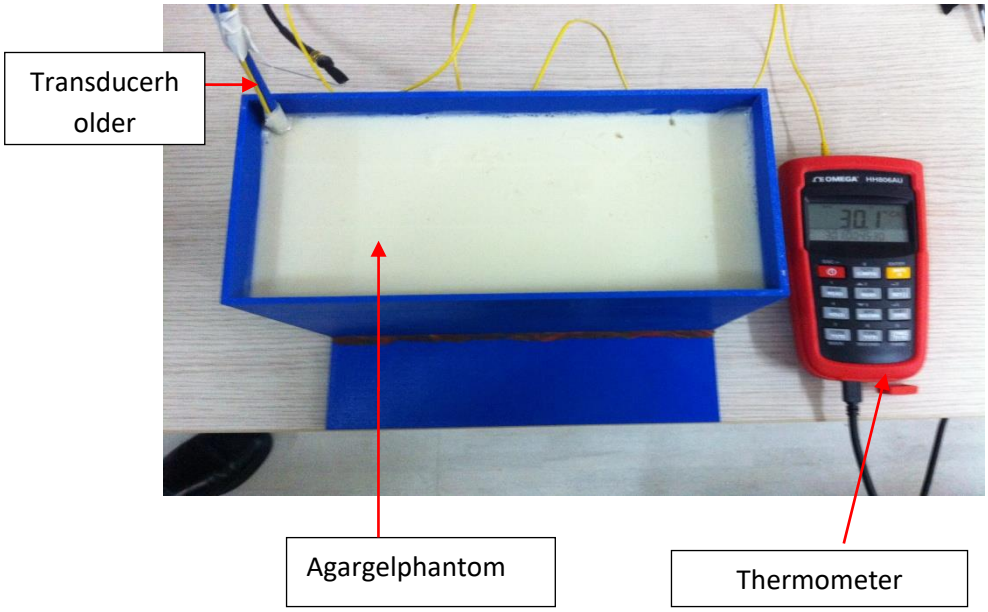

Figure 7.6: Experimental setup for investigating temperature elevation in agar gel phantom using intravascular transducers.

Results

The temperature elevation in the agar/silica evaporated milk phantom using a thermocouple which was placed at the transducer face is shown in fig. 7.8. The maximum temperature difference was almost 30 ℃ for an acoustical power of 9 W for 60 sand 70 ℃ for 16 W acoustical powers for 60 s.

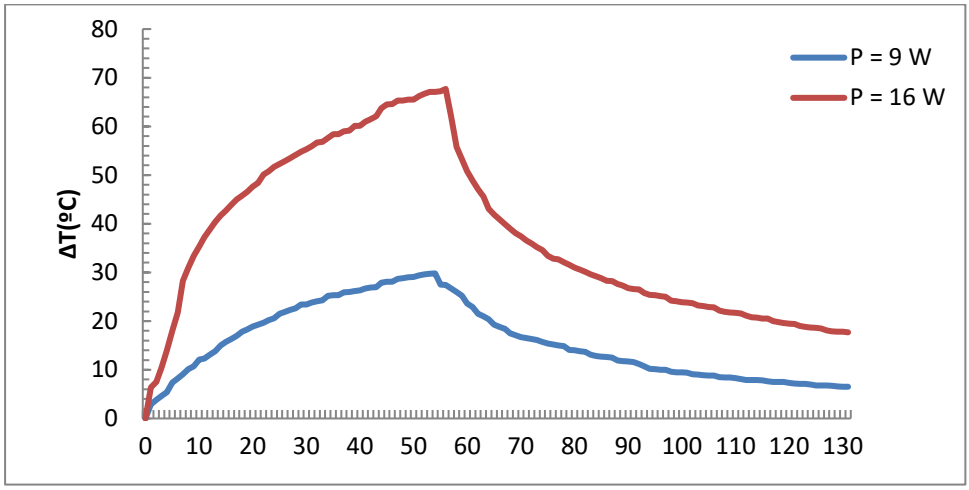

Figure 7.7: Temperature elevation in the agar/silica evaporated milk phantom for a9 W and 16 W acoustical powers of 9 W for 60 s.

7.9 Thermal ablation in the agar/silica evaporated milk phantom

The next step of the evaluation was to assess the creation of thermal lesions in a commercial polyacrylamide gel phantom. The experimental setup is shown in fig. 7.9.

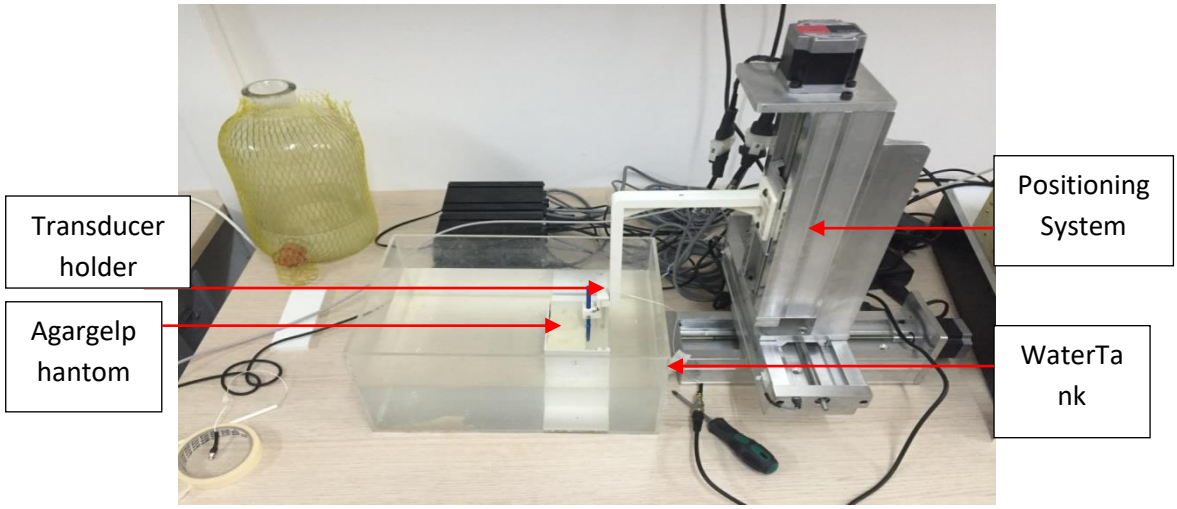

Figure 7.8: Experimental setup for investigating thermal lesion in the agar/silica phantom.

Results

Fig. 7.10 shows thermal lesions on the agar/silica evaporated milk phantom using thermal mode with the 2 x 10 mm^2 transducer operating at 4.0MHz.The 9 lesions at the bottom row were created with acoustical power between 12 W and 15 W for duration of 30 s. The 7 lesions at the top row were created with acoustical power of 20 W for duration of 20 s. The size of the lesions matches the geometry of the transducer. The mean area of the top thermal lesions (n=7) was20.3 ± 5.5 mm^2 and the mean depth (n=7) was 2.3 ± 0.2 mm. Moreover, the mean area of the bottom thermal lesions (n=9) was 20.9 ± 6.9 mm^2 and the mean depth (n=9) was 1.8 ± 0.2 mm.

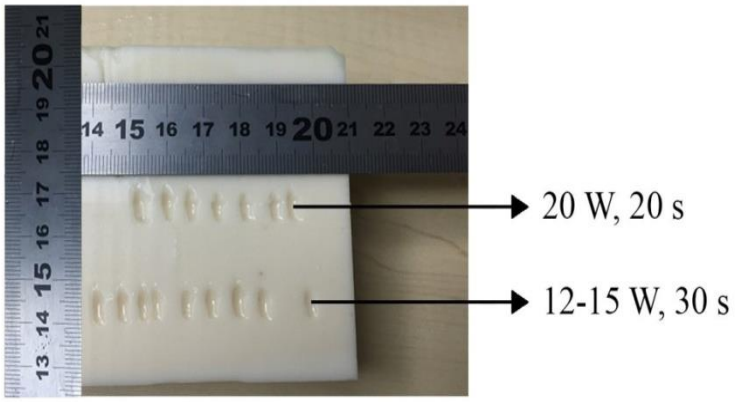

Figure 7.9: Thermal lesions on the agar/silica evaporated milk phantom. Bottom row lesions were created with acoustical power between 12 W and 15 W for duration of 30 s. Top row lesions were created with acoustical power of 20 W for duration of 20 s.

7.10Temperature elevation and distance from the transducer's face in the agar/silica evaporated milk phantom

Materials and methods

The relationship between temperature elevation and the distance from the transducer's face in the agar/silica evaporated milk phantom was investigated. For our arterial model, the temperature elevation near the artery is a critical factor and should be kept below 1 °C. The experimental setup is shown in fig. 7.11.

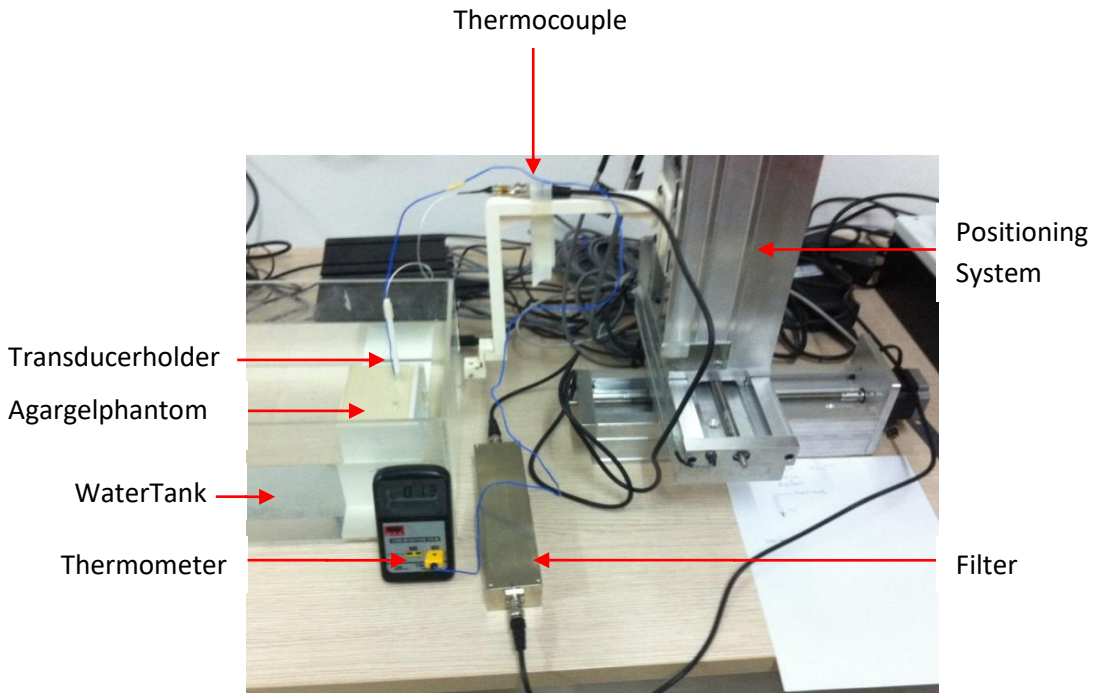

Figure 7.10: Experimental setup for investigating thermal elevation with distance from the transducer's face.

Results

The temperature elevation in the agar/silica evaporated milk phantom against depth from the transducer's face is shown in fig. 7.12. The acoustical power and sonication time were 12 W and 12 s respectively. The maximum and the minimum temperature difference was almost 60 ℃ at 1 mm and 1 ℃ at distance 5 mm from the transducer's face respectively.

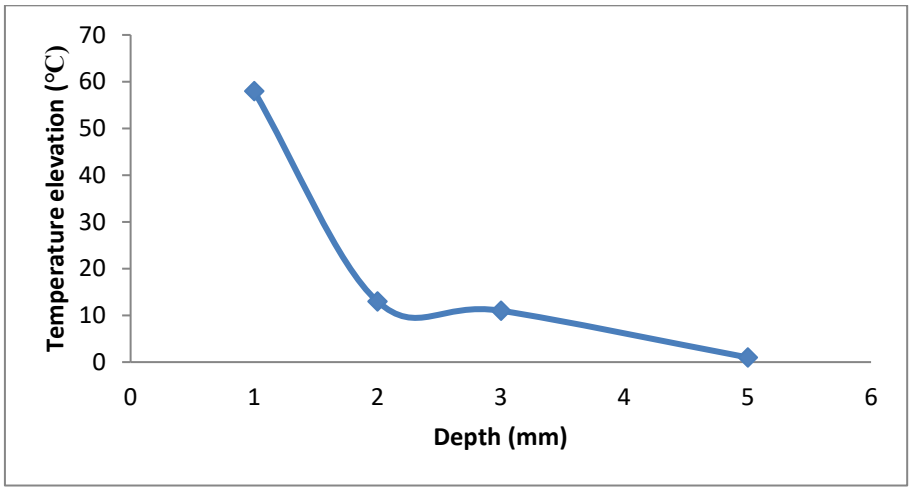

Figure **7**.11: Temperature elevation in the agar/silica evaporated milk phantom using thermocouple which was placed at different depth from the transducer face.

7.11 Investigating the ability of increasing temperature on the agar/silica evaporated milk gel phantom using an intravascular transducer with different active size

Materials and methods

The next step of our investigation was to assess the temperature elevation on the agar/silica evaporated milk gel phantom using a transducer with different active size. The active size of the transducer was 3x8 mm^2. The transducer material was made out of P762-type piezoceramic (Ferroperm, Kvistgaard, Denmark), operating at 4.0MHz (±5%). The agar/silica evaporated milk gel was placed on absorbing material in order to avoid reflections of the beam. The experimental setup is shown in fig.84.

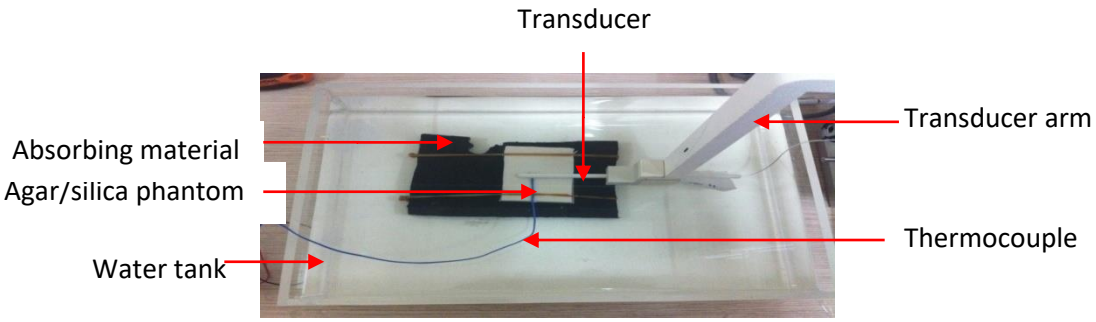

Figure 7. 12: Experimental setup for investigating temperature elevation in agar gel phantom using an intravascular transducer (f=4.0 MHz and 3x8 mm^2 active size).

Results

The temperature elevation in the agar/silica evaporated milk phantom using a thermocouple which was placed at the transducer face is shown in fig. 7.14. Fig. 7.14A shows the unfiltered chart of the temperature elevation. The chart appeared to have a lot of noise because of the vibrations on the thermocouple produced by the transducer during sonication. The maximum temperature difference was almost 65℃ for an acoustical power of 8 W for 60 s. Fig. 7.14B shows the filtered chart of the temperature elevation with the same acoustical power and sonication time.

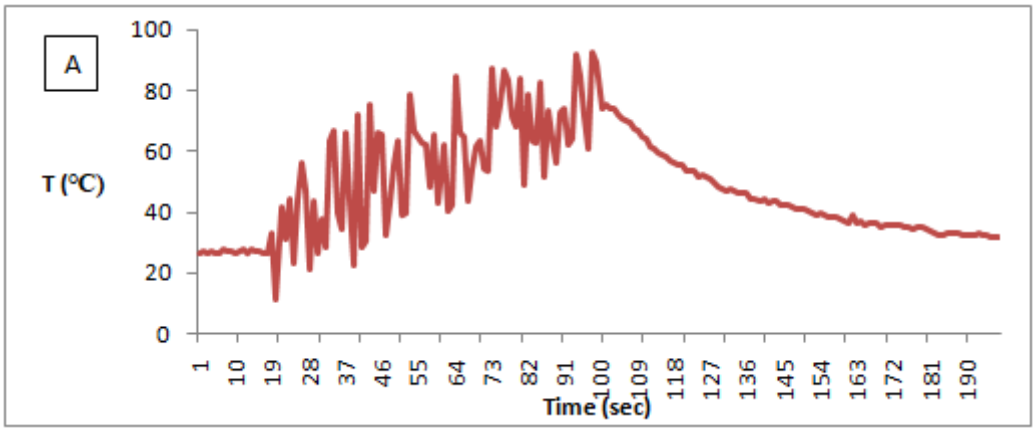

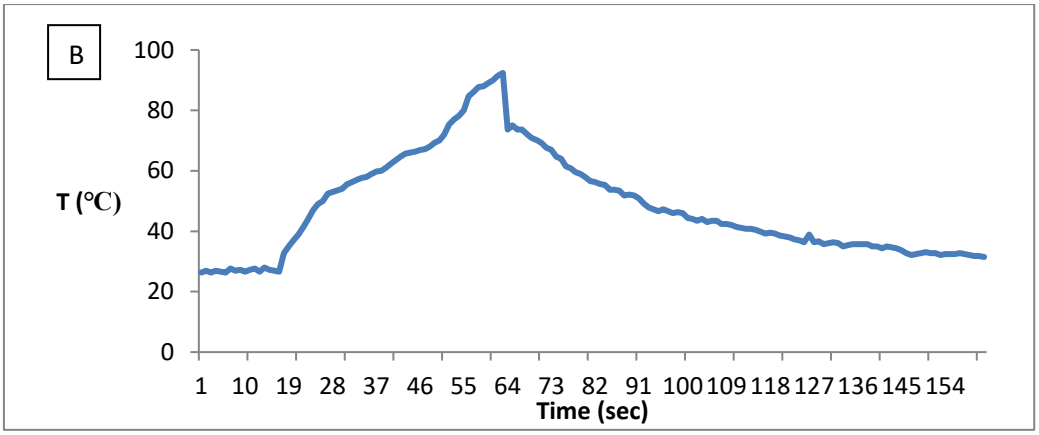

Figure 7.13: A) The unfiltered chart of the temperature elevation. The max temperature difference was almost 65°C for an acoustical power of 8 W for 60 s, B) The filtered chart of the temperature elevation with the same acoustical power and sonication time.

7.12 Investigating the ability of increasing temperature on the agar/silica evaporated milk gel phantom using an intravascular transducers with different element areas

Material and methods

Transducers with different element dimensions were evaluated for creating thermal lesion in agar/silica evaporated milk gel phantom. The active sizes of the transducer element were 2 x 10 mm^2 and 1 x 10 mm^2respectively. The transducer was operating at 4.0 MHz ($\pm$5%).

Results

Fig.7.15 shows the thermal lesions created from the two transducers using the evaporation method. The size of the lesions matches the geometry of each transducer. The first 3 lesions (1-3) at the top section were created from the 2 x 10 mm^2 transducer with acoustical power of 18 W for duration of 10 – 30 s. The last 3 lesions (4-6) at the bottom section were created from the 1 x 10 mm^2 with acoustical power of 18 W for duration of 10 – 30s. The size of the lesions matches the geometry of the transducer. The mean depth of the top (n=3) and bottom (n=3) thermal lesions were 1.83 ± 0.24 mm respectively 1.33 ± 0.47 mm.

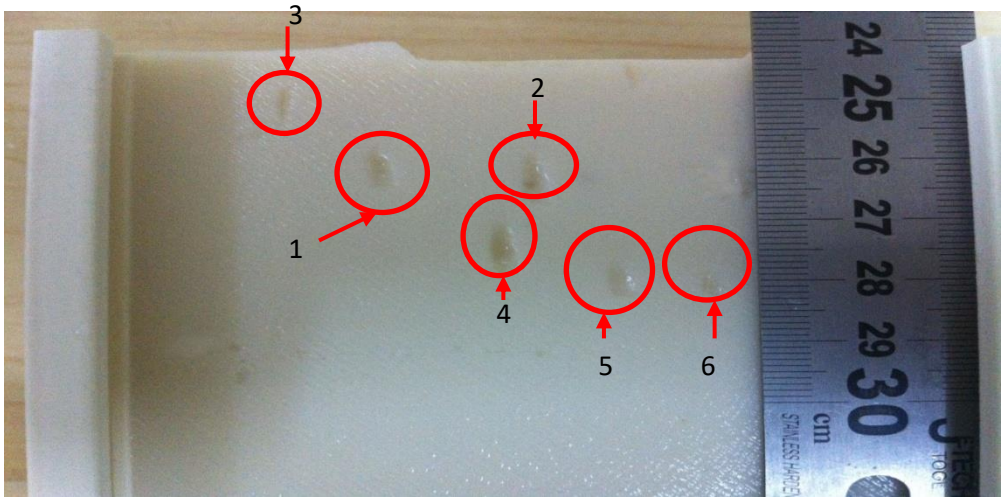

Figure 7.14: Thermal lesions in agar/silica evaporated milk gel phantom using two transducers with different active sizes.

7.13Temperature elevation at various depths from the transducer's face in the agar/silica evaporated milk phantom for different acoustical powers and depths

Materials and methods

The relationship between temperature elevation and depth from the transducer's face in the agar/silica evaporated milk phantom using different acoustical powers and depths was investigated. The experimental setup is shown in fig. 7.16.

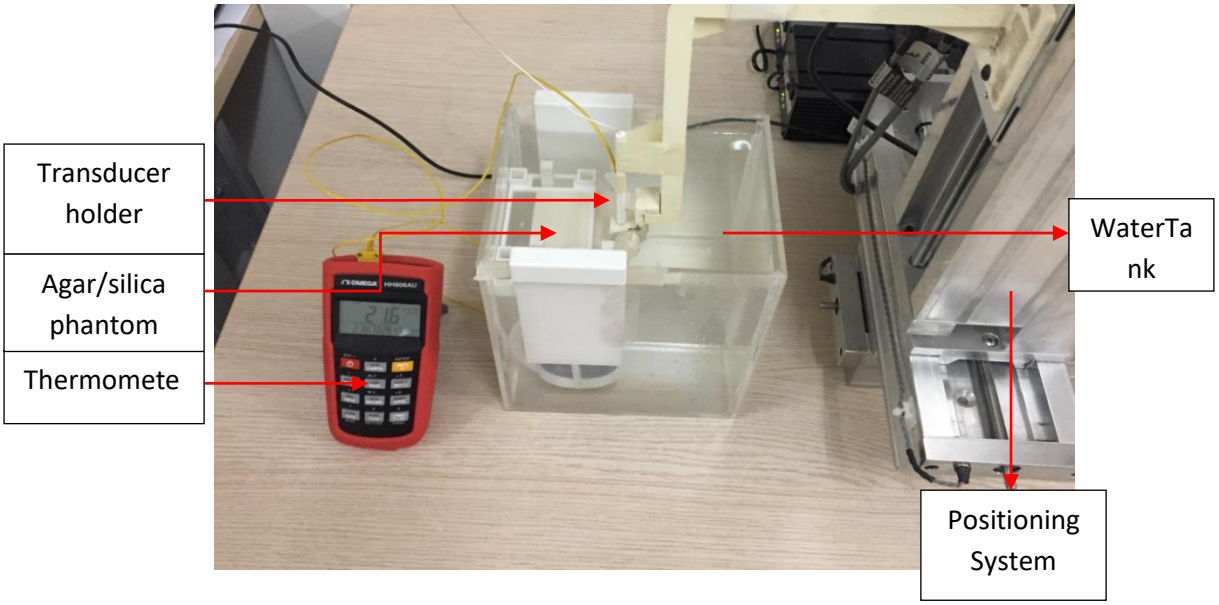

Figure 7.15: Experimental setup for investigating the temperature elevation in intravascular transducers using different acoustical power at various depths from the transducer's face.

Results

The sonication time was 60 s for all the experiments. For 10 mm depth from the transducer's face the max temperature elevations were 2.1 ℃ and 1.8 ℃ for 5 W and 10 W acoustical powers respectively. For 5 mm depth from the transducer's face the max temperature elevations were 8.4 ℃ and 16.9 ℃ for 5 W and 10 W acoustical powers respectively. For 0 mm depth from the transducer's face the max temperature elevations were 48.7 ℃ and 49.5 ℃ for 5 W and 10 W acoustical powers respectively.

Figure 7.17 shows the graphs of temperature elevation against time for zero depth and different power levels. Fig. 7.17A and fig.7.17B shows the temperature elevation for 5W acoustical and 10 W acoustical powers respectively.

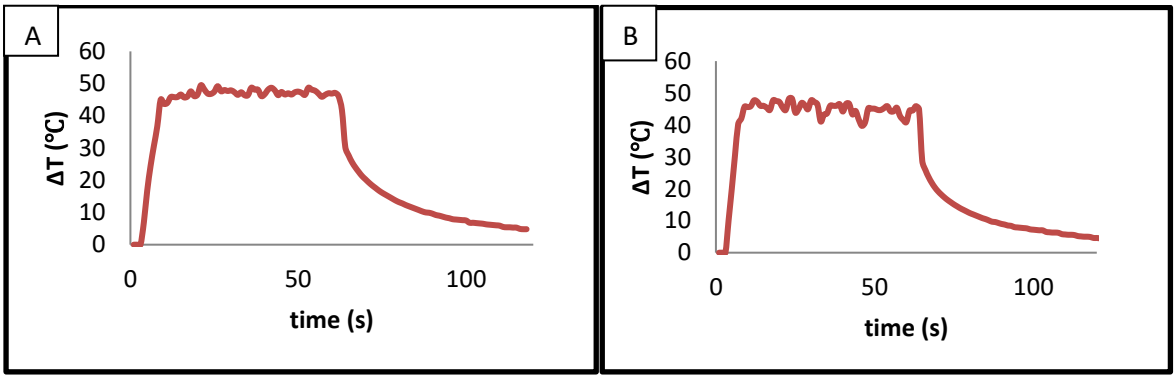

Figure 7.16: A) The 48.7 ℃ temperature elevation for 5 W acoustical power and 60 s sonication time, B) The 49.5 ℃ temperature elevation for 10 W acoustical power and 60 s sonication time.

Figure 7.18 shows the graphs of temperature elevation against time for 5 mm depth and different power levels. Fig. 7.18A and fig.7.18B shows the temperature elevation for 5 W acoustical and 10 W acoustical powers respectively.

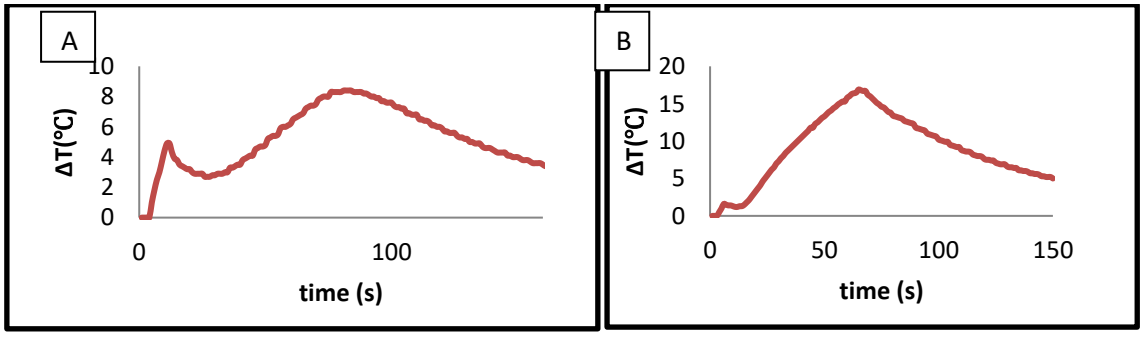

Figure 7.17: The 8.4 ℃ temperature elevation for 5 W acoustical power and 60 s sonication time, B) The 16.9 ℃ temperature elevation for 10 W acoustical power and 60 s sonication time for 5 mm depth.

The graphs of temperature elevation against time for 10 mm depth and different power levels are shown in fig.7.19. Fig. 7.19A and fig. 7.19B shows the temperature elevation for 5 W acoustical and 10 W acoustical powers respectively.

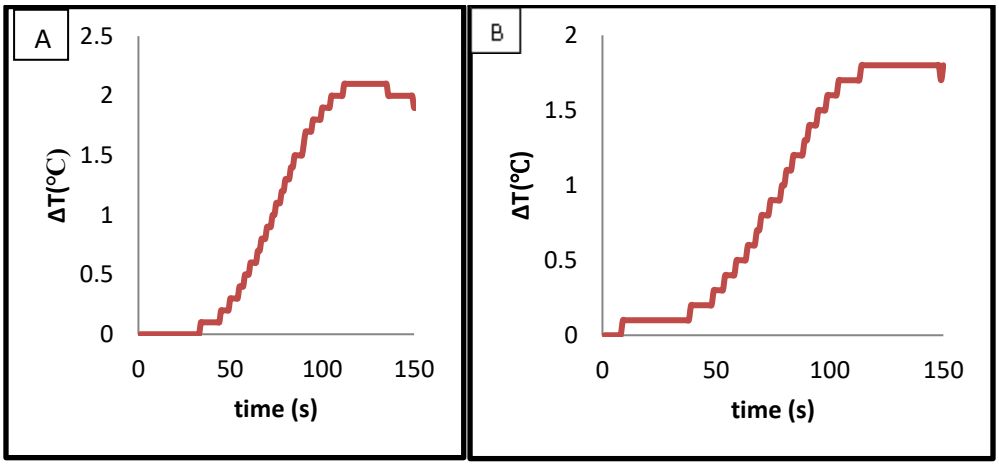

Figure 7.18: A) The 2.1 ℃ temperature elevation for 5 W acoustical power and 60 s sonication time, B) The 1.8 ℃ temperature elevation for 10 W acoustical power and 60 s sonication time for 10 mm depth.

Figure 7.20 shows the graphs of temperature elevation against time for the same acoustical power and different depths. Fig. 7.20A and fig. 7.20B shows the temperature elevation for 5W acoustical and 10 W acoustical powers for different depths respectively.

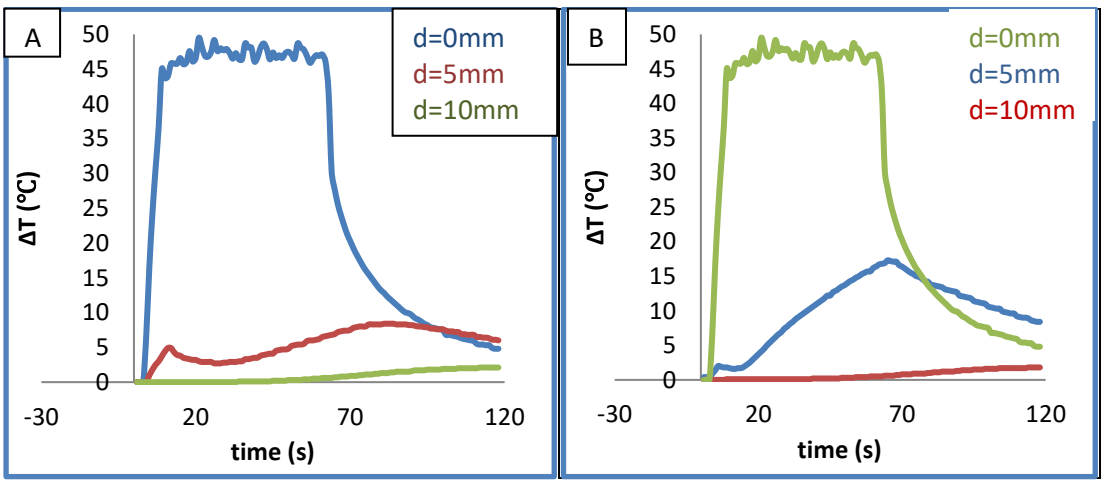

Figure 7.19: A) The temperature elevation for 5 W acoustical power, B) 10 W acoustical power and different depths.

7.14Investigating the ability of increasing temperature on the agar/silica evaporated milk gel using mechanical mode

Materials and methods

The next step of our investigation was to assess the temperature elevation on the agar/silica evaporated gel using mechanical mode. The recipe of the tissue mimicking agar gel was 4% w/v agar, 4% w/v silica dioxide and 30% v/v evaporated milk. The experimental setup is shown in fig. 7.21.

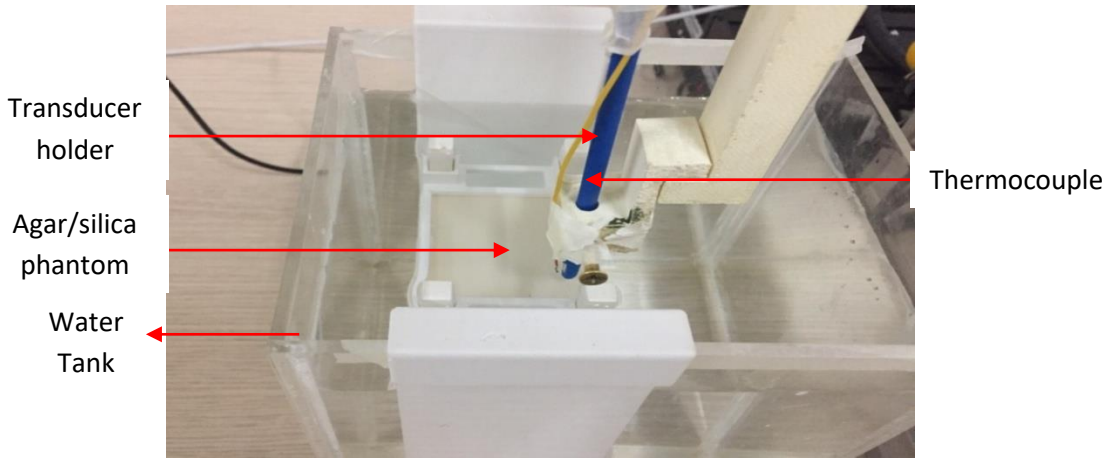

Figure 7.20: Investigating temperature elevation in agar/silica phantom using mechanical mode.

Results

The temperature elevation against pulse repetition period (PRP) for different acoustical powers is shown in fig. 7.22. Sonication time and duty factor (DF) were 60 s and 10 % respectively. Figures7.22 A-D shows the temperature elevation against PRP for 16 W, 20 W, 25 W and 33 W acoustical powers respectively. The max temperature elevation was 0.3 ℃, 0.7 ℃ and 0.9 ℃ 1.5 ℃ for 1000 ms.

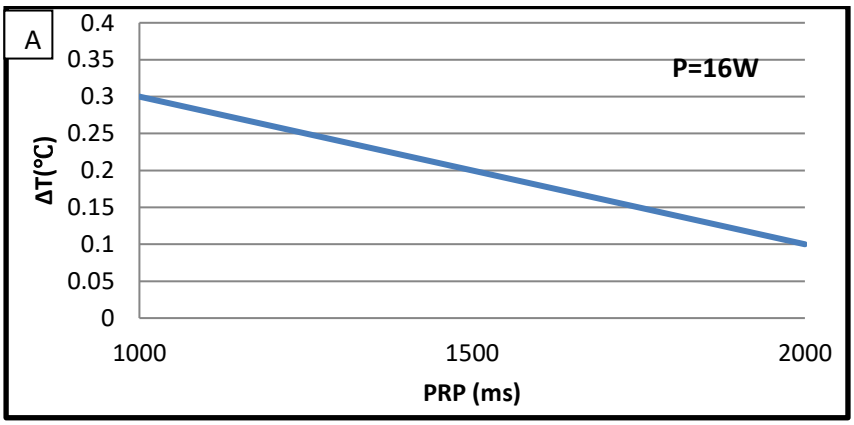

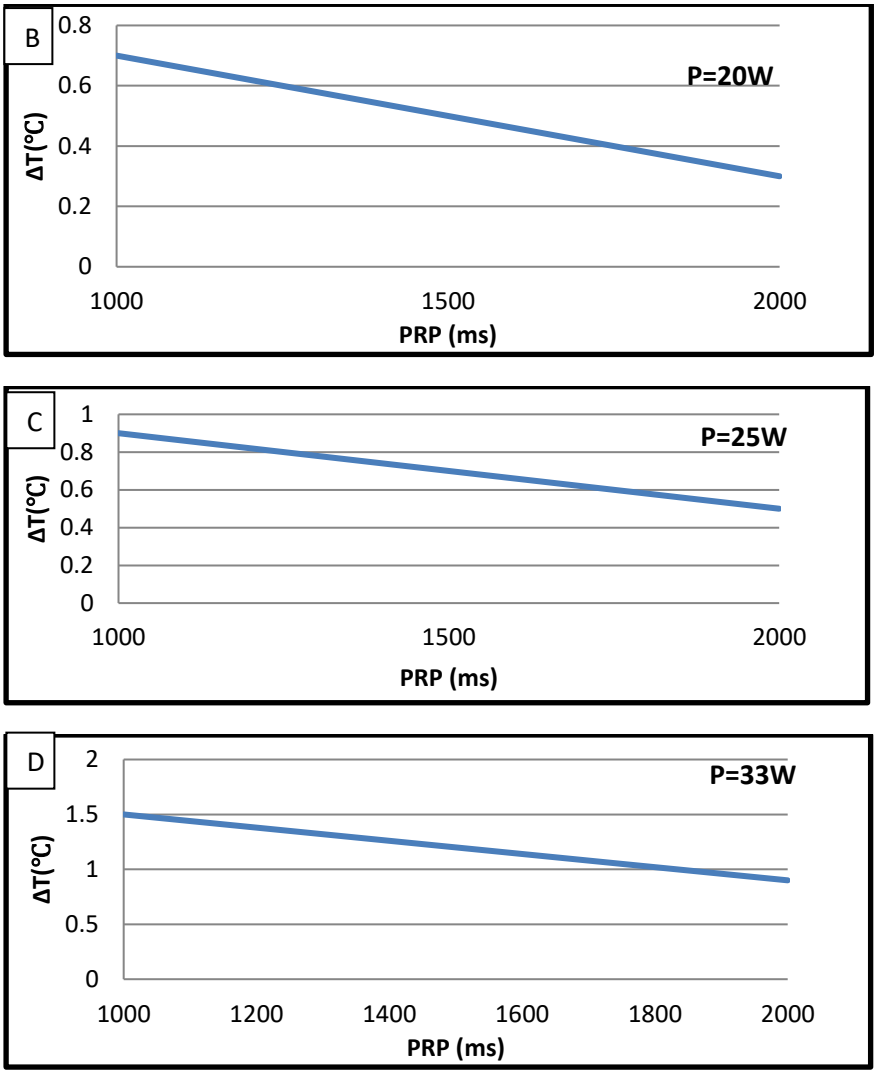

Figure7. 21: A)Temperature elevation against PRP for 16 W, B) 20 W, C) 25 W and D) 33 W acoustical power respectively.

Figure 7.23 shows the temperature elevation in agar/silica phantom against PRP for different acoustical power levels.

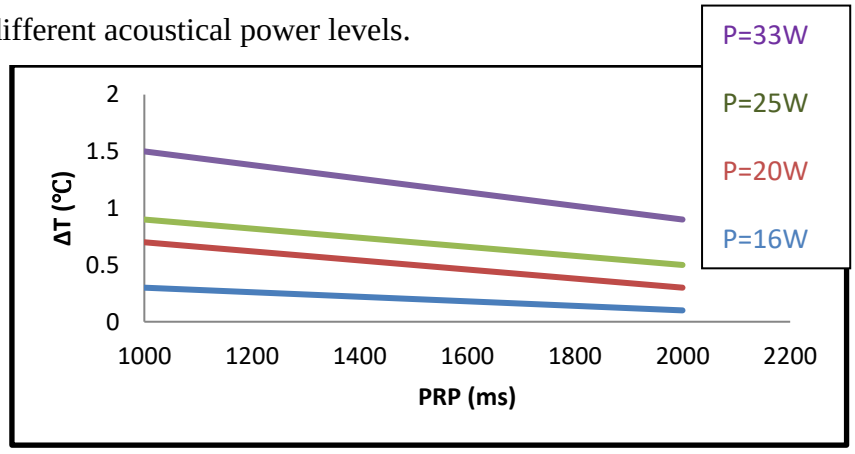

Figure 7.22: Temperature elevation against PRP for different acoustical power levels.

7.15 Discussion

In this chapter, an evaluation of ultrasonic ablation in different tissue phantoms was presented regarding different sonication parameters such as acoustical power and sonication time. The first step of our investigation was to assess thermal lesions in freshly excited turkey tissue with different acoustical power with the same sonication time. The size and the shape of the lesions were similar to the geometry of the transducer. When acoustical power increased by 7 W the mean area of thermal lesions increased by 42.6% and the mean depth by 20%. The higher the acoustical power the higher the area and depth of thermal lesion because higher acoustical energy per unit time is transferred to the same area. This result is very important during thermal ablation of tissues because the correct determination of the power before the sonication will optimize the treatment. The area and the size of thermal lesions matched the geometry of the transducer also during the assessment of thermal lesions in a commercial polyacrylamide gel phantom.

The next step of the evaluation was to assess the temperature elevation on the agar/silica evaporated milk gel phantom. Temperature elevation is very important for thermal therapy which can be divided into two sections. The first is low-temperature hyperthermia, where temperatures in the range of 43–45 °C are applied for several minutes to kill cancer cells directly or to sensitize them to cytotoxic agents and/or radiation [231]. The second is high-temperature thermal ablation, where temperatures in the range of 50–80 °C or higher are applied for a shorter amount of time to rapidly coagulate the tissue and induce necrosis through processes such as protein denaturation [232]. The temperature elevation increased by 57 % when acoustical power increased by 7 W for 60 s. The 70 °C temperature elevation with16 W acoustical power was in the range of thermal ablation.

Moreover, the relationship between temperature elevation and the distance from the transducer's face in the agar/silica evaporated milk phantom was investigated. For our arterial model that was discussed in chapter 4, the temperature elevation near the artery is a critical factor and should be kept below 1 °C. The temperature elevation was kept below 1 °C at distance 5 mm at the face of the transducer for 12 W acoustical powers and 12 s sonication time. Another similar

evaluation was done with increased sonication time at 60 s. The different combination of depths and acoustical power did not maintain the temperature elevation below 1 ℃. The minimum 1.8 ℃ temperature elevation was achieved for 10 W acoustical powers at 10 mm depth from the transducer's face.

The last part of this study was to assess the temperature elevation on the agar/silica evaporated gel using mechanical mode. During the treatment of atherosclerotic plaque both thermal and mechanical mode of ultrasound can be used. The first mode can be used at the beginning to destroy as much as possible plaque and the second at the end of the treatment where the temperature elevation should be kept below 1℃ near the artery. During this evaluation the temperature elevation kept below 1℃ for acoustical powers up to 25 W and 2000 ms PRP.

7.16 Conclusion

An evaluation of ultrasonic ablation in different tissue phantoms was presented in this chapter. Different sonication parameters were used such as acoustical power and sonication time. Tissue phantoms consisted of agar/silica evaporated milk gel phantom, a commercial polyacrylamide gel and freshly excited turkey tissue. The size and the shape of the lesions were similar to the geometry of the transducer. The temperature elevation was assessed because is an important part during destruction of atherosclerotic plaque in human arteries. The temperature elevation should be kept up to 1 ℃ in the artery. The distance from the transducer's surface and the mechanical mode were evaluated for achieving this goal.

8. Evaluating acoustic and thermal properties of a plaque phantom

8.1 Introduction

Atherosclerosis is a systemic disease that mainly affects large and medium-sized arteries. The disease starts as an endothelial dysfunction, which initiates recruitment of inflammatory cells and lipids within the arterial wall [227]. This combination with smooth muscle hyperplasia develops a slowly growing atherosclerotic plaque that can create ischemia or stenosis leading to heart attack or stroke. Atherosclerosis treatment requires special surgical procedures such as balloon angioplasty [228-230], balloon angioplasty and stenting [231, 232], cutting balloon [233-235], atherectomy [236, 237] and surgical bypass [238, 239], to open an artery and improve blood flow. The degree of luminal stenosis and patient's symptomatology, among other factors, determine the best treatment option for each patient [240]. High intensity focused ultrasound (HIFU) [241] may present an innovating option for treatment of localized atherosclerotic plaques in terms of providing a completely non-invasive treatment paradigm for ablation of atherosclerotic plaques.

HIFU beams can be precisely focused within a small focal volume, resulting in a rapid rise of the local tissue temperature. This temperature elevation causes localized tissue damage through coagulative necrosis [241, 242]. The ideal choice of operating frequency and transducer design can lead to this result without significant biological damage to the intervening tissue [243, 244]. Moreover, the presence of image guidance modalities such as MRI and ultrasound has allowed for completely non-invasive thermal therapy procedures [245-248].

Thermal effect of ultrasound is mainly due to a phenomenon called absorption, in which the mechanical energy is converted into heat. Heating is related to the distribution of intensity in the absorbed beam and the frequency-dependent absorption coefficient (characteristic of each type of tissue). However, the transducer itself can be a source of heat by conduction, and one should also consider blood perfusion which plays a key role in reducing heating significantly. The temperature rise in the body is always a matter of great concern because of its influence in cellular activity [249]. There is a need to continuously propose techniques to assess the effects

produced by ultrasound in the human body with higher confidence and accuracy. Tissue-mimicking phantom materials have been largely explored in ultrasound research in the last decades [250-254]. Concerning atherosclerotic plaque, plaque phantoms have been used in several studies. Some of the studies specified only mimicking lipid plaques [255-259], calcified plaques [260-262], lipid and fibrous cap/tissue plaques [263-273]; lipid and calcified plaque [274] and only one study [275] mimicked the main three components (fibrous tissue, lipid core and calcium).

Apart from the obvious capability of withstanding ablation temperatures, phantoms need to mimic all the acoustic and thermal properties required for the relevant application method. The most frequently reported acoustic properties for tissues and phantoms include speed of sound, acoustic attenuation coefficient, acoustic impedance and density. On the other hand, thermal properties include thermal conductivity, specific heat capacity and thermal diffusivity. To our knowledge, no previous study was performed for evaluating atherosclerotic plaque phantoms *in vitro* with their main three components for evaluating the acoustic and thermal properties. The main acoustic and thermal properties of soft tissues (fatty, muscle; brain, breast, liver, kidney and blood) are reported by McGarry et al. [276]. The average acoustic and thermal properties of tissues with standard deviation are summarized on table 8.1.

Table 8.1: Acoustic and thermal properties of soft tissues (fatty tissue, muscle, brain, breast, liver, kidney, blood)

Properties of tissues	Meanvalue± SD
Speed of sound (m/s)	1548 ± 39
Attenuation coefficient (dB/cm-MHz)	0.63 ± 0.30
Acousticimpedance (MRayl)	1.61 ± 0.08
Density (kg/m^3)	1039 ± 23
Thermal conductivity (W/mK)	0.42 ± 0.11
Volumetric specific heat capacity (MJ/m^3K)	3.27 ± 0.05
Thermal diffusivity (mm^2/s)	0.13 ± 0.02

The acoustic characterization of tissue in terms of attenuation, absorption, scattering, and propagation speed is very important for the effective implementation of ultrasound for diagnosis or treatment. The pulse-echo and through-transmission methods are used for measuring the acoustic speed and attenuation of ultrasound in

several media [277]. The various techniques require immersion of the sample in a liquid agent, most often water, and have different advantages, experimental set-ups, and assumptions with different modifications of previously utilized methods [278, 279]. For the through-transmission method one transmitting and one receiving transducer is used, with attenuation either given as a ratio between signals recorded in the reference water path and in presence of the sample between the transducers [54] or with the variable thickness method, as a ratio of the independent attenuations of two sample specimens of different thicknesses [281]. In contrast, in the pulse echo technique a transducer operates in transmit and receive mode sends signals through the sample which are reflected on a high impedance material [282]. Attenuation is calculated by considering echoes arising in the reference water frame and in presence of the sample. However, this technique is only valid for equal transmission and refection coefficients at both sides of the sample [277]. Moreover, the mechanisms affecting attenuation have been extensively reported in literature [283, 284].

The mechanism of acoustic absorption is important in therapeutic applications because it controls the amount of energy deposition in the form of heat. Acoustic absorption becomes the main property contributing to tissue temperature rise, when short pulses are used, because the effect of perfusion and conduction is minimized [283]. Experimental methods for estimating the fundamental property of absorption coefficient have been proposed [285]. It was shown that there are two main phases during the temperature rise immediately after the application of the acoustic pulse. During the first phase, the increase of temperature is due to the action of viscous forces between the wire of the thermocouple and the medium, while the second phase is due to the absorption of sound in the medium. The absorption coefficient is independent of the intensity of the incident wave and increases as temperature increases [286].

In 1979, Goss et al. [287] identified the magnitude and frequency dependency of ultrasonic absorption coefficient in various biological tissues (brain, heart, kidney, liver, tendon, and testis) using the transient thermoelectric method (TTM). Heat conduction can contribute a significant error to the measurement of the ultrasonic absorption coefficient when using the TTM method [288]. In this paper, the experimental set up designed in a previous study was used to determine the absorption

coefficient of atherosclerotic plaque phantoms using the TTM method [289]. The whole experimental setup provides stability for the transducer and the phantom, minimizing errors from the motion of the phantom and thermocouple.

Although acoustic and thermal properties of atherosclerotic plaque are very important for the effective implementation of ultrasound on diagnosis and treatment of diseases, as it is evidenced from the literature, not many research efforts were dedicated towards measuring both acoustic and thermal properties. The purpose of this study aims to describe the development of an atherosclerotic plaque phantom and test its suitability as such by characterizing its acoustic and thermal properties.

8.2. Materials and Methods

8.2.1 Atherosclerotic Plaque Phantom

The atherosclerotic plaque phantom consisted of Agar-agar granulated, purified and free from inhibitors for microbiology, (Merck KGaA, EMD Millipore Corporation, Darmstadt, Germany), gypsum (Peletico Building Gypsum, Peletico Ltd, Strovolos, Cyprus), butter (FLORA original, UNILEVER TC LTD, Nicosia, Cyprus) and water. Agar was used for mimicking fibrous tissue, gypsum for calcium and butter for lipid core. The produced sample was isotropic and homogeneous. The amount of ingredients used each time was varied. The steps for the preparation were described in Menicou et al. [277].

8.2.2 Estimation of acoustic propagation speed

Acoustic propagation speed of the plaque phantoms having different lipid, gypsum and butter concentration was measured using the pulse-echo technique. The pulse-echo technique was used for measurement of the acoustic propagation speed for the different recipes of atherosclerotic plaque phantoms. Each phantom was immersed in an acrylic water tank filled with deionised/degassed water. A pulse/receiver (500 PR, GE Panametrics, Waltham, USA) was utilised to send ultrasound waves to a planar transducer working in transmit/receive mode, operating at a frequency of 2.7 MHz and having an active element diameter of 10 mm. A holder made from

Acrylonitrile Butadiene Styrene (ABS) was printed utilising an industrial 3D printer (FDM 270, Stratasys Ltd., Minessota, USA) to accommodate the transducer and phantom. A digital oscilloscope (TDS 2012, Tektronix Inc., USA) was connected to the pulse/receiver to measure the signal from the transducer which is transmitted through the sample and reflected back using a metal reflector. Fig. 8.1 shows the schematic diagram of the experimental set-up used for measurement of the acoustic propagation speed.

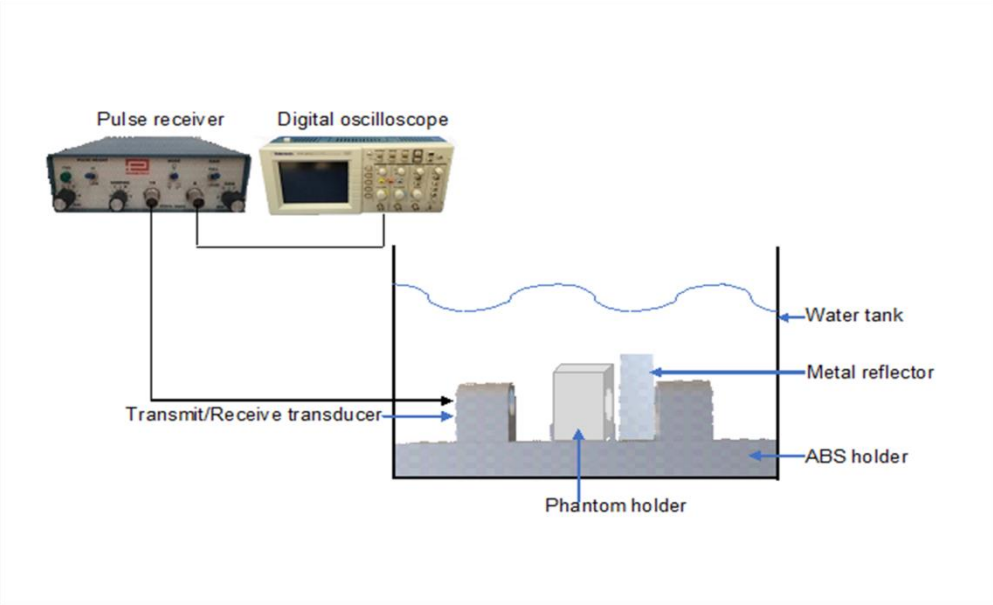

Fig.8.1 Schematic diagram of the experimental set-up used for measurement of the acoustic propagation speed

Initially, acoustic echoes were recorded as the reference water path and then with each of the phantoms fixed on the sample holder. The group velocity within each phantom was calculated using the Eq. (1) [290]:

$$v_s = v_w \left[\frac{(t_w - t_s)}{\Delta t} + 1\right] \quad (1)$$

where v_w is the acoustic propagation speed in water, t_w is the time needed for the wave to travel to the reflector and back to the transducer in the reference water path, t_s is the time required for the wave to travel the same distance in the presence of the phantom and Δt is the time difference between echoes arising from the front and back surfaces of the phantom.

8.2.3 Measurement of attenuation coefficient

Attenuation of the plaque phantoms having different lipid, gypsum and butter concentration was measured using the through-transmission technique. The planar transmitting transducer operating at 1.1 MHz was inserted in the ABS holder facing the respective 1.1 MHz receiver transducer, which was connected to a spectrum analyzer (HP8590L, Keysight Technologies, California, USA) for recording the attenuated signal. Each phantom was accommodated between the transducers. Figure 8.2 shows the schematic diagram of the experimental set-up. Signals were recorded in the reference water path and then with the phantom samples fixed between the transducers.

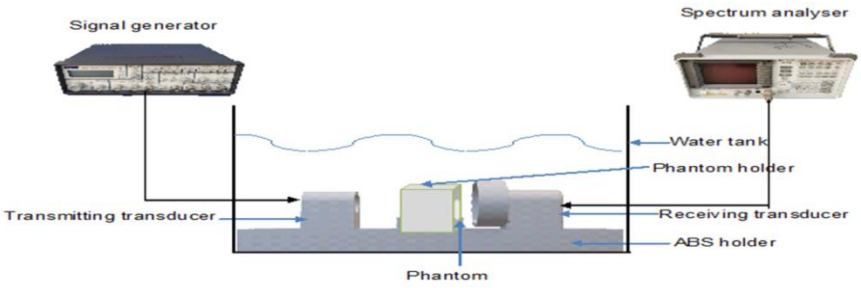

Fig.8.2 Experimental set-up used for measurement of the attenuation coefficient of different plaque phantoms

The attenuation coefficient of each phantom was calculated using the Eq. (2) [277]:

$$a = a_w + \frac{20 \log e}{x} \times \ln\left(\frac{A_w}{A_s} T\right) \quad (2)$$

where a_w is the attenuation coefficient of water, x is the thickness of each phantom, A_w is the signal received in the reference path, A_s is the signal received in presence of each phantom and T is the transmission coefficient. The transmission coefficient of each phantom was inserted in the equation to account for ultrasonic reflection induced by each different surface of the phantoms. It was calculated using the following equation:

$$T = 1 - R \quad (3)$$

Where R is the reflection coefficient calculated using the Eq. (4):

$$R = \left(\frac{Z_1 - Z_2}{Z_1 + Z_2}\right)^2 \quad (4)$$

Where Z_1 and Z_2 are the acoustic impedances of phantom and water respectively and can be calculated using the Eq. (5):

$$Z = \rho \cdot c \quad (5)$$

Where ρ is the mass density and c is the acoustic propagation speed of either the water or phantom under investigation. The phantom's mass density was calculated using the water displacement method [277]. A piece of phantom was weighed (1479 V, Tanita Corporation of America, Inc, USA) and its volume was extracted by measuring displacement of water in a volumetric tube.

8.2.4 Estimation of absorption coefficient

A method to estimate fast and accurately the absorption coefficient of an agar-based gel phantom using a novel experimental setup [289]. According to this, the agar-based gel phantom was exposed to a focused US beam and the absorption coefficient was determined by measuring the rate of temperature rise using a thermocouple (5SC-TT-K-30–36, type K insulated beaded wire, 100 μm thick, Omega Engineering, Norwalk, Connecticut, USA). For the absorption coefficient measurement, a signal generator (HP 33120A, Agilent technologies, Englewood, CO, USA), an RF amplifier (AG1012, T & C Power Conversion, Inc., Humboldt St., Rochester, NY) and a spherically focused transducer (Sonic Concepts, Inc., Seattle, USA) operating at 0.4 MHz (focal length of 70 mm and diameter of 40 mm) were utilized in the experimental setup as described by Drakos et al. [289]. The transducer is of wide beam thus minimizes the conduction effects. Also, the temperature elevation is low thus minimizes the conduction effects. A temperature reader (HH806AU, Omega Engineering) was used to record the temperature over time in the TMM. The thermocouple was placed at the focal position which was located 4 cm deep from the bottom face of the TMM (the transducer was 3 cm below the front surface of the TMM facing upwards). Fig. 8.3 illustrates the schematic diagram of the experimental setup to estimate the absorption coefficient of plaque phantoms.

8.2.5 Estimation of plaque phantom thermal properties

The thermal properties of the plaque phantoms were measured using the instrument Isomet (model 2104, Applied Precision, Ltd., Bratislava, Slovakia). The instrument was used according to the manufacturer's recommendation for estimating thermal conductivity (W/mK), thermal diffusivity (mm^2 /s), and specific heat capacity (kJ/kgK). The transient method was used to perform the thermal conductivity measurements, which were carried out automatically by a needle sensor. The selected sensor was able to accurately measure in the range of 0.2–1 W/ m K. According to the manufacturer, the accuracy of the device for thermal conductivity measurements was 5% of reading +0.001 W/m K. Thermal diffusivity is derived by dividing conductivity with density whereas specific heat capacity describes how quickly a material reacts to a change in temperature. A spherical volume of the material around the needle probe with a minimum diameter of 5 cm was needed for accurate measurement. Due to this limitation of the system, a specimen of appropriate dimensions (5 cm height, 7 cm wide and 15 cm long) was prepared. The needle probe was inserted in the plaque phantom, and the 3 thermal properties (thermal conductivity, thermal diffusivity, and volumetric specific heat capacity) were calculated simultaneously by the device. The procedure was repeated five times and the mean and standard deviation values of each thermal property were deduced.

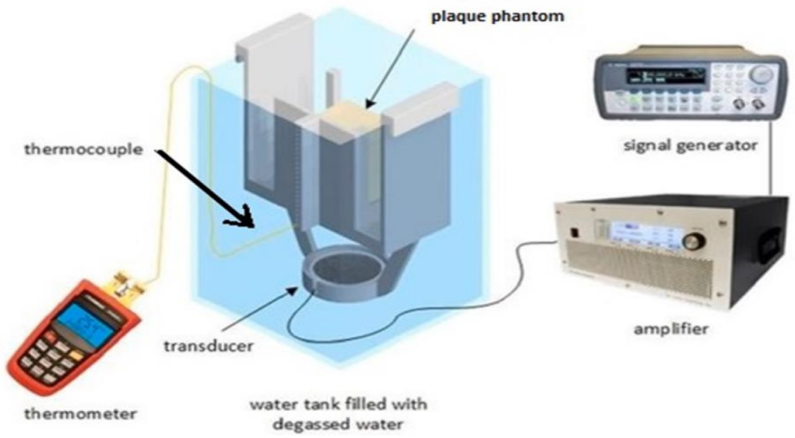

Fig.8.3 Schematic diagram of the experimental set up to measure the absorption coefficient of the plaque phantoms

8.2.6 Experimental setup and HIFU sonication parameters

The absorption experimental setup described previously was used to apply high-power sonication in the phantom. The scope of the high-power sonication was to test the ability of the phantom to reach high temperatures and create lesions. The phantom was fitted tightly into the holder and a transducer (Sonic Concepts, Inc., Seattle, USA) operating at 0.4 MHz (radius of curvature of 70 mm and diameter of 40 mm) was positioned below the phantom facing upwards for a bottom to top sonication inside an acrylic water tank filled with degassed/deionised water. The experimental HIFU system included a signal generator (HP 33120A, Agilent Technologies), a radio-frequency power amplifier (AG1012, T&C Power Conversion, Inc.), and the spherically-focused transducer. Prior to sonication, the phantom was allowed to reach thermal equilibrium with the degassed/deionised water to minimize conduction effects. The sonication time was 60 s and the acoustical power was 10 W. The transducer position was adjusted in order to focus at 3 cm deep inside the phantom.

8.2.7 Temperature measurement using a thermocouple

During sonication, the temperature change at the focal point of the phantom was recorded. The temperature reader (HH806AU, Omega Engineering) was used to record the temperature change in the phantom. The thermocouple (5SC-TT-K-30–36, type K insulated beaded wire, 100 μm thick, Omega Engineering) was inserted in the sample at the focus which was 3 cm deep. The thermocouple tip was rigid enough and it was inserted from one end of the phantom, all the way to the target with the phantom immersed in degassed/deionised water. The thermocouple tip was selected to be sufficiently thin to reduce possible artifacts. Although the focal length was known, precise localization of the focal point was achieved by changing the position of the thermocouple at low power until the highest temperature change was achieved.

8.3. Results

Plaque phantoms with different amounts of agar, butter and gypsum were prepared following a simple preparation procedure [277]. Thermal properties (thermal

conductivity, volumetric specific heat capacity and thermal diffusivity) were evaluated by inserting a needle probe in the plaque phantom. Initially, experiments were performed to assess thermal properties by varying butter concentration. Figure 8.4 shows thermal properties against butter concentration for 10% w/v and 6% w/v gypsum respectively. The lower the percentage of gypsum the lower the thermal conductivity, volumetric heat capacity and thermal diffusivity. When gypsum increased by 4 % w/v, thermal conductivity increases by 1.9 – 2.2%, volumetric heat capacity by 0.6 % and thermal diffusivity by 1.7 – 2.1%.

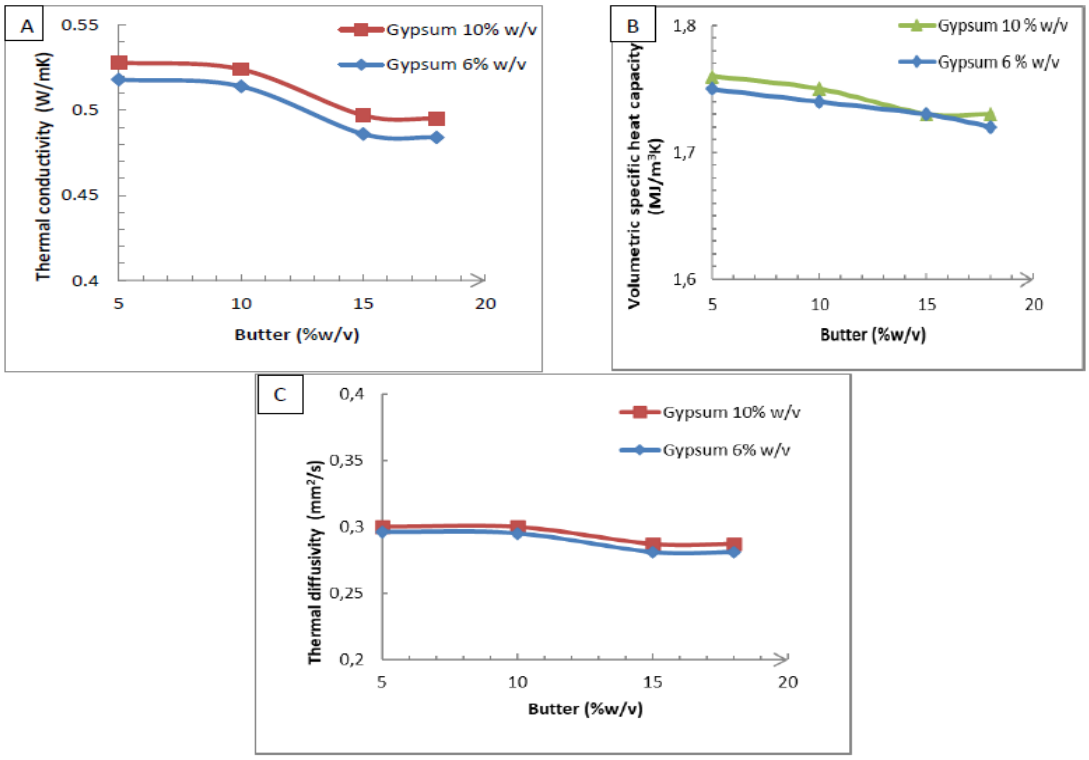

Fig 8.4a) Thermal conductivity, b) Volumetric specific heat capacity and c) Thermal diffusivity of plaque phantoms against butter concentration for 10 % w/v and 6 % w/v gypsum respectively.

Furthermore, experiments were performed to assess thermal properties by varying agar concentration. Figure 8.5 shows thermal properties against gypsum with 10% w/v butter and 10% w/v gypsum. For the phantom with 2% w/v agar was impossible to take measurements because the phantom did not solidify. The agar changed slightly the thermal properties of the plaque phantom. Specifically, when

agar increased by 2 % w/v, thermal conductivity decreased by 3.2 – 4.6 %, volumetric heat capacity by 0.6 % and thermal diffusivity by 3.1 – 3.7 %.

Gypsum, the mimicking material of calcium was lastly assessed regarding thermal properties. Thermal properties of plaque phantoms against gypsum for 10% w/v and 18% w/v butter concentration are shown in fig.8.6. Thermal conductivity k and thermal diffusivity D followed a similar relationship with gypsum concentration. Both of them increased from 2% w/v to 10% w/v gypsum and then decreased slightly until reaching 14% w/v gypsum (calcified material). Furthermore, the amount of reduction from 10% w/v to 14% w/v gypsum was larger when the amount of lipid concentration was larger. Moreover, volumetric specific heat capacity was constant from 2% w/v to 6% w/v gypsum, and then increased slightly by 0.6% from 6% w/v to 10% w/v gypsum and then remained constant up to 14% w/v gypsum. For all the measurements, thermal properties of atherosclerotic plaque phantoms decreased when lipid concentration increased.

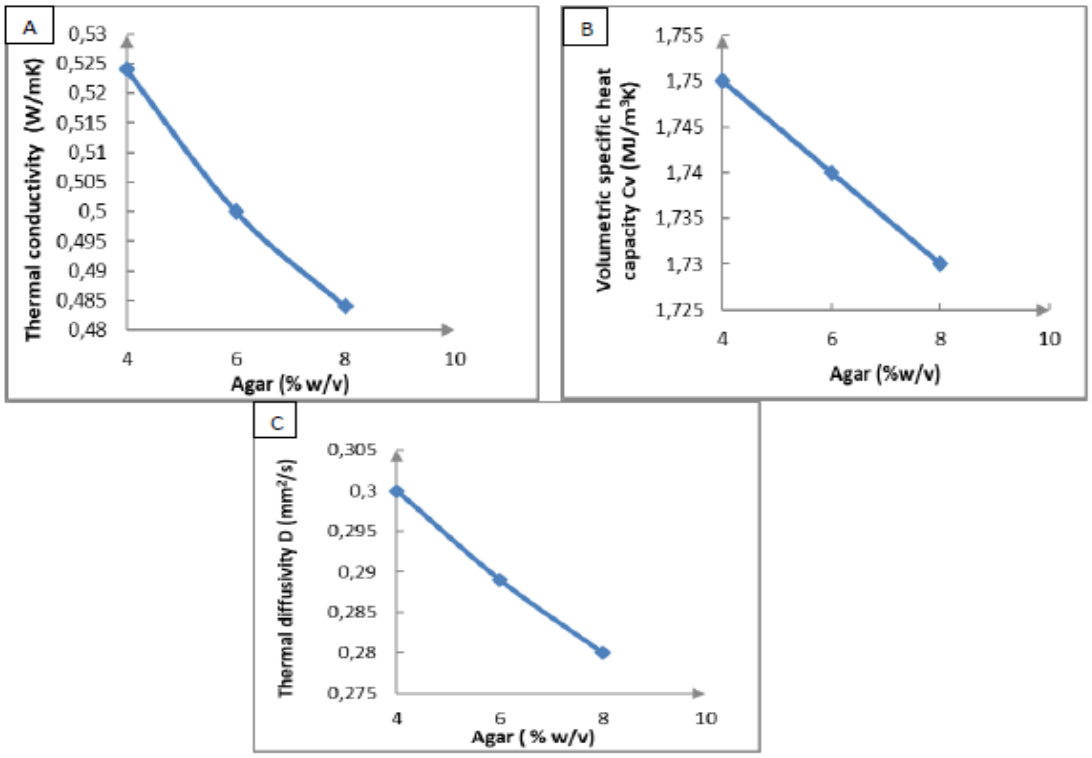

Fig 8.5a) Thermal conductivity, b) Volumetric specific heat capacity and c) Thermal diffusivity of plaque phantoms against agar for 10% w/v lipid and10% w/v gypsum.

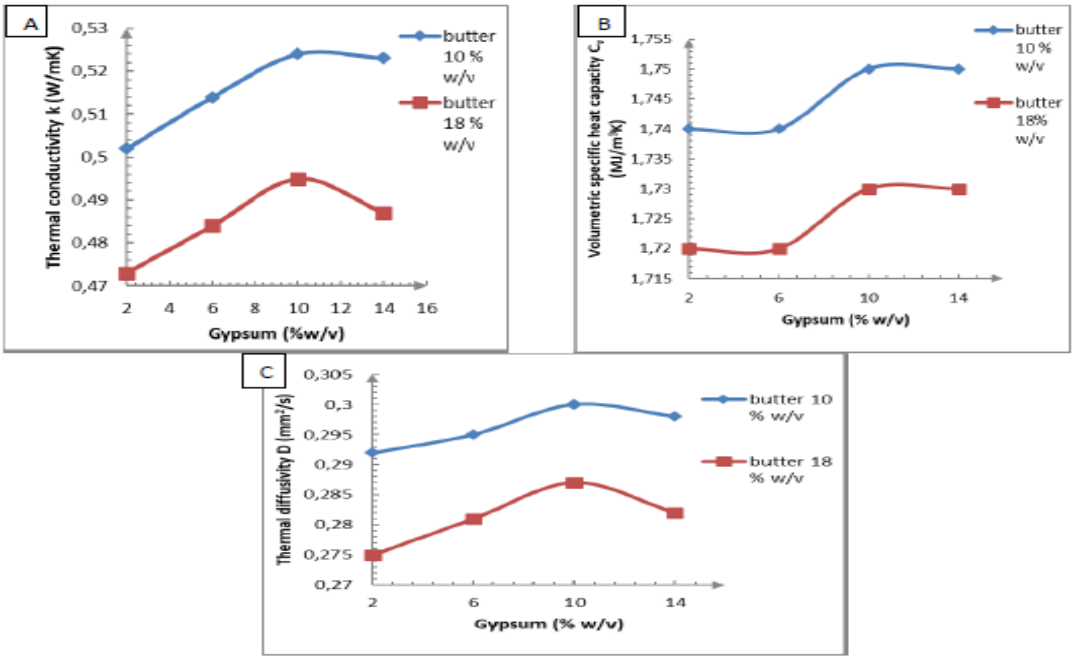

Fig 8.6a) Thermal conductivity, b) Volumetric specific heat capacity and c) Thermal diffusivity of plaque phantoms against gypsum for 10% w/v and 18% w/v butter respectively.

The absorption coefficient was estimated by applying an ultrasonic protocol that produces a low-temperature change between 2 and 3 ℃, which correspond to an acoustic power of 1 W [289]. During the sonication, the temperature increased linearly with time as expected since conduction effects are eliminated. The temperature maintained its linearity for a long sonication of 60 s, which is representative of low conduction. The maximum temperature and the rate of temperature recorded for different plaque phantoms. Based on the temperature-time gradient, the absorption coefficient calculated for each plaque phantom. The attenuation coefficient of each phantom was calculated using the through-transmission immersion technique. Acoustic properties of plaque phantoms against lipid concentration are shown in fig.8.7. Absorption coefficient increases as lipid concentration increases. Absorption coefficient increased up to 78.2 % when lipid concentration increased by 10% w/v. Attenuation coefficient increased as the lipid concentration increased for 1.1 MHz frequency. Attenuation coefficient increased up to 4.7 % when lipid concentration increased by 10% w/v. As the lipid concentration of

plaque phantom increases, the acoustic propagation speed decreases. Specifically, acoustic propagation speed decreased by 1.2 % when lipid concentration increased by 10% w/v. Depending on the agar, gypsum and butter concentration the ultrasonic attenuation coefficient can vary.

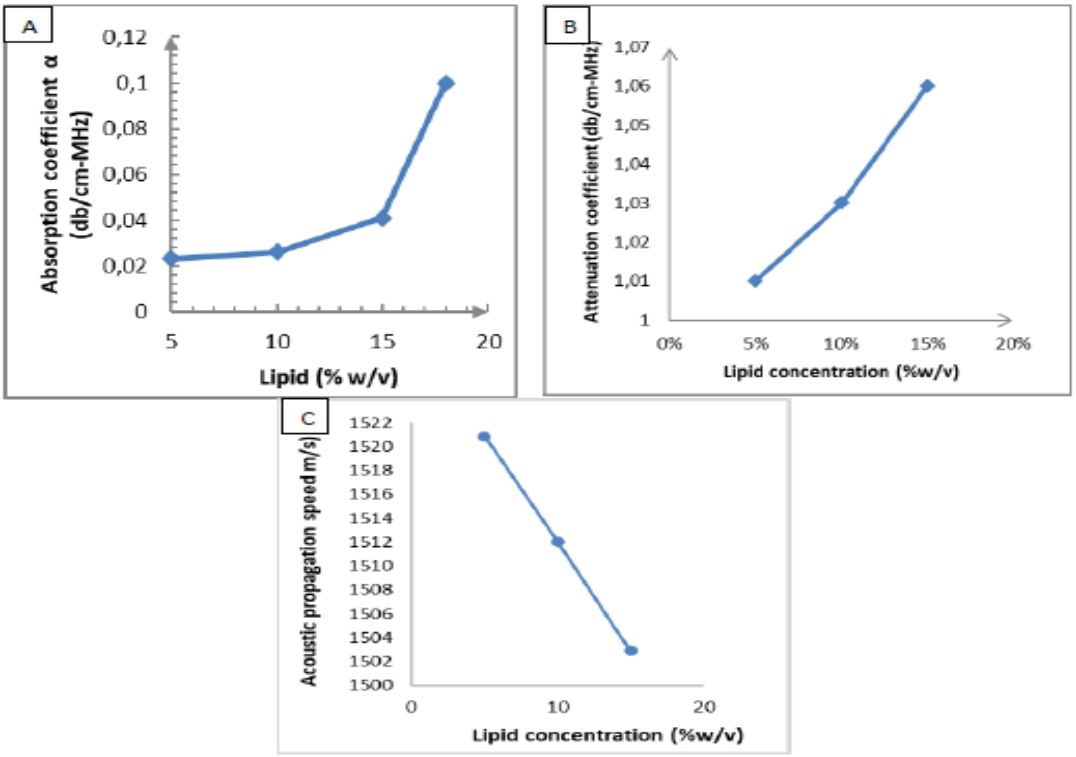

Fig 8.7a) Absorption coefficient, b) Attenuation coefficient and c) Acoustic propagation speed of plaque phantoms against lipid concentration. Agar and gypsum was 4 % w/v and 6 % w/v respectively.

Additionally, experiments were performed to assess acoustic properties by varying agar concentration. Figure 8.8 shows acoustic properties against agar with 10 % w/v butter and 10 % w/v gypsum. As the agar concentration increased by 6 % w/v, the ultrasonic absorption coefficient increased up to 138 %. For this experiment, the minimum value measured for absorption coefficient was 0.26 dB/cm-MHz (2 % agar, 6 % gypsum, 18 % butter) and the maximum 0.62 dB/cm-MHz (8% agar, 6% gypsum and 18 % butter). Attenuation coefficient increased as the agar increased for 1.1 MHz frequency. Attenuation coefficient increased up to 70% when agar concentration increased by 3 % w/v. The measured attenuation coefficient value was founded in the range of 1-3 dB/cm-MHz that was reported in a previous study [291]. Moreover, the

acoustic propagation speed was founded in the range of soft tissues [292]. Acoustic speed increased when agar concentration increased by 1% w/v and then decreased slightly until 6 % w/v agar concentration.

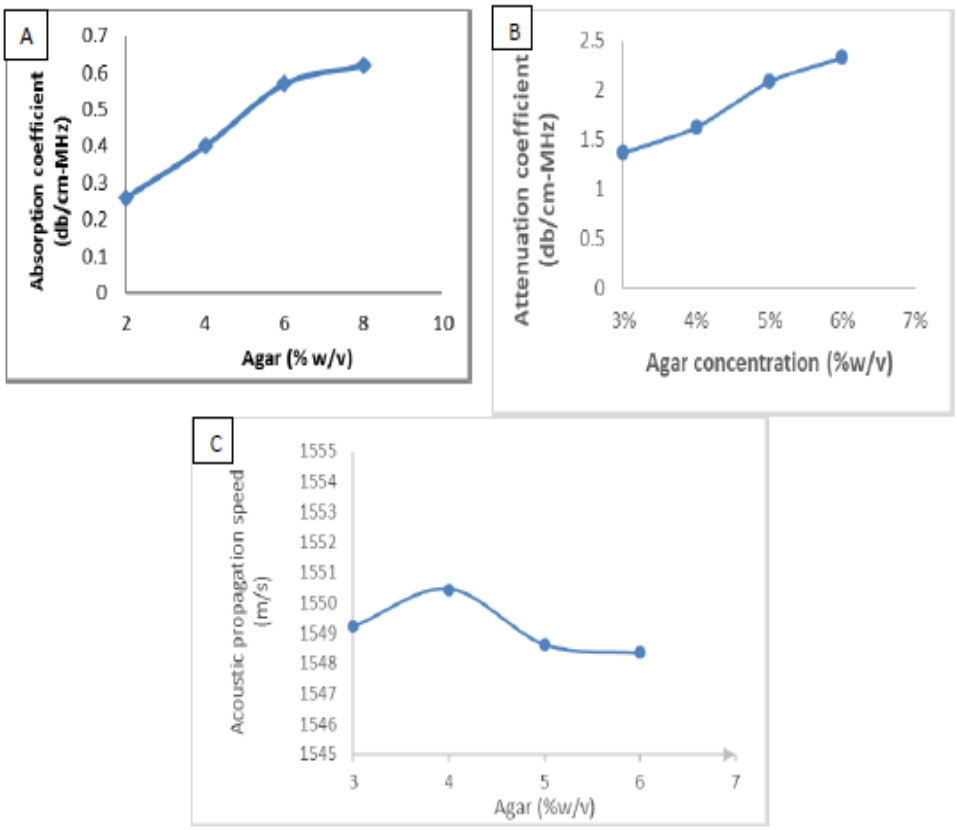

Fig 8.8a) Absorption coefficient, b) Attenuation coefficient and c) acoustic propagation speed of plaque phantoms against agar concentration. Gypsum and butter was 6 and 15 % w/v respectively.

Finally, acoustic properties of plaque phantoms against gypsum for 4% w/v agar and 15% w/v butter concentration are shown in fig. 8.9. As the gypsum concentration increased, the ultrasonic absorption coefficient decreased. Absorption coefficient decreased up to 55% when gypsum concentration increased by 12% w/v. Attenuation coefficient increased up to 45% when gypsum concentration increased by 12 % w/v. As the gypsum concentration of plaque phantom increases, the acoustic propagation speed decreases while attenuation coefficient increases. Acoustic propagation speed decreased by 3.3 % when gypsum concentration increased by 12% w/v.

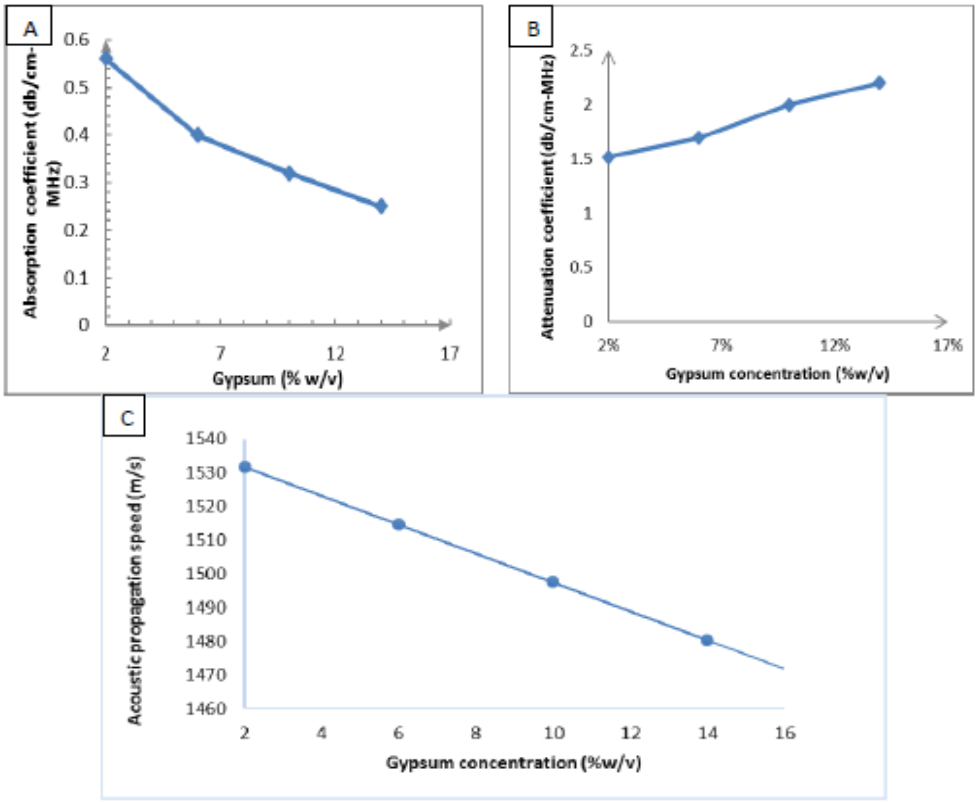

Fig 8.9a) Absorption coefficient, b) Attenuation coefficient and c) acoustic propagation speed of plaque phantoms against gypsum concentration. Agar and butter concentration was 4 % w/v and 15% w/v respectively.

8.4. Discussion

The purpose of this study is to describe the evaluation of an atherosclerotic plaque phantom by characterizing its acoustic and thermal properties. The phantoms consisted of agar, gypsum, butter and water. Agar was used for mimicking fibrous tissue, gypsum for calcium and butter for lipid core. Although acoustic and thermal properties of atherosclerotic plaque are very important for the effective implementation of ultrasound on diagnosis and treatment of arteriosclerosis diseases, as it is evidenced from the literature, not many research efforts were dedicated towards measuring both acoustic and thermal properties. Range of phantoms ingredients, range of acoustic and thermal properties and their mean value with standard deviation of atherosclerotic plaque phantoms are shown in table 8.2. The

range of densities of plaque phantoms was varying from 900 to 1100 kg/m^3. The higher the amount of lipid, the lower the density.

Table 8.2: Range of phantoms ingredients, range of acoustic and thermal properties and their mean value with standard deviation of atherosclerotic plaque phantoms

Range of agar (%w/v)	Range of gypsum (%w/v)	Range of butter (%w/v)	Acoustic and thermal properties	Range of acoustic and thermal properties	Mean value ± SD
4 only	10 only	10-15	Acoustic speed (m/s)	1498 - 1550	1523±23
4-6	6-10	5-10	Absorption coefficient (dB/cm-MHz)	0.023-0.620	0.30±0.21
4 only	2-10	15 only	Acoustic Impedance (MRayl)	1.30 -1.40	1.35±0.03
4-6	6-10	5-10	Attenuation coefficient (dB/cm-MHz)	1.00-2.34	1.63±0.46
4 only	6-10	5-18	Thermal conductivity k (W/mK)	0.44 - 0.52	0.50±0.02
4 only	6-10	5-18	Volumetric specific heat capacity C_v (MJ/m^3K)	1.69-1.77	1.73±0.02
4 only	6-10	5-18	Thermal diffusivity D (mm^2/s)	0.26 - 0.30	0.29±0.01

The experiments were initially conducted in plaque phantoms with different amount of agar, gypsum and butter for evaluation of thermal properties (thermal conductivity, volumetric specific heat capacity and thermal diffusivity). As lipid concentration increases, thermal conductivity, volumetric specific heat capacity and thermal diffusivity decreases. The calcified material (gypsum) changed slightly the thermal properties of the plaque phantoms. As gypsum concentration increases,

thermal properties increase slightly. Furthermore, as agar concentration increases, thermal conductivity, volumetric specific heat capacity and thermal diffusivity decreases.

Table 8.2 shows the range of phantoms ingredients, range of acoustic and thermal properties and their mean value with standard deviation of atherosclerotic plaque phantoms. Thermal conductivity, volumetric specific heat capacity and thermal diffusivity mean values with standard deviations were 0.50±0.02 $Wm^{-1}K^{-1}$, 1.73 ± 0.02 $MJm^{-3}K^{-1}$ and 0.29 ± 0.01 mm^2s^{-1} respectively. The plaque phantom with the maximum amount of butter (agar 4% w/v agar, 6% w/v gypsum and 18% w/v butter) had the minimum amount of thermal conductivity (0.48 $Wm^{-1}K^{-1}$), volumetric specific heat capacity (1.69 $MJm^{-3}K^{-1}$) and thermal diffusivity (0.26 mm^2s^{-1}) respectively. Moreover the plaque phantom with the minimum amount of butter and increased gypsum (4% w/v agar, 10 % w/v gypsum and 5 % w/v butter) had the maximum amount of thermal conductivity (0.52 $Wm^{-1}K^{-1}$), volumetric specific heat capacity (1.77 $MJm^{-3}K^{-1}$) and thermal diffusivity (0.30 mm^2s^{-1}). Thermal conductivity values for the plaque phantoms are in the range of those of biological tissues and arterial plaques. [293,294]. For our evaluated phantom, the thermal conductivity values are in the range of those of body internal organs, such as kidney (0.58 ± 0.07 $Wm^{-1}K^{-1}$), muscle (0.54 ± 0.06 $Wm^{-1}K^{-1}$) and liver (0.48 ± 0.06 $Wm^{-1}K^{-1}$). On the other hand, there is an important difference of our phantom with volumetric heat capacity (liver: 3.27 ± 0.01 $MJm^{-3}K^{-1}$, kidney: 3.76 ± 0.44 $MJm^{-3}K^{-1}$, muscle: 3.61 ± 0.42 $MJm^{-3}K^{-1}$) and thermal diffusivity (liver, kidney, and muscle: 0.15 ± 0.02 mm^2s^{-1}) [293]. Different tissues have different thermal properties and our plaque phantom is a combination of four different materials (agar, butter, gypsum and water) with different percentages.

Moreover, the pulse-echo technique was used to measure the acoustic propagation speed within different atherosclerotic plaque phantoms. Attenuation of the plaque phantoms having different lipid, gypsum and butter concentration was measured using the through-transmission technique. As lipid concentration increases, acoustic propagation speed decreases while attenuation coefficient increases (fig.8.7). As gypsum concentration increases, thermal properties increase slightly. Furthermore, as agar concentration increases, acoustic propagation speed reaches the maximum

value at 4% w/v agar and then decreases slightly while attenuation coefficient increases (fig.8). Finally, as gypsum concentration increases, acoustic propagation speed decreases while attenuation coefficient increases (fig.9).

Acoustic speed, acoustic impedance and attenuation coefficient mean values with standard deviations were 1523±23 m/s, 1.35±0.03 MRayl and 1.63±0.46 dB/cm-MHz (table 8.2). The plaque phantom with agar 4 % w/v agar, 10 % w/v gypsum and 10 % w/v butter had the maximum acoustic speed (1550 m/s) and the phantom with increasing concentration of 5 % w/v butter, the minimum acoustic speed (1498m/s). Additionally, the plaque phantom with agar 4 % w/v agar, 6 % w/v gypsum and 5 % w/v butter had the minimum attenuation coefficient (1.00 dB/cm-MHz) and the phantom with increasing concentration of 2 % w/v agar, 4 % w/v gypsum 5 % w/v butter the maximum acoustic speed (2.34 dB/cm-MHz). As the amount of calcified material in human atherosclerotic plaque increases, the ultrasonic attenuation increases [295]. Moreover, the plaque phantom with agar 4 % w/v agar, 10 % w/v gypsum and 15 % w/v butter had the minimum acoustic acoustic impedance (1.30 MRayl) and the phantom with decreasing concentration of 8 % w/v gypsum, the maximum acoustic acoustic impedance (1.40MRayl). The measured attenuation coefficient value was founded in the range of 1-3 dB/cm-MHz that was proposed in previous studies [296-298]. Moreover, the acoustic propagation speed was founded in the range of soft tissues [292]. Depending on the agar, gypsum, and butter concentration the ultrasonic attenuation coefficient can vary.

Additionally, the experimental set up designed in a previous study was used to determine the absorption coefficient of atherosclerotic plaque phantoms using the TTM method [289]. As lipid and agar concentration increases the absorption coefficient increases too (fig. 8.7, 8.8). Moreover, when gypsum concentration increases the absorption coefficient decreases (fig.8.9). The plaque phantom with agar 4% w/v agar, 6% w/v gypsum and 5% w/v butter had the minimum absorption coefficient (0.023 dB/cm-MHz) and the phantom with increasing concentration of 2% w/v agar, 4% w/v gypsum 5% w/v butter the maximum absorption coefficient (0.620 dB/cm-MHz). The absorption coefficient mean value with standard deviation was 0.30 ± 0.21 dB/cm-MHz. Absorption coefficient of soft tissues (liver, brain, kidney and heart) reported by Goss et al [287]. The desired absorption coefficient for

soft tissues and was 0.22 dB/cm-MHz. The concentration of agar, gypsum and butter concentration can alter the ultrasonic absorption coefficient. Finally, ultrasonic absorption coefficient values were inside the range of reported values for soft tissues [287] and an agar-based phantom [289].

The present study aims to enhance the available quantitative data on acoustic and thermal properties of atherosclerotic plaque and especially for ultrasonic absorption coefficient. As it was already mentioned earlier, not many data exist on the value of the ultrasonic absorption but only for soft tissues. According to the aforementioned literature reported within the scope of this study, it is concluded that acoustic and thermal properties of atherosclerotic plaque phantoms fall well within the range of values reported for atherosclerotic plaque and slightly different for thermal diffusivity and volumetric specific heat capacity for soft tissues.

The limitation of this study include that macrophages were not used during this study which is an important part of atherosclerotic plaque [300], but in general as it was investigated; no study has evaluated them in their model. In future studies, the optimum recipe of the atherosclerotic plaque phantoms that mimics the human atherosclerotic plaque (agar 4% w/v, gypsum 10% w/v and butter 10% w/v) can be used with the proper choice of operating frequency and transducer design for HIFU therapy and would be focused only for arteries that have at least 50 % blockage. Patients with at least 50% of coronary or carotid artery blockage may need more aggressive treatment, especially if they have symptoms while surgery is usually advised for carotid or coronary narrowing of more than 70%. This technology can be used in the future for clinical trials to treat plaques in the coronary arteries.

8.5. Conclusion

An evaluation of acoustic and thermal properties of plaque phantoms to test their suitability for ultrasound therapy was presented in this chapter. The evaluation included measurements of the acoustic propagation speed using pulse-echo technique, ultrasonic attenuation coefficient using through transmission immersion technique, and absorption coefficient using an ultrasonic protocol that produces a low-

temperature change method. Moreover, thermal properties (thermal conductivity, volumetric specific heat capacity and thermal diffusivity) were measured using the transient method using a needle probe. It is concluded that acoustic and thermal properties of atherosclerotic plaque phantoms fall well within the range of values reported for atherosclerotic plaque and slightly different for thermal diffusivity and volumetric specific heat capacity for soft tissues. The goal of this work was to assess acoustic and thermal properties of plaque phantoms in order to mimic the human arterial atherosclerotic plaque so can be used for ultrasound therapy in the future. However, macrophages which are an important part of atherosclerotic plaque should be investigated in upcoming studies. Finally, future studies should be focused on the optimum recipe of the atherosclerotic plaque phantoms that mimics the human atherosclerotic plaque (agar 4% w/v, gypsum 10% w/v and butter 10% w/v) and can be used for HIFU therapy and would be focused only for arteries that have at least 50 % blockage.

1

9. Conclusion and future work

This dissertation examined the design of an in vitro model to assess the thermal ablation of atherosclerotic plaque using different parameters of intravascular transducers. The first study was concentrated on the design and creation of a suitable plaque phantom to be used in HIFU application on the atherosclerotic plaque. To our knowledge, no previous study was performed for evaluating atherosclerotic plaque phantoms *in vitro* for ultrasound therapy. The second objective of this dissertation was the evaluation of porcine atherosclerotic plaque phantoms for US therapy. The plaque phantom was evaluated in abdominal porcine arteries that mimic the elasticity of human arteries. The next study included the evaluation of our phantom and a TMM phantom for US therapy using MR thermometry for evaluating the temperature elevation. Then US ablation was assessed in different phantoms and a turkey tissue. Temperature elevation was examined again by altering different parameters such as the distance from the transducer face, different active size of the transducer, different element area and different acoustical power. Finally, the last study examined the acoustic and thermal properties of plaque phantoms to test their suitability for ultrasound therapy.

Initially, for the first study the effect of therapeutic ultrasound for destruction of atherosclerotic plaque phantoms was described. A low cost arterial plaque model was evaluated with different atherosclerotic plaque phantoms using different acoustic parameters such as acoustic power and treatment time. The arterial mimic tube base was made by thermoplastic polyurethane (TPU) and the other components from co-polyester extended (CPE+) material for mimicking the elastic properties of the artery. Atherosclerotic plaques were mimicked with their three main components: fibrous tissue with agar, lipid core with butter and calcium with gypsum and the optimum treatment process that maximized the destruction of atherosclerotic plaque in minimum time duration was achieved. In order to succeed this, the influence of acoustic parameters such as acoustic power and treatment time was investigated. The acoustic power and treatment time range was 6 – 15 W and 6 – 30 s respectively. Fibrotic, PIT, TCFA, ThCFA and FC phantoms were mimicked to cover the different types of atherosclerotic plaques. Same plaque phantoms are evaluated separately with a portable X-Ray system and an overall conclusion has

been analyzed for all the phantoms. The max and minimum percentage plaque destruction was evaluated for same plaque phantoms and the relationship between the percentage plaque destruction and their ingredients was analyzed. A fibrotic and TCFA phantom was destructed completely with different acoustic powers and treatment times. The fibrotic phantom was destructed with 8 W acoustical power and 30 s treatment time while TCFA phantom with 15 W acoustical power and 20 s treatment time. FC phantom was not destructed because of the very high percentage of gypsum (50 %) that has been used. The maximum amount of lesion depth was 2.61 mm. This is very important for the future purpose of this study because the main coronary arteries are usually between 3 and 4 mm in diameter, so the transducer can be used in the future to destroy at least 65 % blockage of a coronary artery.

Moreover, the second study was based on the creation and evaluation of porcine atherosclerotic plaque phantoms for ultrasound therapy. Abdominal porcine arteries were selected due to their lumen size, so the transducer can fit inside them. The evaluation was made with an X-ray system and focused on PIT and TCFA atherosclerotic plaque phantoms which cover the main types of human atherosclerotic plaques. The maximum depth lesions for the PIT and TCFA porcine plaque phantom with 15 W acoustical powers were 2.94 mm and 2.90 mm for 25 and 30 s of sonication time respectively. On the other hand, the minimum depth lesions for the PIT and TCFA porcine plaque phantom with 15 s sonication time were 0.9 mm and 0.97 mm for 10 W and 15 W acoustical powers respectively. The findings of this study are very important for optimizing the acoustical parameters of the transducer during US ablation of atherosclerotic plaque.

An evaluation of atherosclerotic plaque and TMM phantom for ultrasound therapy using MR thermometry which is a noninvasive temperature real time MR monitoring during minimally invasive thermal therapy was assessed during the third study. The purpose of the first part of this evaluation was to destroy an area of a plaque-mimicking phantom using a planar transducer, obtain MR thermometry images during the sonication and assess the destroyed area of the phantom using high-resolution imaging. The average lesion depth was 1.77 mm for 30 s sonication time and acoustic power of 10 W. X-ray image and T2W-FSE image (sagittal plane) were used for the evaluation of the size and the depth of the plaque lesion. The size was

evaluated with the same accuracy while the depth of the lesion was evaluated more precisely with the X-Ray image. Moreover, a TMM phantom was evaluated for heating with a planar transducer. The readings near the planar transducer were completely masked by electricity artifacts.

The fourth study had as its main objective to evaluate the creation of thermal lesions with US in different phantoms such as agar/silica evaporated milk gel phantom, a commercial polyacrylamide gel and freshly excited turkey tissue. For the freshly excited turkey tissue, as the acoustical power increased by 7 W, the mean area and depth of thermal lesions increased by 42,6% and 20% respectively. The temperature elevation was assessed because is an important part during destruction of atherosclerotic plaque in human arteries and should be kept up to 1 ℃. The distance from the transducer's surface and the mechanical mode were evaluated for achieving this goal. During the evaluation of the agar/silica evaporated milk gel phantom, the temperature elevation kept below 1℃ at distance 5 mm for the face of the transducer for 12 W acoustical powers and 12 s sonication times. During the treatment of atherosclerotic plaque both thermal and mechanical mode of ultrasound can be used. When the sonication time increased at 60 s, the different combination of depths and acoustical powers did not achieve to keep the temperature elevation below 1 ℃. The minimum 1.8 ℃ temperature elevation was achieved for 10 W acoustical powers at 10 mm depth from the transducer's face 1℃.

Finally, the last study focused on evaluating of acoustic and thermal properties of plaque phantoms to test their suitability for ultrasound therapy. The pulse-echo technique, through transmission immersion technique and an ultrasonic protocol that produces a low-temperature method were used to measure the acoustic propagation speed, ultrasonic attenuation coefficient and absorption coefficient respectively. Moreover, the transient method using a needle probe was used for evaluating the thermal properties (thermal conductivity, volumetric specific heat capacity and thermal diffusivity. The acoustic and thermal properties of atherosclerotic plaque phantoms fall well within the range of values reported for atherosclerotic plaque and slightly different for thermal diffusivity and volumetric specific heat capacity for soft tissues. Thermal conductivity values for the plaque phantoms are in the range of those of biological tissues and arterial plaques. [293-294]. For our evaluated phantom, the thermal conductivity values are in the

range of those of body internal organs, such as kidney (0.58 ± 0.07 $Wm^{-1}K^{-1}$), muscle (0.54 ± 0.06 $Wm^{-1}K^{-1}$) and liver (0.48 ± 0.06 $Wm^{-1}K^{-1}$). On the other hand, there is an important difference of our phantom with volumetric heat capacity (liver: 3.27 ± 0.01 $MJm^{-3}K^{-1}$, kidney: 3.76 ± 0.44 $MJm^{-3}K^{-1}$, muscle: 3.61 ± 0.42 $MJm^{-3}K^{-1}$) and thermal diffusivity (liver, kidney, and muscle: 0.15 ± 0.02 mm^2s^{-1}) [293]. Different tissues have different thermal properties and our plaque phantom is a combination of four different materials (agar, butter, gypsum and water) with different percentages.

A future development of this study should include macrophages which is an important part of atherosclerotic plaque [300] and may alter not only the optimum treatment result but also the acoustic and thermal properties of atherosclerotic plaque phantoms. Furthermore, in future studies, the optimum recipe of the atherosclerotic plaque phantoms that mimics the human atherosclerotic plaque (agar 4% w/v, gypsum 10% w/v and butter 10% w/v) can be used with the proper choice of operating frequency and transducer design for HIFU therapy and would be focused only for arteries that have at least 50% blockage. However, the pulsatile motion of the artery, which is rather important for the positioning of the ultrasound and the addition of a suction mechanism with this ultrasound technology that would collect the debris during sonication should be investigated in upcoming studies. Finally, future studies should be focused on the temperature elevation at the artery wall by placing a thermocouple in the transducer's face inside the arterial model. Different type of plaques may have different temperature elevation at the artery wall and they would be very difficult to be destroyed by US. The proposed phantom can be used also in the future for evaluating the treatment protocols of MRgFUS robots of our group [47, 170, 301-345] and also for our sonothrombolysis models [169, 346-351].

10. References

[1] Joseph Serrone, Hasam Kocaeli, Douglas Mast, Mark T. Burgess, Mario Zuccarello, "The potential applications of high-intensity focused ultrasound (HIFU) in vascular neurosurgery," *Journal ofClinical Neuroscience*, Vol.19, pp.214-221, 2012.

[2] Schwartz D, Samples J and Korosteleva O. "Therapeutic ultrasound for glaucoma: clinical use of a low-frequency low-power ultrasound device for lowering intraocular pressure,"*J Ther Ultrasound*, Vol.2 No.15, 2014.

[3] Ilya Digel, Inna Kern, Eva Maria Geenen and Nuraly Akimbekov "Dental Plaque Removal by Ultrasonic Toothbrushes,"*Dentistry Journal*, Vol.8, No. 8, 2020.

[4] Salah Shebl Zeidan, "Evaluation of ultrasonic ureteral lithotripsy in the management of distal ureteric stones, single center experience,"*Int. J. Urol. Nephrol*, Vol. 5, No.3, pp. 156-154, 2017.

[5] Nathaniel M. Fried, Yegor D. Sinelnikov, Bharat B. Pant et al. " Noninvasive Vasectomy Using a Focused Ultrasound Clip: Thermal Measurements and Simulations,"*IEEE Transactions on Biomedical Engineering*, Vol.48, No.12, 2001.

[6] W. Jeffrey Elias, Diane Huss, Tiffini Voss et al. " A pilot study of Focused Ultrasound Thalamatomy for Essential Tremor, "*N Engl J Med*, Vol.369, pp. 640-648, 2013.

[7] Kaory Nakamura, Shiro Baba, Ritsu Fukazawa et al. " Treatment of benign prostatic hyperplasia with High Intensity Focused Ultrasound: An initial clinical trial in Japan with magnetic resonance imaging of the treated area,"*Int J Urol*, Vol. 2, pp.176-180, 1995.

[8] Karthik M. Sundaram, Sam S. Chang, David F. Penson et al. "Therapeutic Ultrasound and Prostate Cancer, "*Semin Intervent Radiol*, Vol.34, pp. 187-200, 2017.

[9] Foster RS, Bihrle R, Sanghvi N, et al. " Production of prostatic lesions in canines using transrectally administeres high intensity focused ultrasound," *Eur Urol*, Vol. 23, pp.330-336, 1993.

[10] Susani M, Madersbacher S, Kratzik C, et al. "Morphology of tissue destruction induced by focused ultrasound," *Eur Urol*, Vol.23, pp.34-38, 1993.

[11] Daniel Pajek, Alison Burgess, Yuexi Huang et al. "High intensity focused ultrasound sonothrombolysis: the use of perfluorocarbon droplets to achieve clot lysis at reduced acoustic powers,"*Ultrasound Med. Biol.*,Vol.40, no.9, pp. 2151-2161, 2014.

[12] Damianou et al, "Removing atherosclerotic plaque created using high cholesterol diet in rabbit using ultrasound," *Journal of Therapeutic Ultrasound*, Vol. 3, no.3, 2015.

[13] Qiu- Lan Zhou, Zhi-Yi Chenm, Yi-Xiang Wang et al. "Ultrasound-Mediated Local Drug and Gene Delivery Using Nanocarriers,"*BioMed Research International*, 2014.

[14] Lun Wu, Wenbo Zhou, Shiji Zhou, Changan Liu et al. "Effects of hypoxia inducible factor-2a on promoting angiogenesis of residual hepatocellular carcinoma after high intensity focused ultrasound ablation,"*Zhonghua Gan Zang Bing Za Zhi*, Vol.23, No. 2, pp.112-7, 2015.

[15] L.B. Feral, K. Tachibana, "Advances in therapeutic ultrasound: HIFU & LIPUS," *Philippine Physics Journal*, Vol.39, pp.78-88, 2017.

[16] Shehata IA, "Treatment with high intensity focused ultrasound: Secrets revealed," *Eur J Radiol*, Vol.81, pp.534-541, 2012.

[17] Poissonnier L, Gelet A, Chapelon J, Bouvier R, Rouviere, " Results of transcrectal focused ultrasound for the treatment od localized prostate cancer 120 patients with PSA or +10 ng/mL," *Prog Urol*, Vol. 13, pp.60-72, 2003.

[18] Gardner T, Koch M, Shalhav A, Bihrele R, Foster R, Steidle C, et al, "Minimally invasive treatment of benign prostatic hyperplasia with high intensity focused ultrasound using Sonablate TM system: An updated report of phase III clinical studies conducted in the USA," *Proc SPIE*, Vol.4609, pp.107-114, 2002.

[19]Sanghvi N, Syrus J, Foster R, Bihrle R, Casey R, Uchida T, "Noninvasive surgery of prostate tissue by high intensity focused ultrasound: An updated report," *Eur J Ultrasound*, Vol. 9, pp.19-29, 1999.

[20] Sheng L, Pei-Hong W, "Magnetic resonance image-guided versus ultrasound-guided high-intensity focused ultrasound in the treatment of breast cancer," *Chin J Cancer*, Vol. 32, pp.441-442, 2013.

[21] Ziadloo A, Vaezy S, " Real-time 3D image-guided HIFU therapy," *Conf Proc IEEE Eng Med Biol Soc*, Vol.2008, pp.4459-4562, 2008.

[22] Penna M, Dines K, Seip R, Carlson R, Sanghvi N, "Modeling prostate anatomy from multiple view TRUS images for image guided HIFU therapy," *IEEE Trans Ultrason Ferroelectr Freq Control*, Vol.54, PP.52-69, 2007.

[23] Chan A, Fujimoto V, Moore D, Martin R, Vaezy S, "An image guided high intensity focused ultrasound device for uterine fibroid treatment," *Med Phys*, 2002, Vol.29, pp.2611-2620, 2002.

[24] C.J. Shaw, G. R. ter Haar, I. H. Rivens, D. A. Giussani and C. C. Lees, "Pathophysiological mechanisms of high intensity focused ultrasound-mediated vascular occlusion and relevance to non-invasive fetal surgery," *J. R. Soc. Interface*, Vol.11, no.29, 2014.

[25] Cline HE, Schenck JF, Hynynen K, Watkins RD, Souza SP, Jolesz Fa, "MR - guided focused ultrasound surgery," *J. Comput. Assist. Tomogr*, Vol.16 , pp.956-965, 1992.

[26] Clarke RL, ter Haar GR," Temperature rise recorded during lesion formation by high-intensity focused ultrasound," *Ultrasound Med. Biol*, Vol. 23, pp.299-306, 1997.

[27] Shi X, Martin RW, Rouseff D, Vaezy S, Crum LA. "Detection of high-intensity focused ultrasound liver lesions using dynamic elastometry," *Ultrasound Imaging*, Vol. 21, pp. 107-126, 1999.

[28]Fry WJ, Barnard JW, Fry EJ, Krumins RF, Brennan JF, "Ultrasonic lesions in the mammalian central nervous system," *Science*, Vol. 122, pp.517-518, 1955.

[29] Ter Haar GR, Robertson D, " Tissue destruction with focused ultrasound in vivo," *Eur Urol*, Vol.23, pp.8-11, 1993.

[30] Jacques Curie and Pierre Curie, "Bulletin de la Societe Mineralogique de France," Vol.3, p.90, 1880.

[31] P. Langevin, "French Patent," Vol. 505, p. 703, 1920.

[32] H. Freundlich, K. Sollner and F. Rogowski, "Klin, Wochenschr," Vol. 11, p.1512, 1932.

[33] J. Lynn, R.L. Zwemer, Arthur J. Chick and A.E. Miller, " A new method for the generation anf use of focused ultrasound in experimental biology," *JGP*, Vol.26, No.2, pp.179-193, 1942.

[34] Fry W, Mosberg W, Barnard J, et al. "Production of focal destructive lesions in the central nervous system with ultrasound," *J Neurosurg*, Vol.11, pp.471-478, 1954.

[35] Chapelon JY, Margonari J, Theillere Y, et al. " Effects of high-energy focused ultrasound on kidney tissue in the rate and the dog," *Eur Urol*, Vol. 42, pp.147-152, 1992.

[36] Vykhodtseva NI, Hynynen K, Damianou C, "Histologic effects of high intensity pulsed ultrasound exposure with subharmonic emission in rabbit brain in vivo," *Ultrasound Med Biol*, Vol.21, pp.969-979, 1995.

[37] Adams JB, Moore RG, Anderson JH, et al. "High intensity focused ultrasound ablation of rabbit kidney tumors," *J Endourol*, Vol. 10, pp.71-75, 1996.

[38] Chen W, Zhu H, Zhang L, Li K, Su H, Jin C, et al. "Primary bone malignancy: effective treatment with high-intensity focused ultrasound ablation," *Radiology*, Vol.255, pp.967-978, 2010.

[39] Kennedy JE, Wu F, ter Haar GR, Gleeson FV, Pillips RR, Middleton MR, et al. "High-intensity focused ultrasound for the tratment of liver tumours," *Ultrasonics*, Vol.42, pp.931-935, 2004.

[40] Ritchie RW, Leslie T, Phillips R, Wu F, Llling R, ter Haar G, et al, " Extracorporeal high intensity focused ultrasound for renal tumours: a 3-year follow-up," *BJU Int*, Vol.106, pp.1004-1009, 2010.

[41] Zhang L, Chen WZ, Liu YJ, Hu X, Zhou K, Chen L, et al, "Feasibility of magnetic resonance imaging-guided high intensity focused ultrasound therapy for ablating uterine fibroids in patiens with bowel lies anterior to uterus," *Eur J Radiol*, Vol.73, pp.396-403, 2010.

[42] Ahmed HU, Hindley RG, Dickinson L, Freeman A, Kirkham AP, Sahu M, et al. "Focal therapy for localized unifocal and multifocal prostate cancer: a prospective development study," *Lancet Oncol*, Vol.13, pp.622-632, 2012.

[43] Strickberger SA, Tokano T, Kluiwstra JU, Morady F, Cain C,"Extracardiac ablation of the canine atrioventricular junction by use of high-intensity focused ultrasound," *Circulation*, vol.100, pp.203-208, 1999.

[44] Otsuka R, Fujikura K, Abe Y, Okajima K, Pulerwitz T, Engel DJ, et al. " Extracardiac ablation of the left ventricular septum in beating canine hearts using high-intensity focused ultrasound,",*J Am Soc Echocardiogr*, Vol.20, pp.1400-1406, 2007.

[45] Takei Y, Muratore R, Kalisz A, Okajima K, Fujimoto K, Hasegawa T, et al "In vitro atrial septal ablation using high-intensity focused ultrasound," *J Am Soc Echocardiogr*, Vol.25, pp.467-472, 2012.

[46] Lisa A, Lee M.D, Claudio Simon, Edward L, Bove, Ralph S. Mosca, Emad S. Ebbini, Gerald D. Adams and Assau Ludomirsky, "High Intensity Focused Ultrasound Effect on Cardiac Tissues: Potential for Clinical Application," *Echocardiography:* A Jrnl of CV *Ultrasound& Allied Tech*, Vol.7, no. 6, 2000.

[47] Christakis Damianou, K. Ioannides, V. Hadjisavvas, N. Mylonas, A. Couppis and D. Iosif, "In vitro and in vivo brain ablation created by HIFU and monitored by MRI," *IEEE Transactions on Ultrasonics, Ferroelectrics, an Frequency Control*, Vol.56, No. 6, 2009.

[48] A. Couppis, C. Damianou, Panayiotis Kyriacou, C. Lafon, F. Chavrier, J.Y. Chapelon, A. Birer, "Heart ablation using a planar rectangular high intensity ultrasound transducer and MRI guidance," *Ultrasonics*, Vol. 52, No.7, pp.821 - 829, 2012.

[49] Lisa A. Lee, Claudio Simon, Edward L. Bove, Ralph S. Mosca, Emad S. Ebbini, Gerald D. Abrams, Achiau Ludomirsky, "High Intensity Focused Ultrasound Effect on Cardiac Tissues: Potential for Clinical Application," *Echocardiography*, Vol.17, No.6, pp.563-566, 2000.

[50] Delon-Martin C, Vogt C, Chignier E, et al. " Venous thrombosis generation by means of high intensity focused ultrasound," *Ultrasound Med Biol*, Vol.21, pp.113-119, 1995.

[51] Harpaz D, Chen X, Francis CW et al. " Ultrasound enhancement of thrombolysis and reperfusion in vitro," *J Am Coll Cardiol*, Vol.21, pp.1507-1511, 1993.

[52] Kimura M, Iijima S, Kobayashi K, et al "Evaluation of the thrombolytic effect of tissue-type plasminogen activator with ultrasonic irradiation:In vitro experiment involving assay of the fibrin degradation products from the clot," *Biol Pharm Bull*, Vol.17, pp.126-130, 1994.

[53] Luo H, Nishioka T, Fishbein MC, et al "Transcutaneous ultrasound augments lysis of arterial thrombi in vivo," *Circulation*, Vol.94, pp.775-778, 1996.

[54] Luo H, Steffen W, Cercek B, et al "Enhancement of thrombolysis by external ultrasound," *Am Heart J*, Vol.125, pp.1564-1569, 1993.

[55] Nilsson AM, Odselius R, Roijer A, et al "Pro and antifibrinolytic effects of ultrasound on streptokinase induced thrombolysis,"*Ultrasound Med Biol*, Vol.21, pp.833-840,1995.

[56] Shlansky-Godberg RD, Cines DB, Sehgal CM, "Catheter-delivered ultrasound potentiates in vitro thrombolysis," *J Vasc Interv Radiol*, Vol.7, pp.313-320, 1996.

[57] Tachibana K, "Enhancement of fibrinolysis with ultrasound energy," *J Vasc Interv Radiol*, Vol.3, pp.299-303, 1992.

[58] Jacob I. Laughner, Matthew S. Suklin,Zigi W, Cheri X. Deng, Igor R. Efimov, "Three potential mechanisms for failure of High Intensity Focused Ultrasound Ablaton in Cardiac Tissue, "*Circ Arrythm Electrophysiol*, Vol.5, pp.409-416, 2012.

[59] Y. Okumura, M.W. Kolasa, S.B. Johnson, T.J.Bunch, B.D.Henz, C.J. O'Brien, D.V.Miller, D.L.Packer, "Mechanism of Tissue Heating During HIFU Pulmonary Vein Isolation: Implications for Atrial Fibrillation Ablation Efficacy and Phrenic Nerve Protection," *Journal of Cardiovascular Electrophysiology*, Vol. 19, No. 9, 2008.

[60] B. Bochert, T. Lawrenz, B. Hansky, C. Stellbrink, "Lethal atrioesophageal fistula after pulmonary vein isolation using high-intensity focused ultrasound (HIFU)," *Heart Rhythm*, Vol.5, No.1, pp.145-148, 2008.

[61] Shunkang Rong, Kamsang Woo, Qi Zhou, Que Zhu, Qi Wu, Qi Wang, Changming Deng, Dichuan Liu, Gang Yang, Yonghong Jiang, Zhibiao Wang, Jing Huang, "Septal ablation induced by transthoracic high-intensity focused ultrasound in canines," *Journal of the American Society of Echocardiography*, Vol.26, no.10, pp.1228-1234, 2013.

[62] P. D. Dobrakowski, A.K. Machowska - Majchrzak, B. Labuz-Roszak, K.G.Majchrzak and E. Kluczewska, "MR-Guided Focused Ultrasound: A New Generation Treatment of Parkinson's disease, Essential Tremor and Neuropathic Pain," Vol.20, No.3, pp.275-282, 2014.

[63] Elias WJ, Huss D, Voss T, et al "A pilot stusy of focused ultrasound thalamotomy for essential tremor, " N Engl J Med, Vol. 369, No. 7, pp.640-648, 2012

[64] Jeanmonod D, Moser D, Magara D et al, " Study on incisionless transcranial MR-guided focused ultrasound treatment of Parkinson's disease; safety accuracy and initial outcomes. Current and future applications of focused ultrasound," 2012.

[65] Jeanmonod D, Werner B, Morel A, et al, "Transcranial magnetic resonance imaging-guided focused ultrasound: noninvasive central lateral thalamotomy for chronic neuropathic pain," *Neurosurg Focus,* Vol. 32, No. 1, pp.1-11, 2012.

[66] C. Delon-Martin, Vogt C, E. Chignier, C. Guers, JY Chapelon, Cathignol D, "Venous thrombosis generation by means of high-intensity focused ultrasound," *Ultasound Med. Biol,* Vol. 21, pp.113-119, 1995.

[67] K. Hynynen, Colucci V, Chung A, F. Jolesz, "Noninvasive arterial occlusion using MRI-guided focused ultrasound," Ultrasound Med. Biol, Vol.22, pp.1071-1077, 1996.

[68] Rivens IH, Rowland IJ, Denbow M, Fisk NM, ter Haar GR, Leach MO, "Vascular occlusion using focused ultrasound surgery for use in fetal medicine," *Eur J Ultrasound*, Vol.9, pp.89-97, 1999.

[69] Denbow ML, Rivens IH, Rowland IJ, Leach MO, Fisk NM, ter Haar GR, "Preclinical development of noninvasive vascular occlusion with focused ultrasonic surgery for fetal therapy," *Am J ObstetGynecol*, Vol.182, pp.387-392, 2000.

[70] Fujiwara R, Sasaki K, Ishikawa T, Suzuki M, Umemura S-I, Kushima M, Okai T, "Arterial blood flow occlusion by high intensity focused ultrasound and histologic evaluation of its effect on arteries and surrounding tissues," *J. Med. Ultrasonics*, Vol. 29, pp.85-90, 2002.

[71] Hwang JH, Vaezy S, Martin RW, Cho MY, Noble ML, Crum LA, Kimmey MB, "High-intensity focused ultrasound: a potential new treatment for GI bleeding," *Gastrointes. Endosc*, Vol 58. pp.111-115, 2003.

[72] Ishikawa T, Okai T, Sasaki K, Umemura S, Fujiwara R, Kushima M, Ichihara M, Ichizuka K, " Functional and histological changes in rat femoral arteries by HIFU exposure," *Ultrasound MedBiol*, Vol. 29, pp.1471-1477, 2003.

[73] Ishikawa T, Okai T, Sasaki K, Umemura S, Fujiwara R, Kushima M, Ichihara M, Ichizuka K, "Functional and histological changes in rat femoral arteries by HIFU exposure," *Ultrasound Med. Biol*, Vol.29, pp. 1471-1477, 2003

[74] Ichihara M, Sakaki K, Umemura S, Kushima M, Okai T, "Blood flow occlusion via ultrasound image-guided high-intensity focused ultrasound and its eddect on tissue perfusion," *Ultrasound MedBiol*, Vol.33, pp.452-459, 2007.

[75] Mahoney K, Martin H and Hynynen K, " Focused utrasound effects on blood vessels in vivo limits for vascular interventions," *Ultrasonics Symposium IEEE*, Vol. 2, pp.1405-1408, 2000.

[76] Vaezy S, et al, " Liver hemostasis using high-intensity focused ultrasound," *Ultrasound Med Biol*, Vol.24, pp.903-910, 1998.

[77] Vaezy S, et al, " Hemostasis of punctured blood vessels using high-intensity focused ultrasound," *Ultrasound Med Biol*, Vol. 24, pp.903-910, 1998.

[78] Martin RW, Vaezy S, Kaczkowski P, Keilman G, Carter S, Caps M, Beach K, Plett M, Crum L, " Hemostasis of punctured vessels using Doppler-guided high intensity ultrasound," *Ultrasound Med. Biol*, Vol.25, pp.985-990.

[79] Vaezy et al, "Use of high-intensity focused ultrasound to control bleeding," *J. Vasc Surg*, Vol.29, pp.533-542, 1999.

[80] Fallon JT, Stehbens WE, Eggleton RC, " Effect of ultrasound on arteries," *Arch. Pathol*, Vol. 94, pp.380-388, 1972.

[81] Kullervo Hynynen, Vincent Colucci, Andrew Chung et al. "Noninvasive arterial occlusion using MRI-guided focused ultrasound,"*Ultrasound in Medicine and Biology*, Vol.22, No.8, pp.1071-1077, 1996.

[82] McGovern PG, Pankow JS, Shahar E, Doliszny KM, Folsom AR, Blackburn H, Luepker RV, "The Minnesota Heart Survey Investigators. Recent trends in acute coronary heart disease: mortality, morbidity, medical care and risk factors," *N Eng J Med*, Vol. 334, pp.884-890, 1996.

[83] P. Minko, A. Buecker, S. Jaeger and M. Katoh, "Three year results after directional atherectomy of calcified stenotic lesions of the superficial femoral artery,"*Cardiovascular and InterventionalRadiology*," Vo. 43, No. 5, pp.1165-1670, 2014.

[84] Axel Brisken, Paulina Moore, Robert Zuk, "Methods, systems, and kits for plaque stabilization," *Pharmasonics Inc*, 2000

[85] Wood SKSHMA,"Catheter Ablation of Cardiac Arrythmias. Philadelphia, PA: Elsevier-Health," *Sciences Division*, 2010.

[86] Kawamura M, Koboyashi Y, Ito H, et al." Epicardial ablation with cooled tip catheter close to the coronary arteries is effective and safe in the porcine heart if

the ventricular potential is being monitored in the epicardium and endocardium," *Circ J*, Vol.70, pp.926-932, 2006.

[87] Angkeow P, Calkins HG, "Complications associated with radiofrequency catheter ablation of cardiac arrhythmias," *Cardiol Rev*, Vol. 9, pp.121-130, 2001.

[88] Q. Wu, Q. Zhou, Q. Zhu, S. Rong, Q. Wang, R. Guo, C. Deng, D. Liu, G. Yang, Y. Jiang, Z. Wang, H. Lei, T-C. He, Z. Wang, J. Huang, "Noninvasive cardiac arrhythmia therapy using High-Intensity Focused Ultrasound (HIFU) ablation," *International Journal of Cardiology*, Vol. 166, pp.28-30, 2013.

[89] F.Lu, W. Huang and D.G. Benditt, " A feasibility study of noninvasive ablation of ventricular tachycardia using high intensity focused ultrasound," *Journal of Cardiovascular Electrophysiology*, Vol.29, No.5, 2018.

[90] Adam Castano, Thomas Crawford, Masatoshi Yamazaki, Uma Mahesh R, Avula MD, Jerome Kalifa,"Coronary artery pathophysiology after radiofrequency catheter ablation: Review and perspectives," *Heart Rhytm*, Vol.8, no. 12, pp. 1975-1980, 2011.

[91] Andrew D. Krahn, Jure Manfreda, Robert B. Tate, Francis A.L. Mathewson, T. Edward Cuddy "The natural history of atrial fibrillation: Incidence, risk factors, and prognosis in the manitoba follow-up study," *The American Journal of Medicine*, Vol. 98, no. 5, pp. 476–484, 1995.

[92] Qi Wu, Qi Zhou, Que Zhu, Shunkang Rong, Qi Wang, Rui Guo, Changming Deng, Dichuan Liu, Gang Yang, Yonghong Jiang, ZhiGang Wang, Han Lei, Tong-Chuan He, ZhiBiao Wang, Jing HuangR. "Noinvasive cardiac arrhythmia therapy using High-Intensity Focused Ultrasound (HIFU) ablation," *International Journal of Cardiology*, vol. 166, no. 2, pp. 28–30, 2013.

[93] Schopka et al. "Ablation of atrial fibrillation with Epicor system: a prospective observational trial to evaluate safety and efficacy and predictors of success,"*Journal of Cardiothoracic Surgery*, Vol.5, no.34, 2010

[94] Prasad SM, Maniar HS, Camillo CJ, Schuessler RB, Boineau JP, Sundt TM, Cox JL, Damiano RJ Jr, "The Cox maze III procedure for atrial fibrillation: long-term efficacy in patients undergoing lone versus concncomitant procedures,"*J Thorac Cardiovasc Surg*, Vol.126, pp.1822-1828,2003.

[95] Kawamura M, Kobayashi Y, Ito H, et al. "Epicardial ablation with cooled tio catheter close to the coronary arteries is effective and safe in the porcine heart if

the ventricular potential is being monitored in the epicardium and endocardium,"*Circ J*, vol. 70, pp. 926–932, 2006.

[96] Angkeow P, Calkins HG and F. Morady. "Complications associated with radiofrequency catheter ablation of cardiac arrhythmias," *Journal of Cardiology in Review*, vol.9, no.3, pp.121-130, 2001.

[97] Ninet J, Roques X, Seitelberger R, Deville C, Pomar JL, Robin J, Jegaden O, Wellens F, Wolner E, Vedrinne C, Gottardi R, Orrit J, Billes MA, Hoffmann DA, Cox JL, Champsaur GL "Surgical ablation of atrial fibrillation with offpump, epicardial, high-intensity focused ultrasound: Results of a multicenter trial," *J Thorac Cardiovasc Surg*, Vol. 130, pp. 803-80, 2003.

[98] Manasse E, Medici D, Ghiselli S, Ornaghi D, Gallotti R "Left main coronary arterial lesion after microwave epicardial ablation,"*Ann Thorac* Surg, Vol. 76, pp.276-277, 2003.

[99] Pappone C, Rosanio S, Oreto G, Tocchi M, Gugliotta F, Vicedomini G et al, " Circumferential radiofrequency ablation of pulmonary vein ostia: a new anatomic approach for curing atrial fibrillation," *Circulation*, Vol.102, pp.2619-2628, 2000.

[100] Verma A, Natale A, "Should atrial fibrillation ablation be considered first-line therapy for some patients? Why atrial fibrillation ablation should be consideres first-line therapy for some patients," *Circulation*, Vol.112, pp.1214-1222, 2005.

[101] Jais P, Hocini M, Sanders P, Hsu LF, Takahashi Y, Rotter M et al, " Long term evalutation of atrial fibrillation ablation guided bt noninducibility," *Heart Rhythm*, Vol.3, pp.140-145, 2006.

[102] Pappone C, Santinelli V, " Atrial fibrillation ablation: state of the art," *Am J Cardiol*, Vol.96, pp.59-64, 2005.

[103] Calkins H, Brugada J, Packer DL, Cappato R, Chen SA, Crijns HJ et al, " HRS/EHRA/ECAS expert Consensus Statement on catheter and surgical ablation of atrial fibrillation: recommendations for personnel, policy, procedures and follow up. A report of the Heart Rhythm Society (HRS) Task Force on catheter and surgical ablation of atrial fibrillation," *Heart Rhythm*, Vol.4, pp.816-861, 2007.

[104] Cappato R, Calkins H, Chen SA et al. "Worldwide survey on the methods, efficacy, and safety of catheter ablation for human atrial fibrillation," *Circulation*, Vol.111, pp.1100–1105, 2011.

[105] Pappone C, Oral H, Santivelli V. et al, "Atrio-esophageal fistula as a complication of percutaneous transcatheter ablation of atrial fibrillation," *Circulation*, Vol.109, pp.2724-2726, 2004.

[106] O'Neill MD, Jais P, Hocini M, Sacher F, Klein GJ, Clementy J et al, "Catheter ablation for atrial fibrillation," *Circulation*, Vol.116, 1515-1523, 2007.

[107] Neumann T, Vogt J, Schumacher B, Dorszewski A, Kuniss M, Neuser H et al, "Circumferential pulmonary vein isolation with the cryoballoon technique results from a prospective 3-center study," *J Am Coll Cardiol*, Vol. 52, pp.273-278, 2008

[108] Andreas Metzner, K.R. Julian Chun, Kars Neven, Alexander Fuernkranz, Feifan Ouyang, Mathhias Antz et al., "Long term clinical outcome following pulmonary vein isolation with high-intensity focused ultrasound ballon catheters in patients with paroxysmal atrial fibrillation," *European Society of Cardiology, Europace*, pp.188-193, 2010.

[109] Zimmer JE, He DS, Hynynen K, Marcus FI, Caruso AC, Lampe LF, Aguirre ML, " Application of ultrasound energy for intracardiac ablation of arrhythmias," *Eur Heart J*, Vol. 16, No. 7, pp.961-966, 1995.

[110] Strickberger, Tokano T, Kluiwstra JU, Morady F, Cain C, " Extracardiac ablation of the canine atrioventricular junction by use of high-intensity focused ultrasound," *Circulation*, Vol. 100, No.2, pp.203-208, 1999.

[111] Nestor R, Villamizar, Jennifer H. Crow, Valentino Piacentino III, Louis R. DiBenardo, Mani A. Daneshmand, Dawn E. Bowles, Mark A. Groh and Camelo A. Milano, " Reproducibility of Left Atrial Ablation with High Intensity Focused Ultrasound Energy in a Calf Model," *J Thorac Cardiovasc Surg*, Vol. 140, No. 6, pp.1381-1387, 2010.

[112] Nakagawa H, Antz M, Wong T, Schmidt B, Ernst S, Ouyang F et al, "Initial experience using a forward directed, high - intensity focused ultrasound balloon catheter for pulmonary vein antrum isolation in patients with atrial fibrillation," *J Cardiovasc Electrophysiol*, Vol.18, pp.136-144, 2007.

[113] Schmidt B, Antz M, Ernst S, Ouyang F, Falk P, Chun JK et al, "Pulmonary vein isolation by high intensity focused ultrasound: first in man study with a steerable balloon catheter," *Heart Rhythm*, Vol.4, pp.575-584, 2007.

[114] Marek Pizon, Norbert Friedel, Monika Pizon, Miriam Freundt, Michael Weyand, Richard Feyrer, "Impact of epicardial ablation of concomitant atrial fibrillation on atrial natriuretic peptide levels and atrial function in 6 months follow up: does

preoperative ANP level predict outcome of ablation," *Journal of Cardiothoracic Surgery*, Vol.8, p.218, 2013.

[115] Garcia R, Sacher F, Oses P, Derval N, Barandon L, Denis A, Hocini M, Roques X, Haissaguerre M, Labrousse L, Jais P, "Electrophysiological study 6 months after Epicor high-intensity focused ultrasound atrial fibrillation ablation," J Interb Card Electrophysiol, Vol.41, No.3, pp.245-251, 2014.

[116] Wagenknecht L, Wasserman B, Chambless L, Coresh J, Folsom A, Mosley T, et al. " Correlates of carotid plaque presence and composition as measured by MRI: the Atherosclerosis Risk in Communities Study," *Circ Cardiovasc Imaging*, Vol 4, pp. 314-322, 2009.

[117] T.J.Romer, J.F.Brennan, M. Fitzmaurice, M. L. Feldstein, G. Deinum, J. L. Myles, J. R Kramer, R. S. Lees and M. S Feld," A rotational ablation tool for calcified atherosclerotic plaque removal biomedical microdevices," *Circulation*, Vol. 97, p.8, 1998.

[118] L.Wexler, B. Brundagr, J. Crouse, R. Detrano, V. Fuster, J. Maddahi, J. Rumberger, W. Stanford, R. White and K. Taubert, "Coronary Artery Calcification: Pathophysiology, Epidemiology, Imaging Methods, and Clinical Implications," *Circulation*, Vol.94, pp.1175-1192, 1996.

[119] M Naghavi, P. Libby, E. Falk, S. W. Casscells, S. Litovsky and J. Rumberger, "From Vunerable Plaque to Vulnerable Patient: A call for new definitions and risk assessment strategies: Part I," *Circulation*, Vol.108, pp.1664-1672, 2003.

[120] Weintraub WS, Mauldin PD, Becker E, Kosinski AS, King SB, "A comparison of the costs of and quality of life after coronary angioplasty or coronary surgery for multivessel coronary artery disease. Results from the Emory Angioplasty Versur Surgery Trial (east)," *Circulation*, Vol. 92, no.10, pp.2831-2840, 1995.

[121] Lan C, Chen SY, Chiu SF, Hsu CJ, Lai JS, Kuan PL,"Poor functional recovery may indicate restenosis in patients after coronary angioplasty," *Arch Phy Med Rehabil*, Vol.84, no.7, pp.1023-1070, 2003

[122] Dake MD, Ansel GM, Jaff MR, Ohki T, Saxon RR, Smouse HB, et al. "Paclitaxeleluting stents show superiority to balloon angioplasty and bare metal sten in femoropopliteal disease: twelve month Zilver PTX randomised study results," *Circ Cardiovasc Inter*. Vol.4 ,no. 5, pp.495-504, 2011

[123] Boyle CJ, Lennon AB, Prendergast PJ, "In silico prediction of the mechanobiological response of arterial tissue:application to angioplasty and stenting," *J Biomed Eng*, Vol. 133, no. 8, p.1001, 2011

[124] Kossivsky N. "Intravascular stents after transluminal angioplasty," *N. Eng J Med*, Vol. 317, no.13, pp.836-837, 1987

[125] Takebayashi H, Haruta S, Kohno H, Ichinose H, Taniguchi M, Shimakura T, et al."Immediate and 3-month follow up outcome after cutting balloon angioplasty for bifurcation lesions," *J Interv Cardiology*, Vol. 17, no. 1, pp.1-7, 2004

[126] Bergersen LJ, Perry SB, Lock JE,"Effect of cutting balloon angioplasty on resistant pulmonary artery stenosis,"*Am J Cardiol*, Vol.91, no. 2, pp.185-189, 2003

[127] Unterberg C, Buchwald AB, Barath P, Schmidt T, Kreuzer H, Wiegand V, "Cutting balloon coronary angioplast-initial clinical experience," *Clin Cardiol*, Vol. 16, no. 9, pp.660-664 1993

[128] Safian RD, Grines CL, May MA, Lichtenberg A, Juran N, Schreiber TL, et al. "Clinical and angiographic results of trasluminal extraction coronary atherectomy in saphenous vein bypass grafts," *Circulation*, Vol.89, no. 1, pp.302-312, 1994.

[129] Mangiacapra F, Heyndrickx GR, Puymirat E, Peace AJ, Wijns W, De Bruyne B, et al."Comparison of drug-eluting versus bare-metal stents after rotational atherectomy for the treatment of calcified coronary lesion," *Int J Cardiol*, Vol. 154, no. 3, pp.373-376, 2012

[130] Forouzannia SK, Abdollahi MH, Mirhosseini SJ, Hosseini H, Moshtaghion SH, Golzar A, et al. "Clinical outcome and cost in patiens with off-pump vs on pump coronary artery bypass surgery," *Acta Med Iran*, Vol. 49, no. 7, pp.414-419

[131] Lee EJ, Choi KH, Ryu JS, Jeon SB, Lee SW, Park SW, et al. "Stroke risk after coronary artery bypass graft surgery and extent of cerebral artery atherosclerosis," *J Am Coll Cardiol*, Vol.57, no. 18, pp.1811-1818, 2011

[132] Jorg E, Brown MM, " The evidence for medicine versus surgery for carotid stenosis," *Eur J Radiol*, Vol.60, pp.3-7, 2006.

[133] Shehata IA, Ballard JR, Casper AJ, Liu D, Mitchell T, Ebbini ES, "Feasibility of targeting atherosclerotic plaques by high-intensity-focused ultrasound: an in vivo study," *J Vasc Interv Radiol*, Vol.24, no.12, pp.1880-1887, 2013.

[134] J.S. Koruth, S. Dukkipati, R. G. Carrillo, J. Coffey, J. Tenf, T. Eby, V. Reddy and A. D. Avila, " Safety and efficacy of HIFU Atop Coronary Arteries During Epicardial Catheter Ablation," *Journal of Cardiovascular Electrophysiology*, Vol. 22, No. 11, 2011.

[135] Warren JA, Jordan Jr WD, Heudebert GR, Whitley D, Wirthlin DJ, "Determining patient preference for treatment of extracranial carotid artery stenosis: carotid angioplasty and stenting versus carotid endarterectomy," *Ann Vasc Surg*, Vol. 17, no.1, pp.15-21, 2003.

[136] Hollenbeak CS, Bowman AR, Harbaugh RE, Casale PN, Han D,"The impact of surgical specialty on outcomes for carotid endarterectomy," *J Surg Res*, Vol. 159, no.1, pp.595-602, 2010.

[137] McDonald RJ, Clofy HJ, Kallmes DF, "Intracranial hemorrhage is much more common after carotid stenting than after endarterectomy: evidence drom the national inpatient sample," *Stroke*, Vol.42, no. 10, pp.2782-2787, 2011.

[138] B. Nazer, F. Ghaghaie, R. Kashima, T. Khokhlova, C. Perez, L. Crum, T. Matula and A. Hata, "Therapeutic ultrasound promotes reperfusion and angiogenesis in a rat motel of peripheral arterial disease," *Circ J*, Vol.79, No. 9, pp.2043-2049, 2015.

[139] Fitzgerald J. Peter, Takagi A, Moore P, Hayase M, Kolodgie F, Corl D, Nassi M, Virmani R, Yock P, "Intravascular Sonotherapy Decreases Neointimal Hyperplasia After Stent Implantation in Swine," *Circulation*, Vol.103, pp.1828-1831, 2001.

[140] Damianou, C. Christofi, N. Mylonas, "Simulation of the thermal and mechanical effects of a planar rectangular high intensity ultrasound transduser to be used for destroying atherosclerotic plaque," *Engineering*, Vol.5, pp.347-351, 2013.

[141] Damianou C, Couppis A, "Feasibility study for removing calcified material using a planar rectangular ultrasound transducer," *J Ultrasound*, Vol.19, No.2, pp.115-123, 2016.

[142] Davidson F, "Output measurements for medical ultrasound," *Ultrasonic power balances. In: Preston RC*, pp.75-90, 1991.

[143] Ruiz-Ares G, Fuentes B, Martinez-Sanchez P, Diez-Tejedor E, "A prediction model for unstable carotid atheromatous plaque in acute ischemic stroke patients: proposal and internal validation," *Ultrasound Med Biol*, Vol.40, No.9, 2014.

[144] Siegel RJ, Gunn J, Ahsan A, Fishbein MC, Bowes RJ, Oakley D, Wales C, Steffen W, Campbell S, Nita H et al "Use of therapeutic ultrasound in percutaneous

coronary angioplasty. Experimental in vitro studies and initial clinical experience," Vol.89, No.4, pp.1587-1592, 1994.

[145] Mohamed K. Almekkaway, Islam A. Shehata and Emad S. Ebbini, "Anatomical-based model for simulation of HIFU-induced lesions in atherosclerotic plaques," Internal Journal Of Hyperthermia, Vol. 31, No. 4, pp.433-442, 2015.

[146] Monteverde - Grether C, Valez y Tello de Meneses M, Nava-Lopez G, Jauregui R, Borges J, Abundes A, Lopez-Cuellar M, Armillia M, "Percutaneous transluminal ultrasonic angioplasty: preliminary clinical report of ultrasound plaque ablation in totally occluded peripheral arteries," *Arch Invest Med (Mex)*, Vol.22, No.2, pp.171-179, 1999.

[147] Zhang Y, Dong H, Xu Y, Shi R, Lang H, Gao J, Zhang W, "External ultrasound for carotid atherosclerotic plaque treatment," J Ultrasound Med, Vol.34, No.3, pp.451-9, 2015.

[148] Siegel RJ, Gunn J, Ahsan A, Fishbein MC, Bowes RJ, Oakley D, Wales C, Steffen W, Campbell S, Nita H et al "Use of therapeutic ultrasound in percutaneous coronary angioplasty. Experimental in vitro studies and initial clinical experience," Vol.89, No.4, pp.1587-1592, 1994.

[149] Regar E, Thury A, Van der Giessen WJ, Sianos G, Vos J, Smits PC, Carlier SG, de Feyter P, Foley DP, Serruys PW, "Sonotherapy, antirestenotic therapeutic ultrasound in coronary arteries: the first clinical experience," *Catheter Cardiovasc Interv*, Vol.60, No.1, pp.9-17, 2003.

[150] V. L. Feigin, C.M.M Lawes, D.A. Bennett and C.S. Anderson, "Stroke epidemiology: A review of population-based studies of incidence, prevalence, and case-fatality in the late 20th century," *Lancet Neurology*, Vol.2, No.1, pp.43-53, 2003.

[151] D. Lloyd -Jones, R. Adams et al, "Heart disease and stroke statistics 2009 update: A report from the American Heart Association Statistics Committee and Stroke Statistics Subcommittee," *Circulation*, Vol.119, No.3, pp.410-528, 2009.

[152] J.Gomes and A. Washman, "Types of stroke," *Handbook of Clinical Nutrition and Stroke*, Vol.114, No. 3, pp.253-257, 2013.

[153] S.T.S Troke and S.T.G Roup, "Tissue plasminogen activator for acute ischemic stroke. The National Institute of Neurological Disorders and Stroke rt-PA Stroke Study Group," *N. Engl. J. Med*., Vol. 333, pp.1581-7, 1995.

[154] S. Meairs, A. Alonso and M.G. Hennerici, "Progress in sonothrombolysis for the treatment of stroke," *Stroke*, Vol.43, No.6, pp.1706-1710, 2012.

[155] Gramiak R, Shah PM, " Echocardiography of the aortic root," *Invest Radiol*, Vol.3, No.5, pp.356-366, 1968

[156] Siegel RJ, Fishbein MC, Forrester J, et al. " Ultrasonic plaque ablation. A new method for recanalization of partially or tottaly occluded arteries," *Circulation*, Vol. 78, No. 6, pp.1443-1448, 1998.

[157] Siegel RJ, Atar S, Fishbein MC, et al, "Noninvasive transcutaneous low frequenct ultrasound enhances thrombolysis in peripheral and coronary arteries," *Echocardiography*, Vol.18, No.3, pp.247-257, 2001.

[158] Damianou C, Hadjisavvas V, Mylonas N, Couppis A, Ioannides K, " MRI - guided sonothrombolysis of rabbit carotid artery," *J Stroke Cerebrovasc Dis*, Vol.23, No.2, pp.113-21. 2014.

[159] Tachibana K, Tachibana S, "Albumin microbubble echo-contrast material as an enhancer for ultrasound accelerated thrombolysis," *Circulation*, Vol. 92, No.5, pp.1148-1150, 1995.

[160] Porter TR, LeVeen RF, Fox R, et al, "Thrombolytic enhancement with perfluorocarbon-exposed sonicated dextrose albumin microbubbles," *Am Heart J*, Vol. 132, No.5, pp.964-968, 1996.

[161] Nishioka T, Luo H, Fishbein MC, et al, " Dissolution of thrombotic arterial occlusion by high intensity, low frequency ultrasound and dodecafluoropentane emulsion: an in vitro and in vivo study," *J Am Coll Cardiol*, Vol. 30, No. 2, pp.561-568, 1997.

[162] Kondo I, Mizushige K, Ueda T, et al, " Histological observations and the process of ultrasound contrast agent enhancement of tissue plasminogen activator thrombolysis with ultrasound exposure," *Jpn Circ J*, Vol/.63, No.6, pp.478-484, 1999.

[163] C.K.Holland, S.S.Vaidya, S. Datta, C.C. Coussios and G.J. Shaw, "Ultrasound-enchanced tissue plasminogen activator thrombolysis in an in vitro porcine clot model," *Thromb. Res*., Vol.121, No.5, pp.663-673, 2008.

[164] K. Spengos, S. Behrens, M. Daffertshofer, C.E. Dempfle and M. Hennerici, "Acceleration of thrombolysis with ultrasound through the cranium in a flow model," *Ultrasound Med. Biol.*, Vol.26, No.5 pp.889-95, 2000.

[165]Birnbaum Y, Luo H, Nagai T, et al, "Noninvasive in vivo clot dissolution without a thrombolytic drug:recanalization of thrombosed iliofemoral arteries by transcutaneous ultrasound combined with intravenous infusion of microbubbles," *Circulation*, Vol.97, No.2, pp.130-134, 1998.

[166] Culp WC, Porter TR, Lowery J, et al. " Intracranial clot lysis with intravenous microbubbles and transcranial ultrasound in swine," *Stroke*, Vol.35, No. 10, pp.2407-2411, 2004.

[167] Cohen MG, Tuero E, Bluguermann J, et al. "Transcutaneous ultrasound-facilitated coronary thrombolysis during acute myocardial infarction," *Am J Cardiol*, Vol.92, No. 4, pp.454-457, 2003.

[168] Eggers J, Konig IR, Koch B, et al. "Sonothrombolysis with transcranial color-coded sonography and recombinant tissue-type plasminogen activator in acute middle cerebral artery main stem occlusion:results from a randomized study," *Stroke*, Vol.39, No.5, pp.1470-1475, 2008.

[169]N. Papadopoulos, G. Menikou, M. Yiannakou, C. Yialloureas, K. Ioannides and C. Damianou, "Evalutaion of a small flat rectangular therapeutic ultrasonic transducer intended for intravascular use," *Ultrasonics*, Vol.74, pp.196-203, 2017.

[170] Christakis Damianou, Venediktos Hadjisavvas, Kleanthis Ioannides, "In vitro and in vivo evaluation of a magnetic resonance imaging-guided focused ultrasound system for dissolving clots in combination with thrombolytic drugs," *Journal of Stroke and Cerebrovascular Diseases*, Vol.23, No. 7, 2014.

[171] S.T. Schaefer, S. Kliner, U. Nixdorff, I. Lucic, H. Kaarmann, W. G. Daniel and F. A. Flachskampf, "High Frequency Ultrasound Thrombolysis: In Vitro Effects of Ultraasound Mode, Duration, Temperature, and Frequency," *JACC*, Vol.43, No. 5, 2004.

[172]Molina CA, Ribo M, Rubiera M, et al, " Microbubble administration accelerates clot lysis during continuous 2-MHz ultrasound monitoring in stroke patients treated with intravenous tissue plasminogen activator," *Stroke*, Vol.37, No.2, pp.425-429, 2006.

[173]Alexandrov AV, Molina CA, Grotta JC, et al, " Ultasound-enhanced systemic thrombolysis for acute ischemic stroke," *N Engl J Med*, Vol.351, No.21, pp.2170-2178, 2004.

[174] Ryo Otsuka, K. Fujikura, K. Hirata, T. Pulerwitz, Y. Oe, T. Suzuki. R. Sciacca, C. Marboe, J. Wang, D. Burkhoff, R. Muratore, F. Lizzi and S. Homma, "In vitro

ablation of cardiac valves using high-intensity focused ultrasound," *Ultrasound in Med & Biol*, Vol.31, No. 1.pp 109-114, 2005.

[175]Huang SK, Graham AR, Hoyt RH, Odell RC, "Transcatheter desiccation of the canine left ventricle using radiofrequency energy: A pilot study," *Am Heart J*, Vol.114, pp.42-48, 1987.

[176] Pichardo et al, " Partial shrinkage of venous tissues near valves using HIFU," *AIP ConferenceProceedings*," Vol.754, No. 1, 2005.

[177] P.W. Henderson, G.K. Lewis, N. Shaikh, A. Sohn, A.L. Weinstein, W.L. Olbricht, J.A. Spector, "A portable high-intensity focused ultrasound device for noninvasive venous ablation," *Journal of Vascular Surgery*, Volume 51, No.3, pp.707-711, 2010.

[178] Y. Abe, R. Otsuka, R. Muratore, K. Fujikure, K. Okajima, K. Suzuki, J. Wang, C. Marboe, A. Kalisz, J. A. Ketterling, F. L. Lizzi, S. Homma, " In Vitro Mitral Chordal Cutting by High Intensity Focused Ultrasound," *Ultrasound in Medicine & Biology*, Vol. 34, No.3, pp.400-405, 2008.

.

[179]Mozaffarian D, Benjamin EJ, Go AS, et al. ‘‘Heart disease and stroke statistics – 2015 update: a report from the American Heart Association ’’, *Circulation*, Vol. 131, 2015.

[180] Davies MJ, Thomas A,‘‘Thrombosis and acute coronary-artery lesions in sudden cardiac ischemic death ’’, *N Engl J Med*, Vol. 310, pp.1137-40, 1984.

[181] Otsuka F, Satoshi Y, Teruo N et al. ‘‘Pathology of coronary atherosclerosis and thrombosis’’, *Cardiovasc DiagnTher*, Vol. 6, pp.396-408, 2016.

[182]Virmani R, Kolodgie F, Burke P. Allen et al. ‘‘Lessons From Sudden Coronary Death: A Comprehensive Morphological Classification Scheme for Atherosclerotic Lesions,’’ *ArteriosclerThrombVascBiol*, Vol.20, pp.1262-1275, 2000.

[183]Virmani R, Kolodgie FD, Bruke AP et al. ‘‘Lessons from sudden coronary death: a comprehensive morphological classification scheme for atherosclerotic lesions’’, *ArteriosclerThrombVasc Biol.*, Vol.20, pp.1262-1275, 2000.

[184] Stary HC, Chandler AB, Glagov S et al. ‘‘A definition of initial, fatty streak and intermediate lesions of atherosclerosis: a report from the Committee on Vascular Lesions

of the Council on Atherosclerosis, American Heart Association, *ArteriosclerThromb*, Vol.14, pp.840 – 856, 1994.

[185] Stary HC, Chandler AB, Dinsmore RE et al. ‘‘A definition of advanced types of atherosclerotic lesions and a histological classification of atherosclerosis: a report from the Comittee on Vascular Lesions of the Council on Arteriosclerosis, American Heart Association, *ArteriosclerThrombVascBiol,* Vol.15, pp.1512-1531, 1995.

[186] Burke AP, Farb A, Malcom GT et al. ‘‘Coronary risk factors and plaque morphology in men with coronary disease who died suddenly,’’ *N Engl J Med*, Vol.336, pp.1276-1282, 1997.

[187] Burke AP, Farb A, Malcom GT et al. ‘‘Plaque rupture and sudden death related to exertion in men with coronary artery disease,’’ *JAMA,* Vol.281, pp.921-926, 1999.

[188] Burke AP, Weber D, Farb A et al. ‘‘Coronary calcification: insights from sudden death victims,’’ *Z Kardiol.* In press.

[189] Burke AP, Farb A, Malcom GT et al. ‘‘Effect of risk factors on the mechanism of acute thrombosis and sudden coronary death in women,’’ *Circulation,* Vol.97, pp.2110-2116, 1998.

[190] Van der Wal AC, Becker AE, Van der Loos CM et al. ‘‘Site of intimal rupture or erosion of thrombosed atherosclerotic plaques is characterized by an inflammatory process irrespective of dominant plaque morphology,’’ *Circulation,* Vol.89, pp.36-44, 1994.

[191]Farb A, Burke AP, Tang AL et al. ‘‘Coronary plaque erosion without rupture into a lipid core: a frequent cause of coronary thrombosis in sudden coronary death,’’ *Circulation,* Vol.93, pp.1354-1363, 1996.

[192]Kragel AH, Reddy SG, Wittes JT et al. ‘‘Morphometric analysis of the composition of atherosclerotic plaques in the four major epicardial coronary arteries in acute myocardial infarction and in sudden coronary death,’’ *Circulation,* Vol.80, pp.1747-1756, 1989.

[193] William Insull, ‘‘The pathology of atherosclerosis: Plaque development and plaque responses to medical treatment’’, *The Americal Journal of Medicine*, Vol.122, No 1A, 2009.

[194] Eggen Da, Solberg LA, ‘’Variation of atherosclerosis with age’’, *Lab Invest*, Vol.18, pp. 571-579, 1968.

[195] Burke AP, Kolodgie FD, Burke AP et al. ‘‘Healed plaque ruptures and sudden coronary death: evidence that subclinical rupture has a role in plaque progression’’, *Circulation,* Vol. 103, pp. 934-940, 2001.

[196] Stary HC, *Atlas of Atherosclerosis: Progression and Regression,* 2nd ed. New York: Parthenon Publishing Group, 2003.

[197] Baigent C, Keech A, Kearney PM, et al, ‘‘The Cholesterol Treatment Trialists (CTT) Collaboratior. Efficacy and safety of cholesterol-lowering treatment: prospective treatment: prospective meta-analysis of data from 90,056 participants in 14 randomised trials of statins ’’, *Lancet,* Vol.366, pp.1267-1278, 2005.

[198] Heart Protection Study Collaborative Group. ‘‘MRC/BHF Heart Protection Study of cholesterol lowering with simvastatin in 20,536 high-risk individuals: a ranadomised placebo-controlled trial.’’, *Lancet,* Vol.360, pp.7-22, 2002.

[199] Sever PS, Dahlof B, Poulter NR, et al, for the ASCOT Investigators. ‘‘Prevention of coronary and stroke events with atorvastatin in hypertensive patients who have average or lower-than-average cholesterol concentrations, in the Anglo-Scandinavian Cardiac Outcomes Trial-Lipid Lowering Arm (ASCOT-LLA): a multicentre randomised controlled trial ’’, *Lancet,* Vol.361, pp.1149-1158, 2003.

[200] ALLHAT Officers and Coordinators for the ALLHAT Collaborative Research Group. ‘‘ The Antihypertensive and Lipid-Lowering Treatment to Prevent Heart Attack Trial (ALLHAT-LLT): major outcomes in moderately hypercholesterolemic, hypertensive patients randomized to pravastatin vs usual care,’’ *JAMA,* Vol. 288, pp.2998-3007, 2002.

[201] Wissler RW, VesselinovitchD,‘‘Comparative pathogenetic patterns in atherosclerosis,’’ *Adv Lipid Res,* Vol.6, pp. 181-206, 1968.

[202] Armstrong ML, Heistad DD, Megan MB et al. ‘‘Reversibility of atherosclerosis,’’ *Cardiovasc Clin,* Vol. 20, pp.113-126, 1990.

[203] Strong JP, Malcom GT, McMahan CA et al. ‘‘Prevalence and extent of atherosclerosis in adolescents and young adults: implications for prevention from the Pathobiological Determinants of Atherosclerosis in Youth Study,’’ JAMA, Vol. 281, pp.727-735, 1999.

[204] Patrick A. Calvert, Daniel R. Obaid, Michael O’ Sullivan et al. ‘‘Association between IVUS Findings and Adverse Outcomes in Patients With Coronary Artery Disease,’’ *JACC: Cardiovascular Imaging,* Vol.4, No.8, pp.894-901, 2011.

[205] Vince DG, Dixon KJ, Cothren RM et al. ‘‘Comparison of texture analysis methods for the characterization of coronary plaques in intravascular ultrasound images,’’ *Comput Med Imaging Graph,* Vol.24, pp.221-229, 2000.

[206] Kawasaki M, Takatsu H, Noda T, et al. ‘‘Noninvasive quantitative tissue characterization and two-dimensional colour-coded map of human atherosclerotic lesions using ultrasound integrated backscatter: comparison between histology and integrated backscatter images,’’ *J Am Coll Cardiol,* Vol. 38, pp.486-92, 2001.

[207]Nasu K, Tsuchikane E, Katoh O, et al. ‘‘Accuracy of in vivo coronary plaque morphology assessment: a validation study of in vivo virtual histology compared with in vitro histopathology,’’ *J Am Coll Cardiol,* Vol.47, pp.2405-12, 2006.

[208] Van Herck J, De Meyer G, Ennekens G, et al. ‘‘Validation of in vivo plaque characterisation by virtual histology in a rabbit model of atherosclerosis,’’ *EuroIntervention*, Vol.5, pp.149-56, 2009.

[209] Rodriquez-Granillo GA, Garcia-Garcia HM, Mc Fadden EP, et al. ‘‘In vivo intravascular ultrasound-derived thin-cap fibroatheroma detection using ultrasound radiofrequency data analysis,’’ *J Am Coll Cardiol,* Vol.46, pp.2038-42, 2005.

[210] Kawasaki M, Sano K, Okubo M, et al. ‘‘Volumetric quantitative analysis of tissue characteristics of coronary plaque after statin therapy using three dimensional integrated backscatter intravascular ultrasound,’’ *J Am Coll Cardiol*, Vol.45, pp.1946-53, 2005.

[211] J Chueh, T Turan, K van der Marel, et al, "An Atherosclerotic Plaque Phantom for Medical Imaging,"*J NeuroInterventional Surgery,* Vol. 8, 2016.

[212] J Chueh, T Turan, T Brown, et al. "An atherosclerotic plaque phantom for medical imaging," *J Neurointerv Surg*, Vol. 7, 2015.

[213] Ju-Yu Chueh, Kajo van der Marel, Matthew J. Gounis, et al, "Development of a High-resolution MRI (HRMRI) Intracranial Atherosclerosis Imaging Phantom," *Science, J Neurointerv Surg,* Vol.10, pp.143-149, 2018.

[214] Shanshan Shang, Zhong Jiang Chen, Yue Zhao, Sihua Yang and Da Xing, "Simultaneous imaging of atherosclerotic plaque composition and structure with dualmode photoacoustic and optical coherence tomography," *Optics Express,* Vol. 25, No.2, 2017.

[215]Kwang Nam Jin, Jin Wook Chung, Euh-Ah Park, Whal Lee, "Dual-energy computed tomograph angiography: virtual calcified plaque substraction in a vascular phantom," *Acta Radiological Open,* Vol.6, No.7 pp.969-979, 2017.

[216] Yingchun Cao, Jie Hui, Ayeeshik Kole, et al. "High-sensitivity intravascular photoacoustic imaging of lipid-laden plaque with a collinear catheter design," *Scientific Reports*, 2016.

[217] Christine P. Fleming, Jocelyn Eckert, Elkan F. Halpern,et al, "Depth resolved detection of lipid using spectroscopic optical coherence tomography," *Biomedical Optics Express*, Vol.4, No.8, 2013.

[218] David P. Cormode, Ewald Roessl, Axel Thran, et al. "Atherosclerotic Plaque Composition: Analysis with Multicolor CT and Targeted Gold Nanoparticles," *Radiology*, Vol. 256, No.3, pp.773-783, 2010.

[219] Satoshi Honda,Yu Kataoka, Tomoaki Kanaya, et al, "Characterization of coronary atherosclerosis by intravascular imaging modalities," *Cardiovasc Diagn Ther*, Vol.6, pp.368-381, 2016.

[220] Zhao Zhihong, He Hua, Luo Jun, et al,"Fibroatheroma Morphological Features of Borderline Coronary Lesion Plaques on Stable Angina Pectoris Patients, " *Enliven: Clinical Cardiology and Research*, Vol.2, 2015.

[221] G. Menicou, C. Damianou, "Acoustic and thermal characterization of agar based phantoms used for evaluating focused ultrasound exposures,"*J Ther Ultrasound*, 5:14, 2017.

[222] E.L. Madsen, G.R. Frank, F. Dong, "Liquid or solid ultrasonically tissue-mimicking materials with very low scatter,"*Ultras. Med. Biol*, Vol.24, No.4, pp.535-542, 1998.

[223] Kim JH, Hahn EW. " Clinical and biological studies of localized hyperthermia,"*Cancer Re*s, Vol.39, pp.2258-2261, 1979.

[224] Thomsen S, "Pathologic analysis of photothermal and photomechanical effects of laser-tissue interactions,"*Photochem Photobiol*, Vol.53, pp.825-835, 1991.

[225] Hokland SL, Pedersen M, Salomir R et al. "MRI-guided focused ultrasound: methodology and applications,"*IEEE Trans Med Imaging*, Vol.25, pp.723-731, 2006.

[226] Diederich CJ, Nau WH, Ross AB et al. " Catheter-based ultrasound applicators for selective thermal ablation: progress towards MRI-guided applications in prostate,"*Int J Hyperthermia*, Vol.20, No.739-756, 2004.

[227] Munger MA, Hawkins DW. ‘‘Atherothrombosis: Epidemiology, pathophysiology, and prevention’’, *J Am Pharm Assoc* 2003;44: S5-12.

[228] Weintraub WS, Mauldin PD, Becker et al., "A comparison of the costs of and quality of life after coronary angioplasty or coronary surgery for multivessel coronary artery disease. Results from the Emory Angioplasty Versur Surgery Trial (east)," *Circulation*, Vol. 92, no.10, pp.2831-2840, 1995.

[229] Lan C, Chen SY, Chiu SF, Hsu CJ, Lai JS, Kuan PL,"Poor functional recovery may indicate restenosis in patients after coronary angioplasty," *Arch Phy Med Rehabil*, Vol.84, no.7, pp.1023-1070, 2003.

[230] Dake MD, Ansel GM, Jaff MR, et al. "Paclitaxeleluting stents show superiority to balloon angioplasty and bare metal sten in femoropopliteal disease: twelve month Zilver PTX randomised study results," *Circ Cardiovasc Inter*. Vol.4 ,no. 5, pp.495-504, 2011.

[231] Boyle CJ, Lennon AB, Prendergast PJ, "In silico prediction of the mechanobiological response of arterial tissue:application to angioplasty and stenting," *J Biomed Eng*, Vol. 133, no. 8, p.1001, 2011.

[232] Kossivsky N. "Intravascular stents after transluminal angioplasty," *N. Eng J Med*, Vol. 317, no.13, pp.836-837, 1987.

[233] Takebayashi H, Haruta S, Kohno H, et al. "Immediate and 3-month follow up outcome after cutting balloon angioplasty for bifurcation lesions," *J Interv Cardiology*, Vol. 17, no. 1, pp.1-7, 2004.

[234] Bergersen LJ, Perry SB, Lock JE,"Effect of cutting balloon angioplasty on resistant pulmonary artery stenosis,"*Am J Cardiol*, Vol.91, no. 2, pp.185-189, 2003.

[235] Unterberg C, Buchwald AB, Barath P, Schmidt T, Kreuzer H, Wiegand V, "Cutting balloon coronary angioplast-initial clinical experience," *Clin Cardiol*, Vol. 16, no. 9, pp.660-664, 1993.

[236] Safian RD, Grines CL, May MA, Lichtenberg A, Juran N, Schreiber TL, et al. "Clinical and angiographic results of trasluminal extraction coronary atherectomy in saphenous vein bypass grafts," *Circulation*, Vol.89, no. 1, pp.302-312, 1994.

[237] Mangiacapra F, Heyndrickx GR, Puymirat E, et al. "Comparison of drug-eluting versus bare-metal stents after rotational atherectomy for the treatment of calcified coronary lesion," *Int J Cardiol*, Vol. 154, no. 3, pp.373-376, 2012.

[238] Forouzannia SK, Abdollahi MH, Mirhosseini SJ, et al. "Clinical outcome and cost in patiens with off-pump vs on pump coronary artery bypass surgery," *Acta Med Iran*, Vol. 49, no. 7, pp.414-419, 2011.

[239] Lee EJ, Choi KH, Ryu JS, et al. "Stroke risk after coronary artery bypass graft surgery and extent of cerebral artery atherosclerosis," *J Am Coll Cardiol*, Vol.57, no. 18, pp.1811-1818, 2011.

[240] Jorg E, Brown MM, "The evidence for medicine versus surgery for carotid stenosis," *Eur J Radiol*, Vol.60, pp.3-7, 2006.

[241] Shehata IA. ‘‘Treatment with high intensity focused ultraosound: Secrets revealed’’ Eur J Radiol 2012; 81:534-41

[242] Poissonnier L, Gelet A, Chapelon J et al. ‘‘Results of transrectal focused ultrasound for treatment of localized prostate cancer 120 patients with PSA or +10 ng/mL,’’ *Prog Urol* 2003; 13:60-72.

[243] Gardner T, Koch M, Shalhav A et al. ‘‘Minimally invasive treatment of benign prostatic hyperplasia with high intensity focuded ultrasound using the Sonablate TM system: An updated report of phase III clinical studies conducted in the USA,’’ Proc SPIE 2002; 4609:107-14.

[244] Sanghvi N, Syrus J, Foster R et al. ‘‘Noninvasive surgery of prostate tissue by high intensity focused ultrasound: An updated report,’’ *Eur J Ultrasound* 1999;9:19-29.

[245] Shenh L, Pei-Hong W. ‘‘ Magnetic resonance iimage-guided versus ultrasound-guided high-intensity focused ultrasound in the treatment of breast cancer,’’ *Chin J Cancer* 2013; 32:441-2.

[246] Ziadloo A, Vaezy S. ‘‘Real-time 3D image-guided HIFU therapy,’’ *Conf Proc IEEE Eng Med Biol Soc* 2008;2008:4459-62.

[247] Penna M, Dines K, Seip R et al. ‘‘ Modeling prostate anatomy from multiple view TRUS images for image guided HIFU therapy,’’ I*EEE Trans Ultrason Ferroelectr Freq Control* 2007:54:52-69.

[248] Chan A, Fujimoto V, Moore D et al. ‘‘ An image guided high intensity focused ultrasound device for uterine fibroid treatment,’’ *Med Phys* 2002:29:2611-20.

[249] Szabo TL. ‘‘Diagnostic ultrasound imaging: inside out,’’ Burlington: Elsevier Academic Press; 2004 p.493-8.

[250] Sun MK, Shieh J, Lo CW, Chen CS, Chen BT, Huang CW, Chen WS. Reusable tissue-mimicking hydrogel phantoms for focused ultrasound ablation. *UltrasonSonochem*. 2015;23:399–405.

[251] Cuccaro R, Musacchio C, Giuliano Albo PA, Troia A, Lago S. Acoustical characterization of polysaccharide polymers tissue-mimicking materials. *Ultrasonics*, 2015;56:210–9.

[252] Manickam K, Machireddy RR, Seshadri S. Characterization of biomechanical properties of agar based tissue mimicking phantoms for ultrasound stiffness imaging techniques. *J Mech Behav Biomed Mater*, 2014;35:132–43.

[253] Maccabi A, Arshi A, Garritano J et al. ‘‘Ultrasound-stimulated vibroacoustography for high-resolution differentiation based on viscoelastic properties of tissue mimicking phantoms,’’ *Stud Health Technol Inform*. 2014; 196:262–4.

[254] Kang ST, Lin YC, Yeh CK. Mechanical bioeffects of acoustic droplet vaporization in vessel-mimicking phantoms. *UltrasonSonochem*, 2014;21:1866–74.

[255] Min Wu, Krista Jansen, Antonius F.W. van der Steen, Gijs Van Soest, "Specific imaging of atherosclerotic plaque lipids with two-wavelength intravascular photoacoustics," *Biomedical Optics Express*, Vol.6, No.9, 2015.

[256] Hyeong Soo Nam, Joon Woo Song, Sun-Joo Jang, et al. "Characterization of lipid-rich plaques using spectroscopic optical coherence tomography," *Journal of Biomedical Optics*, Vol.21, No.7, 2016.

[257] Callum D. Little, Radhika K. Poduval, Richard Caufield, et al. "Micron resolution, high-fidelity three dimensional vascular optical imaging phantoms,"*Journal of Biomedical Optics*, Vol. 24, No.2, 2019.

[258] Yuta Kumagai, Yuhei Aotani, Masanobu Kameda, Kenji Wada, Toshiyuki Matsunaka, Hiromichi Horinaka, "Detection of unstable plaque phantom by ultrasonic velocity-change imaging method under cold exposure," *Jpn J Appl Phys*, Vol.57, 2018.

[259] Krista Jansen, Min Wu, Antonius F.W. van der Steen, Gijs van Soest, "Photoacoustic imaging of human coronary atherosclerosis in two spectral bands," *Photoacoustics*, 2013.

[260] Seifollah Gholampour and Keyvan Hajirayat "Minimizing thermal damage to vascular nerves while drilling of calcified plaque," *BMC Rec Notes*, Vol.12, No.338, 2019.

[261] Taylor Richards, Gregory M. Sturgeon, Juan Carlos Ramirez-Giraldom, et al. "Quantification of uncertainty in the assessment of coronary plaque in CCTA through a dynamic cardiac phantom and 3D-printed plaque model,", Vol.23,*J Med Imaging*, Vol.5, 2018.

[262] Kwang Nam Jin, Jin Wook Chung, Euh-Ah Park, Whal Lee, "Dual-energy computed tomograph angiography: virtual calcified plaque substraction in a vascular phantom," *Acta Radiological Open*, Vol.6, No.7 pp.969-979, 2017.

[263] Nima Kasraie, Peter Mah, Carl R. Keener, D. Clarke "Characterization of atherosclerotic plaque: a contrast-detail study using multidetector and cone-beam computed tomography," *Journal of Applied Clinical Medical Physics*, Volume 15, No.1, 2014.

[264] Katsunori Ishii, Akiko Kitayabu, Ryo Nagao, Kunio Awazu "Observation of Atherosclerotic Plaque Phantoms through Saline or Blood Layers by Near-Infrared Hyperspectral Imaging" *Optics and Photonics Journal*, Vol.4, pp.271-279, 2014.

[265]J Chueh, T Turan, K van der Marel, et al."An Atherosclerotic Plaque Phantom for Medical Imaging,"*J NeuroInterventional Surgery*, Vol. 8, 2016.

[266] J Chueh, T Turan, T Brown, et al. "An atherosclerotic plaque phantom for medical imaging," *JNeurointerv Surg*, Vol. 7, 2015.

[267] Ju-Yu Chueh, Kajo van der Marel, Matthew J. Gounis, et al. "Development of a High-resolution MRI (HRMRI) Intracranial Atherosclerosis Imaging Phantom," *Science, J Neurointerv Surg*, Vol.10, pp.143-149, 2018.

[268] Shanshan Shang, Zhong Jiang Chen, Yue Zhao, Sihua Yang and Da Xing "Simultaneous imaging of atherosclerotic plaque composition and structure with dualmode photoacoustic and optical coherence tomography," *Optics Express*, Vol. 25, No.2, 2017.

[269] Yingchun Cao, Jie Hui, Ayeeshik Kole, et al. "High-sensitivity intravascular photoacoustic imaging of lipid-laden plaque with a collinear catheter design," *Scientific Reports*, 2016.

[270] Changhoon Choi, Joongho Ahn, Chulhong Kim, "Intravascular Photothermal Strain Imaging for Lipid Detection," *Sensors*, Vol.18, 2018.

[271] Ji Guo, David M Saylor, Dinesh V Patwardhan,"Impact of Artificial Plaque Composition on Drug Transport," *J Pharm Sci*, Vol.102, No.6, pp.1905-1914, 2013.

[272] Lysa Legault Kingstone, Wael Shabana, Rebecca Thornhill, Megan White, Joanna Lam, Geoff Currie, "Comparison and Accuracy of Carotid Plaque Analysis Between Two-and Three-Dimensional Ultrasound Imaging," *Journal of Diagnostic Medical Sonography*, Vol.30, No.3,pp.123-130, 2014.

[273] Ryo Nagao, Katsunori Ishii, Daichi Matsui, Kunio Awazu "Quantitative Evaluation of Lipid Volume Fraction in Atherosclerotic Plaque Phantoms by Near-infrared Multispectral Imaging at Wavelengths around 1200nm," *Adv Biomed Eng*, Vol.4, pp.158-163, 2015.

[274] David P. Cormode, Ewald Roessl, Axel Thran, Torjus Skajaa, et al. "Atherosclerotic Plaque Composition: Analysis with Multicolor CT and Targeted Gold Nanoparticles," *Radiology*, Vol. 256, No.3, pp.773-783, 2010.

[275] Christine P. Fleming, Jocelyn Eckert, Elkan F. Halpern, Joseph A. Gardecki, Guillermo J. Tearney, "Depth resolved detection of lipid using spectroscopic optical coherence tomography," *Biomedical Optics Express*, Vol.4, No.8, 2013.

[276] Conor K McGarry, Lesley J Grattan, Aoife M Ivory et al. ‘‘Tissue mimicking materials for imaging and therapy phantoms: a review,’’ *Phys. Med. Biol*. 65, 2020.

[277] G. Menicou, C. Damianou, ´´ Acoustic and thermal characterization of agar based phantoms used for evaluating focused ultrasound exposures,´´*J Ther Ultrasound*, 5:14, 2017.

[278] Nolle AW, Mowry SC (1948), ‘‘Measurement of ultrasonic bulk-wave propagation in high polymers,’’ *J Acoust Soc Am* 20(4):432-439.

[279] Kline RA (1984), ‘‘Measurement of attenuation and dispersion using an ultrasonic spectroscopy technique,’’ *J Acoust Soc Am* 76(2):498-504.

[280] He P, Zheng J, ‘‘Acoustic dispersion and attenuation measurement using both transmitted and reflected pulses,’’ *Ultrasonics*, 39(1):27-32,2001

[281] Umchid , ‘‘Frequency dependent ultrasonic attenuation coefficient measurement,’’ ISBME 234-238, 2008.

[282] Youssef MH, Gobran NK, ‘‘ Modified treatment of ultrasonic pulse-echo immersion technique,’’ *Ultrasonics*, 39(7):473-477, 2002.

[283] Damianou CA, Sanghvi NT, Fry FJ et al. ‘‘Dependence of ultrasonic attenuation and absorption in dog soft tissues on temperature and thermal dose,’’ *J Acoust Soc Am* 102(1):628-634, 1997.

[284] Bamber JC, Hill CR, ‘‘Ultrasonic attenuation and propagation speed in mammalian tissues as a function of temperature,’’ *Ultrasound Med Biol* 5:149-157,1979.

[285] J. William, Fry et al. ‘‘Determination of absolute sound levels and acoustic absorption coefficients by thermocouple probes-experiment,’’ *J Acoust Soc Am,* 26 (3) , 311-317, 1954.

[286] Floyd Dunn, ‘‘Temperature and amplitude dependence of acoustic absorption in tissue,’’ *J. Acoust Soc Am,* 14(10) 1545-1547, 1962.

[287] S.A. Goss, LA Frizzell, F. Dunn et al, ‘‘Ultrasonic absorption and attenuation in mamalian tissues,’’ *Ultrasound Med. Biol* 5, 181-186, 1979.

[288] J.I Drewniak, L.A Frizzell, F. Dunn, ‘‘Errors resulting from finite beamwidth and sample dimensions in the determintaion of the ultrasonic absorption, ’’ *J Acoust Soc Am*. 88 (2), 967-977, 1990.

[289] T. Drakos, M. Giannakou, G. Menikou et al. ‘‘An improved method to estimate ultrasonic absorption in agar-based gel phantom using thermocouples and MR thermometry,’’ *Ultrasonic*, 103, 2020.

[290] Selfridge AR, ‘‘ Approximate material properties in isotropic materials,’’ *IEEE Trans Son Ultrason,* 32(3): 381-394, 1985.

[291] Shi et al., Relationship between Ultrasonic Attenuation, Size and Axial Strain Parameters for ex-vivo Atherosclerotic Carotid Plaque, *Ultrasound Med Biol*, 2008 October; 34(10): 1666–1677.

[292] Cujat et al. ‘A review of tissue substitutes for ultrasound imaging’ Ultrasound in Med. & Biol., Vol. 36, No. 6, pp. 861–873, 2010.

[293] Silva N.P, Bottiglieri A, Conceicao et al. "Thermal properties of ex vivo biological tissue at room and body temperature," In Proceedings of the 14th European Conference on Antennas and Propagation (EuCAP), Copenhagen, Denmark, 15 – 20 March 2020.

[294] Valvano, JW and B Chitsabesan, ‘‘Thermal conductivity and diffusivity of arterial wall and atherosclerotic plaque,’’ *Lasers Life Sci*., 1, 219-229, 1987.

[295] Picano E., Landini L, Distante A et al, ‘‘In Vitro Atherosclerosis Detection by Ultrasonic Attenuation,’’ *Circulation Research*, Vol.56, No.4, 1985.

[296] Shi et al., Relationship between Ultrasonic Attenuation, Size and Axial Strain Parameters for ex-vivo Atherosclerotic Carotid Plaque, *Ultrasound Med Biol*. 2008 October; 34(10): 1666–1677.

[297] Almekkaway K. Mohamed, Islam A. Shehata & Emad S. Ebbini, ‘‘Anatomical-based model for simulation of HIFU-induced lesions in atherosclerotic plaques,’’ *International Journal of Hyperthermia*, 31:4, 433-442.

[298] Lei W, Hu J, Liu Y et al, ‘‘Numerical evaluation of high-intensity focused ultrasound-induced thermal lesions in atherosclerotic plaques,’’ Mathematical Biosciences and Engineering, Vol.18, No.2, 1154-1168, 2021

[299] Yang et al. ‘‘High-intensity focused ultrasound ablation: an in vitro agar gel model,’’ *Int J Clin Exp Med*, 2017.

[300] Rohan Bhavane, Cristian Badea, Ketan B. Ghaghada, et al. "Dual-Energy Computed Tomography Imaging of Atherosclerotic Plaques in a Mouse Model Using a Liposomal-Iodine Nanoparticle Contrast Agent," *Circ Cardiovasc Imaging*, Vol.6, pp.285-294,2013.

[301] C. Damianou, "In vitro and in vivo ablation of porcine renal tissues using High Intensity focused Ultrasound", Journal of Ultrasound in Medicine and Biology, Vol. 29 (9), pp. 1321-1330, 2003

[302] C. Damianou, M. Pavlou, O. Velev, K. Kyriakou, M. Trimikliniotis ‘High intensity focused ultrasound ablation of kidney guided by MRI’, Journal of Ultrasound in Medicine and Biology Vol. 30 (3), pp. 397-404, 2004

[303] C. Damianou **“**MRI monitoring of the effect of tissue interfaces in the penetration of high intensity focused ultrasound in kidney in vivo” Journal of Ultrasound in Medicine and Biology , Vol. 30 (9), pp. 1209-1215, 2004.

[304] Damianou, C., Ioannides, K., Milonas, ‘Positioning device for MRI-guided high intensity focused ultrasound system’, Computer-Assisted Radiology and Surgery, 2 (6) pp. 335-345, 2008.

[305] Mylonas N., Ioannides K., Hadjisavvas V., Iosif D., Kyriacou P., Damianou C, ’Evaluation of fast spin echo MRI sequence for an MRI guided high intensity focused ultrasound system for in vivo rabbit liver ablation’ J. Biomedical Science and Engineering, 2010, 3, 241-246

[306] C. Damianou, Ioannides K., Hadjisavas V., Milonas N., Couppis A., D. Iosif, P. Kyriacou' MRI monitoring of lesions created at temperature below the boiling point and of lesions created above the boiling point using High Intensity Focused ultrasound', J. Biomedical Science and Engineering, 3, 763-775, 2010.

[307] Hadjisavvas V., Ioannides K., Komodromos M., Mylonas N., Damianou C., 'Evaluation of the contrast between tissues and thermal lesions in rabbit in vivo produced by high intensity focused ultrasound using fast spin echo MRI sequences', J. Biomedical Science and Engineering, 4, 51-61, 2010.

[308] Yiallouras C., Mylonas N., Damianou C. 'MR compatible positioning device for guiding a Focused ultrasound system for transrectal treatment of prostate cancer', Computer-Assisted Radiology and Surgery, Vol. 4,Page 745-753, 2014. DOI 10.1007/s11548-013-0964-x 2013.

[309] Mylonas N., Damianou C. 'A Prototype MR Compatible Positioning Device for Guiding a Focused Ultrasound System for the Treatment of Abdominal and Thyroid Cancer, International Journal of monitoring and surveillance technologies research, October-December, Vol.1 (4), pp. 48-61, 2013.

[310] Mylonas, N. and Damianou, C., MR compatible positioning device for guiding a focused ultrasound system for the treatment of brain diseases. Int. J. Med. Robotics Comput. Assist. Surg., 2014 Mar;10(1):1-10. doi: 10.1002/rcs.1501. Epub 2013 Jun 7.

[311] Yiallouras C., Damianou C., 'Review of MRI positioning devices for guiding focused ultrasound systems', Int J Med Robotics Comput Assist Surg, 11 (2); (2014), Published online in Wiley Online Library (wileyonlinelibrary.com) DOI: 10.1002/rcs.1601.

[312] Menikou G, Dadakova T, Pavlina M, Bock M, Damianou C., MRI compatible head phantom for ultrasound surgery. Ultrasonics. 2015, Mar; 57:144-52. doi: 10.1016/j.ultras.2014.11.004. Epub 2014 Nov 20.

[313] Yiallouras C., Ioannides C., Dadakova T., Pavlina M., Bock M., Damianou C., 'Three axis MR conditional robot for high intensity focused ultrasound for treating prostate diseases', Journal of Therapeutic Ultrasound, 2015, 3:2, DOI 10.1186/s40349-014-0023-2.

[314] Epaminonda E, Drakos T, Kalogirou C, Theodoulou M, Yiallouras C, Damianou C., MRI guided focused ultrasound robotic system for the treatment of gynaecological tumors, Int J Med Robot. 2016 Mar; 12 (1):46-52. doi: 10.1002/rcs.1653

[315] Yiannakou M, Trimikliniotis M, Yiallouras C, Damianou C. Evaluation of focused ultrasound algorithms: Issues for reducing pre-focal heating and treatment time. Ultrasonics. 65 (2016), pp. 145-153. doi: 10.1016/j.ultras.2015.10.007.

[316] Sagias G., Yiallouras C., Ioannides K., Damianou C., An MRI-conditional motion phantom for the evaluation of high-intensity focused ultrasound protocols, Int J Med Robot. 2016 Sep;12(3):431-41. doi: 10.1002/rcs.1709. Epub 2015 Sep 29.

[317] G. Menikou, C. Yiallouras, M. Yiannakou, C. Damianou, 'MRI guided Focused Ultrasound Robotic System for the Treatment of bone cancer', Int J Med Robotics Comput Assist Surg 2017; 13: e1753.

[318] Menikou G., Yiannakou M., Yiallouras C., Ioannides C., Damianou C., 'MRI-compatible bone phantom for evaluating ultrasonic thermal exposures', Ultrasonics. 2016 Sep;71:12-9. doi: 10.1016/j.ultras.2016.05.020.

[319] N. Papadopoulos, C. Yiallouras, C. Damianou, The enhancing effect of focused ultrasound on TNK- Tissue Plasminogen Activator induced thrombolysis using an in vitro circulating flow model", J Stroke Cerebrovasc Dis. 2016 Dec; 25(12):2891-2899. doi: 10.1016/j.jstrokecerebrovasdis.2016.07.052.

[320] C. Damianou, M. Yiannakou, G. Menikou, C. Yiallouras, 'MRI guided coupling for a Focused Ultrasound system using a top to bottom propagation', Journal of Therapeutic Ultrasound, 5(1), 6. doi: 10.1186/s40349-017-0087-x

[321] M. Yiannakou, G. Menikou C. Yiallouras, K. Ioannides, C. Damianou, MRI guided focused ultrasound robotic system for animal experiments, the International Journal of Medical Robotics and Computer Assisted Surgery, 13(4), e1804 2017. DOI: 10.1002/rcs.1804

[322] T. Alecou, M. Yiannakou, C. Damianou, 'Amyloid beta plaque reduction with antibodies crossing the blood brain barrier opened in 3 sessions with focused ultrasound in a rabbit model', Journal of ultrasound in medicine 36 (11), 2257-2270, 2017. doi: 10.1002/jum.14256

[323] G. Menikou, M. Yiannakou, C. Yiallouras, C. Ioannides, C. Damianou, 'MRI-compatible breast/rib phantom for evaluating ultrasonic thermal exposures', The International Journal of Medical Robotics and Computer Assisted Surgery 14(1), 2017. DOI: 10.1002/rcs.1849

[324] C. Yiallouras, G. Menikou, M. Yiannakou, C. Damianou, 'Software that controls a magnetic resonance imaging compatible robotic system for guiding high-intensity focused ultrasound therapy, Digital Medicine, 3(3), 123-132 July-September 2017 DOI: 10.4103/digm.digm_19_17

[325] C. Yiallouras, M. Yiannakou, G. Menikou, C. Damianou, A multipurpose positioning device for magnetic resonance imaging-guided focused ultrasound surgery, Digital Medicine, 3(3), 138-144 July-September 2017. DOI: 10.4103/digm.digm_33_17

[326] C. Damianou, M. Yiannakou, C. Yiallouras, G. Menikou, 'The role of 3-D printing in MRI guided focused ultrasound surgery', Digital Medicine, 4(1), 22-26, 2018.

[327] Giannakou M, Yiallouras C, Menikou G, Ioannides C, Damianou C. MRI-guided frameless biopsy robotic system with the inclusion of unfocused ultrasound transducer for brain cancer ablation. Int J Med Robotics Comput Assist Surg. 2019; 15: e1951. https://doi.org/10.1002/rcs.1951

[328] Drakos T, Giannakou M, Menikou G, Ioannides C, Damianou C, 'An improved method to estimate ultrasonic absorption in agar-based gel phantom using thermocouples and MR thermometry'. Ultrasonics. 2020, Jan 31;103:106089.doi: 10.1016/j.ultras.2020.106089

[329] Christakis Damianou, Marinos Giannakou, Nikolas Evripidou, Stefan Kege, Peter Huber, Juergen Jenne, 'Focused ultrasound robotic system for very small bore magnetic resonance imaging', Int J Med Robotics Comput Assist Surg, 16 (6), DOI: 10.1002/rcs.2165, 2020.

[330] Theoharis Drakos, Marinos Giannakou, Georgios Menikou, Christakis Damianou, 'MRI-guided focused ultrasound positioning system for preclinical studies in small animals' J Ultrasound Med 2020; 9999:1–10. doi:10.1002/jum.15514.

[331] M Giannakou, G Menikou, K Ioannides, C Damianou, Magnetic resonance image-guided focused ultrasound robotic system with four computer-controlled axes with endorectal access designed for prostate cancer focal therapy Digital Medicine 6 (1), 32

[332] C Damianou, M Giannakou, G Menikou, L Ioannou, Magnetic resonance imaging-guided focused ultrasound robotic system with the subject placed in the prone position, Digital Medicine 6 (1), 24.

[333] Theocharis Drakos Marinos Giannakou Georgios Menikou Georgios Constantinides Christakis Damianou, 'Characterization of a soft tissue-mimicking agar/wood powder material for MRgFUS applications', Ultrasonics, Volume 113, May 2021, https://doi.org/10.1016/j.ultras.2021.106357.

[334] T Drakos; M Giannakou; G Menikou; A Filippou; N Evripidou; K Spanoudes; L Ioannou; C Damianou, MRI-Guided Focused Ultrasound Robotic System for Preclinical use, J Vet Med Animal Sci. 2020; 4(1): 1049.

[335] Anastasia Antoniou, Nikolas Evripidou, Marinos Giannakou, Georgios Constantinides, Christakis Damianou, 'Acoustical properties of 3D printed thermoplastics', Journal of acoustical society of America (JASA), 2021, 149 (4).

[336] Anastasia Antoniou, Theocharis Drakos, Marinos Giannakou, Nikolas Evripidou, Leonidas Georgiou, Theodora Christodoulou, Natalie Panayiotou, Cleanthis Ioannides, Nikolaos Zamboglou, Christakis Damianou, 'Simple methods to test the accuracy of MRgFUS robotic systems', Int J Med Robot. 2021;e2287, https://doi.org/10.1002/rcs.2287.

[337] Anastasia Antoniou, Marinos Giannakou, Nikolas Evripidou, Georgios Evripidou, Kyriakos Spanoudes, Georgios Menikou, Christakis Damianou, 'Robotic system for magnetic resonance guided focused ultrasound ablation of abdominal cancer', Int J Med Robotics Comput Assist Surg, DOI: https://doi.org/10.1002/rcs.2299.

[338] Spanoudes K, Evripidou N, Giannakou M, Drakos T, Menikou G, Damianou C. A high intensity focused ultrasound system for veterinary oncology applications. J Med Ultrasound 2021; 29:195-202

[339] Anastasia Antoniou, Christakis Damianou, Review of MR relaxation properties of tissue-mimicking phantoms, Ultrasonics, Volume 119, 2022, https://doi.org/10.1016/j.ultras.2021.106600.

[340] Anastasia Antoniou, Marinos Giannakou, Nikolas Evripidou, Stylianos Stratis, Samuel Pichardo,Christakis Damianou, Robotic system for top to bottom MRgFUS therapy of

multiple cancer types, , Int J Med Robotics Comput Assist Surg https://doi.org/10.1002/rcs.2364

[341] Anastasia Antoniou, Leonidas Georgiou, Theodora Christodoulou, Natalie Panayiotou, Cleanthis Ioannides, Nikolaos Zamboglou, Christakis Damianou, MR relaxation times of agar-based tissue mimicking phantoms, Journal of Applied Clinical Medical Physics

[342] Antoniou A, Giannakou M, Georgiou E, Kleopa KA, Damianou C. Robotic device for transcranial focussed ultrasound applications in small animal models. Int J Med Robot. 2022 Aug 3:e2447. doi: 10.1002/rcs.2447. Epub ahead of print. PMID: 35924335

[343] Marinos Giannakou; Anastasia Antoniou; Christakis Damianou, 'Preclinical robotic device for magnetic resonance imaging guided focussed ultrasound', The International Journal of Medical Robotics and Computer Assisted Surgery, 2022-10, DOI: 10.1002/rcs.2466

[344] A Antoniou, C Damianou, 'Simple, inexpensive, and ergonomic phantom for quality assurance control of MRI guided Focused Ultrasound systems', Journal of Ultrasound, 2022.

[345] A Antoniou, L Georgiou, N Evripidou, C Ioannides, C Damianou 'Challenges regarding MR compatibility of an MRgFUS robotic system' ,Journal of Magnetic Resonance, 2022

[346] Damianou C., Mylonas N., Ioannides K., 'Sonothromblysis in Combination with Thrombolytic Drugs in a Rabbit Model Using MRI-Guidance', *Engineering*, 2013, 5, 352-356, http://dx.doi.org/10.4236/eng.2013.510B071

[347] N. Papadopoulos, C. Damianou, 'Microbubble-based sonothrombolysis using a planar rectangular ultrasonic transducer', Journal of Stroke and Cerebrovascular Diseases, 26 (6), 2017. DOI: 10.1016/j.jstrokecerebrovasdis.2017.01.023

[348] N. Papadopoulos, C. Damianou, 'Microbubble-based sonothrombolysis using a planar rectangular ultrasonic transducer', Journal of Stroke and Cerebrovascular Diseases, 26 (6), 1287-1296, 2017.

[349] N. Papadopoulos, C. Yiallouras, C. Damianou, The enhancing effect of focused ultrasound on TNK- Tissue Plasminogen Activator induced thrombolysis using an in vitro

circulating flow model", J Stroke Cerebrovasc Dis. 2016 Dec; 25(12):2891-2899. doi: 10.1016/j.jstrokecerebrovasdis.2016.07.052.

[350] N. Papadopoulos, C. Damianou, 'In vitro evaluation of focused ultrasound enhanced TNK-TPA mediated thrombolysis' Journal of Stroke and Cerebrovascular Diseases, ;25(8):1864-77, 2016. doi: 10.1016/j.jstrokecerebrovasdis.2016.03.05

[351] Damianou C., Hadjisavvas V., Mylonas N., Couppis, A., Ioannides K., 'MRI-Guided Sonothrombolysis of Rabbit Carotid Artery', Journal of Stroke and Cerebrovascular Diseases, Vol 23 (2), pp. e113-21, 2014.